Design and Application of Fibre Laser Systems for Gas Spectroscopy

NORHANA ARSAD

Department of Electrical and Electronic Engineering
Centre for Microsystems and Photonics

A thesis submitted to the Department of Electronic and Electrical Engineering
at the University of Strathclyde for the degree of Doctor of Philosophy

February 2010

Abstract

A growing number of applications for trace gas sensing and measurement have emerged in a wide variety of fields. All-fibre systems with spectroscopic measurements are capable of providing accurate gas measurement both remotely and in multiple locations. Low power (10mW) fibre lasers can be easily constructed using an erbium-doped fibre amplifier (EDFA) connected in a fibre loop configuration and can be designed to operate over a broad wavelength range of 1480-1620nm. These fibre lasers provide a possible source for multi-gas spectroscopy to detect the near-infrared (near-IR) absorption lines of gases such as CO, CO_2, C_2H_2, H_2S, etc., in safety, pollution and industrial monitoring. This thesis investigates the feasibility of four types of erbium fibre laser systems using different spectroscopic methods for measurement of gas parameters.

The first system consists of an erbium doped fibre laser (EDFL) in a ring cavity using a saturable absorber (SA) to produce a stable output. The system uses a wavelength scan and pump current modulation to obtain intensity modulation of the laser output, with phase sensitive detection for gas measurements. Results show that the system is feasible but it was difficult to accurately measure gas concentration due to the high background signal level and other noise sources.

The second method involves inserting a micro-optic gas cell into the fibre laser cavity, a technique known as intra cavity laser absorption spectroscopy (ICLAS), and uses the broadband amplified spontaneous emission (ASE) within the cavity at threshold conditions. This

has shown excellent results, with around two orders of magnitude sensitivity enhancement over direct absorption, and is capable of detecting several gas lines with low line strength under room temperature and atmospheric pressure conditions. Results matched well with theoretical data, the system is simple and inexpensive (apart from the OSA) and potentially can be used for multi-gas sensing.

A distributed feedback fibre laser (DFB-FL) was studied as the third system in this thesis. The DFB-FL is more stable and has a narrower linewidth compared to the ring cavity EDFL which tends to suffer from mode hopping problems. The feasibility of using the distributed feedback fibre laser for spectroscopy was investigated, involving a significant cost in setting up the experiments. However due to the DFB-FL being fragile and the lack of proper control in tuning the wavelength it was difficult to implement a working system, and it was deemed to be unsuitable at this stage until improvement and maturity of the current technology has been attained. Furthermore, similar to diode lasers, the DFB-FL operates at a single wavelength only and therefore does not have the capacity for multi-gas sensing with a single source.

The fourth and final method investigated made use of the same EDFL system as in the first technique but with photo-acoustic spectroscopy (PAS). PAS overcomes the key problem of the high background signal level under no-gas conditions and the output gas signal can be recovered in a straightforward manner giving absorption line shapes without extensive signal processing. Good experimental results were obtained under room temperature and atmospheric pressure conditions which agreed well with theoretical data.

Declaration

The copyright of this thesis belongs to the author under the terms of the United Kingdom Copyright Acts as qualified by the University of Strathclyde Regulation 3.51.Due acknowledgement must always be made of the use of any material contained in, or derived from, this thesis.

Signed:..**Date:**.............................

Acknowledgement

I acknowledge the support of Minister of Higher Education (Malaysia) and Universiti Kebangsaan Malaysia (UKM) scholarship.

I would like to give a huge thank you to my supervisor Prof. George Stewart for his guidance, support and encouragement over the last three years. I know it has been a strain on you at times but you always smile and wholeheartedly give me support and motivation in getting through all this. I don't think that I can come this far without your help.

Many thanks to members of the CMP that I have been part of, for their guidance and support, Prof. Culshaw, Prof Johnstone, Prof Uttamchandani, Dr Li, Dr Thursby, Dr. Amstrong, Dr Flockhart, Dr Sheridan, Dr Lengden, Mr. Brown, Dr. Mirza, Mr. Mitchell, Mr Keith, Mr Arup, Mrs. Binnie, Mrs. Smart. Also to Dr. Duffin and Dr. Mauchline from OptoSci Ltd. Special thanks to Dr. Cleary for proof reading my thesis and has reduced Prof Stewart's headache. To my adored friend Ms. Li Li, Dr Li Min, Ms Li Li and Dr Lim (PEDEC), sincerely appreciate your help.

Thank you to my father and all my family members with Uncle Manaf & family in London for their encouragement and support.

To my beloved husband, Azlim Zamberi, I thank you for being the best man in the world and to my wonderful son, Ali Imran for cheering me all the time. I love both of you and always will. Last but not least to my friends if i have missed your name it's only on paper as you all have a special place in my heart MANY Thanks....

In my memory.... Mum

Contents

Nomenclature

DFB   Distributed Feedback Fibre Laser

EDFA Erbium Doped Fibre Amplifier

EDFL Erbium Doped Fibre Laser

FBG   Fibre Bragg Grating

FM   Frequency Modulation

FMS   Frequency Modulation Spectroscopy

FMS   Frequency Modulation Spectroscopy

FPF   Fabry Perot Filter

FPS   Fabry Perot Spectrometer

FSR   Free Spectral Range

GRIN Graded Index

HITRAN High-resolution Transmission Molecular Absorption

ICLAS Intra-cavity Laser Absorption Spectroscopy

IR   Infrared

LIA   Lock-in Amplifier

LM   Loop Mirror

M   Mirror

PA   Photoacoustic

PAS   Photoacoustic Spectroscopy

PD   Photoreceiver

PM   Polarization Maintaining

PSD   Phase- sensitive Detection

PZT   Piezo-transducer

RBW   Resolution Bandwidth

RF   Radio Frequency

RIN   Relative Intensity Noise

RIN   Relative Intensity Noise

SA   Saturable Absorber

SHB   Spatial Hole Burning

SLF   Sagnac Loop Filter

SMSR   Side Mode Suppression Ratio

STP   Standard Temperature and Pressure

TEC   Thermoelectric Cooler

TF Tunable Filter

UV Ultraviolet

WMS Wavelength Modulation Spectroscopy

Chapter 1

INTRODUCTION

1.1 Background of Spectroscopy

Spectroscopy is the study of matter and the use of absorption, emission, or scattering of electromagnetic radiation by matter to qualitatively or quantitatively study physical processes. These bonds can vibrate with stretching motions or bending motions and the interaction of radiation with matter can cause redirection of the radiation and transitions between the atomic or molecular energy levels.

The history of spectroscopy was started when British scientist William Wollaston discovered the existence of dark lines in the solar spectrum in 1802. Thirteen years later, Joseph von Fraunhofer hypothesized that the dark lines were caused by an absence of certain wavelengths of light. In 1859, a German physicist Gustav Kirchhoff showed that each pure substance produces a unique light spectrum which gave rise to the field of analytical spectroscopy[1].

The end of the nineteenth and beginning of the twentieth centuries was marked by significant efforts to quantify and explain the origin of spectral phenomena. Johann Balmer and Johannes Rydberg first developed equations to explain the atom's frequency spectrum and

then Niels Bohr published his famous model in 1913. However, Bohr's model only applied to element that had one electron. In 1925 Werner Heisenberg and Erwin Schrodinger developed quantum mechanics to explain the spectra of most elements. These discoveries marked the beginning of modern spectroscopy[1].

Three commonly used spectroscopic techniques are absorption, emission, and scattering spectroscopy. Absorption spectroscopy, such as Infrared (IR) and Ultraviolet spectroscopy (UV), measures the wavelengths of light that a substance absorbs to give information about its structure whereas emission spectroscopy, including fluorescence and laser emission, quantifies the amount of light that a substance emits at a certain wavelength. Lastly, scattering spectroscopy, such as Raman spectroscopy, is similar to emission spectroscopy but detects and analyzes all of the wavelengths that a substance emits upon excitation [1].

1.2   Motivation of the Study

There is now a growing interest in the application of fibre optic systems for environmental and safety monitoring. Although the near-IR lines of gases are much weaker than the fundamental absorption lines, the availability of standard optical fibres and components is a key stimulus for development of sensors in this spectral region. Fibre optic components are cheap and readily available due to their use in the telecommunications industry, so are ideal for developing systems for the detection of gases.

The benefits in utilizing a fibre optic system include immunity from electromagnetic interference, safety in hazardous environments and fibre lasers can be tuned over a broad spectrum. To compensate for the weak line strengths, high sensitivity spectroscopic techniques such as wavelength modulation spectroscopy, intra-cavity and ring down spectroscopy are among those that have been investigated for these systems.

Even though semiconductor lasers are generally favoured for use in gas detection due

to their stability and compactness, they are wavelength limited to specific gas absorption lines and hence costly to produce. Thus, fibre laser systems are attractive due to their wide spectral range and can be cost effectively used in multiple gas sensing or gas multiplexing [2, 3, 4, 5, 6, 7].

The main purpose of this research is to investigate the feasibility of various types of fibre laser systems for gas spectroscopy using wavelength modulation spectroscopy (WMS), intra cavity laser absorption spectroscopy (ICLAS) and photo-acoustic spectroscopy (PAS) for gas analysis. 1% of acetylene(C_2H_2) gas has been chosen as our first sample gas due to its relatively high line strength at 10^{-20} cm^2/(molecule cm) level which is easy to detect using the EDFL system, followed by lower line strength gases such as carbon dioxide (CO_2) and methane (CH_4) to determine the maximum sensitivity that can be achieved. Absorption lines between 1520 nm and 1570 nm are chosen which are within the bandwidth of erbium doped fibre amplifiers and lasers [8] are thus compatible with the developed fibre laser systems.

1.3   Objective of the Thesis

The work described in this thesis is concerned with the potential of, and the prospects for fibre laser systems in gas spectroscopy, with several techniques being applied during the learning process. Fibre laser systems with spectroscopy techniques such as wavelength modulation spectroscopy (WMS), photoacoustic spectroscopy (PAS) and intra-cavity PAS will be explained in subsequent chapters. The erbium doped fibre laser (EDFL) in a ring cavity was selected as the preferred fibre laser source after a comparison study was made with distributed feedback fibre lasers (DFB-FL) at the preliminary stage of the research. The motivation for choosing these types of fibre lasers is that several absorption lines of different gases fall within the gain region of the erbium doped fibre amplifier (EDFA). Although the general area of research in this study is not entirely new, it was anticipated that the work

would lead to exploration of new techniques and designs which could be adapted to the development of gas spectroscopy systems.

The objectives of the thesis can briefly be summarized as follows:

a. To study the characteristics of the four types of fibre laser systems

b. To determine the suitability and compability of fibre lasers for spectroscopy

c. To explore different spectroscopic techniques for fibre lasers

d. To design and develop a fibre laser system for multi-gas spectroscopy

e. To test and analyse the performance of the developed system

1.4   Scope of Work

As already noted, the aims of the proposed work is to explore the potential of, and the prospects for fibre laser systems in spectroscopy applications and compatibility with various spectroscopy techniques. The study pays significant attention to first developing an understanding of the characteristics of the fibre laser systems, for example, the use of a saturable absorber to get stable operation. Then only would an exploration be carried out using different techniques of spectroscopy to detect the presence of gas.

Simultaneously a preliminary study of photo-acoustic spectroscopy (PAS) using diode lasers was carried out in the initial phase in order to become familiar with the method. Through a significant number of experiments using this method, the compatibility of fibre laser systems was eventually understood for the intended spectroscopy purposes. Figure 1.1 depicts the scope of work covered and describes the study model that will be consistently referred to throughout this thesis with the bold boxes indicating the research path, while the dotted lines are the related topics in the field. The performance of the fibre laser systems was evaluated based on certain design and performance parameters.

The research of this thesis was focussed on trace gas sensing, although spectroscopic tech-

niques can also be used in other forms such as solid and liquid materials. Two categories of detection are studied, namely optical and acoustic detection. Optical detection such as direct detection, intra-cavity laser absorption spectroscopy (ICLAS), wavelength modulation spectroscopy (WMS), and frequency modulation spectroscopy (FMS) are among the methods commonly used whereas acoustic detection involves photo-acoustic spectroscopy (PAS). These techniques will be discussed more in-depth in the following chapters which present theoretical and experimental results obtained for each technique with different types of lasers such as diode lasers, erbium doped fibre lasers and distributed feedback fibre lasers. However, the optimal setup of a fibre laser systems was determined after characterisation, such as steady state and dynamic response, of fibre lasers had been performed.

1.5   Main Contribution of the Research

This thesis makes an original contribution to the research field in the following two aspects:

1) use of intensity (AM) modulation (through pump modulation) with wavelength scanning in an EDFL system incorporating a saturable absorber for both standard and photo-acoustic spectroscopy.

2) demonstration of ~ 2 orders of magnitude sensitivity enhancement and multi-gas sensing in an EDFL using the methods of intra-cavity laser absorption spectroscopy (ICLAS) and the ASE in the cavity.

1.6   Thesis Outline

This thesis is divided into seven main sections which comprise of introduction, chapters explaining the EDFL characteristics and the DFB-FL performance, investigation of ICLAS with an EDFLs, results for photoacoustic spectroscopy (PAS) with fibre laser systems and finally future work and overall conclusions for the whole thesis.
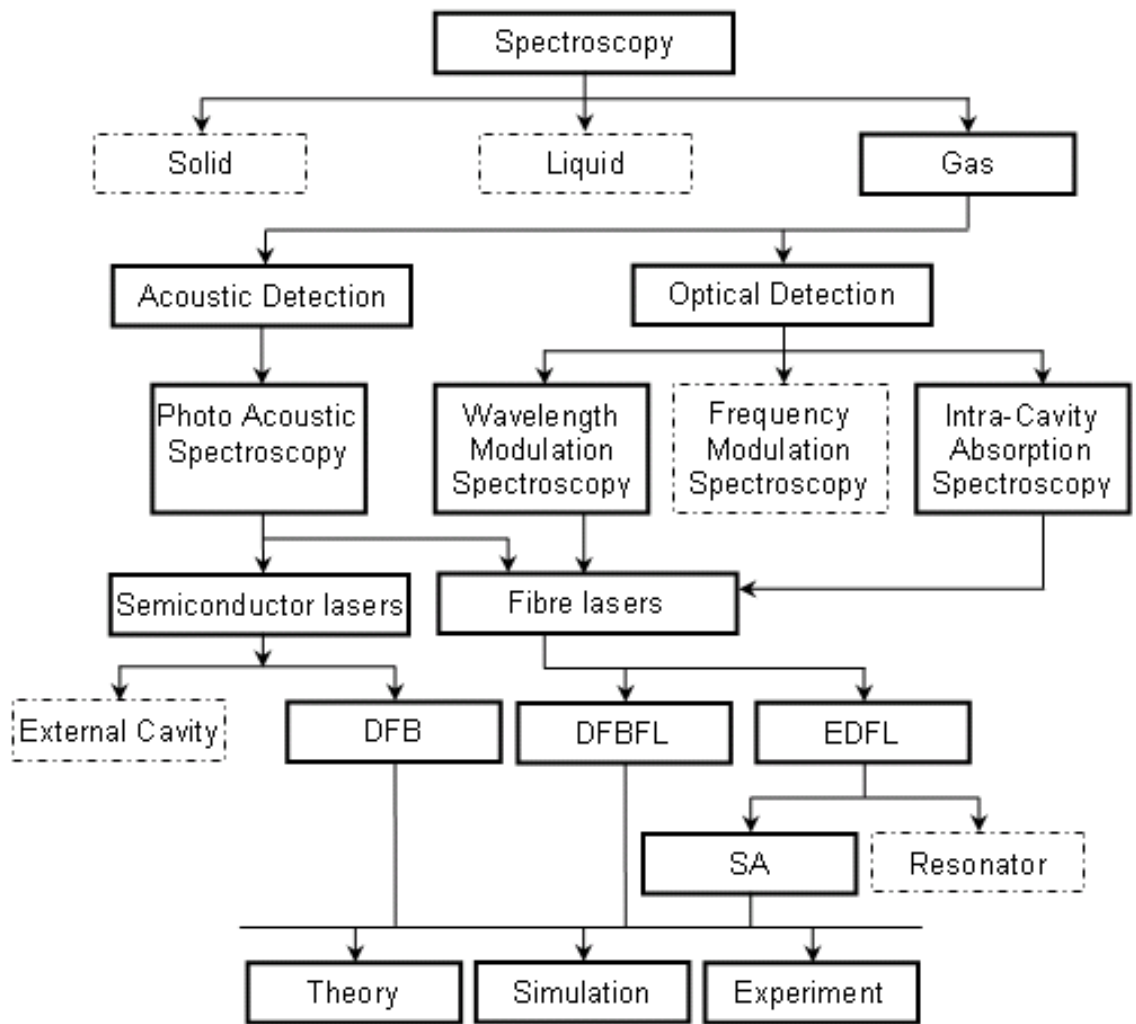
Figure 1.1: Scope of the work

Chapter 2 provides a literature review of gas spectroscopy with a detailed explanation of techniques and methods used throughout the subject area. This is where the technical rationale behind Figure 1.1 is explained. This chapter describes parameters, devices, instrumentation and set-ups associated in achieving the stated objectives.

Chapter 3 investigates the EDFL as a source for spectroscopy using different techniques for detecting the optical signal and focusing intensity modulation (AM).

Chapter 4 introduces intra-cavity laser absorption spectroscopy (ICLAS) with EDFLs and explains the use of ASE for this purpose. After optimization and characterisation, the system was employed for trace gas sensing using various gases with different concentrations for evaluating system sensitivity.

Chapter 5 introduces the DFB-FL as a laser source which uses a FBG in a special fibre to form a laser. One of the advantages of the DFB-FL is its freedom from mode hopping; hence its potential to form a stable laser. The system was studied to determine the feasibility for gas spectroscopy. All the actual experiment setups, applications, optimisations, characteristics, findings and observations are discussed extensively.

Chapter 6 describes an acoustic detection technique, namely photo-acoustic spectroscopy (PAS) for detecting gas. For the preliminary stage, a diode laser was used with the technique to become familiar with the working principles of the system. The experimental setup is similar to conventional spectroscopy except for the gas cell which uses a microphone to detect the acoustic wave. The aim was to give an idea how to implement the system with a fibre laser using PAS to enhance the sensitivity.

Finally Chapter 7 concludes this thesis with a summary and future work.

1.7 Publications by the author

Publications through the study of this research are as follows:

1. George Stewart, Walter Johnstone, Norhana Arsad and Kevin Duffin, "Tunable diode and fibre laser spectroscopy in the near-IR for measurement of gas parameters", (Invited paper) SPIE Photonics Europe, Italy, April 2008.

2. N. Arsad and G Stewart, "Stable, tunable and single-mode operation of an erbium-doped fibre laser system using a saturable absorber for gas spectroscopy applications", SPIE Photonics West, USA, Jan 2009.

3. N Arsad and G Stewart, " Intra-cavity spectroscopy using amplified spontaneous emission in erbium fibre lasers", OFS20, UK, Oct 2009.

4. N Arsad and G Stewart, "Intra-cavity spectroscopy using amplified spontaneous emission in erbium fibre lasers", In preparation for Journal of Measurement Science Technology.

5. N Arsad and G Stewart, "Gas detection using erbium doped fibre lasers with photo acoustic spectroscopy", To be submitted: Journal.

Chapter 2

REVIEW OF GAS SPECTROSCOPY

2.1 Introduction

Gas sensing is very important for environmental, safety and industrial monitoring. Optical fibre gas sensors operating in the near-IR region (1-2μm wavelength) have several advantages, including the availability of low cost components, remote access to hazardous environments and networking capabilities. Fibre laser sources offer interesting possibilities for gas sensors since they can operate over an extended wavelength range and micro-optic gas cells may be readily connected either external to, or within, the fibre laser cavity. Erbium fibre lasers can operate over the wavelength range of the C band but a major problem is that the overtone absorption lines of gases in the near-IR are typically two or three orders of magnitude weaker than their fundamental lines in the mid-infrared [6]. Thus, sensitivity enhancement of spectroscopy is desired in order to detect trace concentration of these gases.

Molecular spectroscopy involves the study of the interaction of radiation between the energy levels of the atoms or molecules of the gas sample. A transition from a lower level to a higher level with transfer of energy from the radiation field to the atom or molecule is called absorption. When a broad band light source is passed through the gas sample, only the light

whose energy is associated with the allowed energy level transitions within the molecule will be absorbed whereas all other light will pass through un-attenuated as depicted in the Figure 2.1.

This chapter describes different techniques of optical detection with a review for each of them, including components used and theoretical methods applied in the study. Finally, types of lasers are also discussed for highlighting their relative advantages and disadvantages as part of this study.
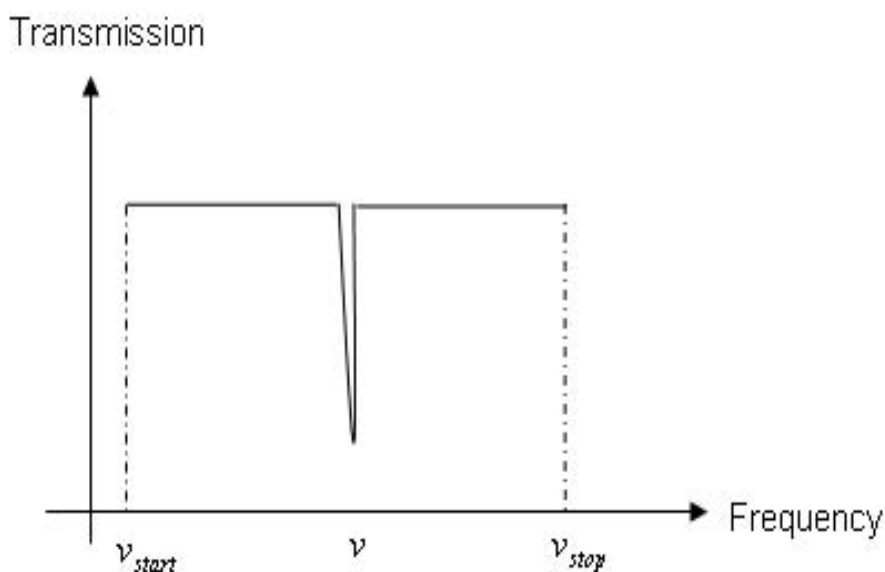
Figure 2.1: Absorption of laser intensity at frequency, v

2.2 Spectroscopy Techniques

The principle behind spectroscopic sensing is rather simple. Every chemical substance exhibits a distinctive light absorption pattern. This pattern is produced as incident light of a specific wavelength is absorbed in a cell of length (l) containing a chemical species that has an absorption line. Optical attenuation characterises the transmission of light through a gas cell. This attenuation is given by Beer-Lambert-Bouger's Law or the Beer-Lambert Law (or

simply Beer's Law):

$$P_{out} = P_{in}exp[-\sigma(v)Nl] \tag{2.1}$$

where P_{in} is the incident intensity of light, $\sigma(v)$ is the absorption cross-section per molecule, v is the wave number, N is the concentration of gas molecules per unit volume and l is the length of the gas cell.

From the equation above, it is clear that the intensity of the light decreases with absorption by the gas. However, gas concentrations are often expressed as fractions of the pure gas at atmospheric pressure, e.g. parts-per-million (ppm) and thus equation 2.1 can be expressed in the following form for convenience:

$$P_{out} = P_{in}exp[-\alpha(v)Cl] \tag{2.2}$$

where P_{in} is the incident intensity of light, C is the concentration of measured gas at normal fraction of $(0 < C < 1)$, α the absorption coefficient and l is the length of the gas cell.

The concentration of measured gas C can be written as:

$$C = \frac{N}{N_0} \tag{2.3}$$

where N_0 is the number of molecules of gas per unit volume at standard temperature and pressure (STP), T=273.15 K, P=10^5 Pa and N is the actual molecular number of measured gas molecules per unit volume at the same condition, i.e. STP.

According to the ideal gas equation, the molecular number of gas molecules per unit volume can be described as:

$$N_0 = \frac{PV}{RT} N_A / V \tag{2.4}$$

where P and T are standard pressure and temperature described above respectively, V is the volume of gas, R is the universal gas constant 3.814472 Jmol^{-1}K^{-1}, and N_A is Avogadro's constant 6.02214×10^{23} mol^{-1}.

The molecular number of gas molecules per unit volume for the case of different pressure and/or temperature also can be calculated by referring to Equation 2.4. Therefore, the actual molecular number per unit volume of measured gas should be modified to meet this particular specific experiment condition ($P = 1$ atm. $= 1 \times 10^5$ Pa, $T = 273.15$ K + room temperature) as they do not correspond to STP conditions.

Referring to Equation 2.2, the absorbance of the measured gas is defined as (for $\alpha Cl \ll 1$)

$$A = \alpha Cl \simeq 1 - \left(\frac{P_{out}}{P_{in}} \right) \tag{2.5}$$

The absorbance is linearly proportional to absorption coefficient, length of cell and concentration; hence the gas concentration can be obtained if the length of the cell and the absorption coefficient are known.

The absorption coefficient $\alpha(v)$ of gas absorption line can be written as:

$$\alpha(v) = N_0 \sigma(v) \tag{2.6}$$

This relationship is given by Equation 2.7 and typical line strengths experimentally can be found between 5×10^{-21} and 2×10^{-19} cm/molecule for gases at room temperature.

$$S = \int_{-\infty}^{\infty} \sigma(v) dv \tag{2.7}$$

The line strength in cm^2/molecule.cm multiplied with the number N_0 gives conversion

from cm/molecule to cm^{-2}/atm.

The gas absorption lineshape in the experiment can be considered as a Lorentzian lineshape since it is collision broadened at atmospheric pressure. Pressure broadened lines are described by the following Lorentzian distribution:

$$\alpha(v) = \frac{N_0 \frac{S}{\pi} \gamma_L}{(v - v_0)^2 + \gamma_L^2} \qquad (2.8)$$

where S is the line strength of gas absorption line in units of cm^2/molecule cm, γ_L is the pressure broadened half-linewidth (in units of cm^{-1}) which associated with the absorption co-efficient are between typically 0.05 and 0.15cm^{-1} for gases at atmospheric pressure.

There are different types of spectroscopic techniques used in different applications, depending on the conditions and requirements of the system. Two categories of detection are studied here which are divided into optical detection and acoustic detection. Optical detection such as direct detection, intra-cavity laser absorption spectroscopy (ICLAS), wavelength modulation spectroscopy (WMS), and frequency modulation spectroscopy (FMS) are among the methods commonly used whereas acoustic detection will focus only on photo-acoustic spectroscopy (PAS). The subsequent section explains each type of technique as used in gas detection systems.

2.2.1 Optical Detection

This topic and the topic to follow are reviews of the major techniques of detection in gas spectroscopy. Figure 1.1 is referred to in order to help describe the techniques.

2.2.1.1 Wavelength Modulation Spectroscopy (WMS)

Wavelength modulation spectroscopy (WMS), also known as a noise-reducing technique [9], is a well-known and commonly used technique in gas spectroscopy. This technique started

when Arndt presented his first models in 1965 [10] and later J Reid et al. performed WMS by use of lead-salt laser diodes in the mid-IR region in 1978 [11]. Improvement in the sensitivity from Reid's experiment marks a significant step forward in gas monitoring of atmospheric pollutants. Ten years later, WMS was applied to optical communication lasers in the near-IR region [12] and recently to novel quantum-cascade lasers [13] and visible laser diodes [14] in 1998 and 2000 respectively.

The importance of the technique is the ability of shifting the detection to higher frequencies, hence reducing 1/f noise. WM is performed by modulating at frequencies that are substantially less than the absorption linewidth. This type of technique is based on sinusoidal modulation of the wavelength of the light while it is slowly tuned through an absorption feature of the species to be detected. The interaction of the modulated light with the absorption feature leads to the generation of signals at the different harmonics of the modulation frequency, which can be detected by using a lock-in amplifier (LIA) [15].

Three requirements in order to perform WMS are (a) narrow linewidth-single longitudinal mode operation, (b) ability to scan across an absorption linewidth and (c) tunability to individual absorption lines of various gases [16]. This can be seen as shown in Figure 2.2 [17]. Acetylene gas has been chosen as a target gas due to its absorption lines being within the EDFA gain; furthermore it has the strongest absorption compared with other gases in this region such as H_2S, NH_3,CO,CO_2.
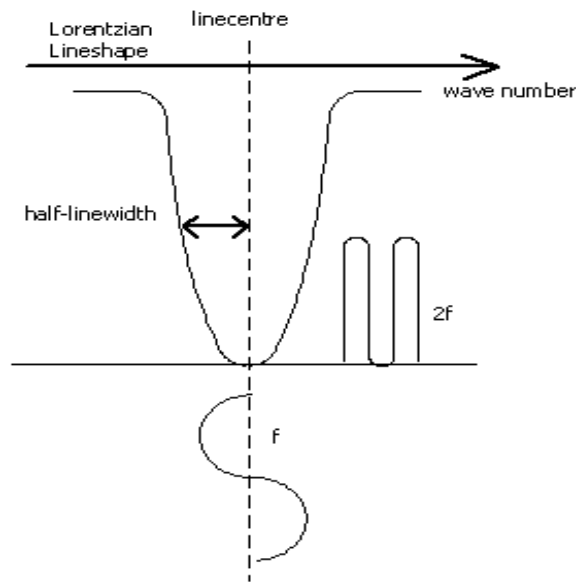
Figure 2.2: Wavelength modulation spectroscopy[17]

As mentioned earlier, a lock-in amplifier (LIA) is usually employed in the system when WM is applied. The LIA detects and measures a very small AC signal by using a technique known as phase-sensitive detection (PSD) to single out the component of the signal at a specific reference frequency and phase. Noise signals at frequencies other than the reference frequency are rejected and do not affect the measurement [18].

Display on Channel 1 and Channel 2 of the LIA are based on the selection of X, Y, R and θ which output display is different from an oscilloscope. Higher harmonic signals can be exploited to obtain more sensitive measurements of spectroscopic parameters, such as lineshape profile, absorption cross-section, temperature, and concentration [19].

2.2.1.2 Frequency Modulation Spectroscopy (FMS)

It has been over two decades since frequency modulation (FM) opened up new applications for spectroscopy with spectrally modulated laser light. FMS and WMS are closely related measurement techniques; they simply operate at different values of modulation index and

15

frequency. FMS is characterised by a modulation frequency that is much higher that the half-width of absorption profile, usually several GHz, and a small FM amplitude. A further description of FMS and WMS in theory is reported in [20, 21]. A low modulation frequency of 2k Hz is employed in our experiments, therefore FMS is not used in this study.

2.2.1.3 Intra-Cavity Laser Absorption Spectroscopy (ICLAS)

In 1992, intra-cavity spectroscopy was employed successfully by V.M. Baev et al [22] using diode lasers as the light source in gas detection [23]. Four years later, a dye laser with intra-cavity absorption spectroscopy was demonstrated which could achieve an absorption length enhancement to 70000km. Then in 1999, a gas sensor based on fibre laser intra-cavity spectroscopy was published by Cordero and Morse [24]. According to the papers reported, intra-cavity laser absorption spectroscopy (ICLAS) is a technique for high sensitivity absorption measurement where photons circulate many times within a laser cavity enhancing the path length of a gas cell in the laser cavity. With a large number of circulations through the cell, it will transform from a short absorption cell into a highly efficient multi-pass system, hence improving the sensitivity of detection.

Furthermore, there is no external modulator needed to create a pulse in this technique compared to ring down spectroscopy [25]. Figure 2.3 depicts an example of ICLAS applied in a fibre laser system for gas spectroscopy as demonstrated in [25] and a theoretical analysis of the dynamics of erbium fibre laser systems is given in [26]. Practical realization of ICLAS with fibre lasers is difficult for several reasons such as the spectrum must be captured during the period of relaxation oscillations and detector arrays for the 1-2 μm region are less capable and more expensive than the silicon CCD arrays used for ICLAS at $<1\mu$m wavelengths. For example, Stark [27] used a rapid scan Fourier Transform (FT) spectrometer to capture the spectrum at each peak of the relaxation oscillations for a thulium-doped fibre laser.
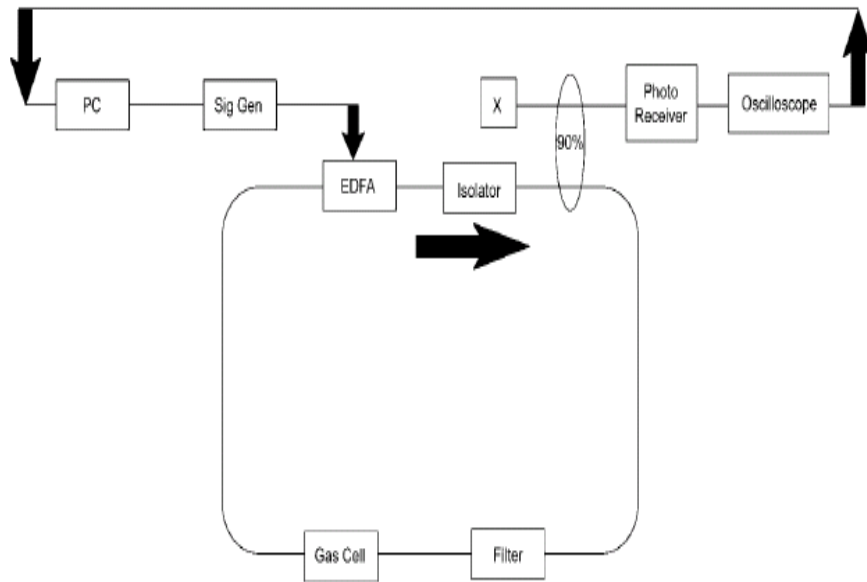
Figure 2.3: Experimental system for intra-cavity analysis[25]

2.2.2 Acoustic Detection

2.2.2.1 Photo-Acoustic Spectroscopy (PAS)

Among spectroscopic techniques, photo-acoustic spectroscopy (PAS) is the oldest type of spectroscopy used for gas analysis. In 1880, Bell discovered the photo-acoustic (PA) effect in solids, which consists of the generation of a sound wave in a medium irradiated by a modulated light beam. This technique was then actively exploited after the microphone and laser were invented [28].

It is well known that PAS is a sensitive gas sensing technique and has been used in many applications including the monitoring of environmental pollution, industrial process control of industry [29, 30, 31] and diagnosis in medicine and biology [32, 33]. It measures directly the amount of modulated laser radiation absorbed in the sample and converted into pressure energy via non-radiative relaxation processes. This constitutes an acoustic wave or sound wave which is later detected by a microphone. A flowchart of how conversion of optical into

electrical form is shown in Figure 2.4 for the acoustic detection.
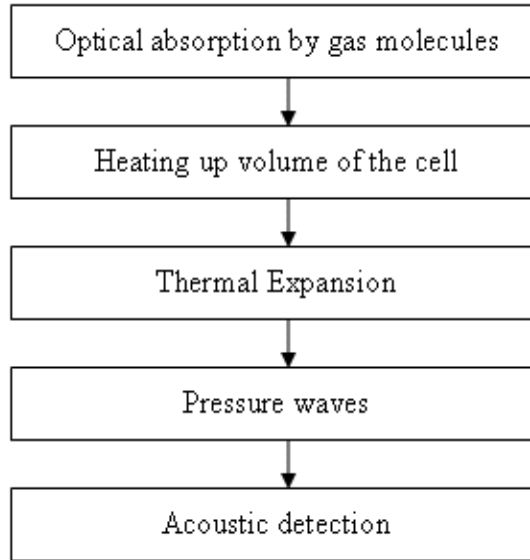
Figure 2.4: Generation of photo-acoustic signal

In the early 1970's, Kreuzer [34] demonstrated the detection of low concentration of methane in nitrogen on the 10^{-8} level by using a 15 mW He-Ne laser operating at 3.39 microns wavelength. Two years later, Dewey and co-workers [35] made a significance improvement by modulating the optical beam at the resonant frequency of the gas cell. Almost at the same time, Goldan and Goto [36] achieved a better result in that the quality factor Q exceeded 750 using the lowest-order radial mode and a multi-pass gas cell. They investigated the microphone coupling characteristics and noise limitations by setting up an electrical equivalent lumped parameter circuit for the condenser microphone. Kamm [37] analyzed the loss mechanism of a resonant cell and presented an optimization method for a photo-acoustic system based on principles derived from experiments and previously published work.

In Chapter 6, detailed experimental work is presented first of all using diode lasers, then an erbium doped fibre laser system is examined with PAS to obtain performance comparison for both lasers. The erbium doped system for PAS is one that has not yet been published.

2.3 Spectroscopy Cell

Here two types of gas cell are discussed, namely, micro-optic gas cell and PA cell as they were used in the experiments. Both have a different layout and are explained in detail in the following section.

2.3.1 Micro-Optic Gas Cell

A micro-optic gas cell consists of two graded index (GRIN) lenses connected to fibre pigtailes positioned at either end of a ceramic V-groove. When a laser beam is launched into the micro-cell, input light is collimated by the GRIN lens at one end and passes through the sensing region and is subsequently collected by the second GRIN lens at the other end. The layout of the module of the micro-optic gas cell employed in our experimental system is depicted in Figure 2.5 (OptoSci Micro Optic Gas Cell) with a 5.9cm path length and an insertion loss of ∼1dB while in Figure 2.6 is the illustration of the micro-optic cell.
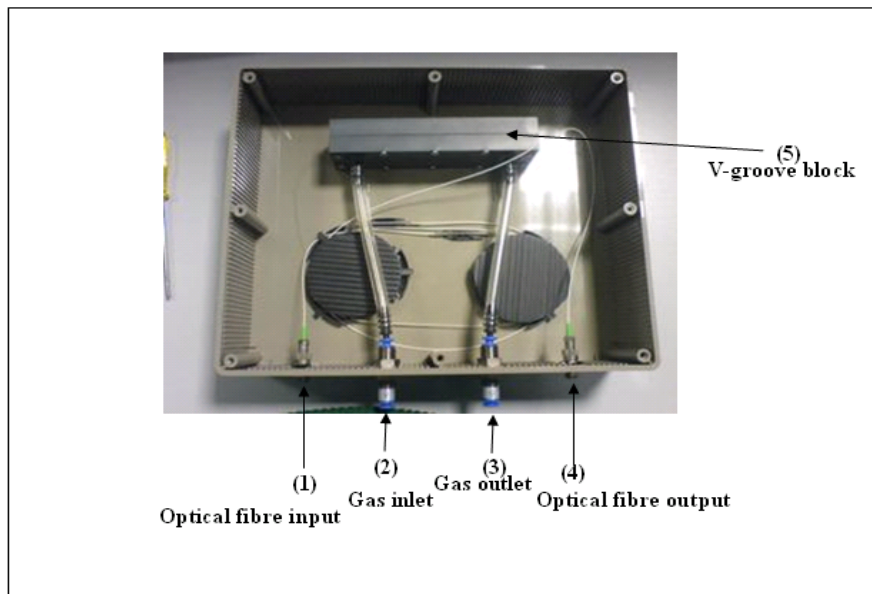
Figure 2.5: Micro-optic gas cell module
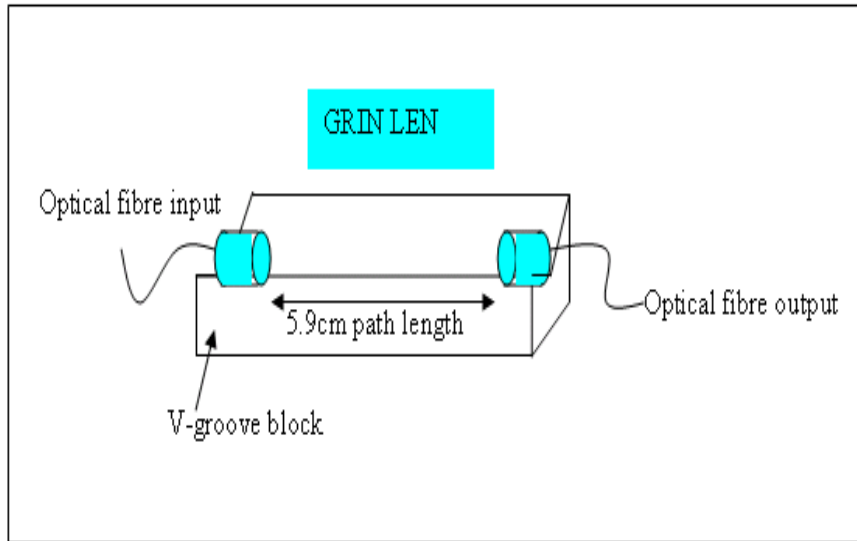
Figure 2.6: Micro-optic gas cell

2.3.2 Photo-Acoustic (PA) Cell

The photo-acoustic (PA) cell layout is shown in Figure 2.7 which is different from the micro-optic gas cell. A crucial part of PA gas detection is the cell in which the PA signal is generated or detected. It includes a resonator, windows, gas inlets and outlets and a microphone.

Energy from the laser beam launched into the gas cell is absorbed by the gas molecules. Ideally, when light power is launched into a gas cell, some or all of the power is absorbed by the gas molecules in the cell and converted into heat. This heat warms up the gas and therefore the gas expands. Variation of the expansion gives variation of pressure and generates a sound wave.

The light is modulated with a frequency depending on the types of signal applied hence the partial pressure will be changed according to this frequency. The strength of the sound wave will be detected by a microphone which is placed in the gas cell. The microphone functions as a transducer which converts one form of energy into other form of energy, for example in this case, the acoustic energy (sound wave) into electric energy (kinetic energy) in

20

units of voltage (V). This form of energy is easier to calculate, and directly feeds into digital data that can be recognised by measurement equipment such as an oscilloscope or computer.

The amplitude (S_{out}) of the acoustic wave produced is directly proportional to the sample heating, incident optical power (P_{in}) and the absorption coefficient (α), which can be represented by the following equation:

$$S_{out} = C_{cell}\alpha P_{in} \tag{2.9}$$

where C_{cell} is a cell constant, describing the conversion from optical to acoustic energy. This conversion depends not only on the gas, but also external parameters such as frequency. The theory of the generation of the PA signal has been described in detail by several authors (see for example [38, 39]).
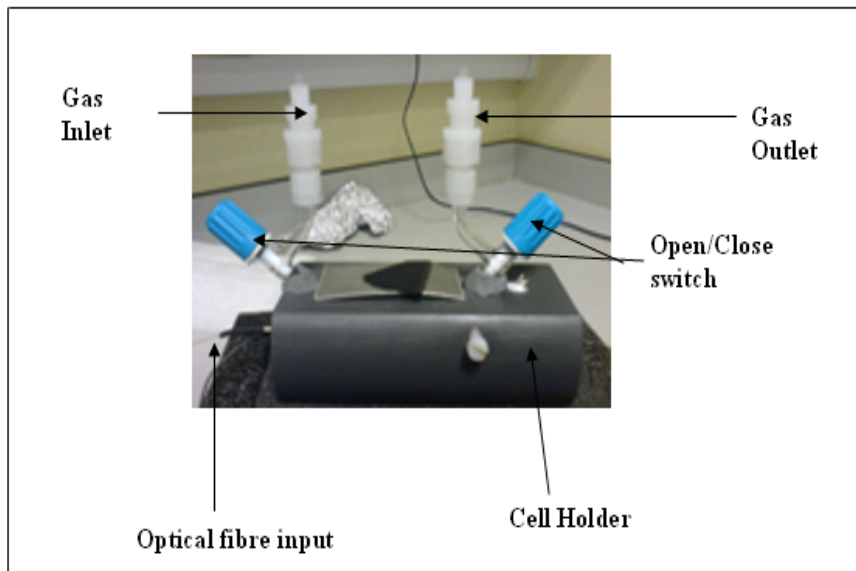
Figure 2.7: Photo-acoustic gas cell

2.4 Absorption Profile Modelling

The HITRAN database is a collection of spectroscopic parameters employed by a computer simulation program developed by Rothman and co-workers at Harvard University to predict the transmission when light is transmitted through gases in the atmosphere. The latest version was released in 2008 [40, 41]. The database contains gas absorption line strengths which are used to compare with experimental results to verify the accuracy and sensitivity enhancement.

There are three computer programs available in the Centre for Microsystem and Photonics (CMP). One is freely accessible on website which uses JavaHAWKS program to plot the line strength values from the HITRAN. The other is a modelling program devised by Dr Moodie from OptoSci. Ltd and a commercial available GATS Spectral Calculator (GATS) [42] to model the absorption profile using the HITRAN 2008 database.

The GATS program was used for all modelling of absorption profiles in this study to compare with experimental results. This is due to the availability and more functions offered by GATS.

2.5 Laser Sources for Spectroscopy

From the definition of [43], lasers are devices that generate or amplify light whose output form depends on the material, atomic system and kinds of pumping or excitation technique. Lasers use a gain medium that is solid, liquid or gas.

The first laser demonstrated by Theodore Maiman in 1960 [44] was a solid state ruby laser; the ruby crystal was pumped by a flash lamp. However, due to their low efficiency, they are only used for some applications. Today, some of the most important industrial solid state lasers are based around rare earth elements such as Neodymium, Chromium, Erbium, or Ytterbium. They are being used in a wide range of applications in medicine, communications,

defence, measurement, and as a precise light source in many scientific investigations.

In the work described in this thesis, the main focus of the research was to select an appropriate laser source as mentioned earlier for constructing a more sensitive or versatile form of gas spectroscopy. Fibre lasers with erbium doped fibre are chosen as our main study. Preliminary experimental work was conducted using diode lasers which are the favoured source for current systems. Distributed feedback fibre lasers (DFB-FL) were also studied as a potential laser source in the future. Their advantages and performance are discussed in the following chapters.

2.5.1 Semiconductor Lasers

Semiconductor lasers are the most basic of all laser types. They are often the preferred light source due to fact that light modulation can be performed simply by modulation of the injection current. Their advantages include their small size, broad range of available wavelengths, stability and compactness.

The advantages of spectroscopy in the near-IR include ready availability of fibres and components from the communications industry, making sensor networks for large area surveillance at an acceptable cost [6]. Tunable diode lasers are used in spectroscopy systems due to their high output power and compatibility with single mode fibre to enable remote sensing to be achieved. However, direct intensity modulation of the laser results in residual amplitude modulation (RAM) thus limiting the sensitivity of tunable diode laser spectroscopy (TDLS) when using 1f detection [11]. Recently, two new calibration-free methods, namely the RAM method [45], and the Phasor Decomposition (PD) method [46], have been reported for the recovery of absolute absorption line shapes from the 1st harmonic signals, but the high RAM background limits the sensitivity of these techniques. Elimination of the RAM to improve the sensitivity of these methods is reported in [47].

There are several other disadvantages of using semiconductor lasers in gas sensing: they

are gas specific and generally quite expensive [17]. However, optical systems operating in the near-IR are still the best option for remote and multi-point sensing and were the driving force in carrying out this research.

2.5.2 Fibre Lasers

Fibre lasers were first introduced by Snitzer in 1961 [48], who demonstrated the use of dielectric waveguides in the form of small fibres as the mode selector in optical masers. The fibre consisted of a core of index of refraction n_1 containing the maser material, surrounded by a cladding of lower index n_2.

The next two decades resulted in development of fibre lasers from Nd-doped fibre lasers, which initially worked in the spatial multimode regime, to the development of continuous wave fibre lasers made of short sections of Nd:YAG single crystal fibres in the 1980s [49]. This improved the coupling efficiency between the fibre laser and a single mode silica optical fibre.

In the 1990s, development of fibre lasers based on an erbium doped fibre in a ring cavity configuration was made after an all-fibre Nd-doped ring cavity laser had been developed by Mears et al. [50]. Much research has been carried out worldwide into the development and applications of rare earth doped fibre in amplifiers and lasers which operate around 1550nm and coincides with the commercially important telecommunications window wavelengths. After many years of research effort, the development of reliable components and equipment for the sake of the technology advancement was possible. For example, the erbium doped fibre amplifier (EDFA) is less complex and more reliable than the earlier optoelectronic repeater technology. Since then, research has been carried out and reported for various applications such as telecommunication, medicine, spectroscopy due to the potential advantages. For a multi-point sensing system, a large number of interrogation points are required which involves considerable distances between a control room and the point at which the presence

of the gas should be monitored. These remote interrogation systems require no electrical power supplies and relatively low optical power densities. In addition the signal can be transmitted from the detection point to the receiver without incurring any penalty due to electromagnetic interference. Several examples of using erbium doped fibre laser (EDFL) for applications in spectroscopy have also been reported [2, 6, 7], for instance the reports demonstrate that fibre lasers are desirable as a laser source with different techniques such as ring down cavity and intra-cavity laser absorption spectroscopy (ICLAS). There are still, however not many applications to spectroscopic sensors due to lack of control and rapid tuning methods [51, 52, 53]. Hence, this study has focused on tackling these problems as detailed throughout the thesis.

2.5.2.1   Erbium Doped Fibre Laser Systems (EDFLs)

As mentioned earlier, lasers use a gain medium to determine type of the device. Similarly, an EDFL cavity consists of a gain medium with regenerative feedback. The gain medium consists of erbium doped fibre with a certain level of population inversion. The population inversion can be achieved through a pump source to excite photons into higher energy level produce a laser. Two types of pump wavelength are prefered, 980nm and 1480nm; an experimental study for these pump wavelengths is reported in [54]. Our work, an EDFA unit is used, manufactured by OptoSci. Ltd. containing a 980nm pump. The EDFA is combined with couplers and isolators to form a ring cavity design. The isolator is used to ensure unidirectional lasing in the cavity. The ring cavity, also known as a travelling-wave cavity is preferred over a linear configuration to avoid spatial hole burning caused by standing waves in the cavity [43].

So far several papers have been reported using the EDFL in sensing applications. Cousin et al. [55] developed a near infrared spectrometer based on a cw continuously tunable EDFL. The author adjusted the temperature of the tunable filter for fine tuning across the bandwidth

and temperature tuning the diode pump was used to tune over the mode hopping gap in order to demonstrate fully continuous frequency tuning [55].

Ryu et al. [51] demostrated a tunable erbium doped fibre ring laser which can be tuned over 102nm by insertion of a fiber Fabry-Perot tunable filter (FFP-TF) in the ring cavity for applied spectroscopy of the absorption lines of acetylene (C_2H_2) and hydrogen cyanide (HCN) [51]. The setup was divided into three parts namely laser amplification, wavelength selection and absorption spectroscopy which results in increased complexity and cost in implementing the system. Both examples were performed under 1mbar of pressure hence with narrower linewidth of absorption line so that wavelength scanning only a few nanometres is enough with.

Based on the reports above, it is shown that the EDFL is a possible alternative as a light source for spectroscopy with several advantages over semiconductor lasers as it can provide a single tunable source over the gain bandwidth of a erbium doped fibre amplifier (EDFA) from 1520-1580nm as well as narrow linewidth. However as mentioned earlier, long cavity fibre lasers have stability problems, i.e. mode hopping occurs frequently, this requires complicated control systems to make them stable and single mode. Hence, measures have been taken to stabilise the system and investigation regarding these fibre laser systems are discussed in Chapter 3.

2.5.2.2 Distributed Feedback Fibre Laser Systems (DFB-FLs)

It is nearly over a decade since Ball [56] proposed the first in-fibre laser formed by arranging two fibre Bragg gratings (FBG) on either side of a short section of erbium doped fibre [57]. The evolution of distributed feedback fibre lasers (DFB-FL) was started and a single mode and stable fibre laser was created by introducing the DFB-FL for stabilizing mode hopping in the system.

Recently, researchers have been progressively demonstrating and enhancing the perfor-

mance of the DFB-FL by use of co-doped fibre [58, 59] and other improvements [60, 61] to provide a robust and efficient single mode optical output. The concept of a DFB laser is commonly used for achieving single frequency operation. The resonator of the laser consists of a periodic structure which acts as a reflector in the wavelength range of laser action and contains a gain medium. The periodic structure contains a phase shift in its middle and this structure is basically the direct concatenation of two Bragg grating with internal optical gain. It has multiple axial modes, but there is only one mode which is favored in terms of losses. Therefore, single frequency operation is often easily achieved despite spatial hole burning (SHB) due to the standing wave pattern in the gain medium. Due to the free spectral range of the laser being large, mode hope-free tuning of the wavelength is possible [62].

DFB fibre lasers possess unique properties that make them more attractive compared to other laser sources. First of all they are an in-fibre laser and therefore are inherently fibre compatible and their output can be connected to transmission fibre using a standard splice. Similarly, the pump power can be delivered to the DFB-FL using standard low-loss transmission fibres. In addition, very simple passive thermal stabilisation is sufficient to ensure the stability of a DFB-FL. A number of active dopants, such as erbium, ytterbium, neodymium and thulium, can be used in order to cover different windows of the optical spectrum and offer extended wavelength coverage [60].

With the benefits described above, the DFB-FL represents an interesting alternative to the semiconductor laser for gas spectroscopy applications. So far, much research work has been based solely on improving the design and fabrication of DFB-FL [63, 64, 65, 66, 67] and not so much on application.

2.6   Conclusion

In this chapter, various types of spectroscopic techniques in both optical detection mode and acoustic detection mode, such as wavelength modulation spectroscopy (WMS), frequency modulation spectroscopy (FMS), intra-cavity absorption spectroscopy and photo-acoustic spectroscopy (PAS) have been presented. The basic parameters and components with definitions that are relevent to gas spectroscopy have also been briefly reviewed to give a general idea of how measurements are carried out before going on to describe laser sources suitable for the study.

Chapter 3

INVESTIGATION OF ERBIUM DOPED FIBRE LASERS SYSTEM (EDFLs) FOR SPECTROSCOPY

3.1   Introduction

Fibre laser systems are potential sources for spectroscopy due to their wavelength tunability and wide bandwidth. A basic erbium fibre laser system consists of an erbium doped amplifier (EDFA) whose gain bandwidth is within the C-band region, corresponding to several gas absorption lines. Furthermore, optical components are readily available due to the boom of optical communications which has also improved technology in other fields such as medicine and spectroscopy. Thus the maturity of the components will enhance the performance and the sensitivity of the system which can be fully exploited in future. Even though diode lasers are the favoured source in most applications, current modulation of the diode laser results in both amplitude and frequency modulation of the output (AM and FM respectively). The residual amplitude modulation (RAM) background creates problems for line-shape recovery

in tunable diode laser spectroscopy (TDLS) and the harmonic signals arising from TDLS have been extensively studied for improved solutions [68, 45, 46]. Recently [47] has reported a method of eliminating the RAM in TDLS by use of an optical fibre delay line. These problems have stimulated the investigation of other laser sources for spectroscopy applications.

This chapter first discusses the basic characteristics of EDFLs, namely, steady-state and dynamic responses. This is followed by an investigation of tuning mechanisms for wavelength scanning and centre wavelength selection by using a fibre Bragg grating (FBG) or a Sagnac loop filter (SLF). The system was further employed to investigate its feasibility for detecting acetylene gas. Since gas absorption lines in the near-IR spectral region are relatively weak, the EDFL was used with intensity modulation (IM) to allow use of a lock-in amplifier in gas detection.

3.2   Principles of EDFLs

The basic setup of an EDFL is shown in Figure 3.1. From this diagram the lasing output characteristics can be determined and are outlined as follows.
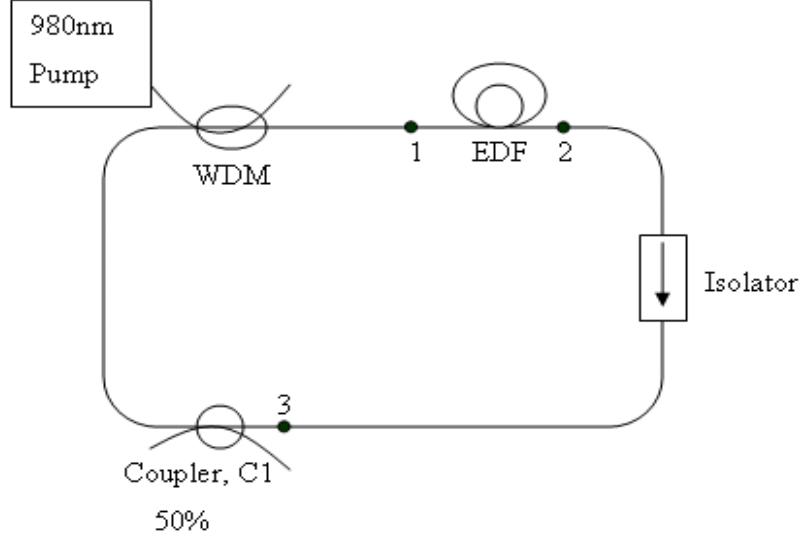
Figure 3.1: Basic ring fibre laser system

The input signal, P_1 is amplified over a length of EDF, from point 1 to point 2. Thus the output of the laser from the coupler is:

$$P_{out} = RP_2 e^{-\alpha_{23}} \tag{3.1}$$

where P_1 and P_2 are the power levels at points 1 and 2 (the input and output of the EDFA respectively) in the loop, $\bar{g}$ is the length-averaged gain of the EDF, and α_{23} is the loss coefficient for section 2→3; $Loss_{23}(dB) = 4.34\alpha_{23}$. R represents the output fraction coupled from the loop by the output coupler.

$$\bar{g} = (\alpha + \gamma)\overline{N}_2 - \alpha \tag{3.2}$$

where is α absorption coefficient, γ is emission coefficient of the erbium doped fibre (EDF) and $\overline{N}_2$ is the upper energy level. When the EDF gain is equal to the loss in the loop cavity, $\bar{g}l = \alpha_c$ for the lasing mode, the power of this mode settles to a steady state, where α_c is the total loss of the loop (external to the amplifier) and l is the length of the EDF. Hence:

$$\bar{g}l = \{(\alpha + \gamma)\bar{N}_2 - \alpha\}l = \alpha_c \qquad (3.3)$$

and, the steady-state value of $\bar{N}_2$ is:

$$\bar{N}_{2ss} = \frac{\alpha_c + \alpha l}{(\alpha + \gamma)l} \qquad (3.4)$$

The atomic rate equation for the EDFA is [17, 69]:

$$P_p(1 - e^{\bar{g}_p l}) = P_1(e^{\bar{g}l} - 1) + \frac{\rho S l \bar{N}_2}{\tau_0} \qquad (3.5)$$

where P_p is pump power, S is the cross-sectional area of the EDF core, ρ is erbium ion density, τ_0 denotes the lifetime at N_2(upper level).

Substituting equation 3.4 into equation 3.5 we obtain an expression for P_1 as:

$$P_1 = \frac{P_p(1 - e^{\bar{g}_p l}) - P_{sat}(\alpha_c + \alpha l)}{(e^{\alpha_c} - 1)} \qquad (3.6)$$

where

$$P_{sat} = \frac{\rho S}{\tau_0(\alpha + \gamma)} \qquad (3.7)$$

with further algebraic simplification [17], the output power from the output coupler is:

$$P_{out} = \eta(P_p - P_{th}) \qquad (3.8)$$

where the threshold pump power, P_{th}, is in photons/sec and η is the slope efficiency.

3.3 Experimental EDFL System

Figure 3.2 illustrates the basic experimental setup of the ring cavity EDFL. In a ring configuration, the direction of the laser light is made to propagate in a uni-directional manner by inserting an optical isolator inside the ring cavity. The unidirectional propagation was important in this configuration because without an isolator, the ring cavity laser tends to be unstable i.e. it lases in one direction then the other. The setup contained an EDFA (Erbium Doped Fibre Amplifier) unit from OptoSci, two couplers with ratio of 80/20 and 90/10, and a tuneable filter (Santec). Single mode fibre pigtails attached with FC/APC connectors were used to reduce back reflection.
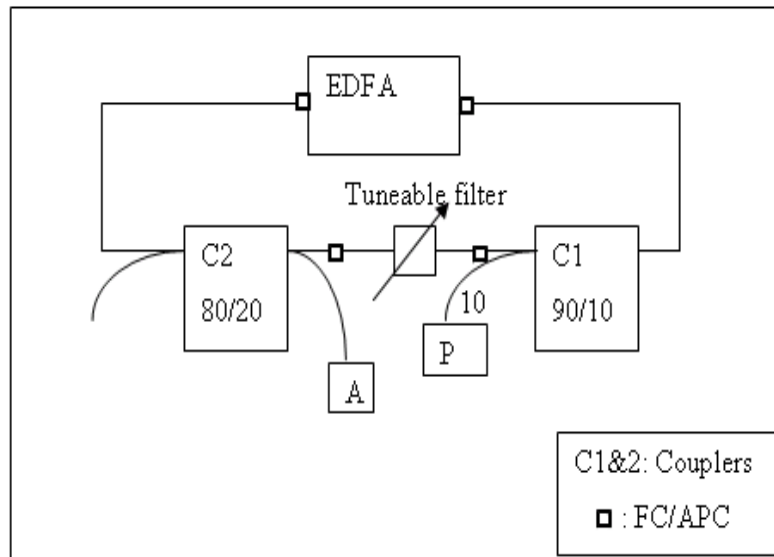
Figure 3.2: Preliminary experimental setup of EDFL in ring cavity

The EDFA unit was formed by a 980nm pump source, two 980/1550nm wavelength division multiplexer (WDM) couplers and two isolators. The front panel of the unit has a pump power controller to vary the input pump signal to measure power characteristics. At C1, 10% of the cavity power of the EDFL is tapped off and an OPTOSCI low noise photoreceiver (PD) was used to receive the signal and provide variable gain through its multiplier

knob. Voltage measurement at the output of the PD was obtained by a Tektronix digital oscilloscope (TDS784D). C2 was used to measure cavity parameters, which will be explained later.

3.4   Power Characteristics of the EDFLs

For the first experiment, three tests were conducted to obtain performance parameters such as laser output power and threshold pump power. Two wavelengths (1530nm and 1560nm) were selected by the tunable filter. For the first test, the pump power was varied from 1mW to 75mW to get the output power for both wavelengths without C2. For the second test; the first test was repeated with C2 included. Lastly, the second test was repeated without C2 to compare the tunable filter position, C1 before the tunable filter and C1 after the tunable filter. The experimental results are shown in Figure 3.3 and Figure 3.4.
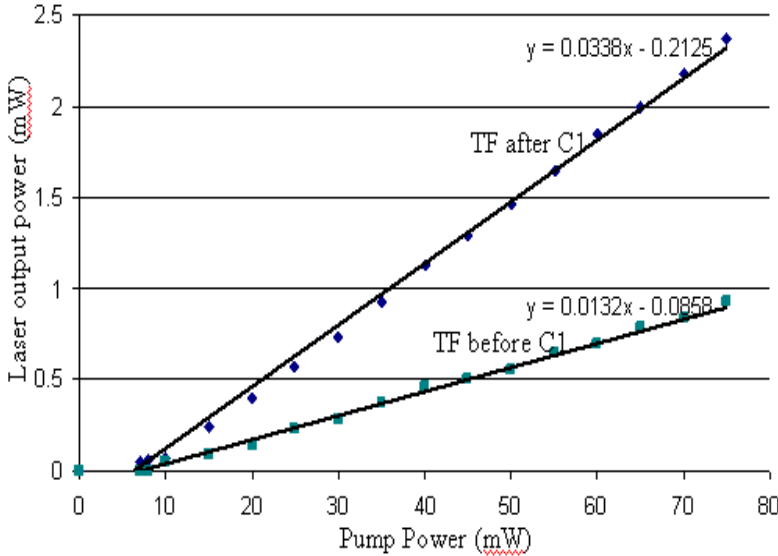
Figure 3.3: Laser power characteristics for different positions of the tunable filter (TF) in the ring cavity EDFL without C2 at 1530nm

34
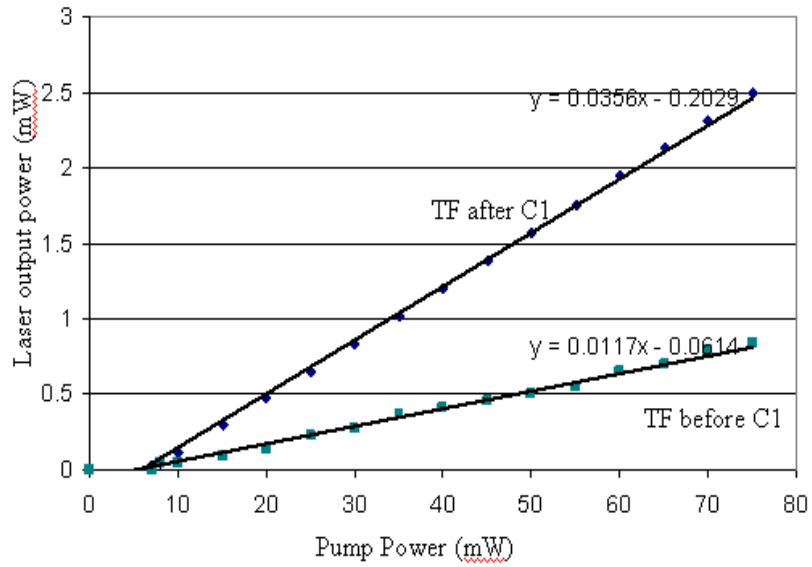
Figure 3.4: Laser power characteristics for different positions of the tunable filter (TF) in the ring cavity EDFL without C2 at 1560nm

From the figures, it can be observed that higher output power is obtained with the tunable filter placed after the coupler compared to the tunable filter placed before the coupler. Thus, the configuration of the system is important in determining the optimum design for the laser system.

Figure 3.5 and Figure 3.6 show the effect of including, or excluding, coupler C2 in the cavity for both wavelengths of 1530nm and 1560nm. Adding the component gives extra losses in the cavity and this reduces the output power of the system.
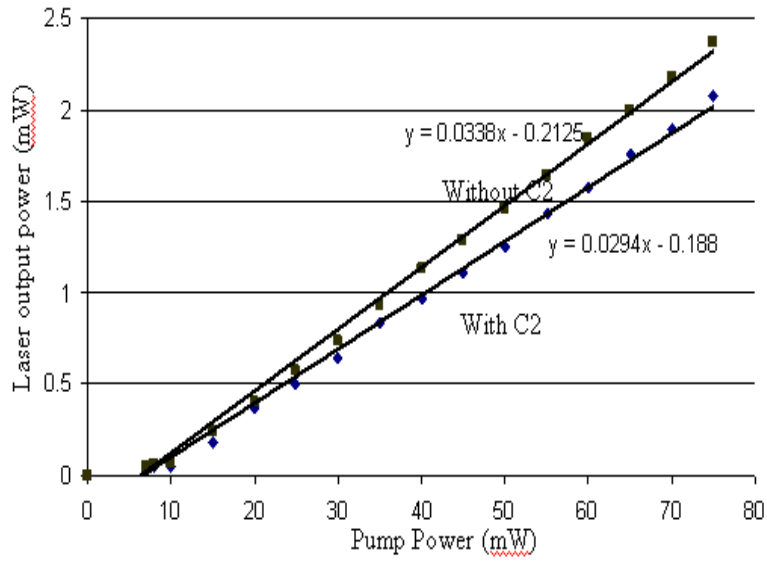
Figure 3.5: Effect on lasing power of EDFL with/without C2 at 1530nm
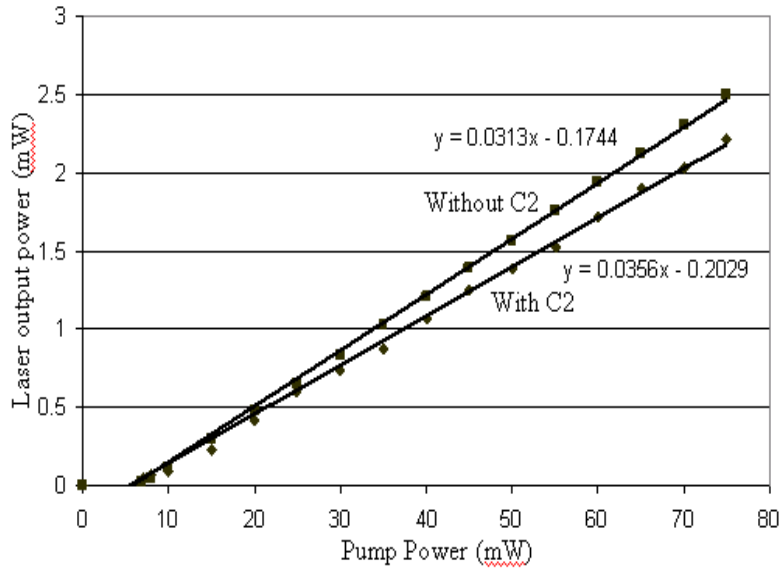
Figure 3.6: Effect on lasing power of EDFL with/without C2 at 1560nm

3.5 Dynamic Response Measurements

For the second experiment, the setup in the first experiment was reused with the addition of a function generator at the back of EDFA unit as shown in Figure 3.7. A square wave with 200mHz frequency and with a range of amplitudes from 0V to 5V peak-to-peak was used to apply step changes to the pump power in order to observe the transient response.

Two tests were conducted to obtain the transient response. The first test was the measurement of the build-up time which is the time delay between the launch of the pump power (t_o) and the start of laser spiking (t_b) with five sets of pump power values; 13.5, 20.2, 33.7, 47.3 and 60.2 mW corresponding to pulse voltages of 1.5, 2, 3, 4 and 5 Volts respectively.
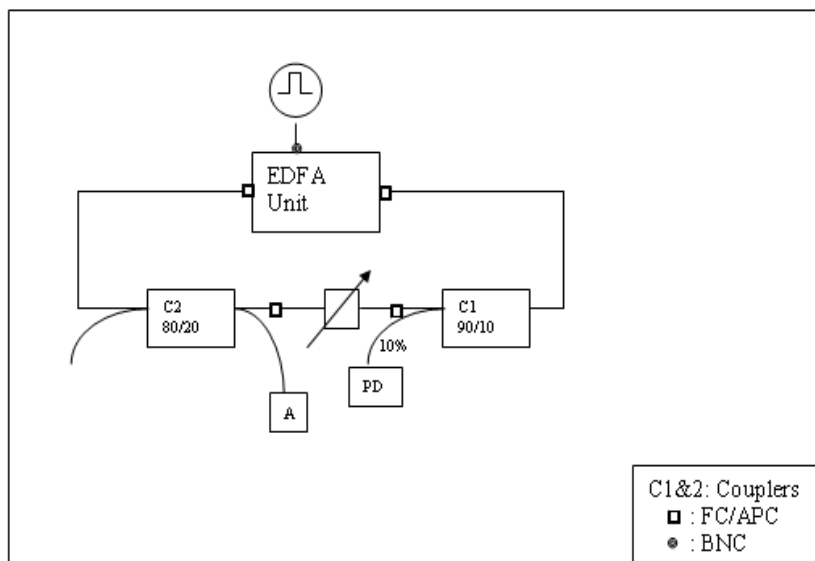
Figure 3.7: Setup for the measurement of the transient response

Secondly, the decay constant and the frequency of relaxation oscillations were measured by fitting a typical under-damped waveform to the measured data. This happened after the build-up time and before the steady-state, where 1560nm was chosen as the wavelength in the experiment.

Results were obtained through a personal computer where LabView was used to record

the signal output. A virtual instrument file "Read Waveform to Voltage Array.vi" was used for storing the complete frame length for one or two scope channels. This data was stored in *.txt format and analyzed using Matlab.
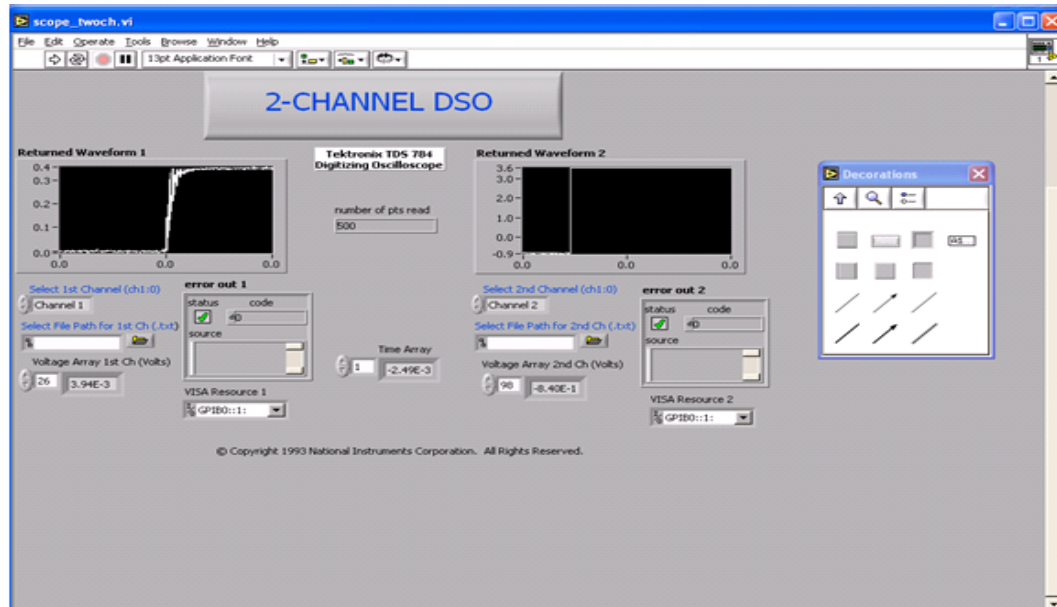
Figure 3.8: LabView 2 Channel DSO

Figure 3.8 shows the interface of the LabView program which was used to obtain and display the data from the oscilloscope. There are two windows: a) experimental results b) signal from the function generator (as reference). These results are shown in detail in Figure 3.9 and used to calculate the build-up time of the EDFL system.
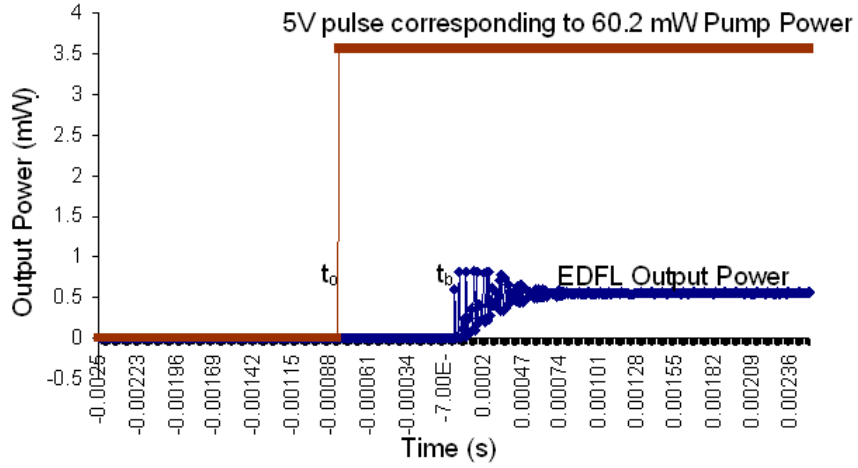
Figure 3.9: Time Delay between the launch of pump power (t_0) and the start of laser spiking (t_b)

Build-up time refers to the time it takes after application of the pump power for the inversion level to rise above threshold and laser spiking to commence. Figure 3.9 shows the laser build up times as a function of the pump power step. From the experiment, it was found that the build-up time was reduced with increase of the pump power and was shorter with the cavity without C2 (lower loss cavity) as shown in Figure 3.10.
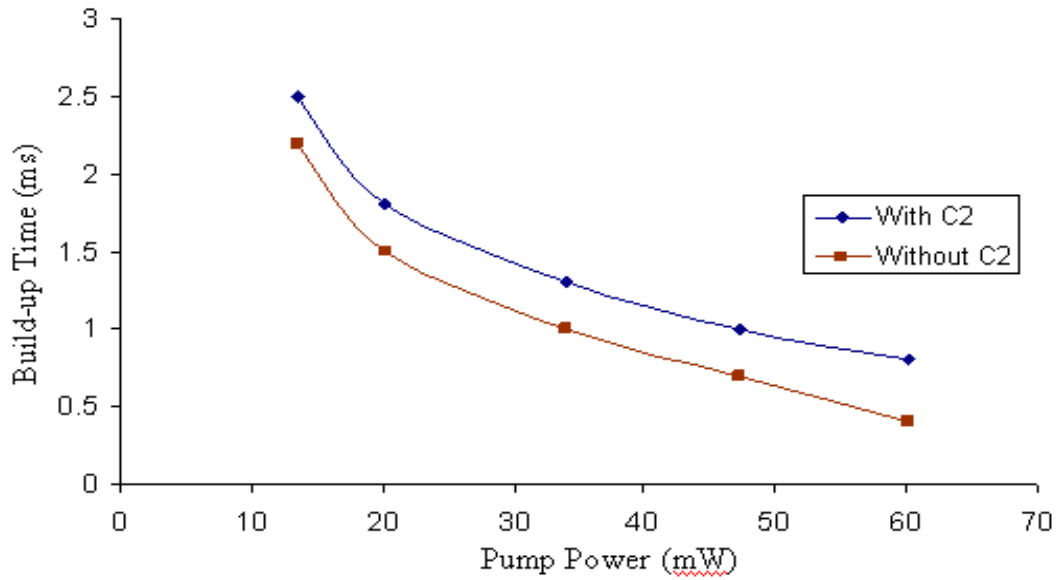
Figure 3.10: Build-up times of EDFL at 1560nm

The decay constant and frequency of relaxation oscillations were also measured. The time it takes for the output power level to stabilize can be observed using the LabView program. The step in pump power for Figure 3.9 was 5V which corresponded to 60.2 mW. As shown in Figure 3.11 for 1530nm, the response deviated significantly from the expected pattern; therefore the decay constant and the relaxation oscillation frequency were not measured at 1530nm wavelength.

However as can be seen in Figure 3.12 at 1560nm wavelength, the laser output power follows a standard decaying oscillatory pattern before stabilizing at its steady-state value.
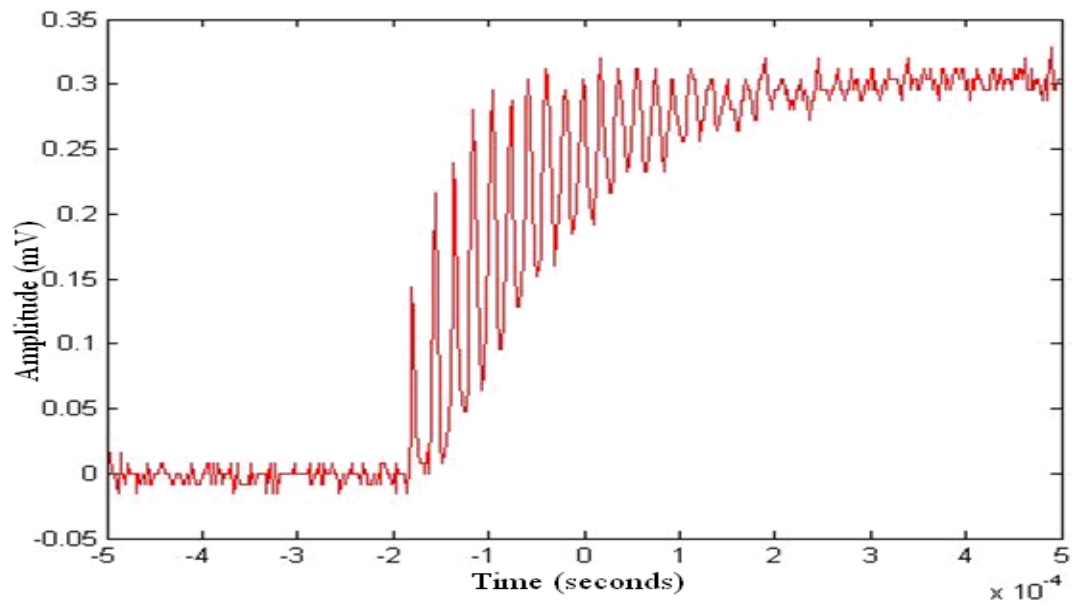
Figure 3.11: Transient Characteristics of EDFL (with C2) at 1530nm
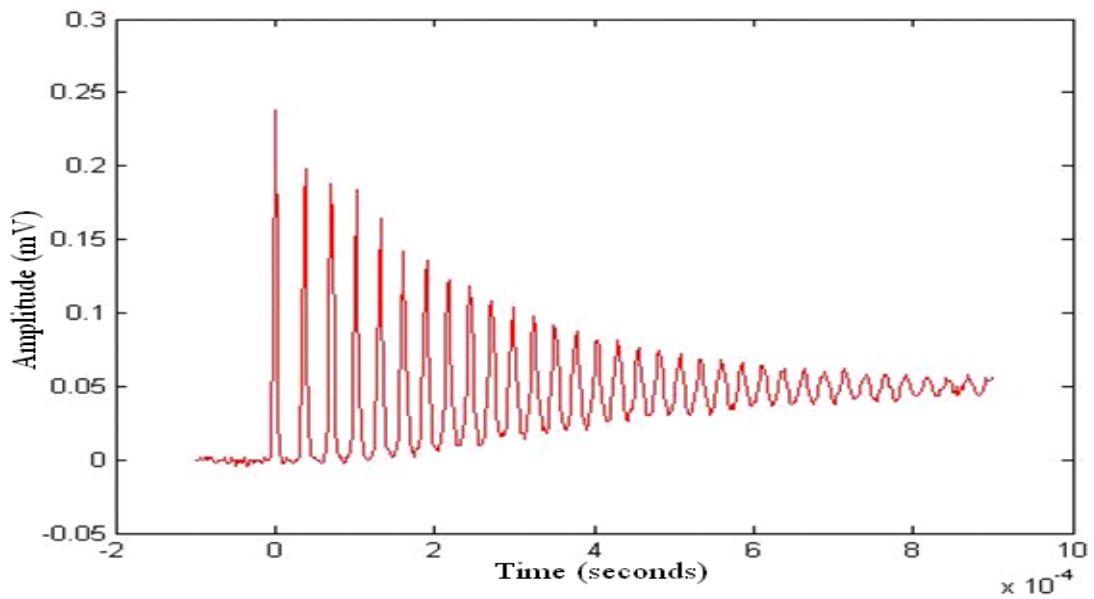
Figure 3.12: Transient Characteristics of EDFL (with C2) at 1560nm

41

3.6　Cavity Parameters of the EDFLs

A number of experiments were conducted to measure the external cavity loss (between points 3 and 6, with/without C2 – see Figure 3.13) and the cavity length from the self beating spectrum of the longitudinal modes on a radio frequency (RF) spectrum analyser.
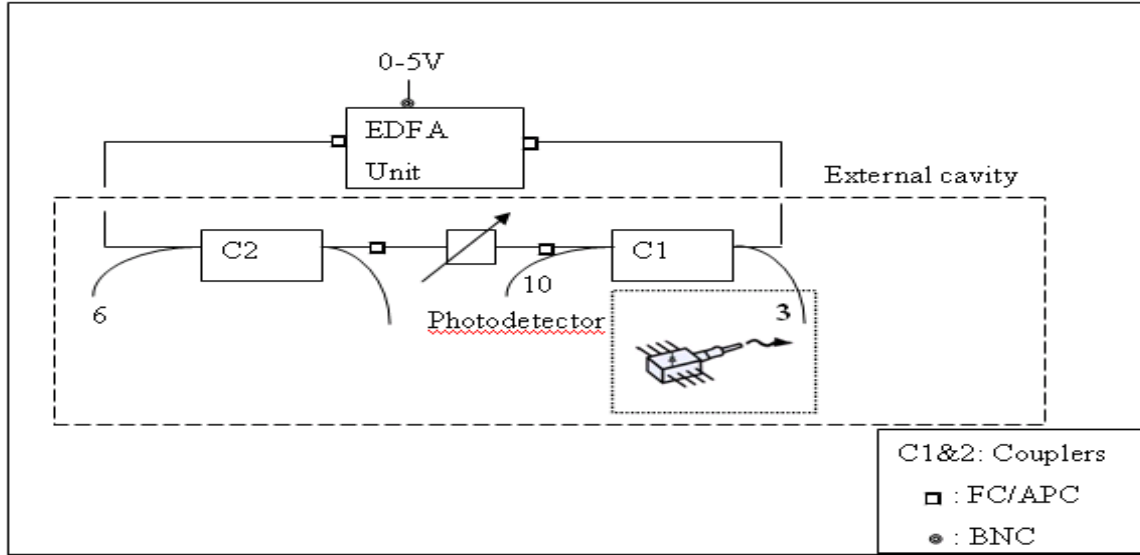
Figure 3.13: Setup for measurement of cavity loss

For the measurement of the external cavity loss, the EDFL was separated into the EDFA unit and the external cavity as shown in Figure 3.13. Light was launched from an external DFB laser at 1532.83 nm into port 3 and the output measured at port 6. Measurements were repeated for every component added into the external cavity. Cavity loss in dB was calculated by using the formula:

$$Loss(dB) = 10\,log\left(\frac{P_{out}(mW)}{P_{in}(mW)}\right) \quad\quad (3.9)$$

The results for both configurations (with or without C2) are tabulated as shown in Table 3.1.

	Cavity Loss (dB) between points 3 and 6	
Wavelength (nm):	Without C2	With C2
1532.83	4.83	6.05

Table 3.1: Cavity Loss with tunable filter included

Spectrum self-beating can be used to calculate cavity length by using the following formula:

$$\triangle f = \frac{c}{n_e L_{cav}} \tag{3.10}$$

For the above formula, c denotes the speed of light while n_e is the effective refractive index of the mode of the fibre. The cavity length, L_{cav} is measured by calculating the frequency spacing between two adjacent modes of the cavity, as depicted in Figure 3.14, where the spectrum was obtained from an Agilent PSA Series spectrum analyzer (E4443A). Table 3.2 summarizes the data obtained from the experimental results.
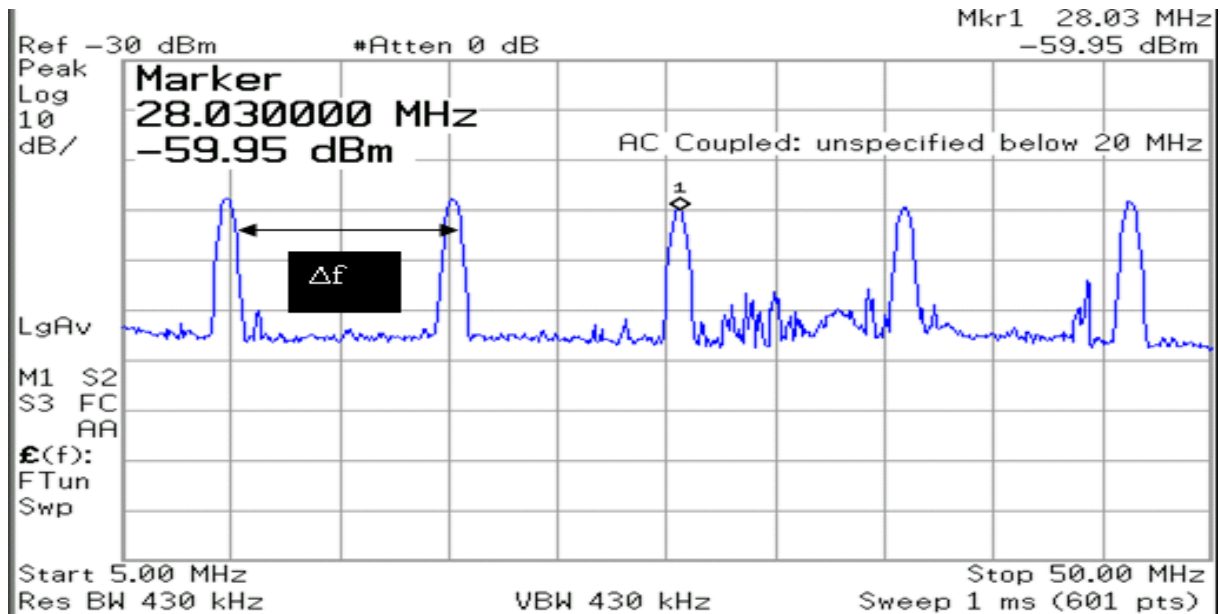
Figure 3.14: EDFL Spectrum at pump power of 40mW at 1560nm

Spectrum self-beating	Δf(MHz)		Cavity Length(m)	
Wavelength (nm):	Without C2	With C2	Without C2	With C2
1560	9.80	9.43	21.11	21.94

Table 3.2: Cavity Length using self-beating spectrum

3.7 Mode Suppression

In an absence of a filter and with a fixed cavity loss, the cavity mode with maximum gain would start lasing and adjacent modes, with nearly similar gain, compete with the lasing mode. As a result, the lasing wavelength can hop from one mode to another mode (mode hopping) if the cavity parameters are perturbed, this also includes environmental factors such as temperature changes (length of the cavity is susceptible to thermal drift) and vibration. A long cavity length laser results in closely spaced longitudinal modes and can severely limit their applications due to multimode oscillation and mode hopping. Hence, several methods have been investigated to solve the mode hopping problem such as use of a Fabry Perot filter (FPF), but the FPF is not easy to fabricate thus of high cost [52]. The Pound-Drever approach [16, 70] uses a PZT modulator to modulate the cavity and a servo-loop to control the position of the main cavity mode within a broader sub cavity mode. However, it is very difficult to operate the system as all cavities need to be controlled simultaneously resulting in complex electronic controls adding noise to the system and causing instability. Therefore a simpler and more effective method for suppressing mode hopping was chosen to stabilise our laser system, using a saturable absorber (SA) with polarization maintaining (PM) components. A comparison/optimization of the setup was performed by employing either a simple mirror, fibre loop mirror or FBG as the reflector with the SA. For gas spectroscopy applications, the performance of the system using a Sagnac loop filter (SLF) or a piezo-transducer

44

(PZT) as the wavelength tuning mechanism was studied, using the loop mirror and the FBG as the reflector for the SLF and the PZT respectively.

3.7.1   Saturable Absorber (SA) for Mode Suppression

A saturable absorber (SA) acts in the laser cavity as a narrow bandwidth filter by incorporating a segment of un-pumped erbium doped fibre in the ring cavity to suppress mode hopping through the establishment of a transient Bragg grating by standing-wave saturation effects in the length of un-pumped fibre. PM-EDF is used to ensure the formation of a stable standing-wave since, with PM fibre, the two counter-propagating waves interfere with each other with their state-of polarizations optimized which enhances single frequency operation. This has improved the performance of the fibre laser and a linearly polarised output is obtained with little mode hopping [52].

Figure 3.15 shows a schematic diagram of the experimental setup of the erbium doped fibre ring laser with the SA. The objective of this experiment is to get stable and narrow linewidth, single mode operation of the fibre laser system. A standard EDFA unit (OptoSci Erbium Doped Fibre Amplifier, ED AMP supplied by Opti-Sci. Ltd) which included a 980nm pump laser, two WDMs, an active gain medium (erbium-doped fibre) and two isolators was used for this setup. The output of the EDFA was connected to a 2 meter length of polarization controller to adjust the polarisation state of the EDFA output. The polarizer controller is connected to a 50/50 polarization maintaining (PM) coupler and 50% of the output of this coupler is connected to a PM circulator (which also ensures unidirectional lasing operation), whereas the other 50% of the coupler (laser output) was connected to a PM isolator to avoid back reflection and eliminate unwanted noise. Port 2 of the PM circulator is connected to the saturable absorber section which comprises of a polarizer with panda fibre (0.8 meters), a PM EDF with bow tie fibre (2 meters length) and various reflectors (simple mirror, fibre loop mirror or FBG) at the end. All of these PM components have a centre wavelength of

1550nm. Finally port 3 of the PM circulator is connected into the EDFA, which made the total cavity length of the system approximately 20 meters, giving a 10 MHz mode spacing.

An optimum design was investigated by comparing the performance of different reflectors used in the SA section, namely a fibre Bragg grating (FBG), fibre loop mirror (LM) and mirror (M). A 50/50 PM coupler was used to form the fibre LM in which two output ports were connected together to get 100% reflection back to input port of coupler. A 15mm length FBG with 1550nm centre wavelength and a mirror formed by coating a thin aluminium film on the end of fibre were used as the other reflectors for comparison.
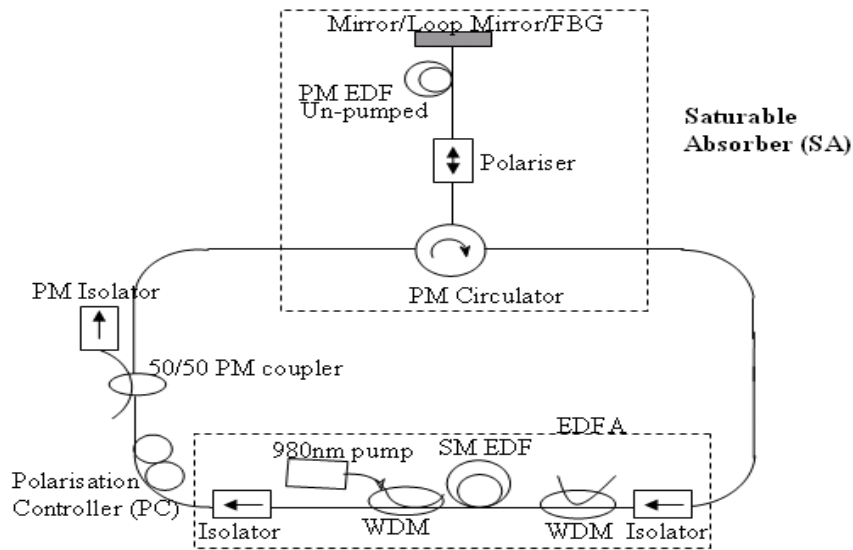
Figure 3.15: Schematic diagram of erbium doped fibre laser (EDFL) ring cavity with a saturable absorber (SA)

3.7.1.1 Power Characteristics of the EDFL with a SA

Figure 3.16 shows the output power characteristics of the EDFL with the FBG, loop mirror and mirror. The loop mirror gave the highest output power with a threshold power of 14.2mW for both the loop mirror and the FBG and 19.9mW for the mirror.
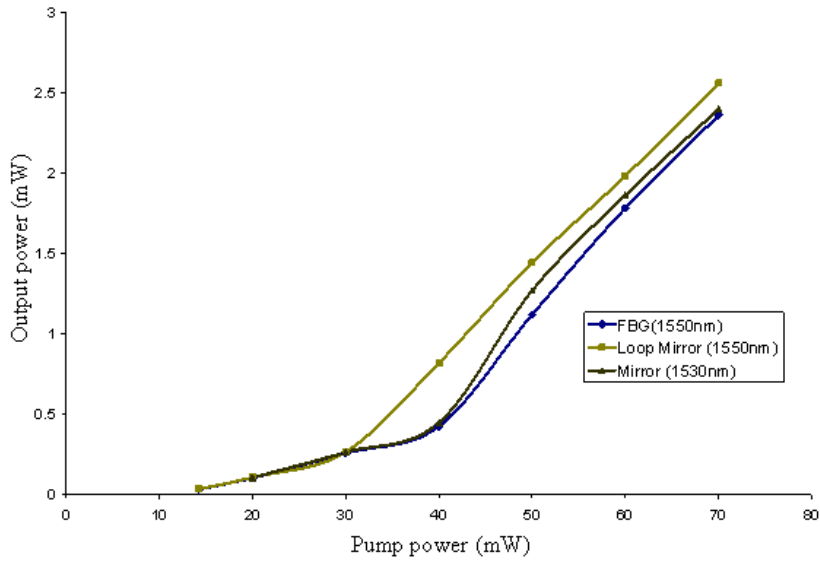
Figure 3.16: Output power of the EDFL (with FBG, loop mirror or mirror) versus input pump power at 980nm

3.7.1.2 Mode Stability

A Fabry Perot Spectrometer (FPS) with 300MHz bandwidth was used to observe the laser stability. The output from the FPS was connected to an oscilloscope (*Agilent Infiniium Oscilloscope 1.5GHz, 8GSa/s, model 54845AR*) as shown in Figure 3.17. The performance of the EDFL system is shown in Figures 3.18, 3.19 and 3.20 for the FBG, LM and M, respectively, which show the laser output as the FPS is wavelength scanned by a ramp voltage on its PZT. It was found that all three reflectors gave stable laser operation and hence worthy of further investigation.
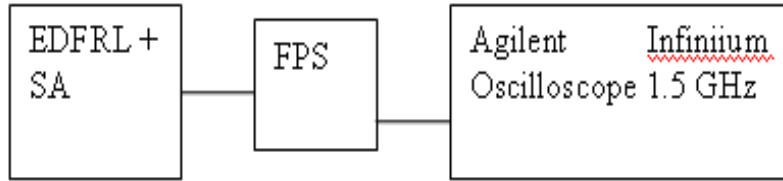
Figure 3.17: Observation of laser modes by FPS configuration
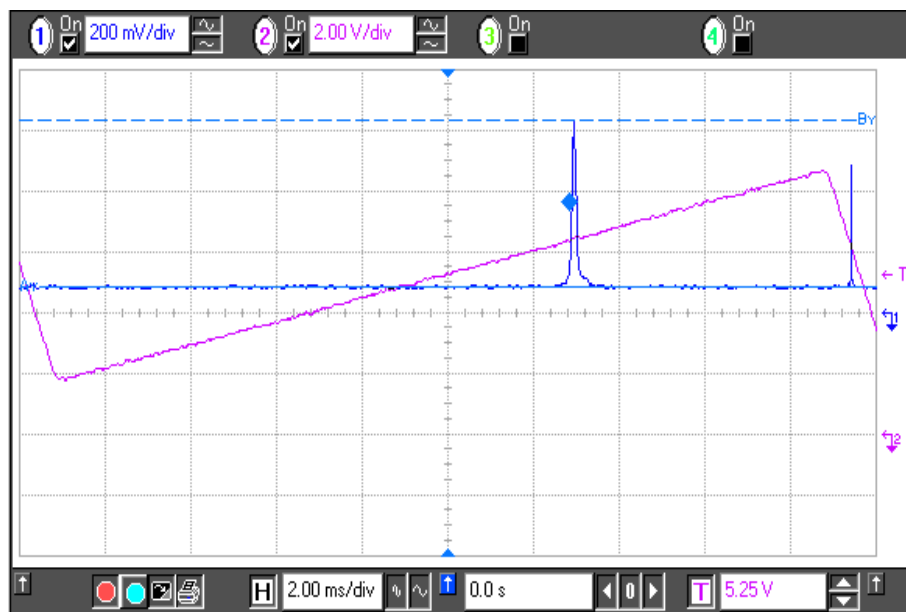
Figure 3.18: Single mode operation with FBG (PZT drive voltage also shown)
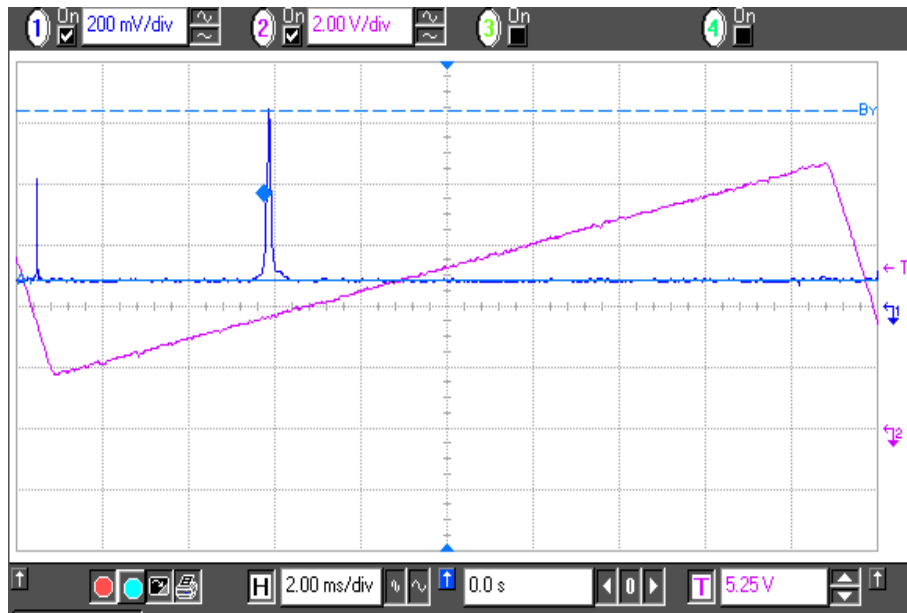
Figure 3.19: Single mode operation with loop mirror (PZT drive voltage also shown)
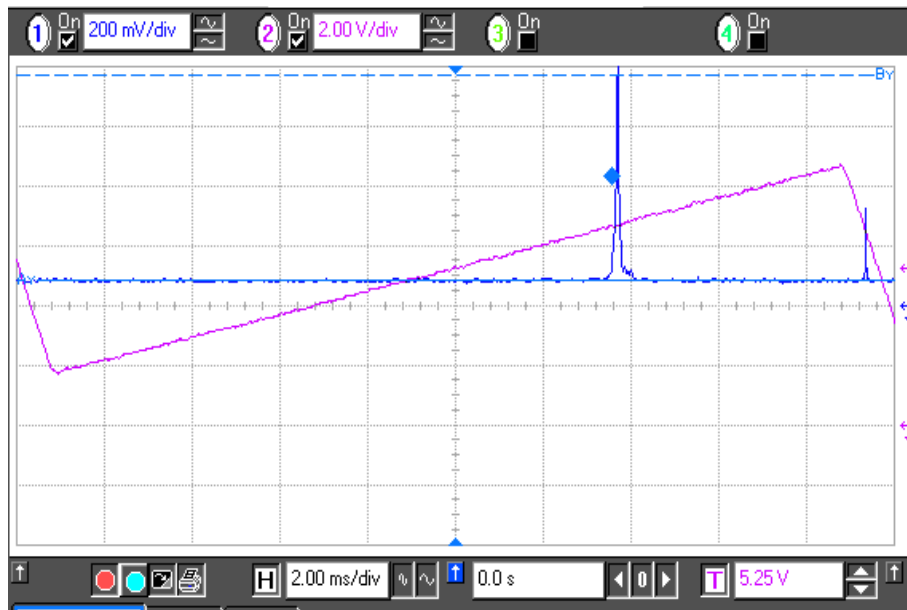
Figure 3.20: Single mode operation with mirror (PZT drive voltage also shown)

3.7.1.3   Dynamic Response of EDFL with SA

Figure 3.21 shows the setup for measuring the transient response using a function generator connected to the rear of the EDFA unit. Five different amplitudes of step or square waveform were applied for the pump power with a modulation frequency of 100Hz and with a positive dc offset to maintain the peak to peak value between 0 to 5V. Amplitudes of 1V, 2V, 3V, 4V and 5V were used, corresponding to pump powers of 10.4mW, 23.8mW, 36.8mW, 49.6mW and 61.4mW respectively, as indicated on the front panel of the EDFA unit. A low noise photoreceiver (OptoSci LNP-2A, 100 Hz-2.24 MHz) was used to detect the output signal and was connected to the oscilloscope to see the response.
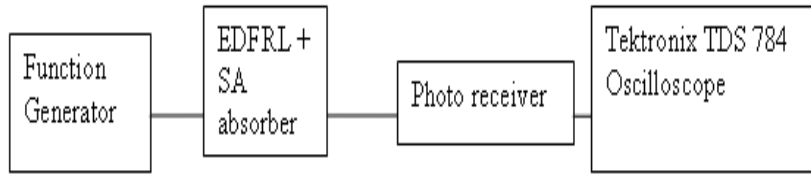
Figure 3.21: Setup for measurement of transient response of EDFL with SA

As previously discussed, the laser build-up time was measured as the time delay between the launch of the pump power and the start of laser spiking. From observation, when 5V was applied from the function generator, the build-up time with the mirror was the fastest response, followed by the FBG and then the loop mirror, 2.84ms, 3ms and 4.8ms respectively. Referring to Figure 3.22, it was observed that the build up time reduces with increase of pump power.
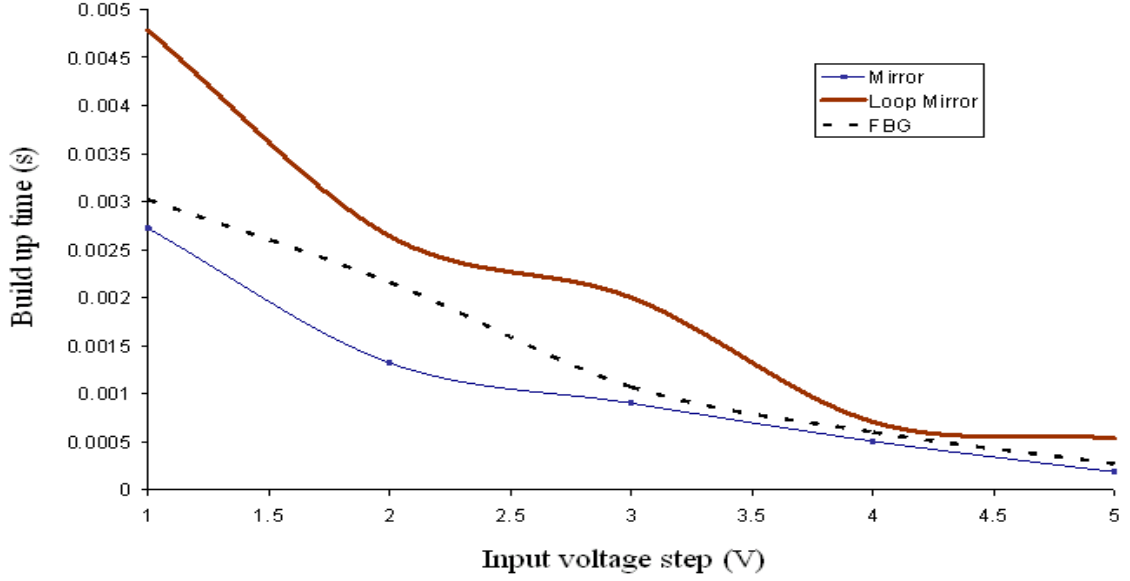
Figure 3.22: Build-up time versus voltage step applied to pump power control

3.7.1.4   Relative Intensity Noise (RIN)

The noise at a given frequency can be described in terms of relative intensity noise (RIN) which increases as pump power decreases [71]. RIN is the defined as

$$RIN = \frac{S_p(\varpi)}{P_T^2} \qquad (3.11)$$

where $S_p(\varpi)$ is the photon noise spectral density (noise per unit frequency interval), and P_T is the total photon number, $P_T = PV_a$. V_a is the volume of the active laser region [71].

The noise is large at the relaxation oscillation frequency which is proportional to the square root of the pump power,P_p according to the equation [26]:

$$\omega^2 = \frac{1}{t_c \tau_0} [\frac{P_P}{P_{th}} - 1] \qquad (3.12)$$

where ω is the relaxation oscillation (angular) frequency, P_P is the DC pump power level, P_{th} is the threshold pump power, τ_0 is the upper state lifetime and t_c is the cavity lifetime.

51

Figure 3.23 shows the measured RIN of the EDFL with SA using the RF spectrum analyser with a laser output power of -6.31dBm on the photoreceiver. With reference to Figure 3.23, a conversion is needed when the value of the resolution bandwidth (RBW) of the instrument is more than 1, which also depends on the frequency. The following equation was used to calculate the RIN:

$$RIN = 10log_{10}data - 10log_{10}RBW \qquad (3.13)$$

The data obtained was already in dBm and hence it was only needed to convert RBW into log form and subtract to get the actual RIN value.
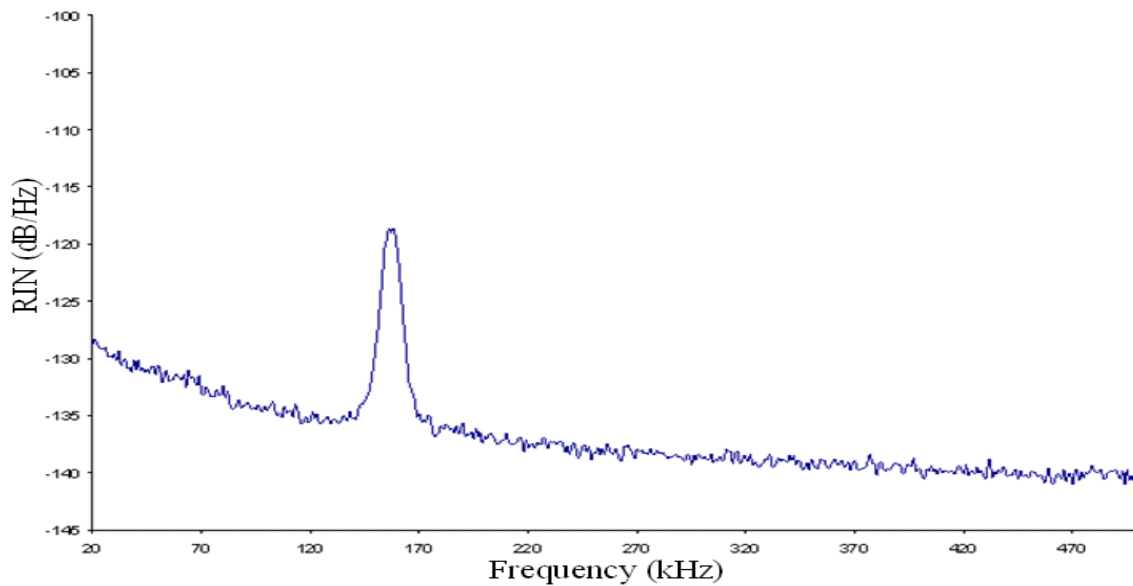
Figure 3.23: RIN of the EDFL with SA with pump power of 70mW

From Figure 3.23 it can be seen that the EDFL has a low RIN except at the relaxation oscillation frequency of 159 kHz where the RIN is maximum at -119 dB/Hz.

3.7.1.5 Tuning Range with a Tunable Filter and a Sagnac Loop Filter (SLF)

An important feature of a laser system for gas spectroscopy is the ability to scan across an absorption line. In the EDF ring cavity laser, the wavelength can be selected within the erbium gain-bandwidth and can be tuned by use of a commercial tunable filter (TF), by use of an all-fibre Sagnac loop filter (SLF) or by thermally stretching a FBG. All these methods have been used and investigated in this study.

Tunable filter (TF) For the EDFL with SA, a tunable filter (Santec, OTF-300) with a wavelength range of 1530-1570nm and 1nm loss at -3dB bandwidth was inserted into the cavity for wavelength selection. A 40nm tuning range, as depicted in Figure 3.24, was achieved with either the loop mirror or the mirror in the SA section. Hence both mirrors are compatible with this form of tuning and give similar performance.
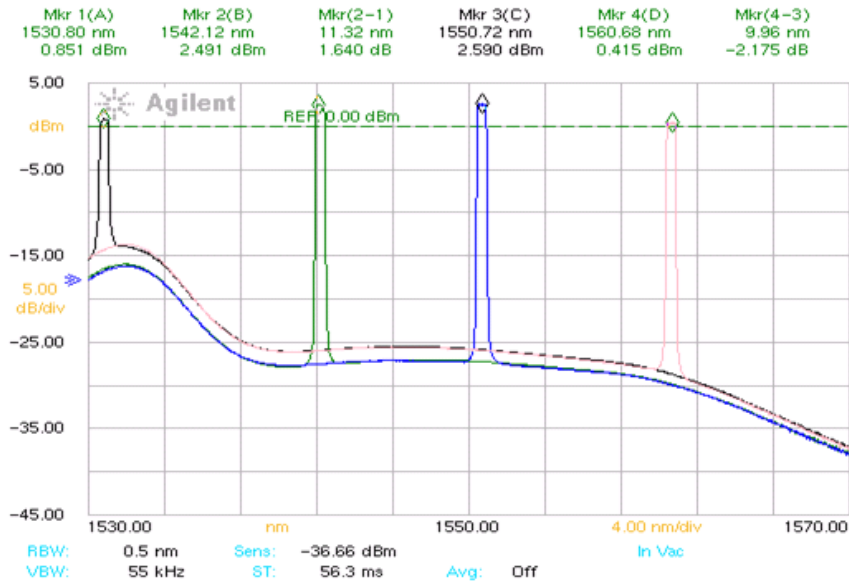
(a)
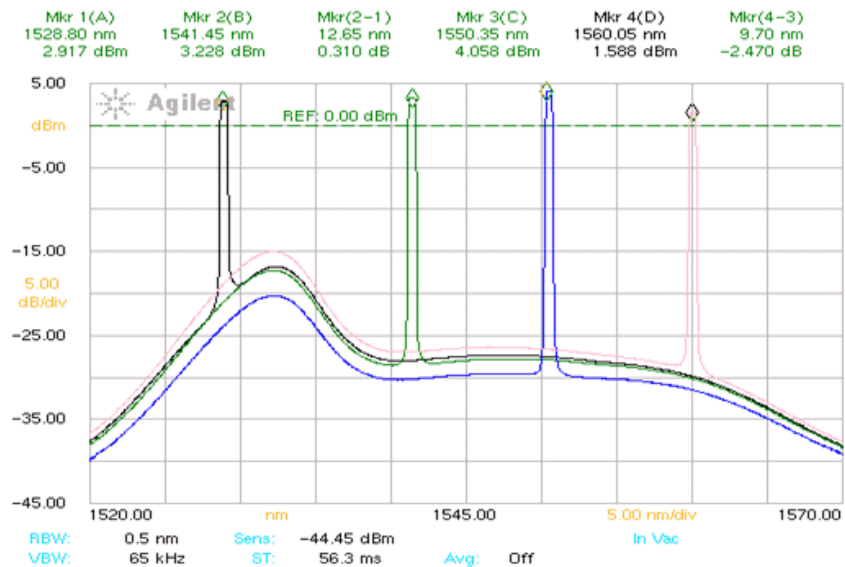
(b)

Figure 3.24: Spectra of laser output using a commercial filter to tune the centre wavelength of the EDFL system with a SA and (a) loop mirror (b) mirror

Sagnac Loop Filter (SLF) The SLF functions as a periodic filter and may be used for step tuning the frequency. The setup shown in Figure 3.25 was used to measure the wavelength characteristics of the SLF. Two EDFA units (to give a higher input power) were

used as a broadband ASE source at maximum pump power (70mW, 75mW). This provided the input for the SLF which consisted of a SM 50:50 coupler connected to a polarisation controller (PC), polarization maintaining fibre (PMF) and a small birefringence loop (SBL). The output of the SLF was monitored on a optical spectrum analyzer (OSA). Three different lengths of PMF were used in the SLF. Each length gives a different channel spacing according to the relation:

$$s = \frac{\lambda^2}{BL} \tag{3.14}$$

where s is channel spacing, B is the birefringence, L is the length of PM fibre, λ is the wavelength of the input light wave.

The channel spacing for the three different lengths of PMF used were 0.8nm, 0.3nm and 0.16nm.
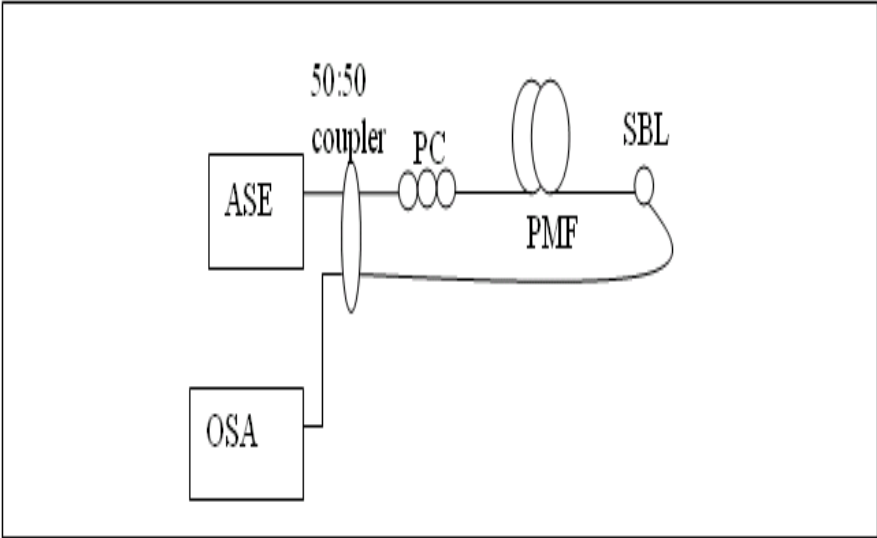
Figure 3.25: Measurement of SLF characteristics

Figure 3.26 shows the SLF output for channel spacings of 0.8nm and 0.16nm. Higher finesse is achieved for the SLF of 0.16nm wavelength spacing. Fine tuning can be performed

using the SBL for selecting the centre wavelength of laser. Figure 3.27 displays the SLF output over the full ASE spectral range of 1520nm to 1580nm (highest peak power at 1532nm due to the characteristics of the EDFA gain).
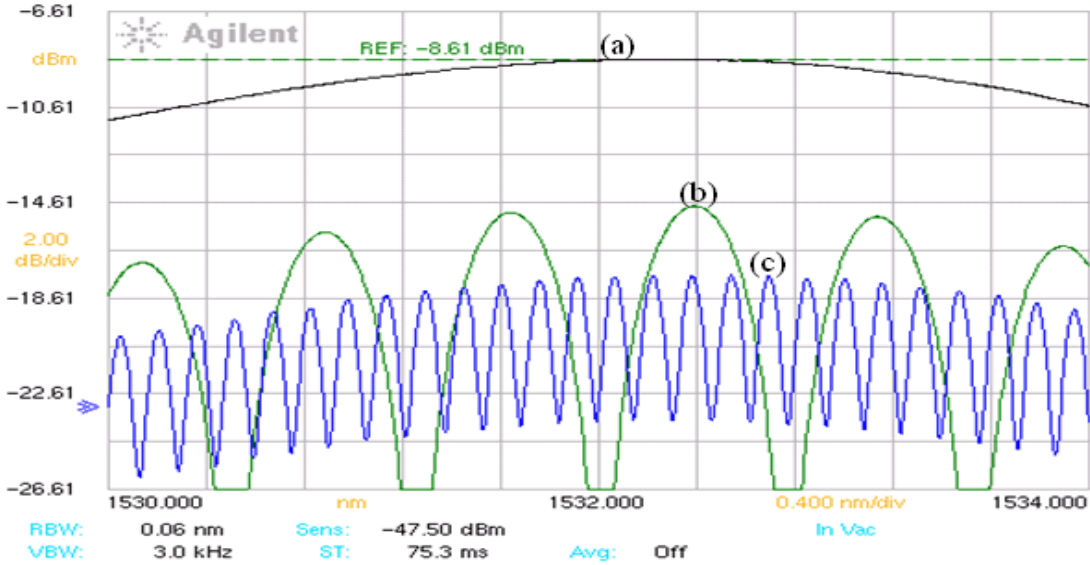
Figure 3.26: (a) EDFA gain profile (b) SLF with 0.8nm wavelength spacing and (c) SLF with 0.16nm channel spacing
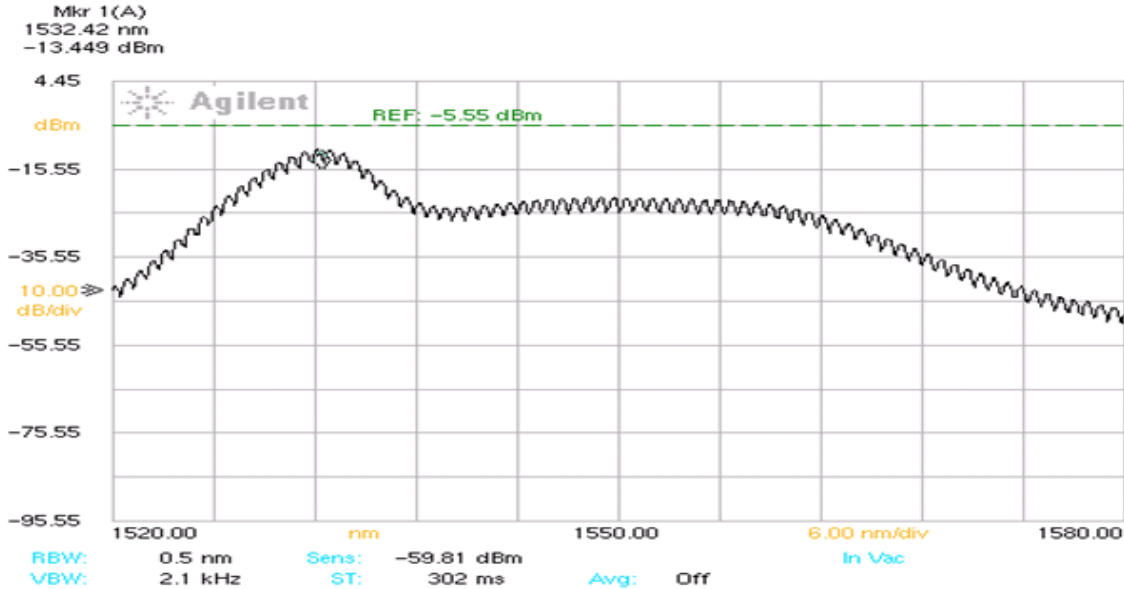
Figure 3.27: SLF output over full spectral range of ASE

Comparing the SLF with the commercial tunable filter (TF), the SLF is a periodic filter with step tuning whereas the TF is a single-wavelength bandpass filter with continuous wavelength tuning. The unique property of the SLF is that the channel spacing can be altered by changing the length of the PMF which is easier and more cost effective than the TF. Therefore depending on the requirements or applications, wavelength tuning will be carried out using either the TF or the SLF in the experimental systems.

3.8 Modulation of the Fibre Laser Output and Application for Spectroscopy

In the following sections we will investigate the application of the various fibre laser systems discussed above for gas detection. As an initial step attenuation measurements will be used to simulate gas absorption. For simplicity and with the eventual goal of accurate line-shape recovery, we will use intensity modulation of the laser output (at a few kHz frequency) which can simply be obtained through pump current modulation. This allows the use of a lock-in amplifier in the detection system. Low frequency (few Hz) wavelength scanning will be applied separately. As discussed earlier, this avoids the problems associated with combined AM and FM modulation which makes recovery of exact line-shapes more difficult (as occurs in DFB diode lasers using conventional wavelength modulation spectroscopy [15]).

Note that in order to get an optimum output intensity modulation from pump power modulation, the amplitude of pump modulation signal, V_{AC} and the DC level or offset voltage, V_{DC} must be set correctly as illustrated in Figure 3.28.
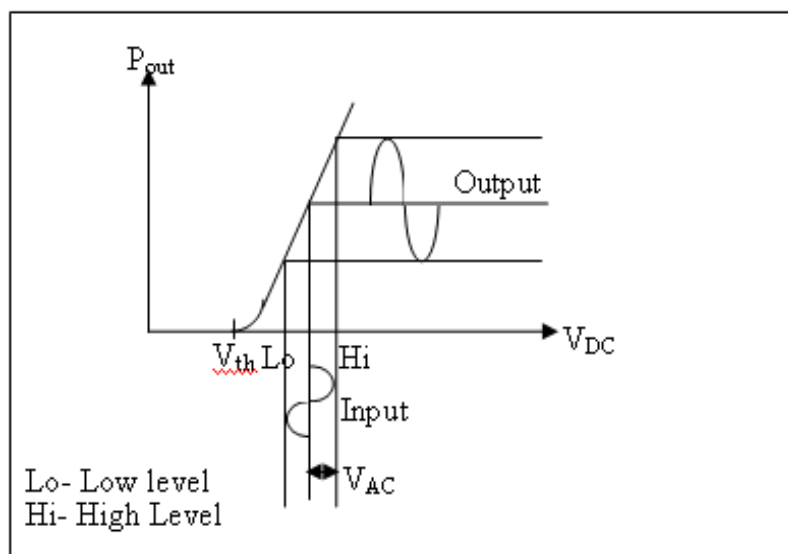
Figure 3.28: Output intensity modulation from pump modulation

3.8.1 System Operation with a Fibre Bragg Grating (FBG) and Piezoelectric Transducer (PZT)

Figure 3.29 shows the first experimental fibre laser system investigated for application to gas spectroscopy. The saturable absorber section uses a FBG as the reflector and a PZT is used to stretch the FBG for wavelength scanning/tuning at 1Hz frequency. A function generator is used to modulate the pump current/power and hence produce intensity modulation at 2kHz on the laser output.

The fibre laser is as described earlier and consists of an Erbium Doped Fibre Amplifier unit (EDFA as supplied by OptoSci. Ltd) which included a 980nm pump laser, two wavelength division multiplexers (WDM), an active gain medium (erbium-doped fibre, ~11m) and two isolators all contained within the EDFA unit. The output from the EDFA is connected to a polarization controller (PC, 2m fibre length) to align the polarization state with the axis of a 50/50 PM coupler. One output of the PM coupler is connected to a PM circulator consisting

58

of three ports in total; the second port of the circulator is connected to the saturable absorber section while the third port is connected to the EDFA input to close the cavity. The total cavity length is approximately 20m ($\sim$10 MHz mode spacing). The SA section comprises of a polarizer (PANDA fibre, 0.8m length) spliced to PM erbium-doped "bow-tie" fibre to form the SA (2 meter length) and a FBG. The fibre laser output is collected from the other port of the 50/50 PM coupler followed by a PM isolator which ensures that no power was reflected back into the system.

The output of the complete fibre laser system was connected to a variable attenuator to simulate gas absorption and detected by a photo-receiver followed by a lock-in amplifier (LIA) for signal processing. The performance of the system was measured by an optical spectrum analyzer (OSA) and an oscilloscope.
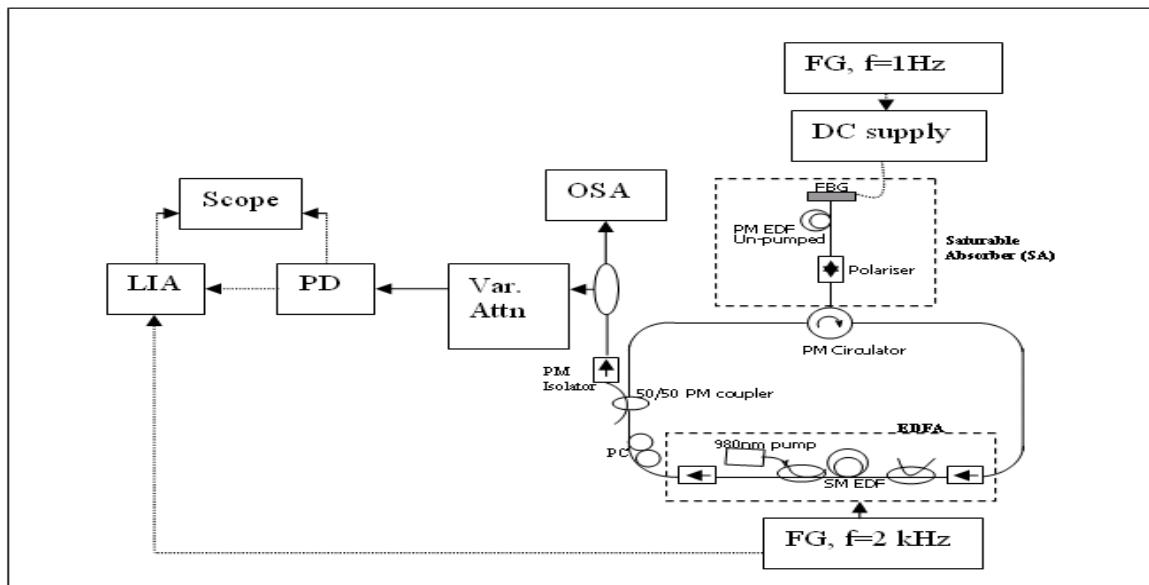
Figure 3.29: Experimental erbium doped fibre laser system with FBG as wavelength selector and reflector for the saturable absorber section

The centre wavelength of the FBG was 1550nm with a high reflectivity of 99% to produce a stable standing wave in the SA section. As discussed earlier, mode stability is an important consideration in this study. To preserve the stability of the laser polarization against envi-

ronmental disturbances, polarization maintaining (PM) components were used in the setup (except for the EDFA). We verified single-mode operation by using a scanning Fabry-Perot interferometer (FPI) with a 300 MHz free spectral range. Figure 3.30 shows the laser output from the FPI while Figure 3.31 was the laser spectrum obtained from the optical spectrum analyzer (OSA).
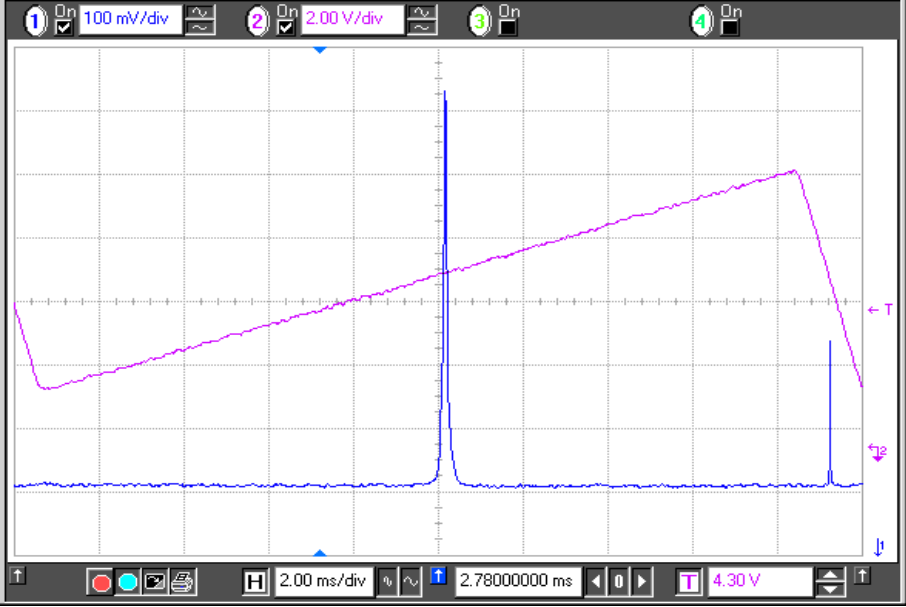
Figure 3.30: Measurement of single mode operation using a Fabry-Perot interferometer (FSR of 300 MHz)
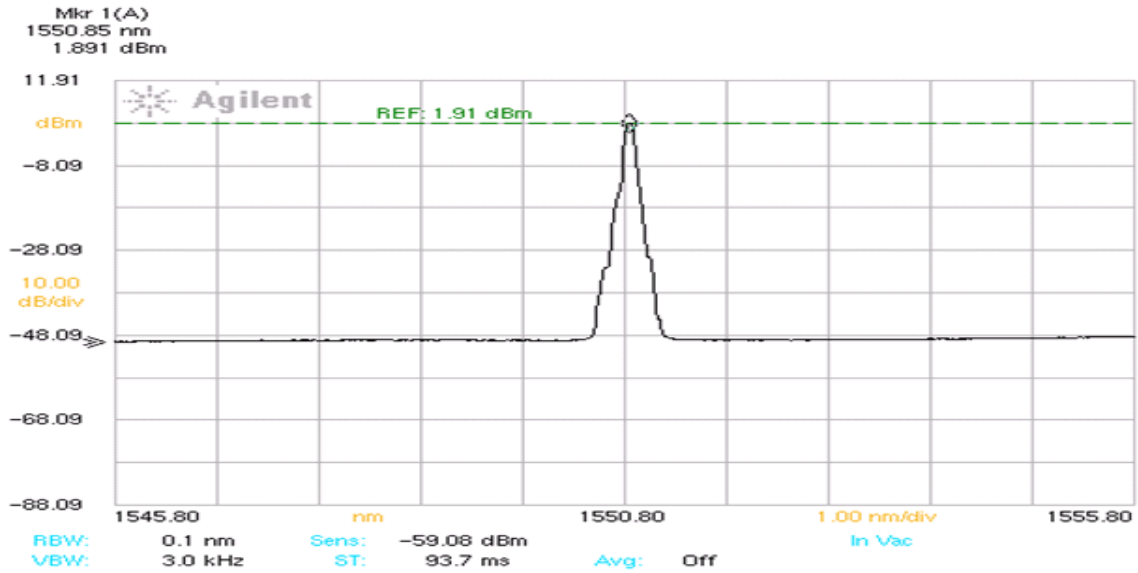
Figure 3.31: Laser output displayed on the Optical Spectrum Analyser (OSA)

As shown in Figure 3.32, the centre wavelength was tuned so that the laser could be scanned across a typical gas absorption line through a slow ramp of the 1Hz frequency with 300V supplied by a voltage amplifier (Xantrex unit, XFR 300-9, 0-300V, 0-9A) to the PZT on the FBG. Figure 3.33 is similar to Figure 3.32 but with the addition of a sinusoidal signal of 800mV peak-to-peak (Vpp) at a frequency of 2kHz applied to the pump input to give intensity modulation on the laser output.
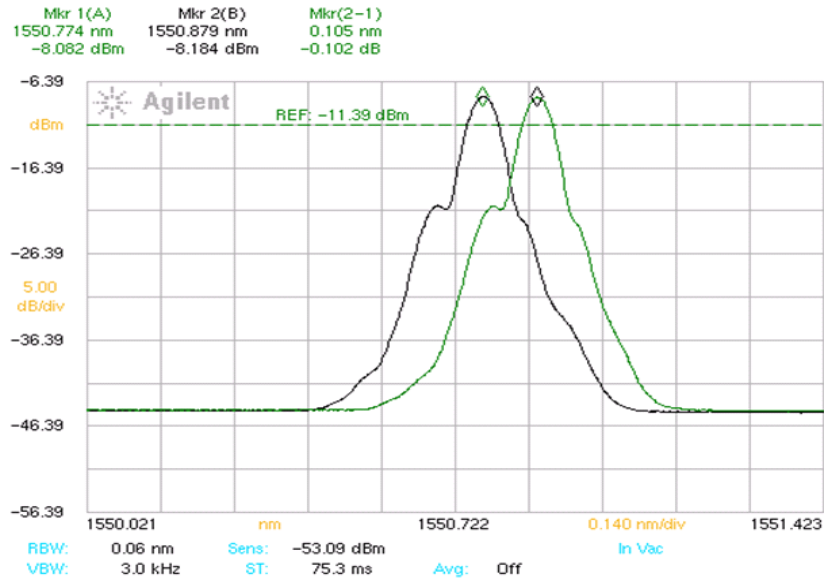
Figure 3.32: Mkr1 (A) shows the laser output before stretching the FBG and Mkr2 (B) shows the output after stretching, with Mkr (2-1) indicating 0.1nm of tuning range obtained by stretching
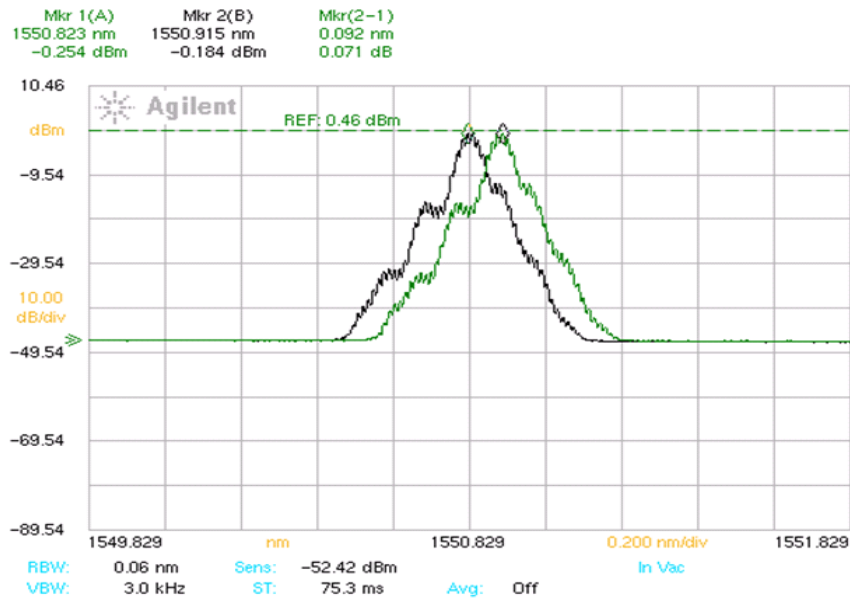
Figure 3.33: Laser output while the FBG is stretched by the PZT (as in Fig 3.32) and simultaneously intensity-modulated by sinusoidal modulation of the pump power at a frequency of 2kHz

An optimum modulation voltage from the function generator is a key requirement so

that a large intensity modulation can be obtained on the laser output. From the laser's DC output characteristics, the amplitude and the offset voltage were determined for modulation optimization. Based on Figure 3.34, which shows the laser output as function of DC voltage applied to the pump, there was a linear increase between at V_{DC} at 1.7V to 2.8V whereas the output abruptly increased after 2.9V. Therefore, V_{DC} set at 2.2V and V_{AC} at 800mVpp with a frequency of 2kHz. This is a simpler modulation scheme compared with using a waveguide phase modulator [72] or a tunable filter by varying its temperature [55] which is costly and complex. As already mentioned, use of a high modulation index can enhance the sensitivity of the system for detecting small attenuation from gas absorption lines.
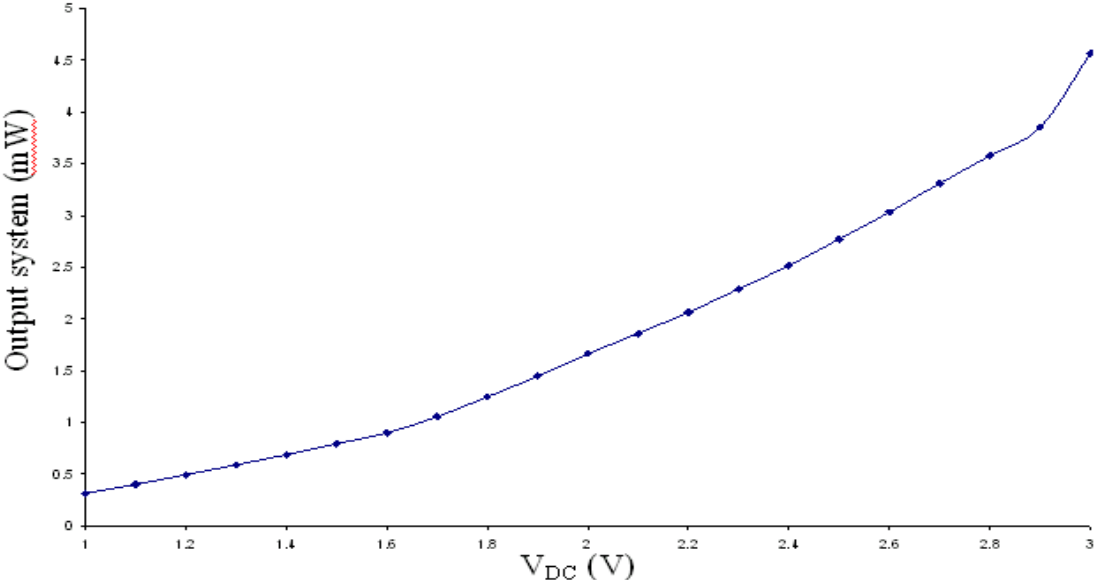
Figure 3.34: Laser output as function of DC voltage applied to pump power

To test the system operation with the intensity modulation applied, a Perkin Elmer Instrument, 7280 DSP Lock-In Amplifier (LIA) with sensitivity of 50mV, time constant of 1ms, phase of 25 ° and first harmonic was used to detect the output signal. An attenuator of 5dB was used at the photo-receiver input to avoid power saturation. Figures 3.35 and 3.36 show the change of output signal amplitude when the variable attenuator shown in Figure

3.29 is adjusted. A linear decrease in output signal was observed when the value of the variable attenuator was increased and, according to the Figure 3.35, the smallest attenuation detected by the LIA is 0.005dB. There was no perturbation on the output with and without stretching of the FBG by the PZT as shown in Figure 3.37.
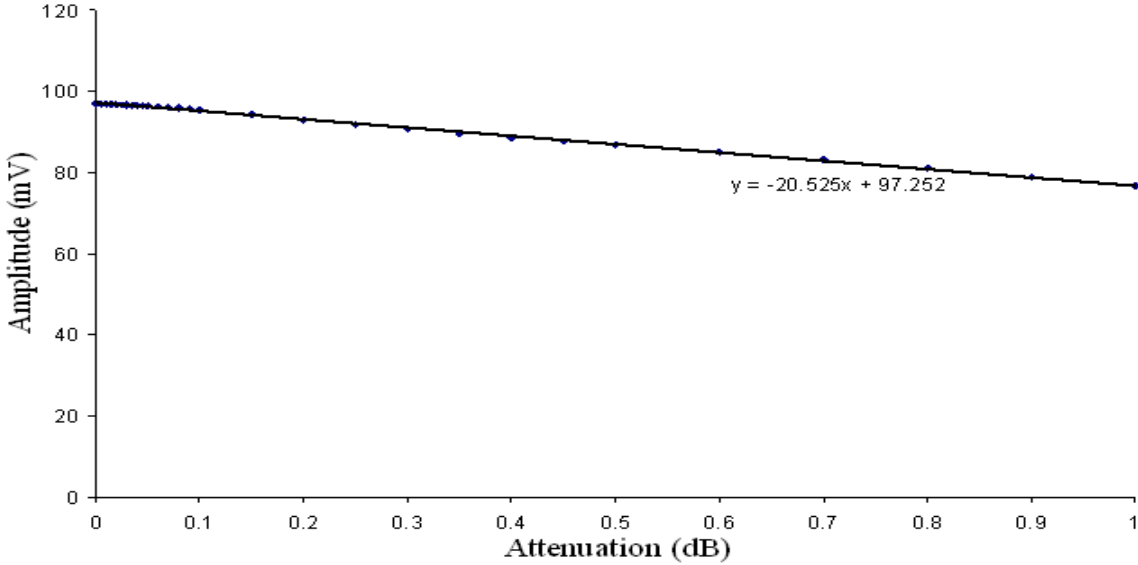
Figure 3.35: Laser AM signal output versus small changes in attenuation applied
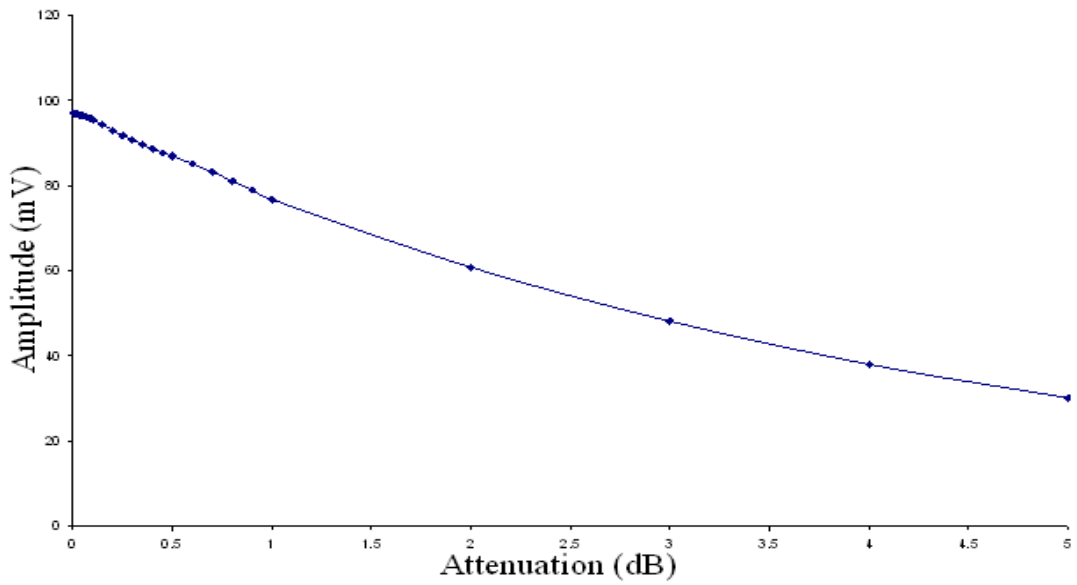
Figure 3.36: Laser AM signal output versus large changes in attenuation applied
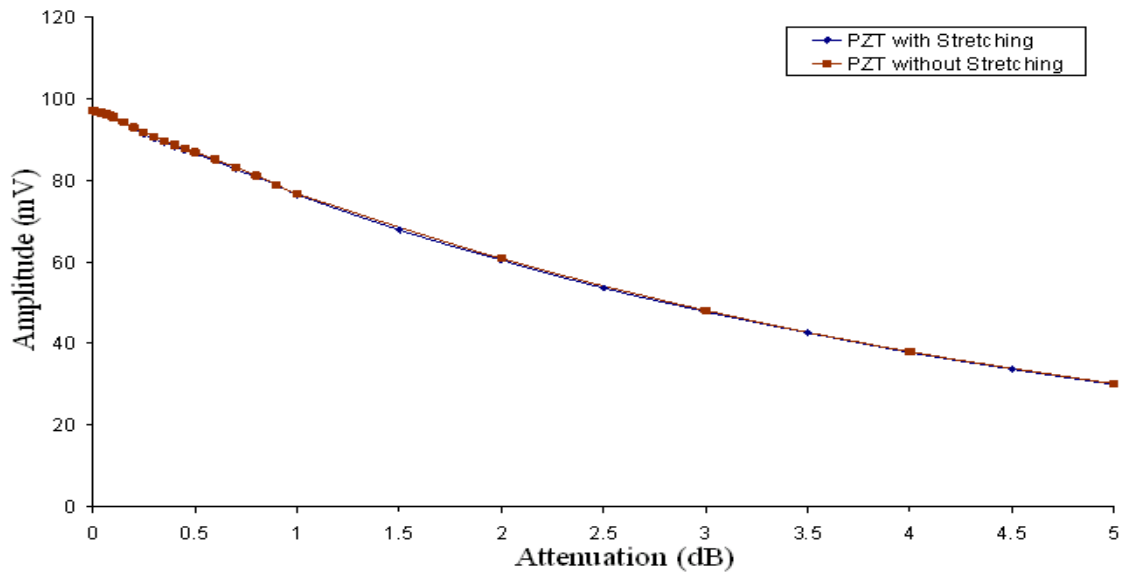
Figure 3.37: Comparison between laser AM signal output as function of attenuation with and without stretching of FBG

65

3.8.2 System Operation with a Sagnac loop filter (SLF) and Loop Mirror (LM)

The disadvantage of using the previous arrangement is that the range of wavelength operation is limited and defined by the FBG characteristics. An alternative scheme is to use a Sagnac Loop Filter (SLF) and a Loop Mirror (LM) to replace the FBG and PZT as shown in Figure 3.38. Further details on the SLF can be found in [73]. The SLF is inserted in the cavity and the LM in the saturable absorber arm. The SLF requires manual tuning in order to scan across a gas absorption line which is inconvenient as compared to the PZT. However, this setup has a higher laser output power since the voltage offset required is larger – compare Figure 3.39 for this setup with Figure 3.34 for the previous case. Figure 3.40 depicts the laser output on the OSA. Referring to Figure 3.41; the system was capable of tuning over 0.1nm (by adjustment of the small birefringence loop, SBL, in the SLF) which is sufficient to scan through a typical pressure-broadened gas absorption line.
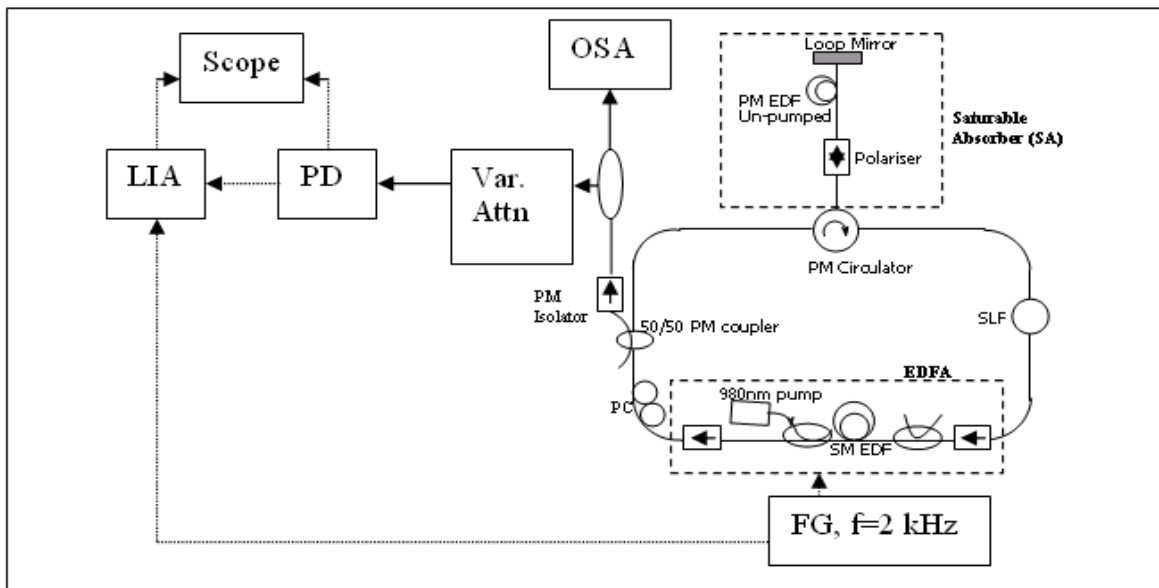
Figure 3.38: Experimental erbium doped fibre laser system with SLF for wavelength tuning and loop mirror as reflector on the saturable absorber

Tuning range can be improved by using a flat-gain erbium doped fibre, employing a gain-flattening filter or cascading erbium doped fibre amplifiers to reduce the length-averaged inversion level [73]. Moreover, finer tuning can be achieved by cascading two or more SLFs and Figure 3.42 illustrated the tuning achieved on the laser output from cascading two SLFs. Figure 3.43 shows the attenuation change that was detected by the system over the range of 0.005dB to 5dB with Figure 3.44 zooming into a smaller scale of attenuation. This system can also detect a 0.005dB change of attenuation which was smallest available value from the variable attenuator used in the experiments.
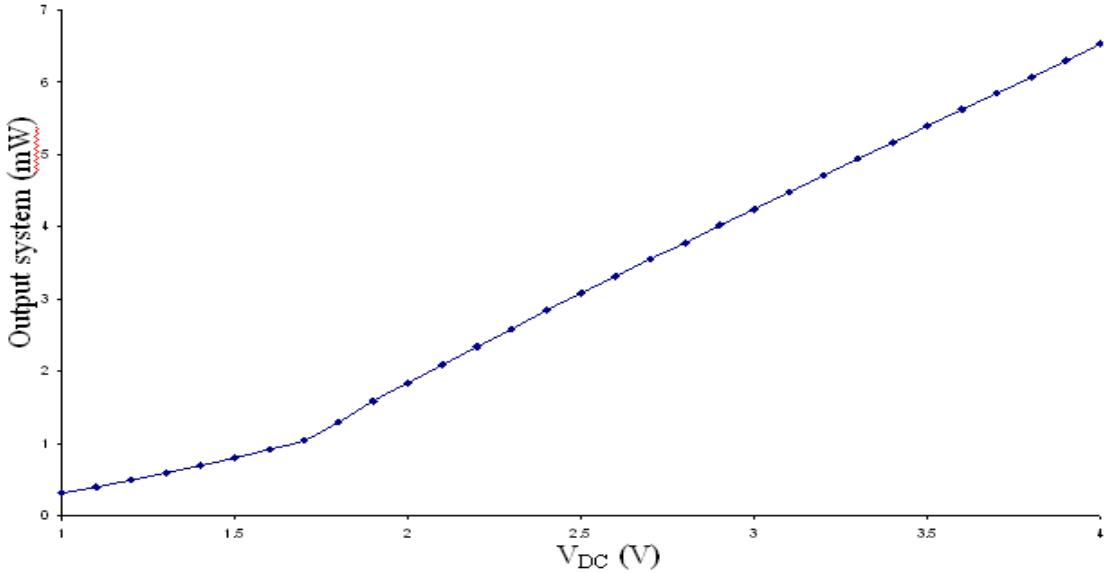
Figure 3.39: Laser output as function of DC voltage applied to pump power
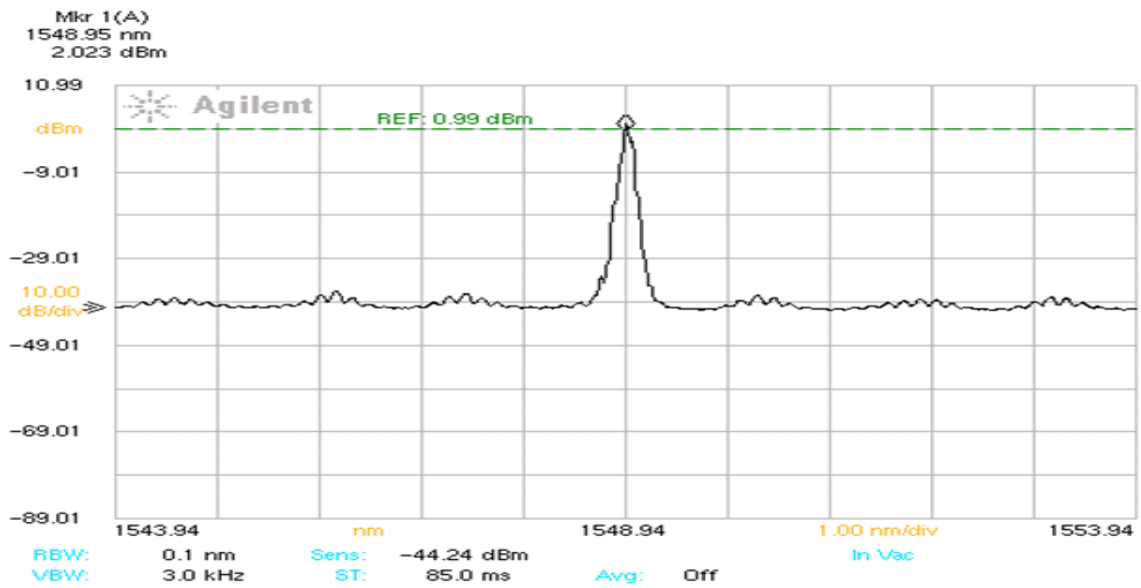
Figure 3.40: Laser output displayed on the Optical Spectrum Analyser (OSA)
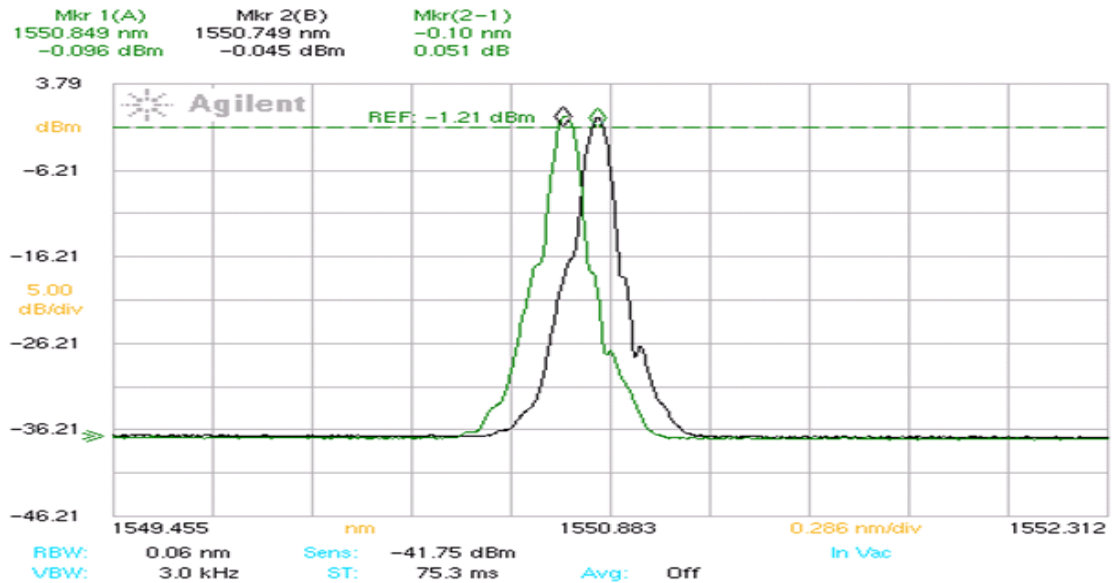
Figure 3.41: Mkr1(A) shows laser wavelength in initial position and Mkr2 (B) shows position after adjusting the SLF with Mkr(2-1) indicating a tuning range of 0.1nm (SLF channel spacing of 0.16nm)
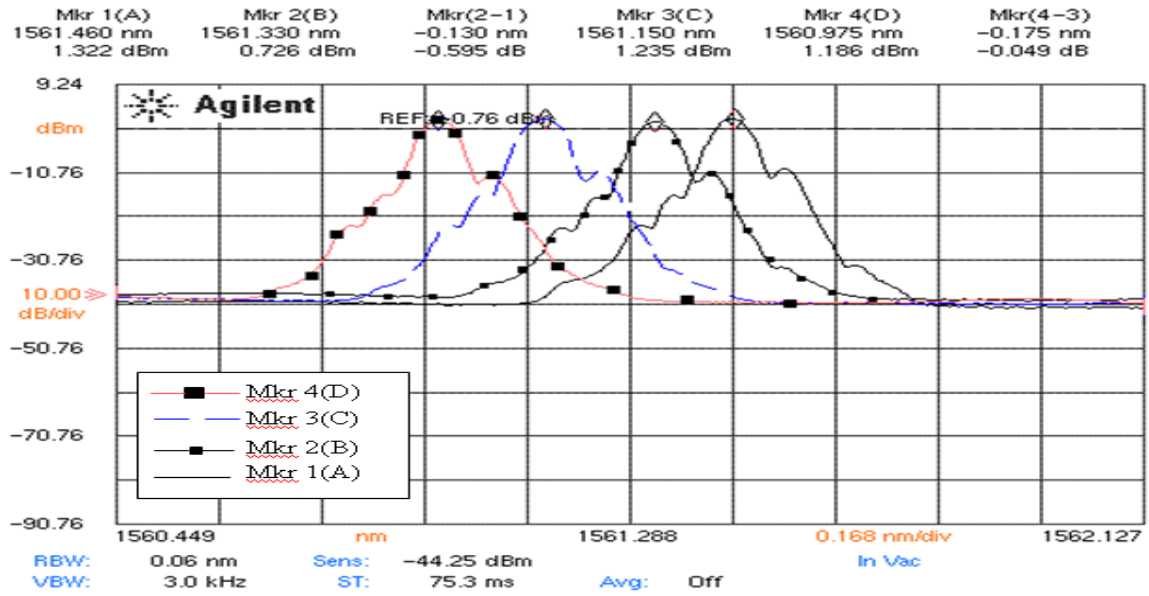
Figure 3.42: Fine tuning of laser centre wavelength by use of two cascaded SLFs
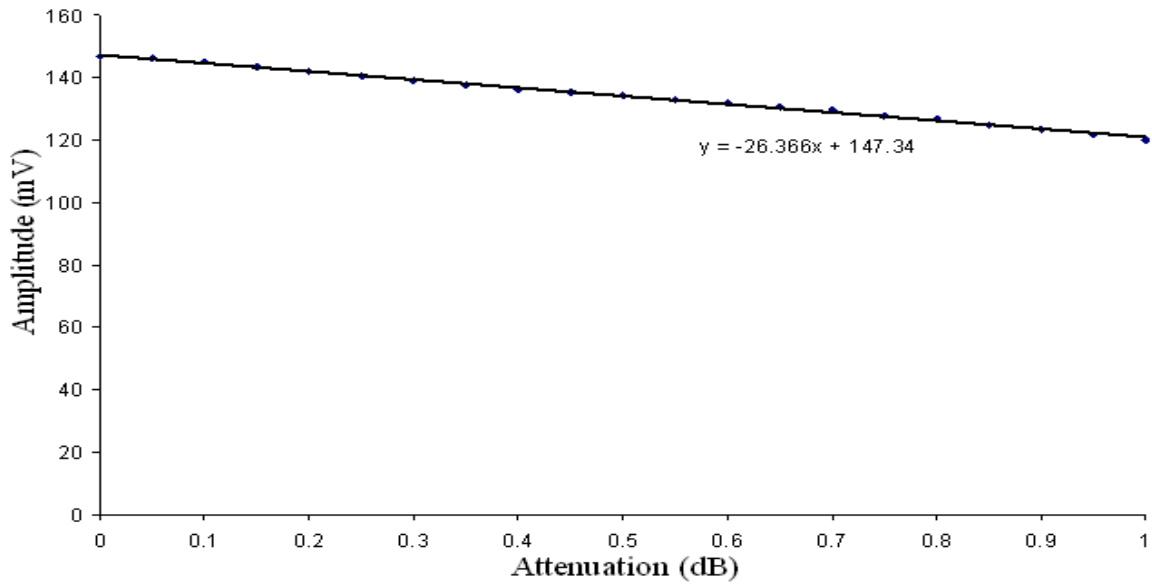
Figure 3.43: Laser AM signal output versus small changes in attenuation applied
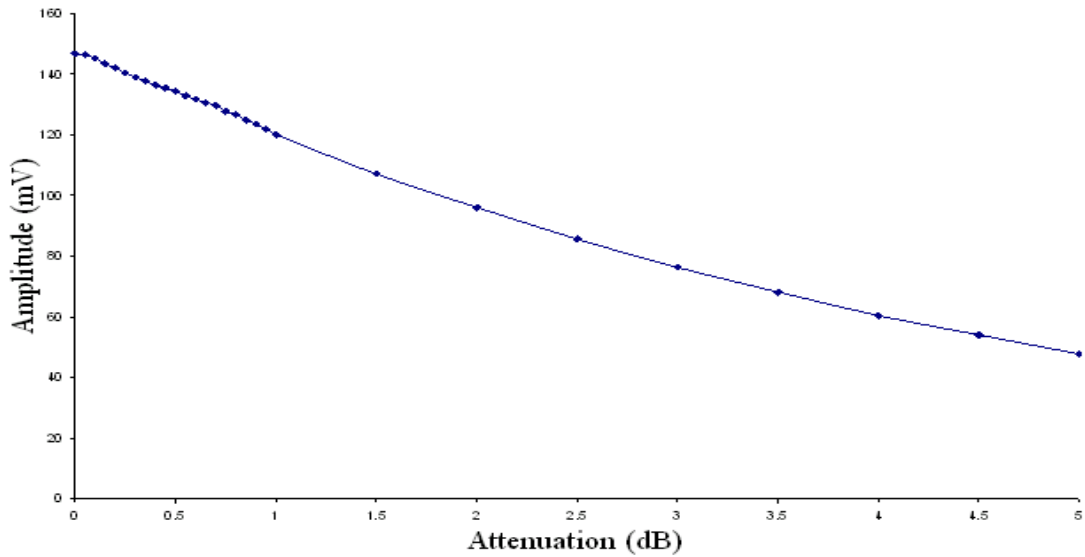
Figure 3.44: Laser AM signal output versus large changes in attenuation applied

Hence both this system and the previous one are feasible for spectroscopy applications with 0.005dB of attenuation detectable with both setups, though scanning methods are different. It should be noted that the performance of the overall system can be improved by splicing all the components together as the results given here are for a connectorized system where cavity losses are higher. As noted, the objective of the research is to develop a simple method of wavelength scanning, with separate amplitude modulation for phase sensitive detection, so that absorption line-shape recovery may be performed without the distorting effects experienced with diode lasers, where injection current modulation produces both AM and FM modulation simultaneously. Further careful investigation is required to ascertain if the pump modulation on the fibre laser as described here produces any modulation of the wavelength.

3.9 Application to Gas Spectroscopy

The previous section used a variable attenuator to simulate gas absorption but in this section, the EDFL system was employed with a fibre-coupled micro-optic cell using intensity modulation spectroscopy to demonstrate the feasibility of the system for trace gas sensing.

3.9.1 Gas Detection with the EDFLs using Intensity Modulation for Spectroscopy

3.9.1.1 Experimental Setup

The experimental system used is shown in Figure 3.45 which is the same as Figure 3.29 except that the variable attenuator has been replaced with a micro-optic cell. The micro-optic gas cell consisted of two graded index (GRIN) lenses positioned at either end of a ceramic V-groove. Input light was collimated by the GRIN lens at one end and passes through the sensing region and subsequently collected by the second GRIN lens at the other end.
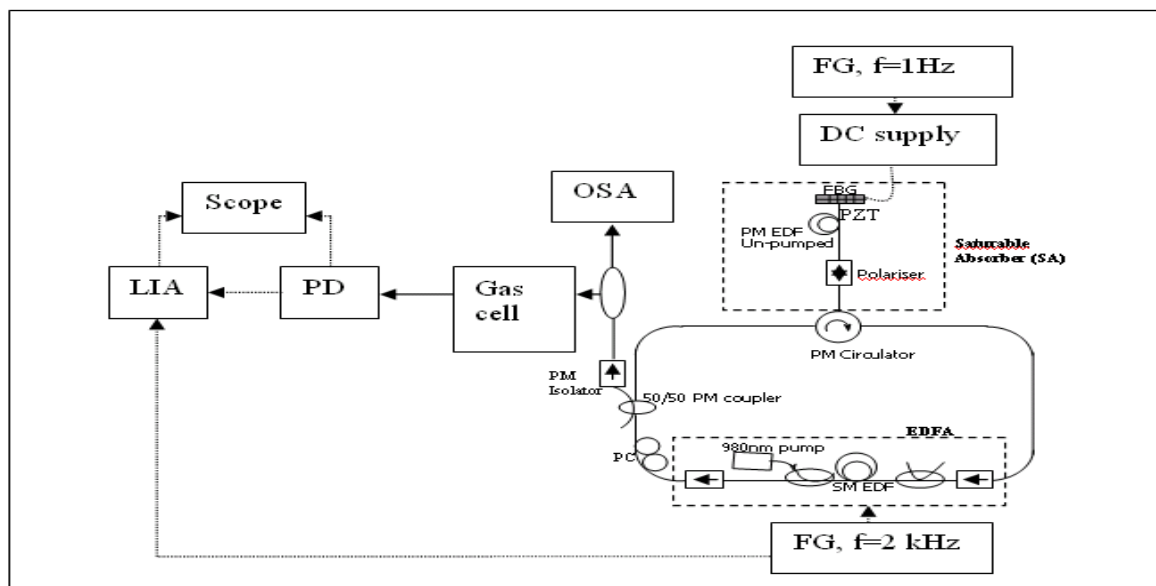
Figure 3.45: Experimental system for gas detection

3.9.1.2   System Characterisation and Calibration

Before attempting to perform gas measurements with the system, it was first necessary to check the system operation and its tuning characteristics to ensure that it was properly set up for gas detection.

The FBG characteristics were first measured and Figure 3.46 shows the Bragg wavelength as a function of the applied voltage which is relatively linear. A wavelength shift of 0.1nm is attained when 100V DC is applied to the PZT, thus yielding a tuning sensitivity of 0.001nm/V. Theoretically, the tuning range of this device was limited only by the breaking strength of the fibre; however due to the limits imposed by the high voltage amplifier (maximum output of 200V) only a 0.2nm shift was achievable; thus a proper selection of the centre wavelength of the FBG to match a particular gas absorption line is crucial for this experiment.
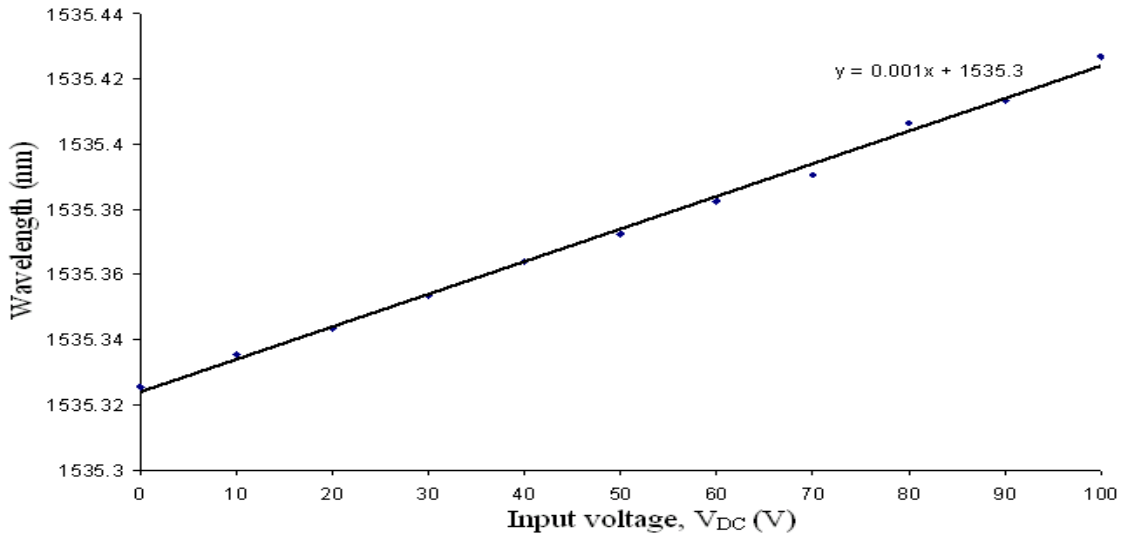
Figure 3.46: Tuning range of the FBG with sensitivity of 0.001nm/V

After verifying the tunability of the FBG, it was necessary to validate the stability of the laser output characteristics. Figure 3.47 shows the output spectra of the laser measured using

72

an OSA with 0.06nm of resolution while the pump power was varied from 45mW to 75mW with maximum laser output of 3mW. Referring to the figure, the side mode suppression ratio (SMSR) and output power of the laser are rising when the pump power was increased, but the centre wavelength of the laser remains fixed proving the system is stable where the centre wavelength is determined by the FBG used in the SA.
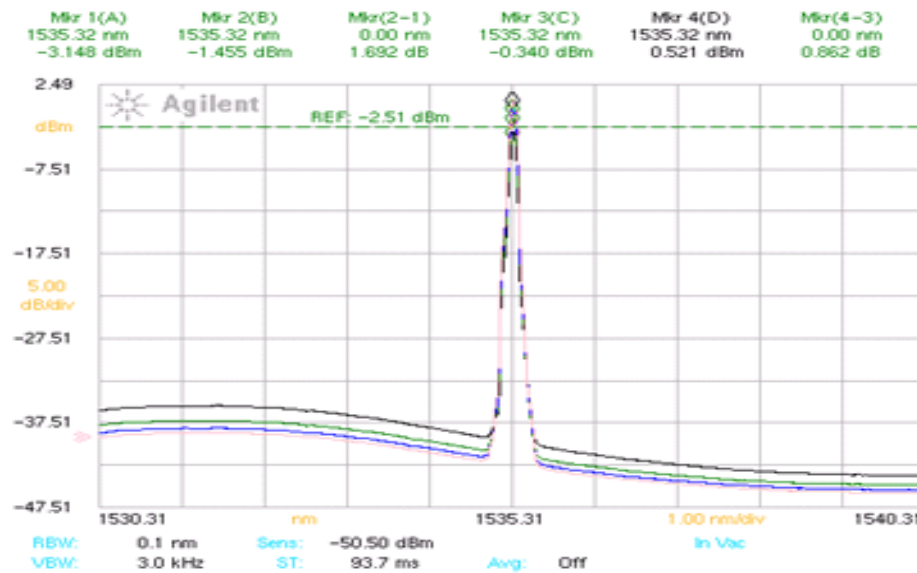
Figure 3.47: Laser output spectra as function of pump power

It was also necessary to verify that the laser wavelength as determined by the FBG could be operated within the wavelength region of a typical gas absorption line. Acetylene was chosen as the target gas. In order to get a clear comparison between the wavelength of the laser and suitable absorption lines of acetylene gas, the (broad-band) amplified spontaneous emission (ASE) was observed on the OSA along with the laser output after passage through the micro-optic cell containing acetylene. Figure 3.48 displays the output from the OSA with (a) indicating the ASE with several (noisy) gas absorption lines, (b) indicating the laser centre wavelength before (or without) stretching and (c) indicating the laser centre wavelength after a considerable amount of mechanical stretch on the FBG. The figure indicates that the laser

wavelength can be swept through the acetylene absorption line at a wavelength of 1535.39nm by the PZT.
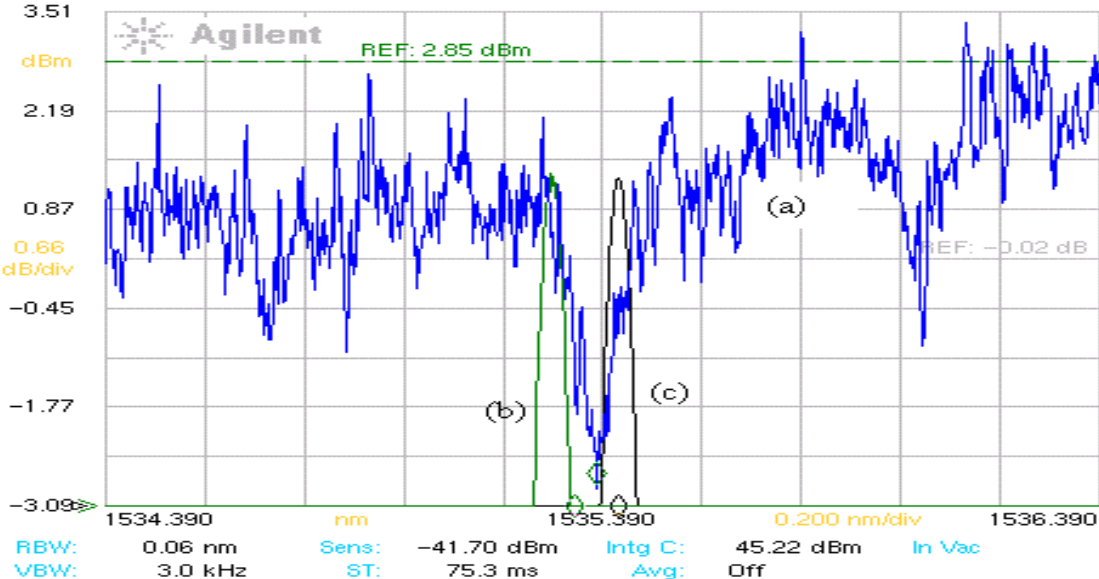
Figure 3.48: Laser tunability sweeping across gas line by using a PZT

3.9.1.3 Measurements on Acetylene Absorption Line

First of all, Figure 3.49 shows the output from the oscilloscope when only the ramp signal is applied to the PZT (no modulation on the pump) with 75mW DC pump power. The gas absorption line can be observed between the spikes (which are likely caused by sudden power recovery of the laser after the rapid change of the ramp signal at the end of each ramp cycle).
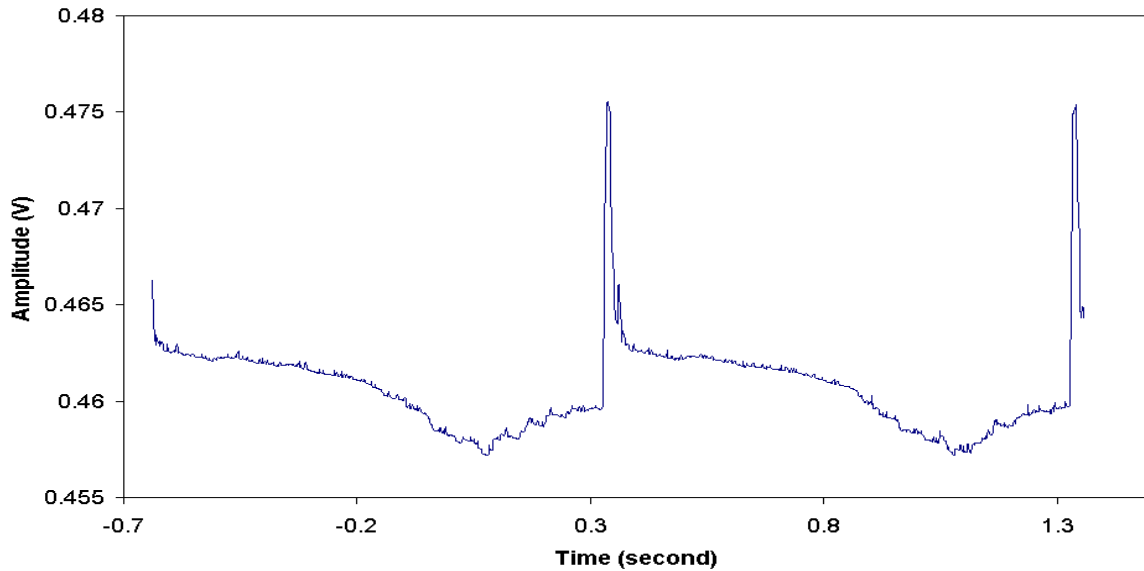
Figure 3.49: Output signal observe on scope as laser wavelength is ramped across the acety-
lene absorption line

Sinusoidal modulation was now applied to the pump so that a lock-in amplifier (LIA)
(phase-sensitive detection) may be employed to measure the amplitude of the output intensity
modulation as the laser wavelength is swept through the absorption line. 1% of acetylene
gas was filled into the cell and the output is shown in Figure 3.50. The peak to peak
amplitude of the signal from the LIA was 130mV at the first harmonic (1f) and almost zero
(0.023mV) as expected at the second harmonic (2f) which was due to the small deviation
of the intensity modulation from purely sinusoidal. The 1f signal obtained approximately
followed the absorption line. The absolute line shape is obtained by normalising to the
background (off-line) signal. Based on the result, a comparison between the theoretical
absorption line for 1% acetylene was made and depicted in Figure 3.51. There is clearly a
problem with the depth of the gas line not matching the theoretical line – this is possibly due
to high background signal occured even no gas presents in the cell. Other possible includes
laser output power variation and normalisation issues, in conjunction with the cooling system
used in setting the actual wavelength of the FBG. From the result obtained, the depth of

the absorption line was 0.13V and noise level was 80mV resulting signal to noise ratio of 1.7. Thus the minimum of 0.5% acetylene can be detected through this technique.

Figure 3.50: Gas detection along the line shape with 1f of LIA output
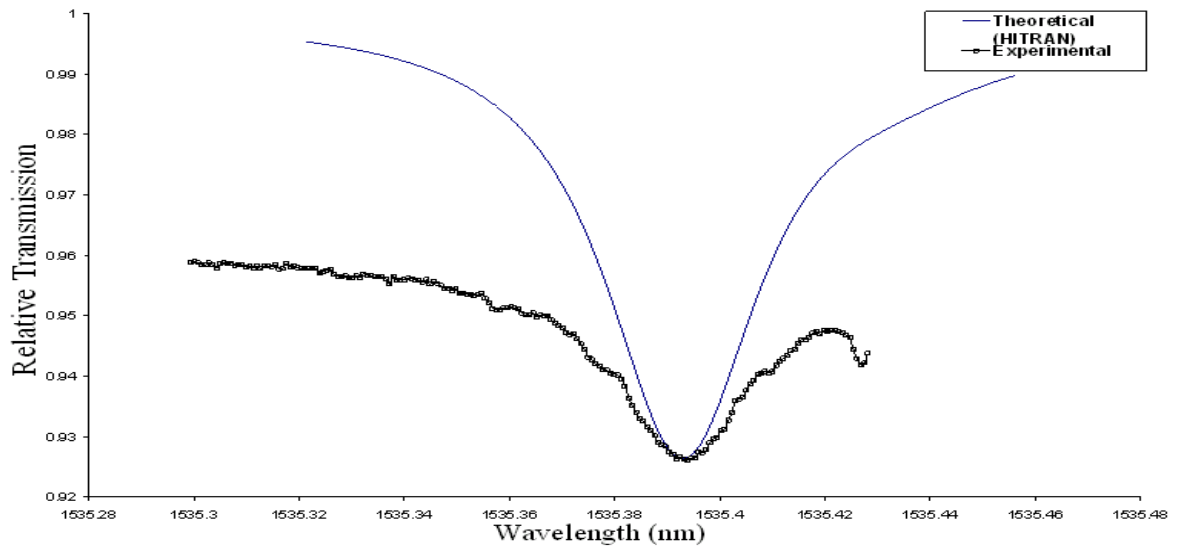
Figure 3.51: Relative transmission for acetylene for 1% of concentration, pressure 1 bar temperature $22°C$

The system is capable of detecting gas absorption lines but better results may be possible by giving attention to the following issues:

It is difficult to confirm that the tuning range is sufficient with the 1Hz ramp modulation used in the experiment. The resolution of the OSA available in the lab is 0.06nm and it is impossible to see every scan performed by the PZT. For measuring gas lines at atmospheric pressure and temperature, a tuning range of $\sim$0.1nm is required. A higher voltage amplifier is needed to get the desired tuning range as currently only 200V is available in the lab. (Measurement of lines at low pressure would be possible since linewidths are narrowed at lower pressures or temperatures)

The FBG wavelength needs to be closely matched to the absorption line wavelength. Due to a slight mismatch, the FBG used in the experiment was connected to a temperature controller to shift its wavelength to the acetylene absorption line and temperature fluctuations in the lab result in wavelength fluctuations.

The setup would be better placed in styrofoam to make the system less sensitive to environmental perturbation such as vibration, acoustic noise and fluctuations in room temperature. Furthermore, the current experimental setup is a testbed so all components are connectorised with FC/APC connector. It is expected that the system performance can be significantly improved by splicing all the connections to reduce noise and get more stable laser.

3.10 Conclusion

This chapter has presented the basic characteristics of several erbium fibre lasers systems with a particular focus for gas spectroscopy. A key objective of the research was to investigate a simple method of wavelength scanning, with separate intensity modulation (for phase sensitive detection) so that absorption line-shape recovery may be performed without the

distorting effects experienced with diode lasers, where injection current modulation produces both AM and FM modulation simultaneously.

The characteristics of a fibre ring laser system using a saturable absorber to suppress mode hopping and improve laser stability was first investigated using two different arrangements for wavelength tuning, namely, a FBG with a PZT and a SLF with a loop mirror. Preliminary results demonstrated that both arrangements are feasible for spectroscopy applications, with 0.005dB of attenuation detectable with both setups, though scanning methods were different. Automatic scanning across an absorption line by using the PZT is more effective than manual tuning of the SLF; however the wavelength tuning range is larger for the latter arrangement. The tuning range of 0.1nm obtained by stretching the PZT or tuning the SLF demonstrated that the laser output can be tuned across a typical pressure-broadened absorption line.

Using simple pump modulation to produce output intensity modulation, along with wavelength scanning by stretching the FBG, the system has been used to detect acetylene absorption lines, although further work is necessary to improve system operation for accurate line shape recovery. However the system is still rather complex and this prompted an investigation into simpler, more effective methods for gas spectroscopy with a fibre laser system. The following chapter investigates the use of intra-cavity methods to achieve these objectives.

Chapter 4

INTRA-CAVITY LASER ABSORPTION SPECTROSCOPY (ICLAS) USING EDFLs

4.1   Introduction

One possible method to enhance the sensitivity of near-IR fibre laser gas sensors is use of the technique known as "intra-cavity laser absorption spectroscopy" (ICLAS) where a gas cell is placed within a laser cavity and the evolution of the output spectrum is captured over the build-up period of laser oscillation in the cavity. Enhancement of the effective path length of the gas cell occurs due to the multiple circulations of light within the cavity during this period. The technique has been successfully demonstrated with solid-state lasers [22] and effective absorption path lengths ranging from tens to thousands of kilometers, depending on the laser type and operation conditions, have been attained. We have previously reported a theoretical analysis of the dynamics of erbium fibre laser systems [26] but practical realization of ICLAS with fibre lasers is difficult for several reasons – the spectrum must be captured during the

period of relaxation oscillations and detector arrays for the 1-2μm region are less capable and more expensive than the silicon CCD arrays used for ICLAS at <1μm wavelengths. For example, Stark [27] used a rapid scan Fourier Transform (FT) spectrometer to capture the spectrum at each peak of the relaxation oscillations for a thulium-doped fibre laser.

In this chapter we present a simple and inexpensive method of ICLAS which makes use of the amplified spontaneous emission (ASE) already present within a fibre laser cavity and we experimentally demonstrate the principle of operation using gases such as acetylene, carbon dioxide and methane. Acetylene gas has a high absorption line strength among other gases in the near-IR which makes it easy to detect whereas low line strength gases such as carbon dioxide and methane are also tested to demonstrate the system's ability for multi-gas sensing. Experimental results are compared with theoretical results obtained from the HITRAN database 2004 and 2008 using a commercial program created by GATS Spectral Calculator.

4.2 Principle of ICLAS using ASE within the Fibre Laser Cavity

The first key principle for attaining path length enhancement within an erbium fibre laser cavity is to ensure a broad, flat erbium gain spectrum which preferable can be tuned over the desired spectral regions where particular gas absorption lines exist. As discussed in Chapter 3, the gain characteristics of erbium-doped fibre amplifiers and lasers may be conveniently described in terms of a length averaged gain coefficient, $\overline{g}$, given by [26, 74]:

$$\overline{g} = (\gamma + \alpha)\overline{N}_2 - \alpha \tag{4.1}$$

where γ is the emission coefficient, α is the absorption coefficient and $\overline{N}_2$ is the length

averaged inversion level ($0 < \overline{N}_2 < 1$) where $\overline{N}_2 = \frac{1}{l} \int_0^l N_2(z) dz$. Figure 4.1 shows $\overline{g}$ as a function of wavelength for different inversion levels, $\overline{N}_2$, for the erbium fibre used in the fibre laser systems. The total gain, G , of a length, L , of erbium fibre is given by $G = \overline{g}L$.
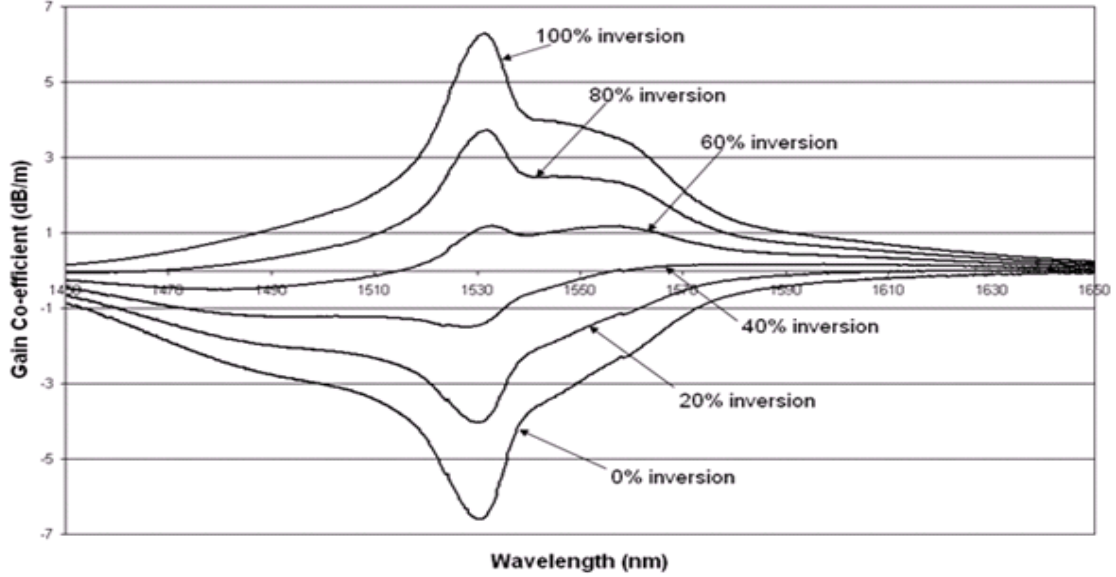
Figure 4.1: Length-averaged gain coefficient of FibreCore EDF at different inversion levels

It is clear from Figure 4.1 that the shape of the gain spectrum is dependent on the inversion level and a reasonably flat spectrum is attained over the 1530-1560nm region when the inversion level is $\sim 60\%$ and $\overline{g} \approx 1\text{dB/m}$. When the cavity is lasing, the inversion level is determined by the external cavity loss since steady-state laser oscillation implies that gain and loss are equally balanced (net round-trip gain of unity). For example, with a cavity loss of 10dB, then an erbium fibre gain of G=+10dB is required for lasing, which means that $\overline{g} \approx 1\text{dB/m}$ for a typical erbium fibre length of 10m and hence the system operates at 60% inversion level. Increasing or decreasing the cavity loss will correspondingly increase or decrease the inversion level, so a variable attenuator within the fibre laser cavity may be used to select a particular gain curve in Figure 4.1. Similarly, increasing the erbium length will reduce the inversion level. Assuming homogeneous broadening is dominant, the actual

81

lasing wavelength is determined by the position of the local maximum on the appropriate gain curve in Figure 4.1 and the lasing wavelength may be switched between ∼1530nm and 1560nm by simple adjustment of the variable attenuator to raise or lower the inversion level around 60%.

The second key principle relates to the characteristics of the ASE within the fibre laser cavity. ASE exists over the full gain-bandwidth of the erbium fibre and provides a convenient broadband source for interrogation of gas absorption lines. As noted above, the net round-trip gain is approximately unity at the lasing wavelength but this is also true for the ASE within the cavity, particularly near the lasing wavelength, if the gain curve is flat. Hence the ASE undergoes multiple circulations within the fibre laser cavity and consequently the effective path-length of an intra-cavity gas cell is greatly increased.

4.3   Experimental Fibre Laser System for ICLAS

The experimental system for demonstration of ICLAS using ASE is shown in Figure 4.2 with different positions of the coupler placed in the cavity. The erbium doped fibre amplifier (EDFA) unit (OptoSci Ltd., ∼1.8dB internal loss) consists of ∼11m of erbium-doped fibre, pumped by a 980nm diode laser with two wavelength division multiplexers for in/out coupling of the pump and an isolator at both the input and the output of the EDFA. A 6cm path-length micro-optic gas cell (insertion loss of ∼1dB) is fibre-coupled within the cavity and a variable attenuator (EXFO, Optical Test System IQ-203, insertion loss of ∼3dB) is also included within the cavity to adjust the inversion levels as discussed above. A 20:80 single mode fibre coupler is used to tap off 20% of the cavity light to an optical spectrum analyzer (OSA: Agilent 86140B resolution of 0.06nm) to monitor the cavity ASE and the laser emission. Total cavity length is ∼13m and all connectors are FC/APC except for the variable attenuator which had FC/PC connectors.
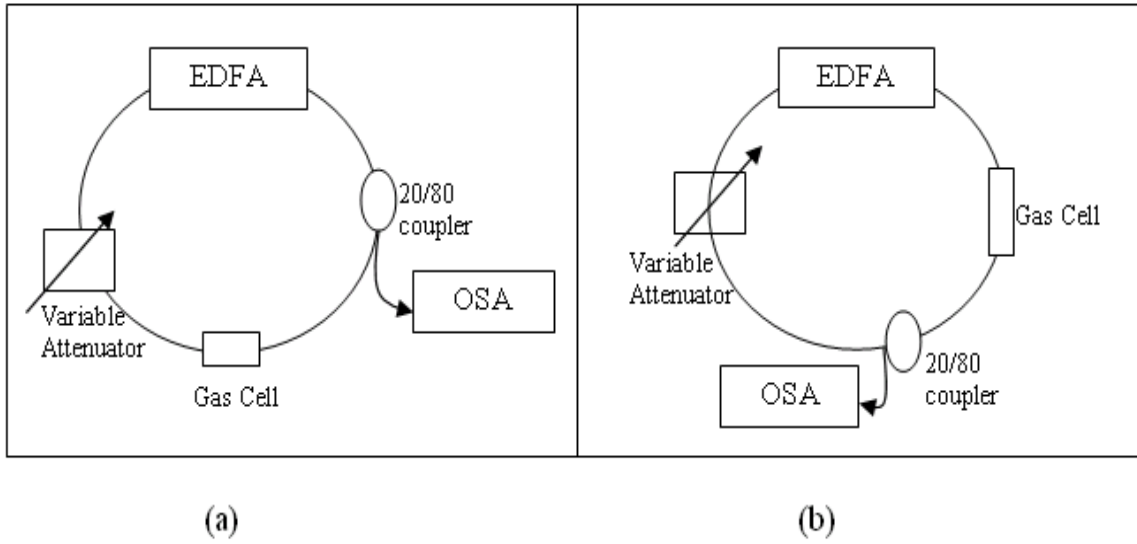
Figure 4.2: Experimental setup for ICLAS with (a) gas cell after coupler and (b) gas cell before coupler

4.4   Experimental Results

Before we present the detailed experimental measurements of absorption lines for various gases and the sensitivity enhancement, we first investigate the effect of the various components used in the design of the system shown above in Figure 4.2.

4.4.1   Position of the Coupler in the Cavity

The output ASE power level for the cell placed after the coupler, Fig 4.2 (a), was higher than that for before the coupler, Fig 4.2(b), as shown in Figures 4.3 and 4.4, with ∼6dB difference, for both 20/80 and 50/50 couplers even though the total round-trip attenuation of the cavity is not changed. The 50/50 coupler depicted in Figure 4.4 gives a higher output due to more power being tapped from the cavity to the OSA. Figures 4.5 and 4.6 shows the (enhanced) acetylene absorption lines extracted from Figures 4.3 and 4.4 after subtraction

83

of the background ASE (using Origin 6.1 software). It shows that the absorption lines from both setups are almost similar, hence the setup with the cell placed after the 20/80 coupler is preferable due to the higher power and lower noise levels and will be used for the rest of the experiments conducted in the following sections.
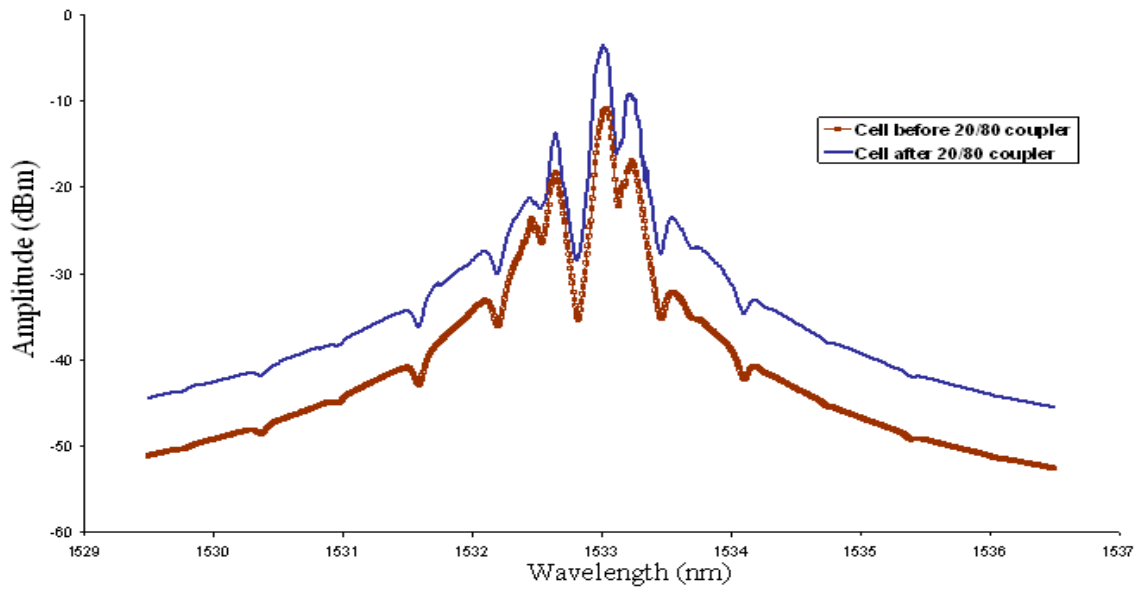
Figure 4.3: ASE spectrum for both setups with 20/80 coupler (acetylene in cell)
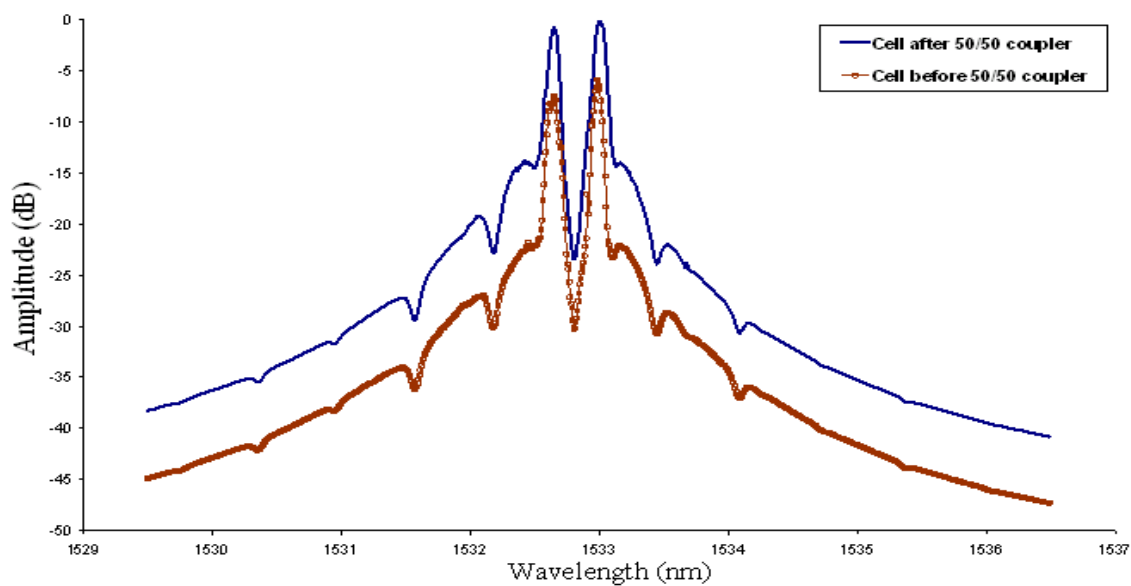
Figure 4.4: ASE spectrum for both setups with 50/50 coupler (acetylene in cell)
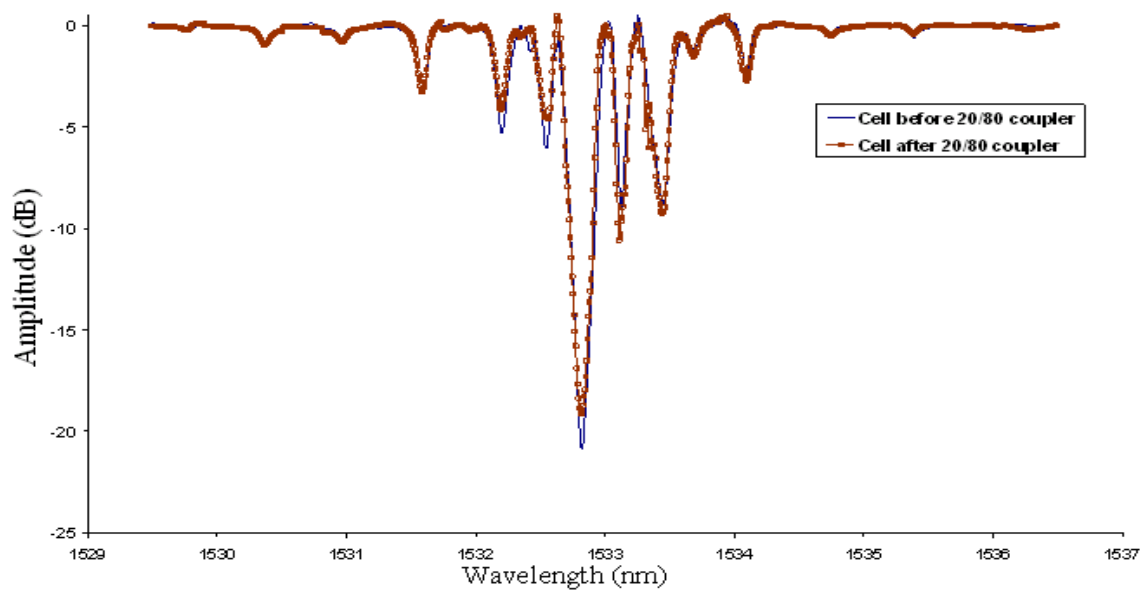
Figure 4.5: Acetylene gas absorption lines using 20/80 coupler
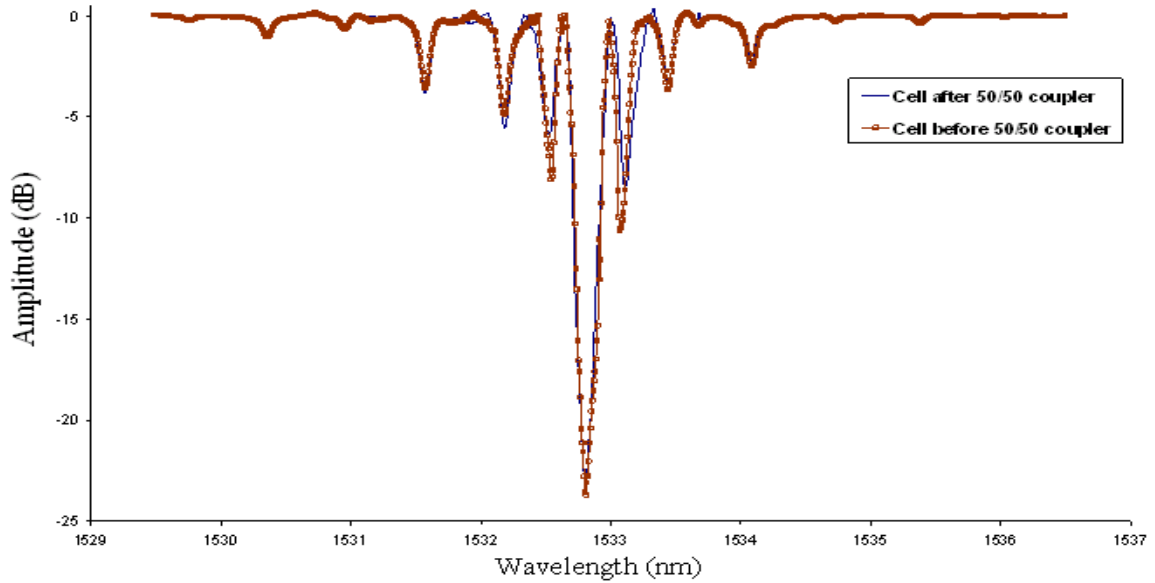
Figure 4.6: Acetylene gas absorption lines using 50/50 coupler

4.4.2 Effect of Inserting a Tunable Filter (TF)

As was discussed in Chapter 3 for a standard EDFL system, a tunable filter may be inserted into the cavity for selecting/tuning the laser wavelength and to reduce mode hopping at high pump powers. However no gas absorption lines can be seen when a TF is used in the system here for ICLAS since the TF has a narrow bandwidth and filters out the ASE. Without the TF, many gas absorption lines appear on the ASE spectrum from the OSA as depicted in Figure 4.7 where the solid curve indicates 'without a TF' and the other curves are representing the TF being tuned to specific wavelengths. Experimental settings are 71.3mW pump power (maximum pump available for the EDFA) and variable attenuator set at 10dB.
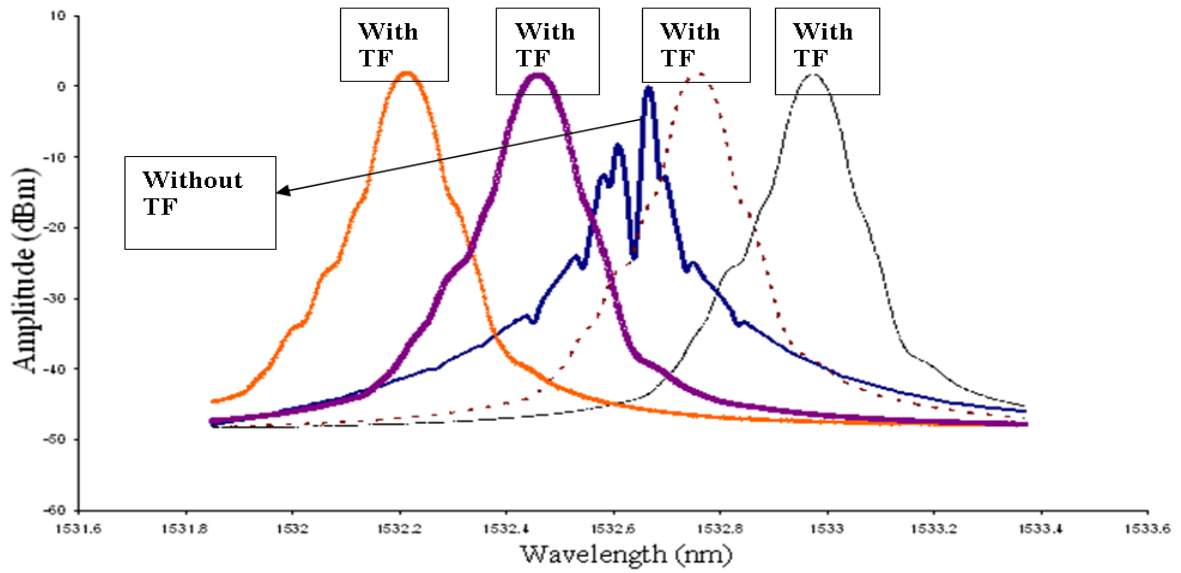
Figure 4.7: ASE spectrum with and without a tunable filter in the cavity

4.4.3 Effect of Pump Power

Pump power is one of the main factors in enhancing the depth of the gas absorption lines observed on the ASE spectrum. Referring to Figure 4.8 below, the depth of the absorbance at a wavelength of 1532.8nm is decreased when the pump power is reduced. This arises when the pump power falls below the threshold value and hence circulation of the ASE within the cavity is greatly reduced. On the other hand, high pump powers tended to enhance laser mode fluctuations and the centre wavelength of laser could also shift towards longer wavelengths (cavity loss set at 9.1dB attenuation) due to the flat gain curve.

87
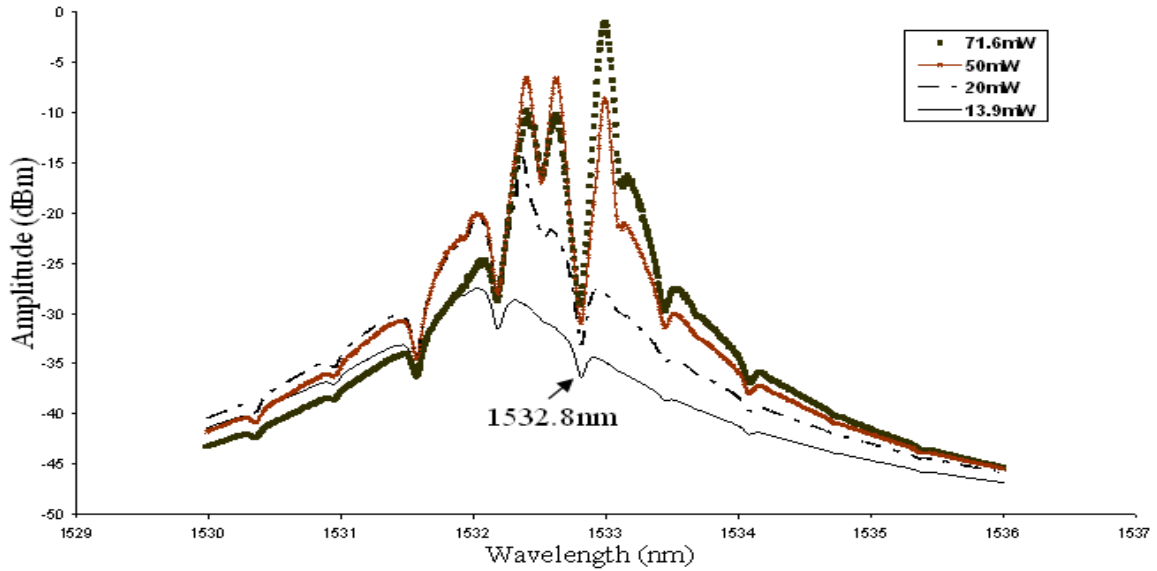
Figure 4.8: Effect of pump power on observed depth of acetylene lines

4.4.4 Effect of Attenuation on Lasing Wavelength

Gain and loss play an important role in determining the lasing wavelength which is based on the position of the maximum in the gain curve shown in Figure 4.1 when there is no filtering element in the cavity. This is also crucial for operation of our system so that there is sufficient ASE near threshold in the vicinity of particular gas absorption lines. As we can observe from Figure 4.9, when the cavity attenuation is changed in the system, the lasing wavelength is also changed. Based on examination of Figure 4.1 in the region of 1530nm, the system tends to lase at longer wavelengths when the cavity attenuation is reduced which is in accordance with the theory. Therefore, we can adjust the lasing wavelength around desired absorption lines by controlling both the pump of the EDFA and the setting of the variable attenuator.
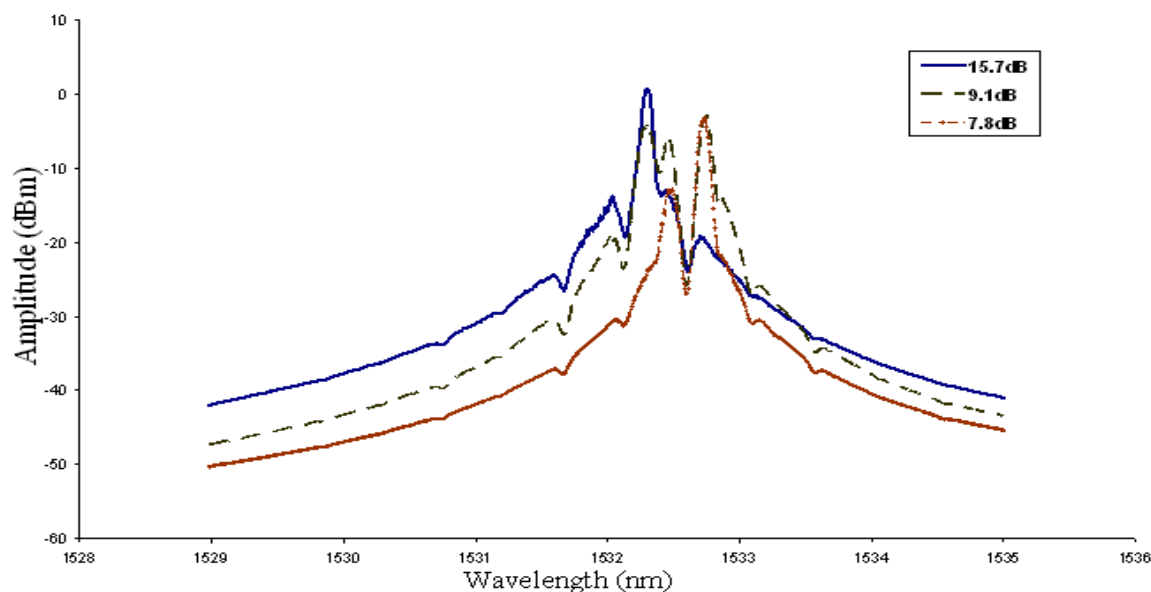
Figure 4.9: Effect of attenuation on the lasing wavelength (with no TF)

4.4.5   Gas Absorption Line Measurements

4.4.5.1   1% Acetylene (C_2H_2) Gas

Compared with other hydrocarbon gases, C_2H_2 has relatively strong lines in the near-IR around 1530nm and hence measurements were performed using 1% C_2H_2 in the micro-optic gas cell to evaluate the performance of the system. Figure 4.10 shows the ASE output observed on the OSA over the wavelength range of 1529-1537nm both with 1% C_2H_2 in the gas cell and after the cell was flushed with nitrogen (no gas) for a pump power of 70.2mW and an added attenuation of 11.8dB from the attenuator in the cavity.

A total of 16 acetylene absorption lines can be observed in Figure 4.10 and, in particular, the lines near the central (lasing region) are greatly enhanced in amplitude. This is illustrated more clearly in Figure 4.11 where the background has been subtracted from the gas line (in units of dB) and the central absorption line appears with ~15dB of attenuation.

In order to compare the results with theory and obtain the sensitivity enhancement factor,

the dB scale of Figure 4.11 was converted to relative transmission„P_g/P_{bg} , in Figure 4.12 using the relationship:

$$P_g/P_{bg} = 10^{(\frac{P_g(dBm)-P_{bg}(dBm)}{10})} \tag{4.2}$$

Figure 4.13 shows the theoretical acetylene absorption lines, calculated from the HI-TRAN database 2004, using commercial software (GATS Spectral Calculator) to calculate the relative transmission for 1% $C_2H_2$with a 6cm path-length (micro-optic cell path length). All 16 acetylene lines observed experimentally correspond with the theoretical line positions allowing for a calibration error on the OSA wavelength scale of ±0.04nm..
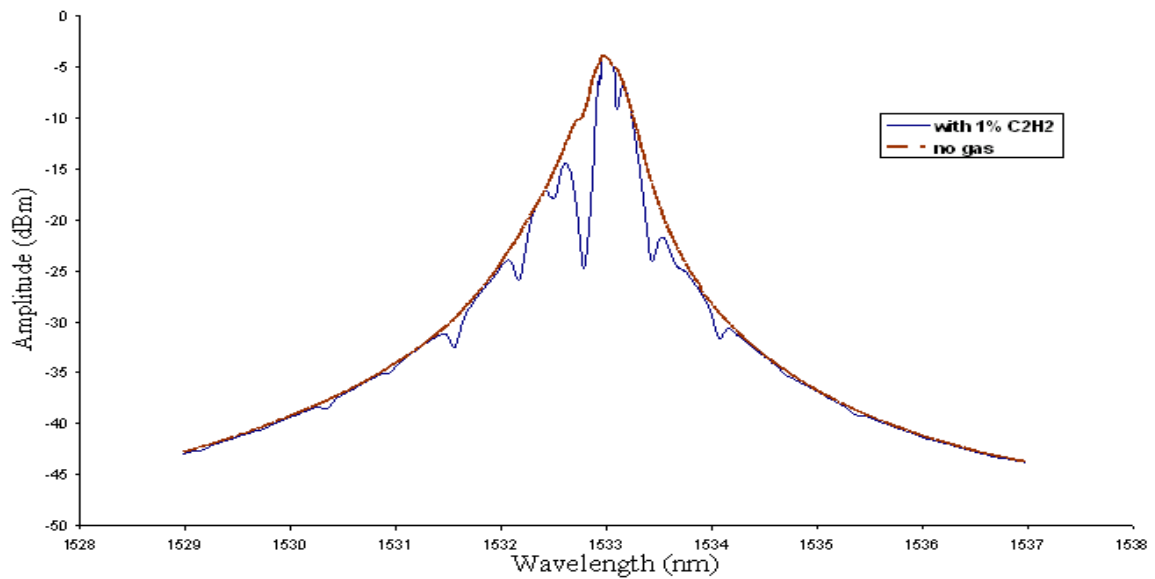
Figure 4.10: ASE spectrum with and without 1% acetylene gas
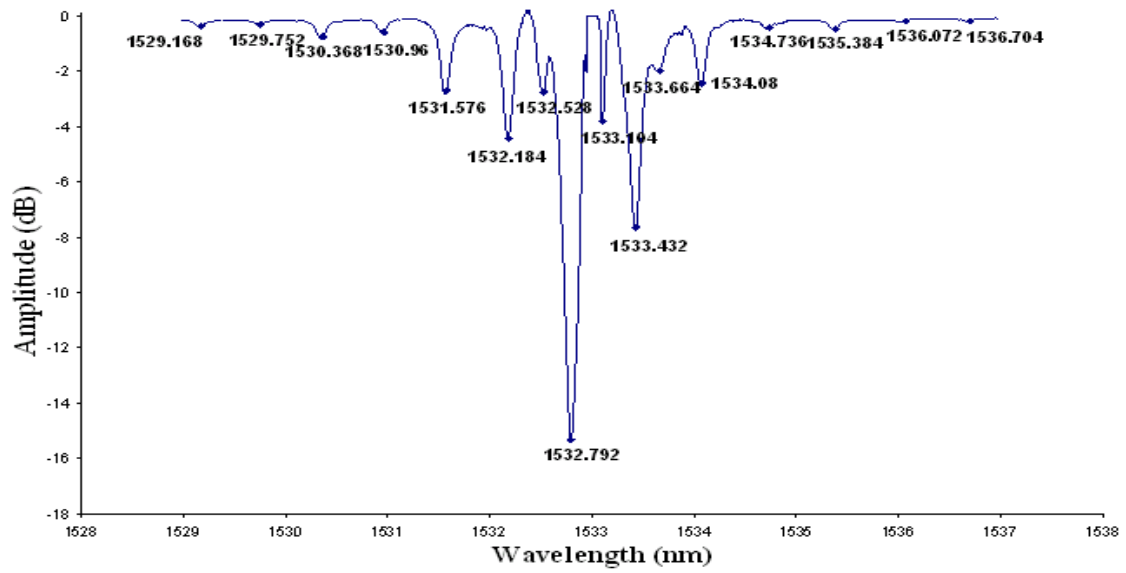
Figure 4.11: Experimental 1% C2H2 lines after background subtraction
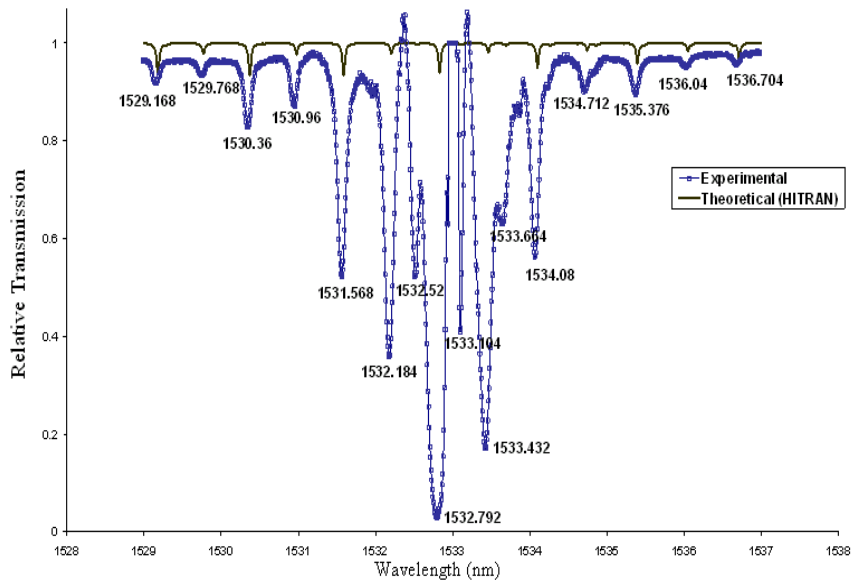
Figure 4.12: Experimental 1% C2H2 lines (relative transmission)

91
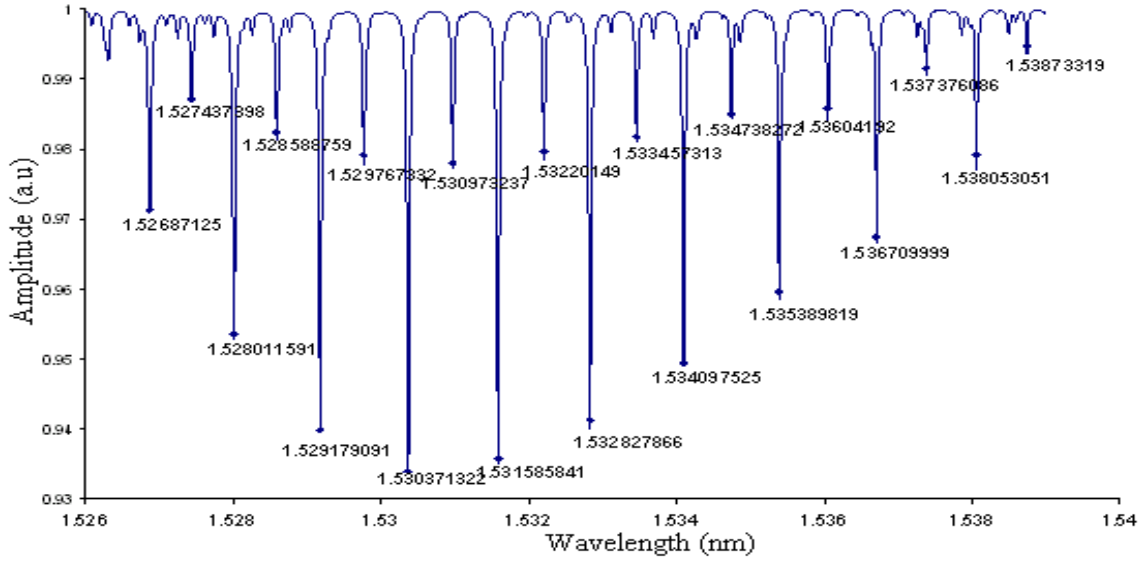
Figure 4.13: Absorption lines from HITRAN database for 1% acetylene gas using GATS Spectral Calculator with a 6cm path length

Among the lines depicted in the Figure 4.11, consider the path length enhancement for the central 1532.79nm line which corresponds to 1532.83nm in the HITRAN database. The experimental attenuation observed is ∼16dB at the line centre which translates to a relative transmission of 0.03 from equation (4.2) and as shown in Figure 4.12. Figure 4.13 shows that the theoretical relative transmission for this absorption line over a 6cm path length is 0.94 for 1% acetylene. Using these figures in Beer's Law, $P_{out}/P_{in} = exp[-\alpha(v)Cl]$, the theoretical line centre absorbance is: $A = \alpha Cl = 0.06$ while the experimental absorbance observed is: $A = \alpha Cl_{eff} = 3.5$. Since the gas concentration, C, and the absorption co-efficient,α, is the same for both cases, this means that the effective experimental path length, l_{eff}, is increased to 3.5m, an enhancement factor of ∼60 over the 6cm cell length. It is clearly evident from Figures 4.4 and 4.5 that the actual enhancement observed is very much dependent on how close the absorption line is to the lasing region.

Even better results are expected with improved flattening of the gain curve over the bandwidth, better flushing of C_2H_2 from the cell and a proper arrangement of the device to

reduce vibration.

4.4.5.2   Carbon Dioxide (CO_2)

Carbon dioxide (CO_2) is among the lowest line strength gases in the near-IR. However we can detect the gas with the ICLAS system here. Figure 4.14 shows the observed ASE spectrum in the 1532-1534nm region with 100% CO_2 and without CO_2 in the cell (the cell was filled with N_2 for the 'without gas' condition). Absorption lines can be seen from Figure 4.15 where the ASE background has been subtracted. However due to dampness and environmental humidity, there is also water vapour (H_2O) lines present in the result. The H_2O lines appear alongside the CO_2 lines in the figure. Figure 4.16 shows the theoretical data obtained from the HITRAN database 2008 for CO_2 in this wavelength region.
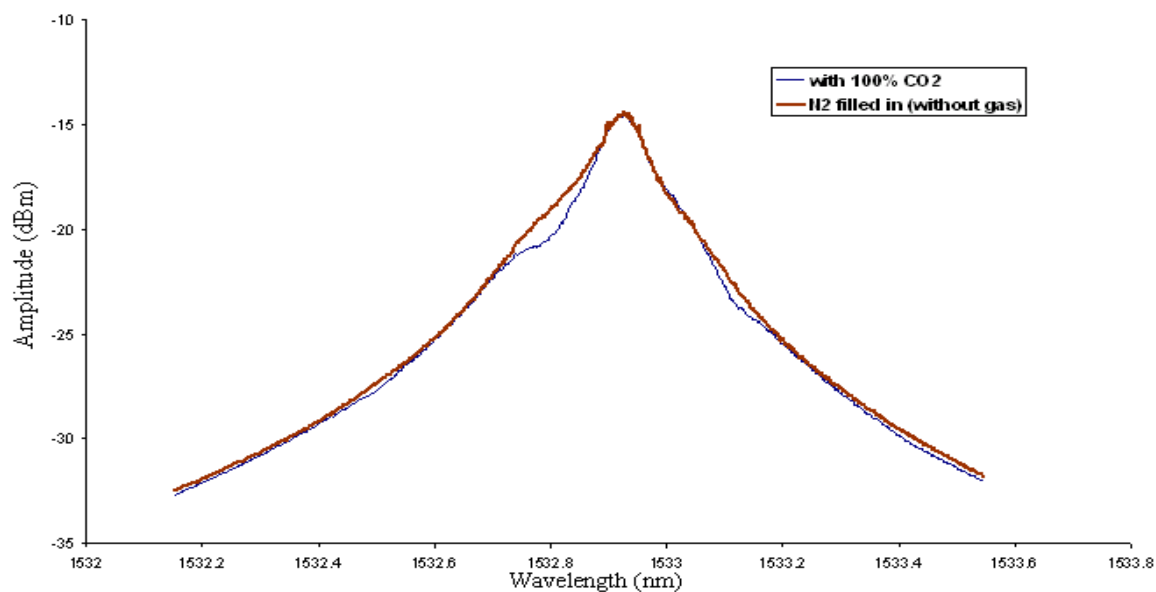
Figure 4.14: Measured ASE spectrum with and without CO_2 gas

93
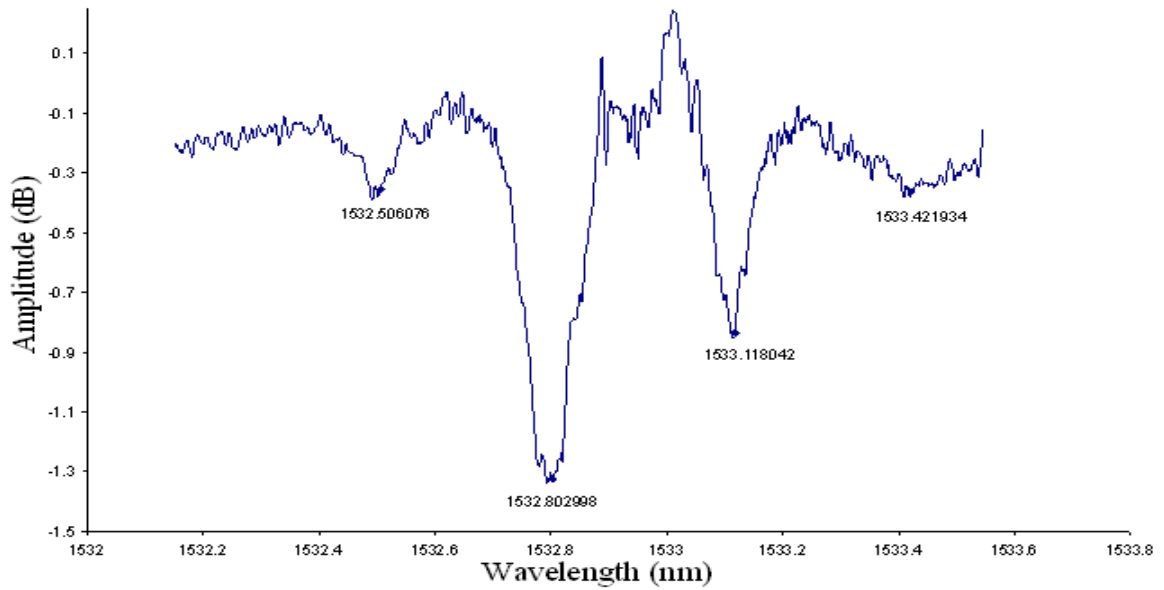
Figure 4.15: Absorption line spectrum with 100% of CO_2 gas
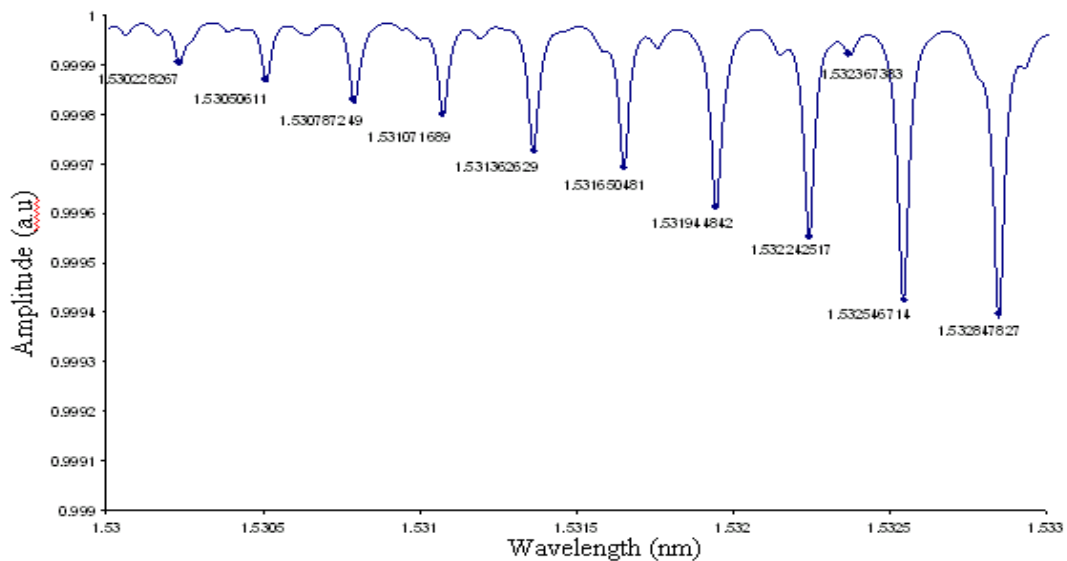
Figure 4.16: Theoretical absorption lines for CO_2 gas using GATS Spectral Calculator

For the weak CO_2 lines, the pump power setting is crucial as with low output power of the laser it is hard to detect the gas presence. This can be demonstrated through Figure 4.17 where low power was applied for this result.

94
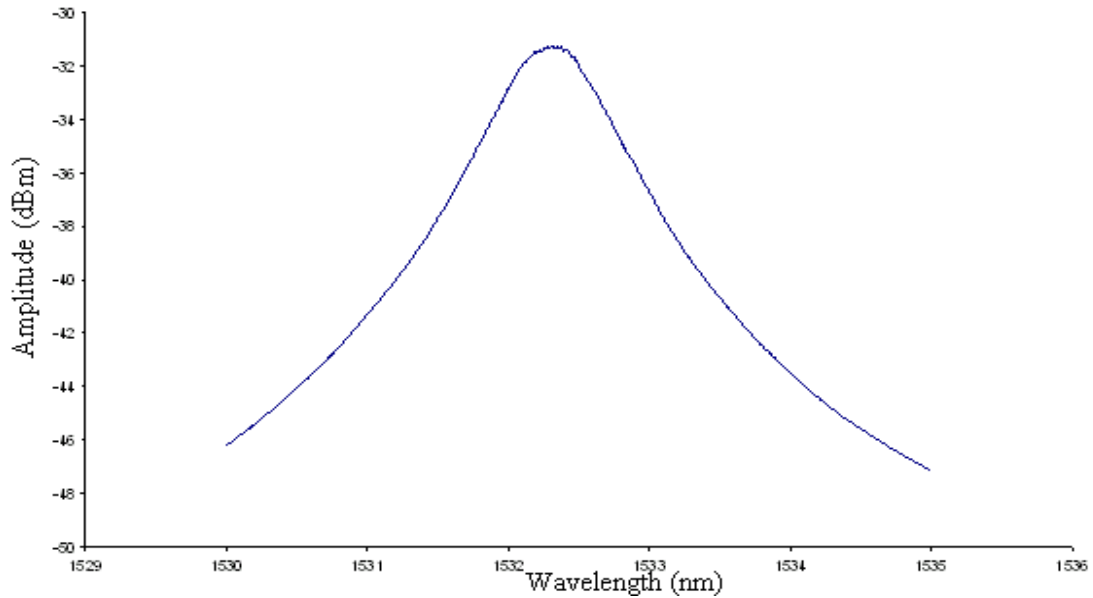
Figure 4.17: No lines can be seen around 1532nm with low output power

Weak CO_2 lines can also be observed at the longer wavelength region around 1555-1558nm as shown in Figure 4.18 taken from the Hitran database. Figure 4.19 show the measured ASE spectrum in the 1556-1559nm region with and without gas in the cell. Due to the low line strength of the gas, only very small dips can be observed in the ASE spectrum. Only two gas lines can be identified as shown in Figure 4.20 where the gas wavelengths are matched with the HITRAN 2008 database.
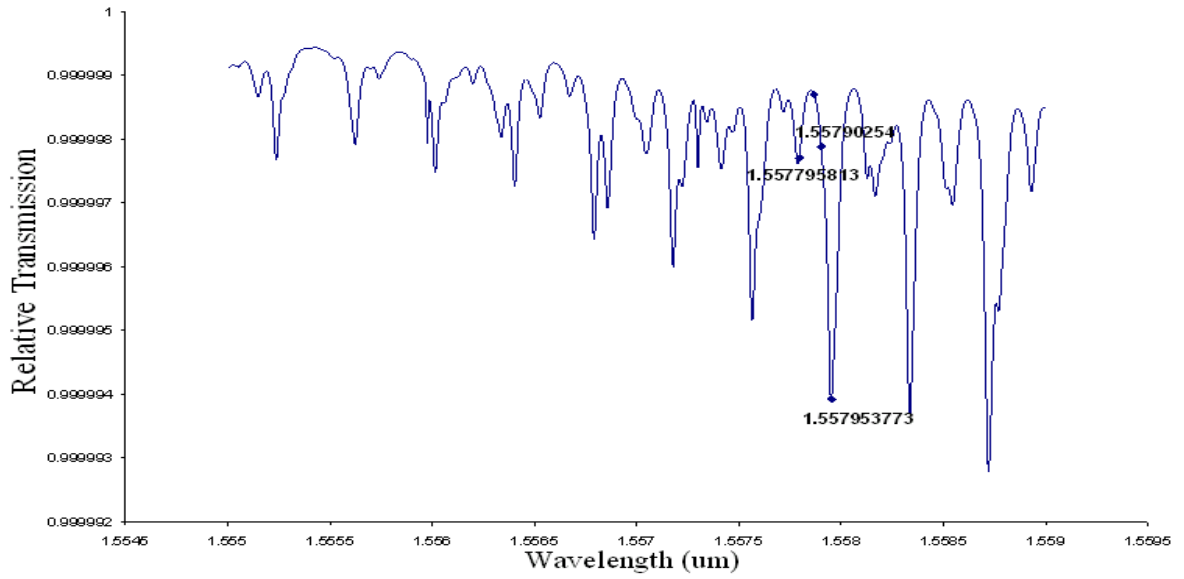
Figure 4.18: Theoretical CO_2 lines at wavelength of 1555nm-1558nm (HITRAN 2004)
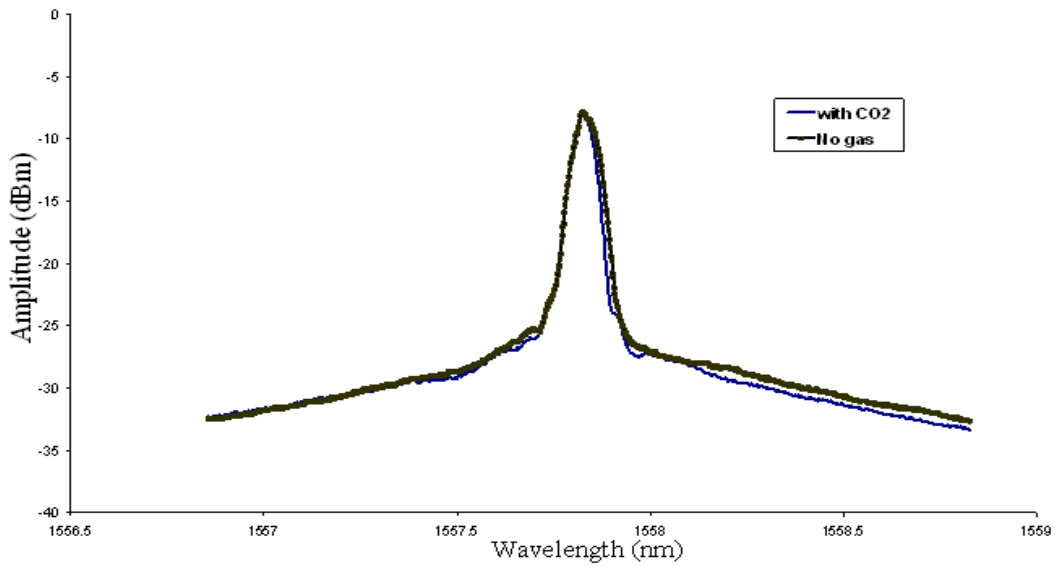
Figure 4.19: Experimental ASE spectrum with CO_2 gas (1556-1559nm) and without (N_2 in cell)
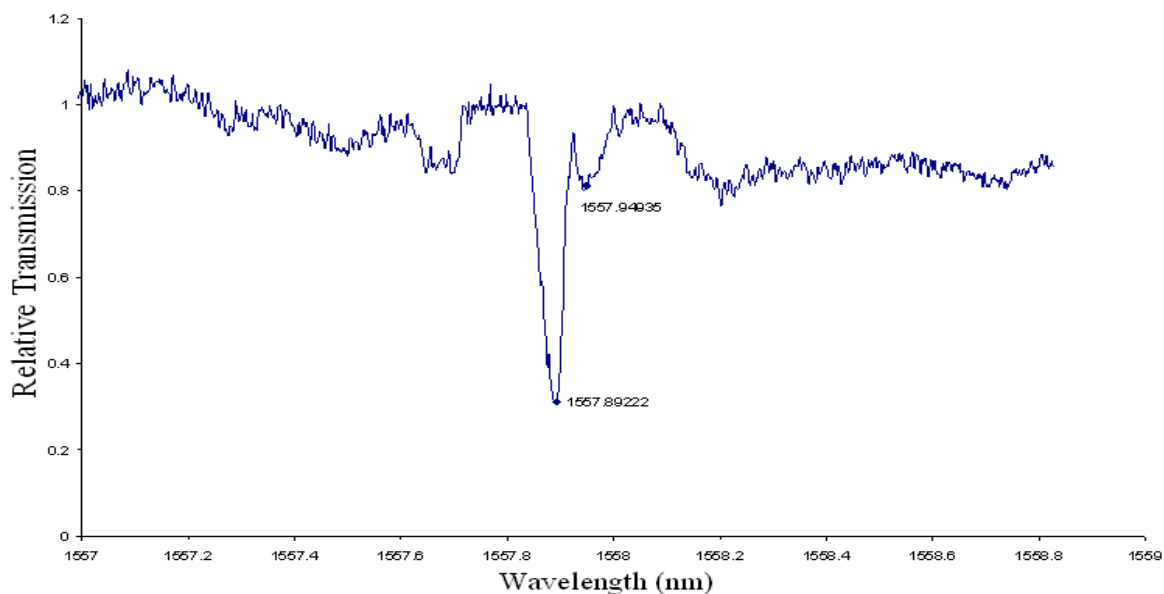
Figure 4.20: Experimental CO_2 lines over wavelengths of 1556nm-1559nm

4.4.5.3   Methane CH_4

Methane can be monitored through its relatively strong near-IR lines around 1650nm but this wavelength cannot be reached with the EDFL. However the HITRAN database indicates that there are several very weak methane lines in the 1530-1560nm region which require a few orders of magnitude enhancement in sensitivity to observe. Figure 4.21 shows the methane lines using GATS commercial software in this C-Band region.
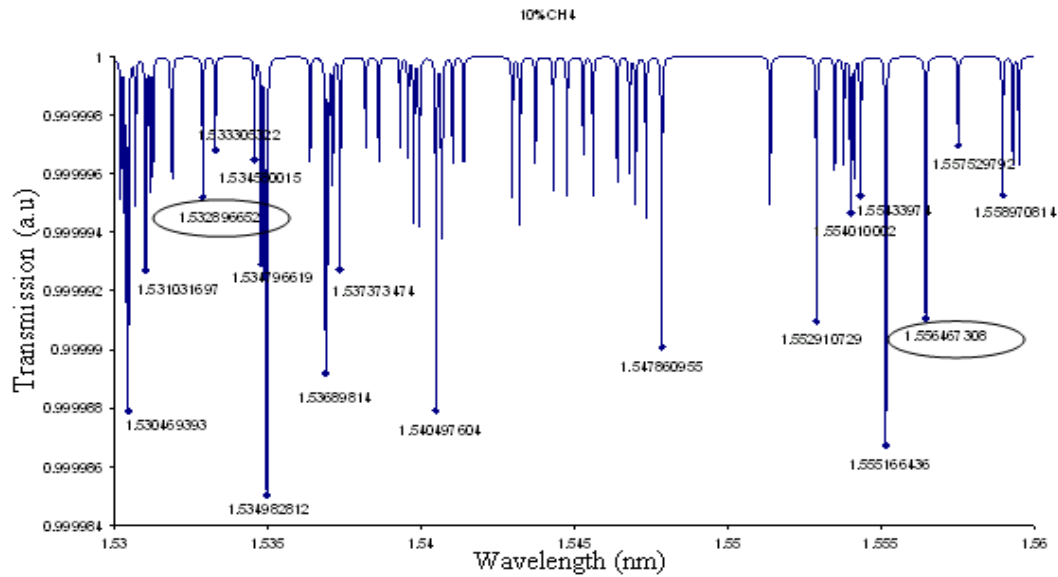
Figure 4.21: Transmission lines for CH$_4$ over the 1530 -1560nm region using GATS Spectral Calculator

The general trends of the experimental results agreed with the theoretical predictions. Only a few lines of CH$_4$ have been found in this area and water vapour lines also appeared due to humidity in the atmosphere and the very low line strength of CH$_4$. Sensitivity enhancement of nearly a hundred thousand with effective absorption path lengths of kilometres has been achieved.

Figure 4.22 and Figure 4.23 display the experimental results for the 1530-1535nm and 1555-1558nm regions respectively with 10% methane and Figures 4.24 and 4.25 show the methane absorption lines with the background subtracted by using a circle as indicator for the CH$_4$ lines. In Figure 4.24, a CH$_4$ line was found at 1532.889nm which is the only line obvious at the peak of the ASE spectrum and is well matched to the theoretical CH$_4$ GATS line at 1532.89nm with a sensitivity enhancement of 55083 times and effective path length of 3km. Referring to GATS, three lines of CH$_4$ can be found in the 1555-1558nm region, but due to the peak of the ASE being around 1556nm to 1557.5nm, only one methane line can be seen from Figure 4.25 at 1556.48426nm with an error of 0.018nm which gives an absorbance of 0.4

and a sensitivity enhancement of 44693 extending the 6cm cell path length to an effective length of 2.64km.
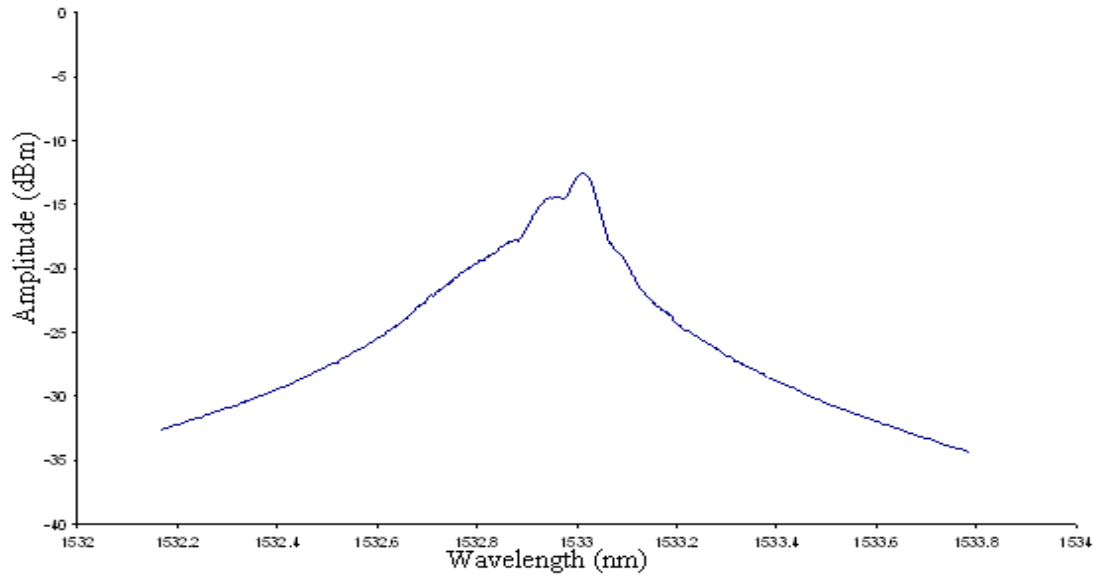
Figure 4.22: ASE spectrum with CH4 gas (1532-1534nm)
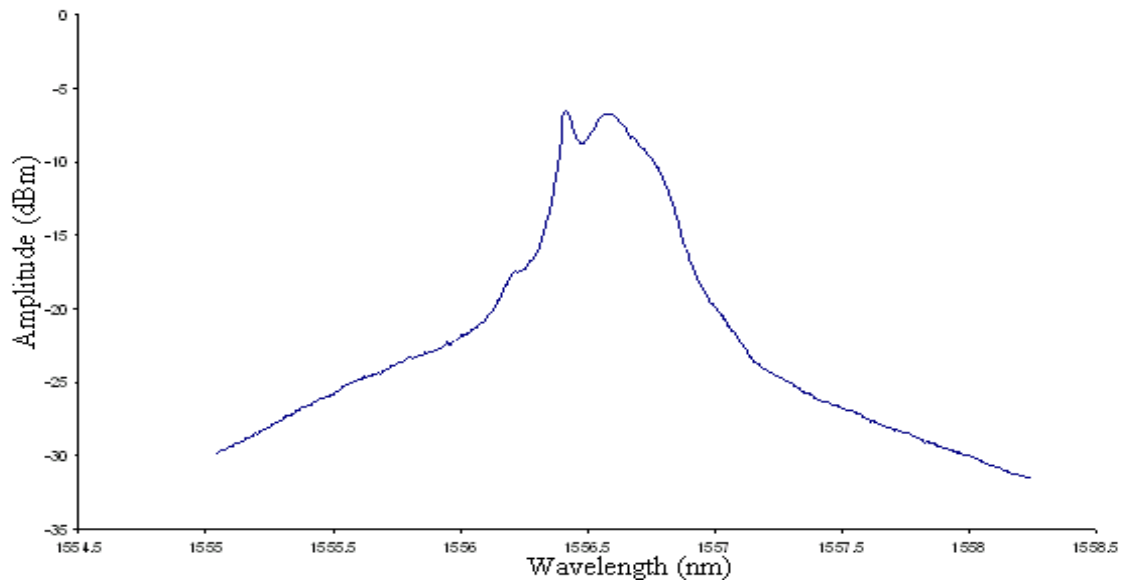
Figure 4.23: ASE spectrum with CH4 gas (1555-1558nm)
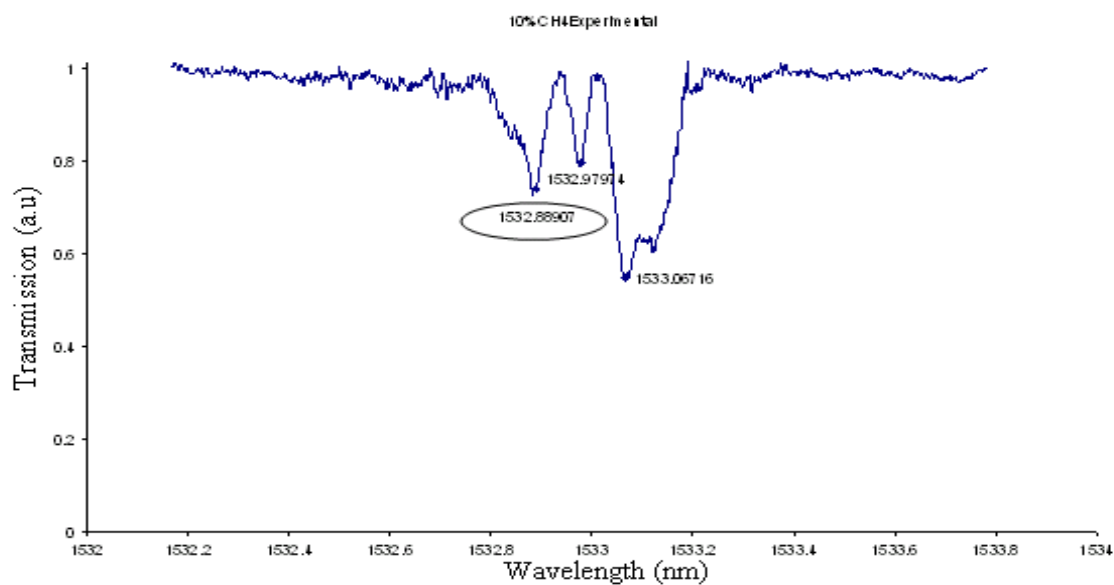
Figure 4.24: Experimental absorption lines for methane in 1532-1534nm region
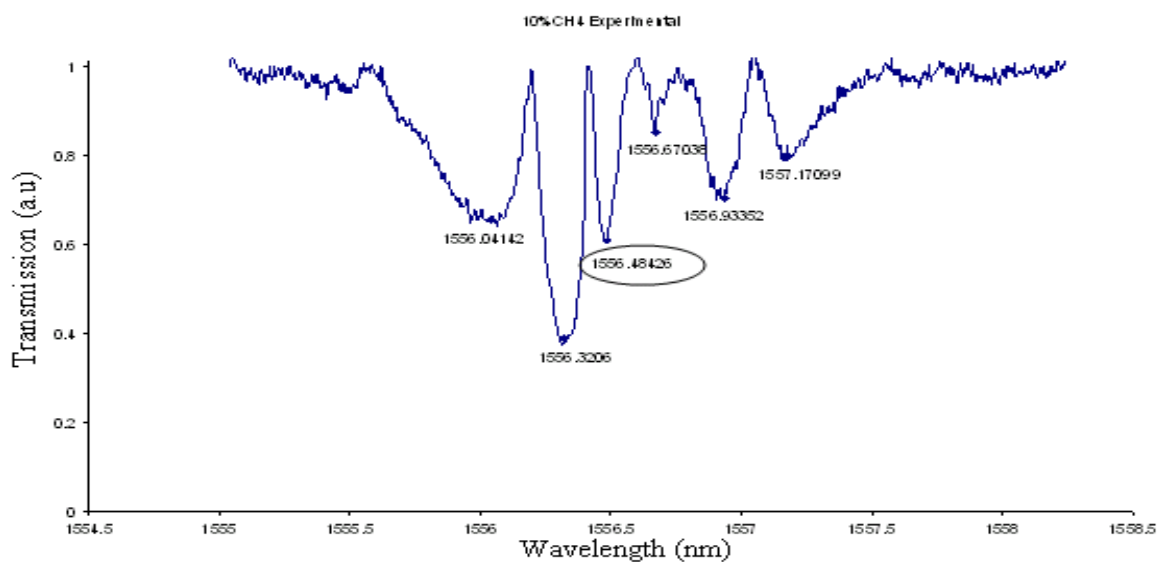
Figure 4.25: Experimental absorption lines for CH_4 gas at 1555-1558nm

4.4.6   Use of a Sagnac Loop Filter (SLF)

As noted, a flat gain curve is required for effective operation of ICLAS and this has been approximately achieved simply by appropriate choice of the inversion level as illustrated in Figure 4.1. However it would be desirable to have a flat curve over a selected wavelength region and to be able to adjust this region across the full ASE spectrum so that particular absorption lines could be selected. As explained earlier, a standard tunable filter (TF) is not suitable for this because it does not possess a sufficiently wide, flat-top pass-band region. As discussed in Chapter 3, a Sagnac Loop Filter (SLF) is simple to construct and has multiple pass-bands whose spacing/width may be adjusted according to the design of the filter (the pass-bands however do not have the ideal flat top).

4.4.6.1   Measurement of SLF characteristics

A SLF was inserted into the cavity but the insertion loss of the SLF was high, about 7dB, and so two EDFA units were cascaded (effectively increasing the length of the erbium doped fibre) so as to maintain a low inversion level. This gives operation up to 1570nm as illustrated in Figure 4.26.
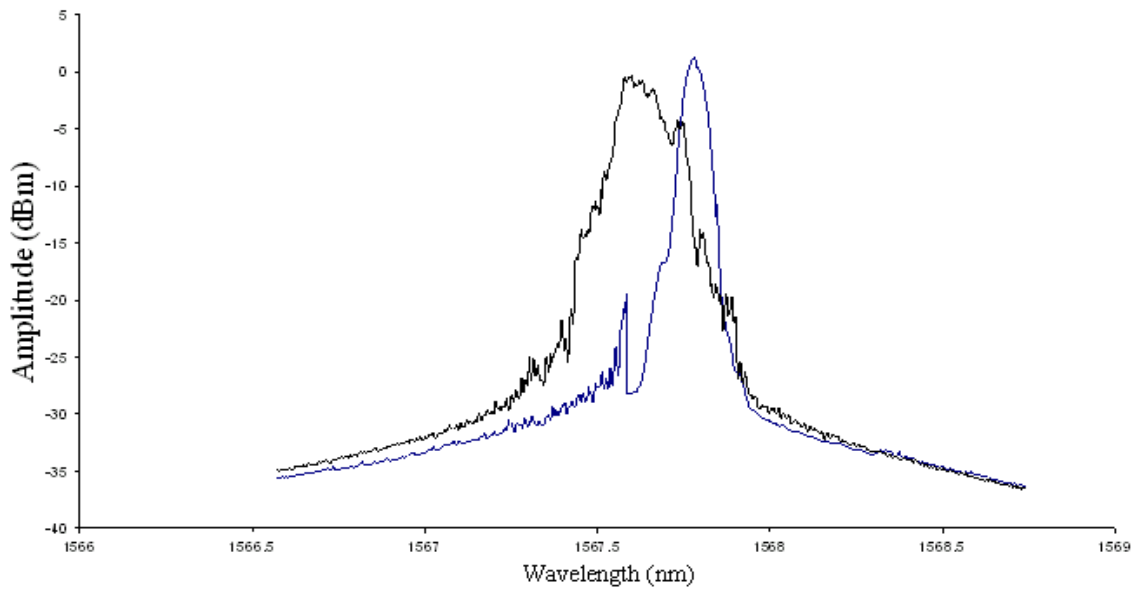
Figure 4.26: Signal is unstable at longer wavelength when tuning PC and SBL of the SLF

A shorter length of PMF used in the SLF gives a wider spacing between the transmission bands and a wider bandwidth for each band. Therefore short lengths of PMF (0.34m and 0.2m) were used and Figure 4.27 shows the tuning range obtained in the 1550-1570nm. Figure 4.28 displays the tuning in the 1530nm region. (The wavelength is tuned by the small birefringence loop, SBL, a component in the SLF – see Chapter 3). Thus, any desired wavelength can be selected through the SLF using the SBL. However, when the wavelength was tuned to longer wavelengths at 1570nm, the signal was unstable and distorted. This is due to the wide bandwidth of the filter tending to encourage mode hopping.
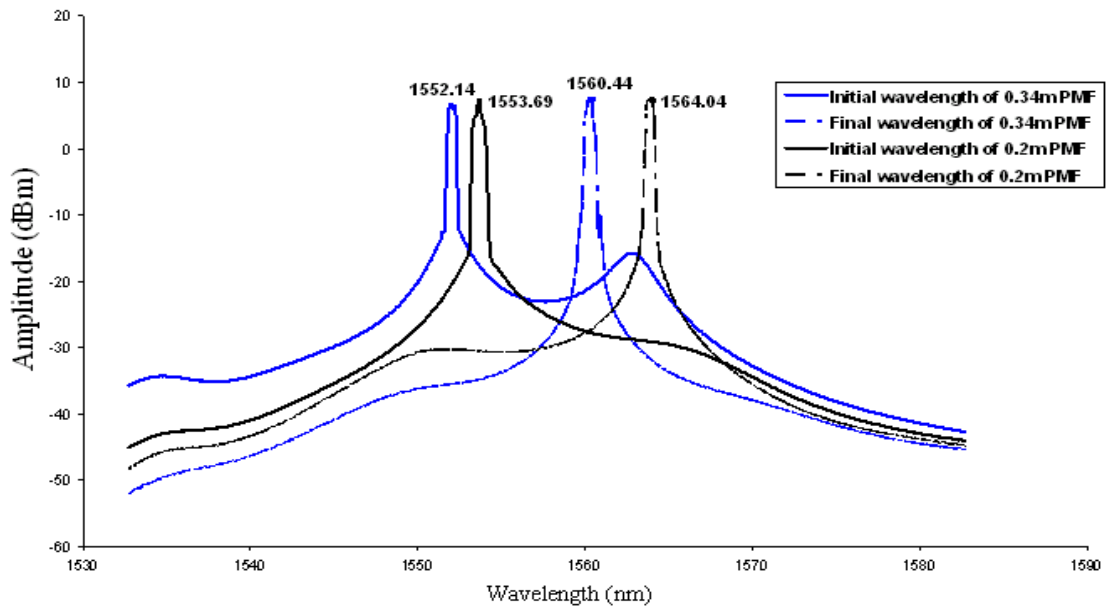
Figure 4.27: Tuning range over 1550-1570nm region for 0.34m and 0.2m of PMF in the SLF
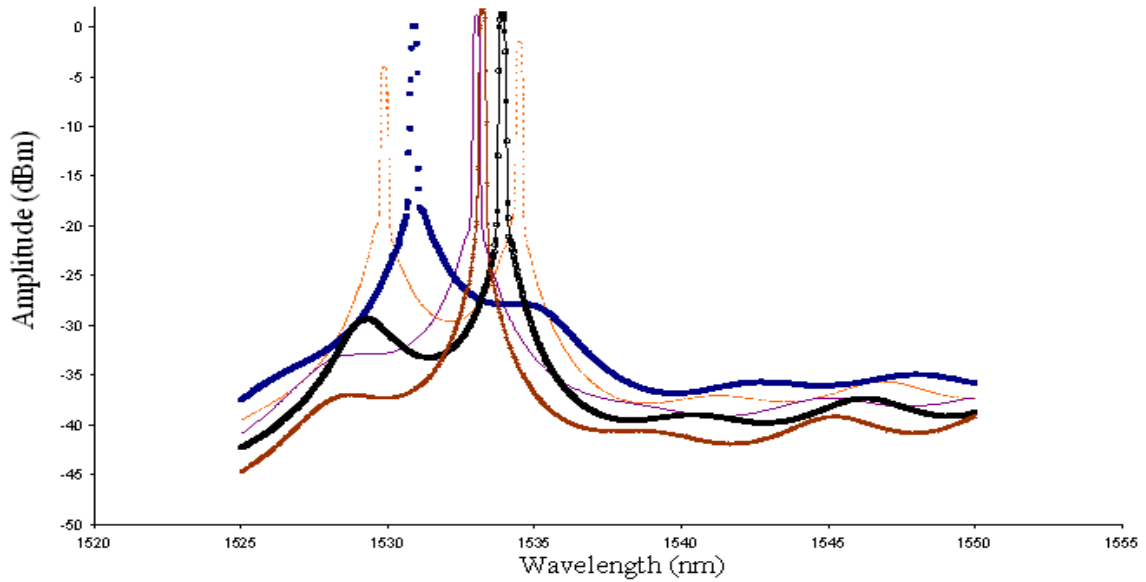
Figure 4.28: Tuning in the 1530nm region using the SBL

4.4.6.2 Gas Measurements with the SLF in the System

Tests were now performed on the system containing the SLF. Figure 4.29 shows experimental gas absorption lines observed on the ASE spectrum with acetylene gas in the cell with 0.34m long of PMF in the SLF. Figure 4.30 is the absorbance obtained by using Origin 6.1 software for background subtraction. Figure 4.31 shows that the wavelength can be tuned by the SBL of the SLF while Figure 4.31 depicts the effect of different settings of the variable attenuator (VA) which alters the inversion and gain curve in Figure 4.1. When the VA is decreased, higher output is attained with the lasing shifting to a longer wavelength. In Figure 4.32 shows shorter length of PMF used in the setup. The shorter the length of the SLF, the broader is the passband of the filter thus more lines can be seen on the ASE spectrum
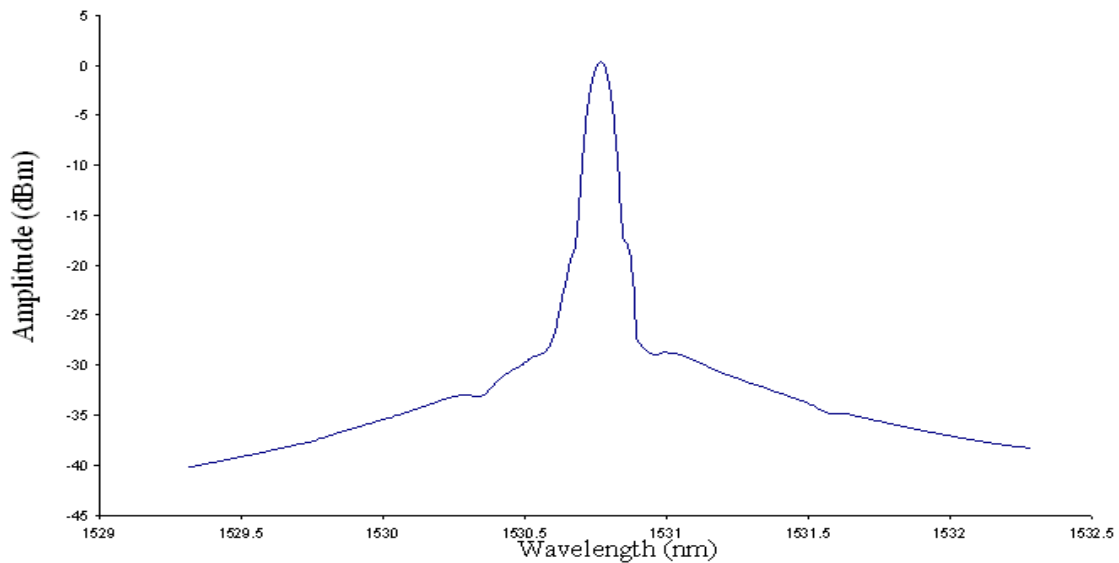
Figure 4.29: ASE spectrum with C_2H_2 gas (0.34m of PMF in the SLF)
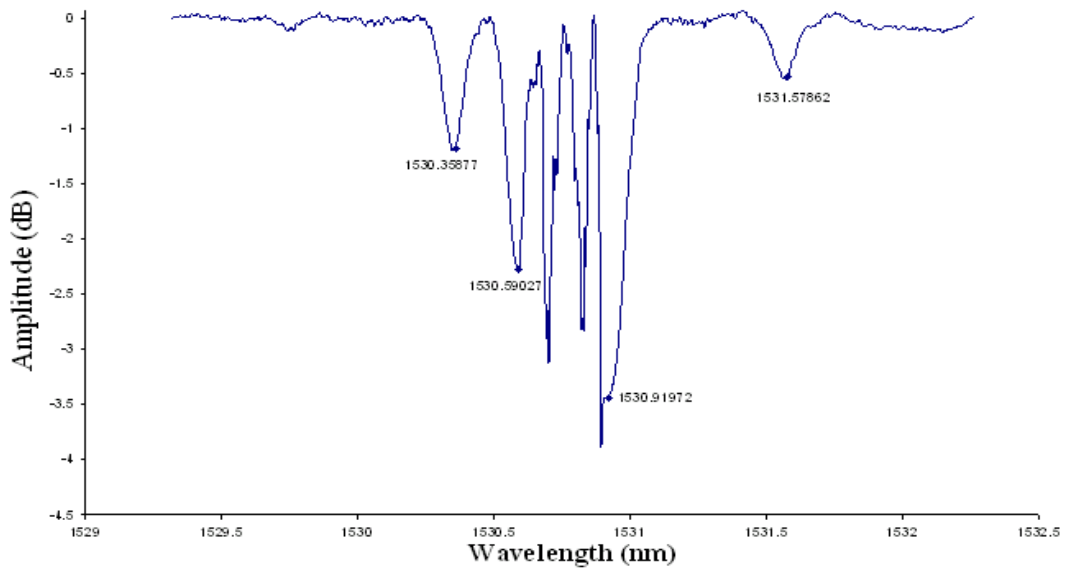
Figure 4.30: Absorption lines after background subtraction in Figure 4.29
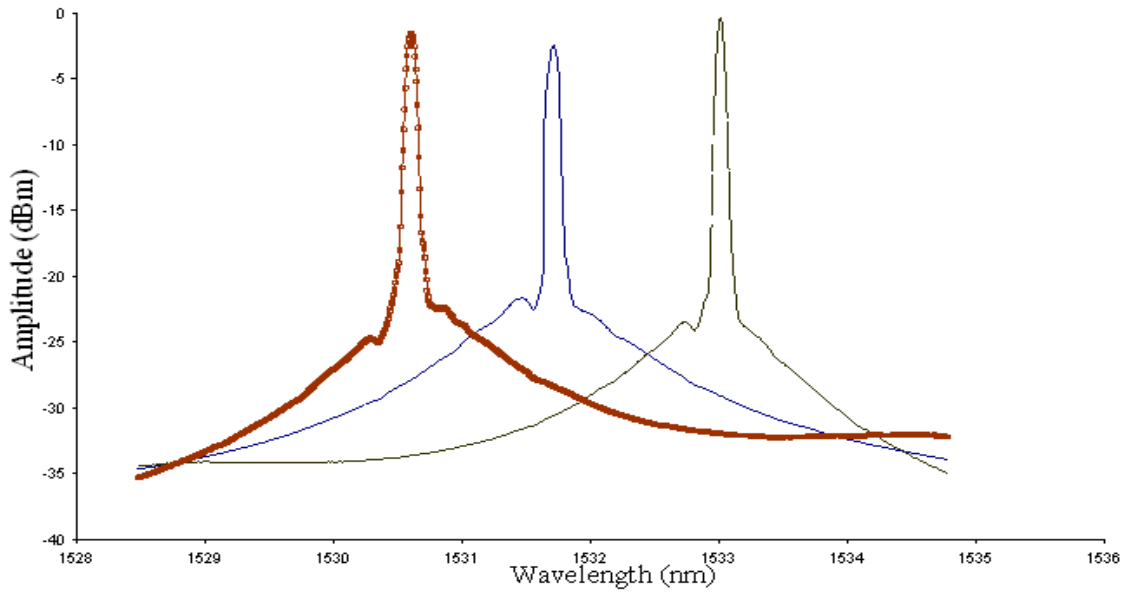
Figure 4.31: Different wavelength regions for lasing and ASE spectrum as the SBL is adjusted
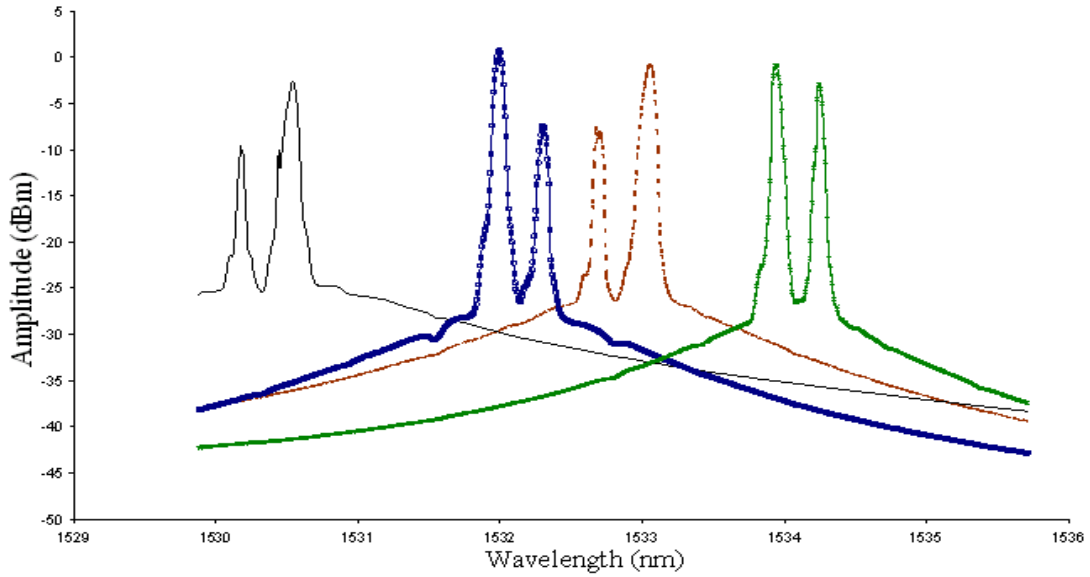
Figure 4.32: Different lasing wavelengths when the SBL is adjusted with 0.2m length of PMF

4.4.7   Effect of Saturable Absorber (SA)

In Chapter 3 we introduced the use of a saturable absorber section in the fibre laser cavity to improve stability and reduce mode hopping. Here we also investigated the use of a saturable absorber (SA) in the ICLAS cavity. As before, the SA section comprised of a three port PM circulator connected to a polarizer (PANDA fibre, 0.8m length), spliced to 2m of un-pumped polarization-maintaining erbium-doped fibre and a loop mirror as reflector.

Figure 4.33 presents the ASE output of the system when 1% C_2H_2 was filled in the cell. We found that the ASE signal is more stable with the SA and some of the gas lines also can be seen but with weak absorption. This is because the ASE near the lasing wavelength has less intensity (the SA section acts a grating filter) and a reduced circulation in the cavity resulting in only small absorption dips. Therefore, it is more difficult to trace a low line strength gas such as CO_2 and CH_4 using the SA.
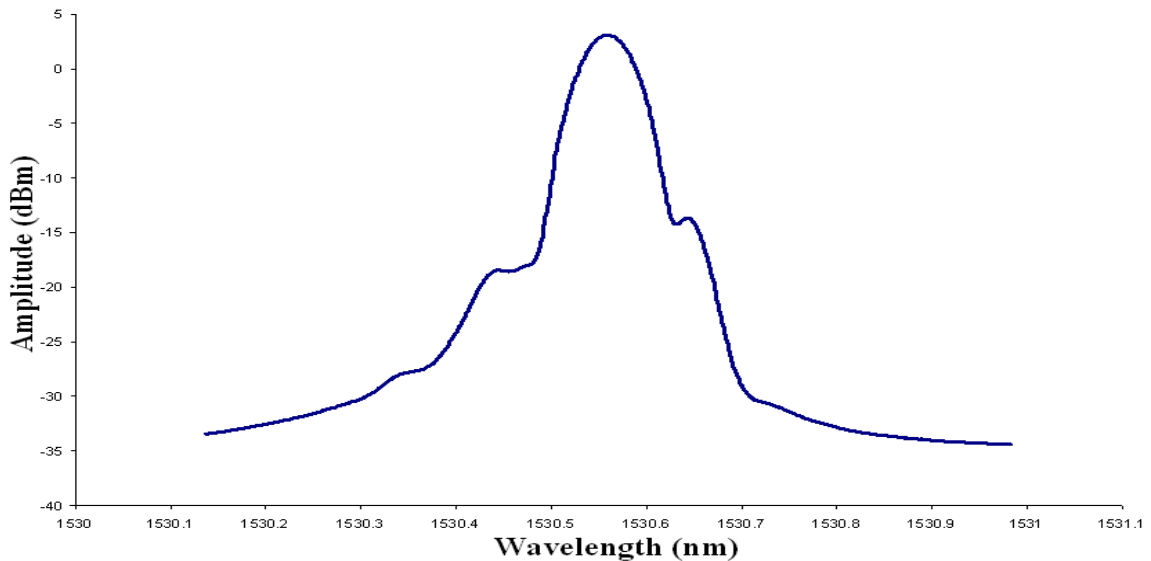
Figure 4.33: Output signal of using a SA in the cavity

4.5 Conclusion

In order to enhance sensitivity for detection of near-IR absorption lines, we have presented in this chapter a simple method of intra-cavity laser absorption spectroscopy (ICLAS) which makes use of the amplified spontaneous emission (ASE) already present within a fibre laser cavity. The ASE provides a convenient broad-band source for the interrogation of several gases within the gain-bandwidth of the fibre laser. The key principle of operation is based on adjusting the cavity attenuation to select an appropriate inversion level and hence flatten the erbium-fibre gain curve. Under this condition, the ASE undergoes multiple circulations within the cavity, enhancing the effective path-length of the micro-optic gas cell placed within the laser cavity. The effect of pump power and the use of wavelength filtering in the cavity to select particular regions of the ASE spectrum have also been investigated.

We have experimentally demonstrated system operation with several gases available in the lab such as 1% C_2H_2, 100% CO_2 and the very low strength lines of 10% CH_4. For 1%

acetylene gas, we have experimentally observed 16 absorption lines in the 1530nm region and a path length enhancement of $\sim$60, transforming the 6cm micro-optic cell into an effective path length of $\sim$3.5m. It was found that the system showed high sensitivity by detecting CO_2 and CH_4 which have very low strengths in the near-IR region. Results were compared with theoretical data from the HITRAN database.

Apart from the OSA, all components are inexpensive and the system is very simple to construct and is fully compatible with an all-optical fibre system. The results show that this technique is the most promising method so far for multi-gas sensing with fibre lasers and has the potential for the simultaneous detection of multiple gas species over a wide wavelength region of the C band where several near-IR gas lines are located.

For practical application, a calibration technique is needed and one method currently under investigation is the use of the weak etalon fringes from a simple intra-cavity etalon formed by reflections from the ends of a $\sim$1cm length silica glass or quartz rod placed within the micro-optic cell.

Chapter 5

DISTRIBUTED FEEDBACK FIBRE LASERS (DFB-FL) FOR SPECTROSCOPY

5.1 Introduction

The importance of this chapter is a demonstration of how knowledge can be transferred from optical fibre telecommunications to fibre optic sensing. Distributed feedback fibre lasers (DFB-FL), where a Bragg grating (with central phase shift) is directly formed within a short length of erbium doped fibre, are potential light sources in sensing due to their freedom from mode hopping. This gives single longitudinal-mode operation with a narrow line-width (typically <10kHz). This chapter presents the experimental setup of a DFB-FL system to study its characteristics and the effect of the design parameters. Optimisation of the system is also carried out to study its compatibility for spectroscopy applications. However, compared with conventional light sources, the advantages of the DFB-FL are outweighed by the high cost due to the early stage of development; hence this study focuses only on the feasibility of

109

using the DFB-FL in gas spectroscopy.

5.2 Review of DFB-FL

Lasing in periodic structures was first described by Kolgenik and Shank [75, 62, 76] who developed the theory of lasing action in periodic structures based on coupled-wave theory back in the early 70s. The DFB configuration then comprised of a laser in a uniform refractive index grating with constant amplitude and period in an active medium, operating with two longitudinal modes. The formation of permanent gratings in photosensitive germanium-doped fibres was then achieved by Hill [77, 75, 78] in 1978. The grating was formed by the interference pattern of ion laser radiation propagating in opposite directions in the fibre.

Significant advancement was established in 1989 by Meltz et al. [77, 79] through a holographic approach which involved exposing photosensitive fibre transversely to the interference pattern produced by two intersecting UV beams to produce the grating. This method was applied to erbium-doped fibre, as reported by Ball and Morey in 1992. Additional enhancement in grating writing techniques followed in 1993 from the introduction of phase masks as demonstrated by Hill and Anderson et al [75, 80, 81, 82].

Further on, Cole et al improved the phase mask method in 1995 by moving the fibre relative to the phase mask while the writing beam was scanning. The method greatly reduced errors in the grating and allowed flexibility for the production of complex grating structures. This is the mature Er-doped DFB fibre laser with permanent phase-shift technology [75, 83].

In 1997 Dong et al [75, 61] improved the DFB-FL by loading a boron- and germanium-doped photosensitive cladding surrounding the active phosphosilicate core doped with Er and Yb, thus boosting the laser efficiency. By the end of 1990s, Laurisden et al and Ibsen et al showed that a better cavity design would be composed of an optimum combination of grating strength and an asymmetrically positioned phase-shift so that the uni-directional

output power is the maximum. [75, 67, 84].

Currently, fibre grating fabrication techniques used for the feedback gratings in the lasers are holographic [75, 79] and phase mask approaches [75, 77]. For the fabrication of the phase shifted DFB-FL the uniform phase mask method is used, based on the moving fibre-scanning beam technique which allows the insertion of the phase shift into the fibre grating [75, 85].

So far DFB-FLs have been demonstrated in wavelength-division multiplexing (WDM) systems in which multiple optical signals are carried on a single optical fibre for a multiplication in capacity [86, 87, 88]. They have also been investigated for gas sensing application as reported by Simonsen et al. [89] who used the DFB-FL to perform WMS on CO_2 at 1578.665nm employing both thermal and PZT tuning. However they observed strong AM of the output induced by the strain modulation from the PZT modulation of the optical wavelength. This resulted in a large distortion of the measured output second harmonic signal.

5.3   Basic Operation of the DFB-FL

A DFB-FL consists of only one grating written into rare earth doped fibre and the lasing wavelength is determined by the grating wavelength. The lasing action is a result of two combined phenomena; signal generation by the active medium and feedback by the grating.

The theoretical analysis for the operation of the DFB-FL is based on coupled-wave theory where two counter-propagating waves are coupled via backward Bragg scattering from the periodic perturbations of the refractive index. As these waves travel in the periodic structure, they receive light along the path by Bragg scattering from the oppositely travelling wave. In this way, the feedback mechanism is distributed throughout the length of the periodic structure, entirely within the gain medium. Because of the gain, these waves grow and their energy is coupled into each other due to Bragg scattering. The gain media of the laser are

analysed using the atomic rate equations which have been discussed in Chapter 3.

5.4 Experimental Investigation of DFB-FL

Several types of measurement were taken during the initial experimental investigation of the DFB-FL such as steady state response, dynamic response, noise and linewidth measurements, temperature effects, pump modulation and wavelength tuning, in order to determine the DFB-FL characteristics.

The experimental arrangement used in this thesis for characterising the DFB fibre lasers is shown in Figure 5.1. A 980/1550 nm WDM was spliced to the 5cm long DFB-FL with a 980nm pump source (referred to as Pump1 or P1). The characteristics of the pump laser at 980nm are shown in Figure 5.2. The output transmission end of the DFB-FL is indicated as port 2 and the reflection end as port 1. A metre long pigtail of standard fibre with FC/APC connectors was spliced onto both ends of the DFB fibre laser to facilitate handling. The output of the DFB-FL was measured by several instruments to characterise the emitted light from the laser such as an Agilent 86140B Optical Spectrum Analyser (OSA), an Agilent E4443A 3Hz-6.7GHz PSA Series Spectrum Analyser (ESA) and a TecOptics Fabry Perot Spectrum Analyser (FPS) Other instruments used in the set-up included a LNP-2A OptoSci Low-noise photoreceiver, Exfo Optical Test System (IQ-200), a Tektronix TDS 784D 1GHz oscilloscope and a SR850 lock-in amplifier.
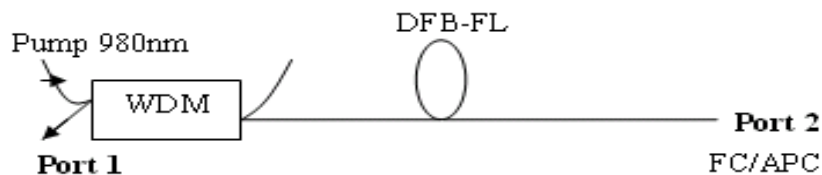
Figure 5.1: Experimental setup of the DFB fibre laser

From Figure 5.3 it can be observed that the output power rises linearly (as anticipated) for both ports as the applied pump power is increased according to the relation:

$$P = \eta(P_p - P_{th}) \tag{5.1}$$

where P is the laser power output of the system, η is the efficiency, P_p is pump power and is P_{th} threshold power. Figure 5.3 shows that the threshold power is $\sim 2.22\text{mW}$ in this case.
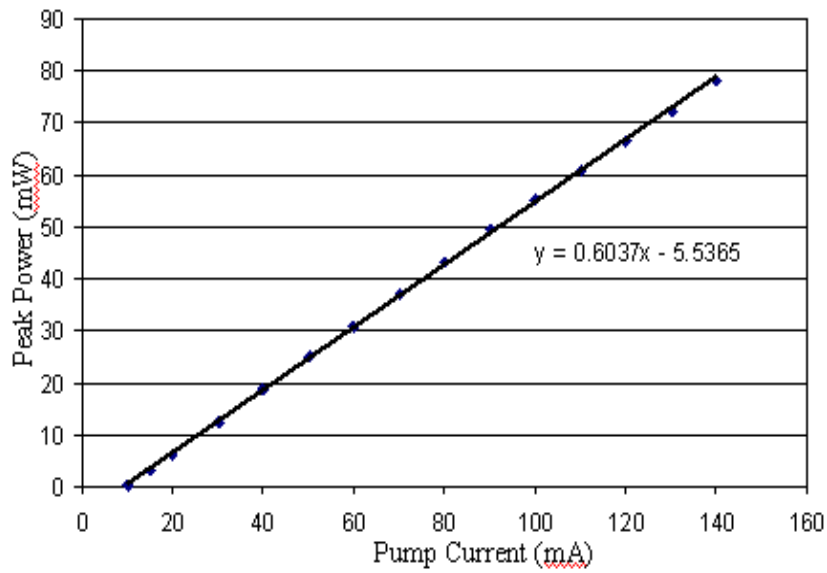
Figure 5.2: Pump power versus diode drive current for 980nm pump laser
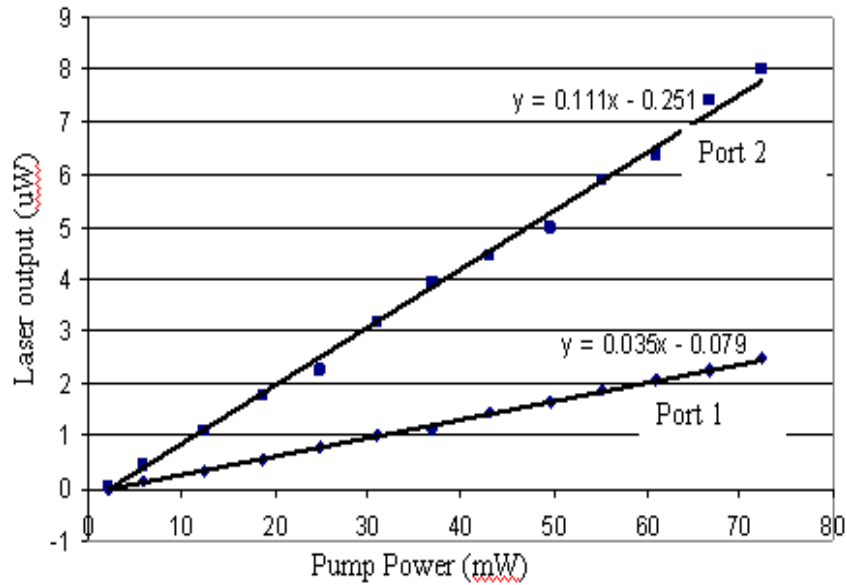
Figure 5.3: Output power of the DFB fibre laser from Port 1 and Port 2

Note that the laser output power of port 2 is higher than that of Port 1, for example, the output power for Port 2 was -21dBm or 8μW, whereas port 1 was -26dBm or 2.47μW at the centre wavelength of 1532.67nm for a pump power of 72.4mW.

5.5   Combination of the DFB-FL with a Power Amplifier EDFA (Amplified DFB-FL)

As was shown in Figure 5.3, the output power of the DFB-FL is in the microwatts range and so an EDFA unit was inserted in the setup to increase the output power. Figure 5.4 shows the combination of the DFB-FL and the EDFA whose input pump is marked as Pump2 or P2 in Figure 5.4. The DFB-FL output reached $\sim$ 5mW output with 50mW applied to Pump1 (P1) and Pump 2 (P2) set at 70mW. Figure 5.5 shows the response for different values of P2 against P1.
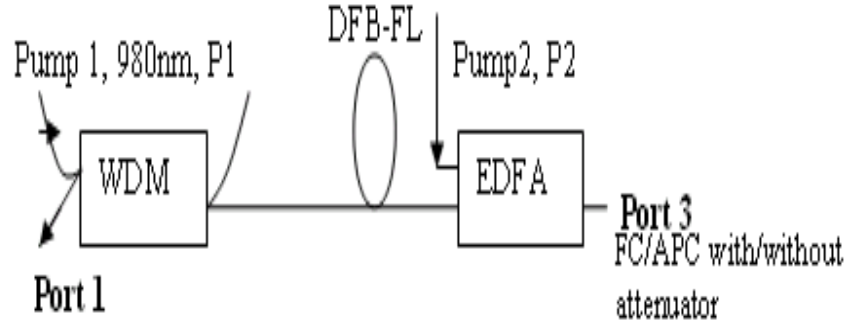
Figure 5.4: Combination of the DFB-FL and the power amplifier arrangement
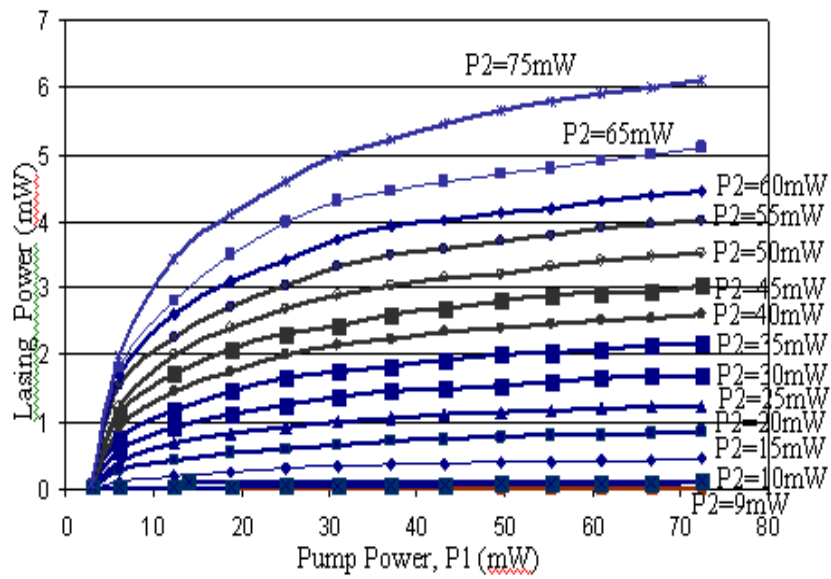
Figure 5.5: Power output versus pump power, P1 with various values of P2

5.5.1 Attenuation Effects

An Exfo Optical Test System (IQ-200) which contains a variable attenuator and a power meter was used to quantify the effect of attenuation. This is important in order to know the sensitivity of the DFB-FL system including the EDFA for future measurement of absorption

lines. The measurement setup is depicted in Figure 5.6 and the effect of attenuation on the power output is displayed in Figure 5.7. (70mW for P1 and 10mW for P2 were chosen to avoid saturation of the photoreceiver). It was found that 0.01dB loss change could be detected with the system.
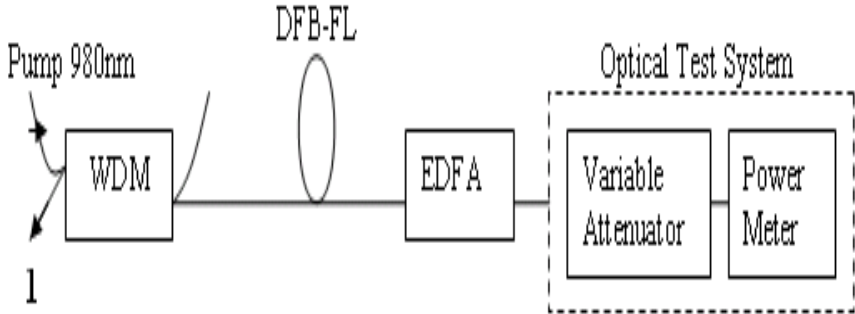
Figure 5.6: Set-up for loss measurements with the DFB-FL and EDFA
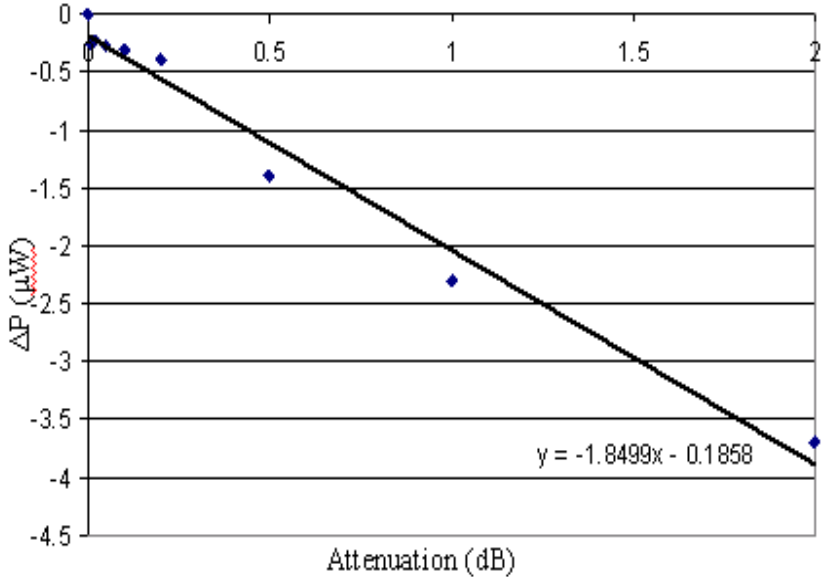
Figure 5.7: Effect of loss on the output power

116

5.5.2   Relative Intensity Noise (RIN) Measurements
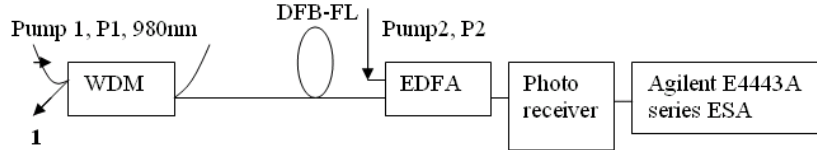
Figure 5.8: Measurement of the RIN of the DFB-FL with EDFA

Figure 5.8 illustrates the setup using an ESA for RIN measurement. Figure 5.9 shows an example of the spectral range of the RIN at a P1 of 25mW and P2 of 10mW, which shows the relaxation oscillation frequency at 165 kHz with a noise of -45.51dB/Hz. Even though this is not the exact RIN value, as extra calculation is needed to deal with the scaling factor used with the instrument setting, the relaxation oscillation frequency is in agreement with the result of the transient response in section 5.5.5 which will be discussed later. Relaxation oscillations reveal important information on the speed with which the system responds to perturbation of the population inversion level.

Figure 5.10 shows the relationship between relaxation oscillation frequency and the input pump power. As expected a linear trend is obtained when the square of the frequency is plotted versus the pump power.

P_{th} is 2.22mW from the graph of Figure 5.10, and using equation 3.12, t_c(cavity lifetime) may be calculated as 1.07ns, assuming $\tau_0 = 10ms$,

Theoretically t_c may be calculated as $t_c = \frac{(4.34)}{\alpha_c + \alpha_q l} = 1.042ns$ where $\tau = \frac{2n_e l}{c} = 0.48ns$ is the round trip time of cavity for $l = 50$mm and $\alpha_c + \alpha_q l \approx 2dB$.
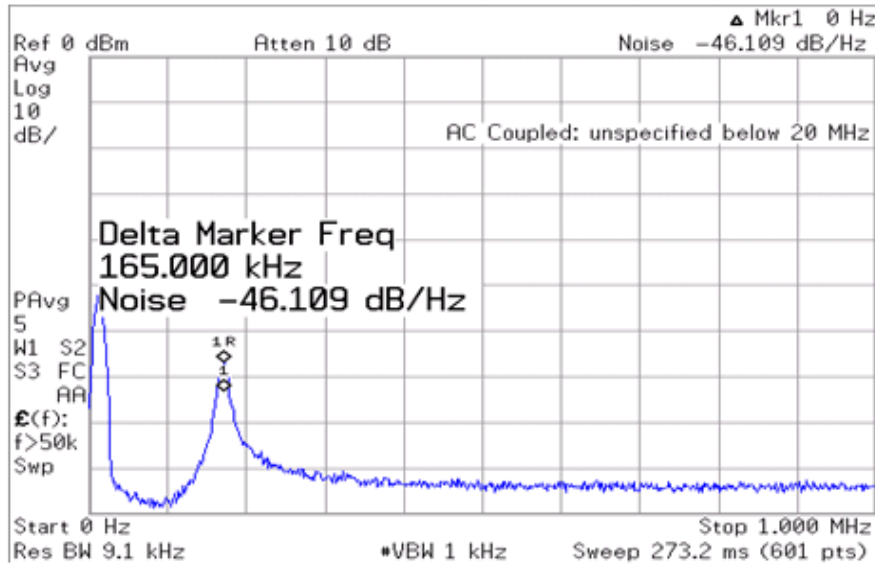
Figure 5.9: RIN at P1 of 25mW and P2 of 10mW
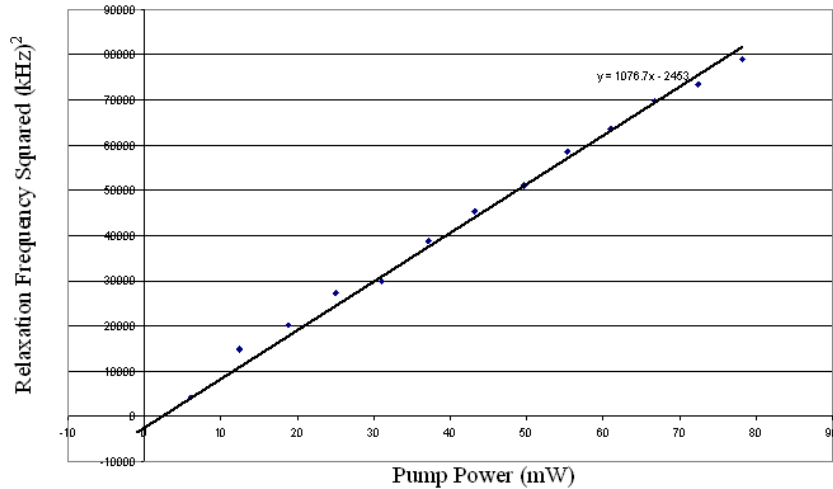
Figure 5.10: Relaxation frequency squared versus pump power, P1, for P2 of 10mW

5.5.3   Linewidth Measurements

Figure 5.11 shows experimental setup to obtain the laser linewidth using the Fabry Perot Spectrometer (FPS) by setting P1 to 72.4mW (130mA) and P2 to 25mW.

118
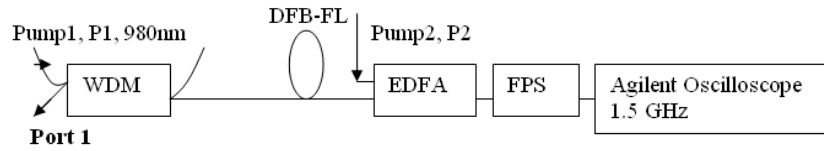
Figure 5.11: Experimental setup to measure the laser linewidth

In principle, a Fabry-Perot cavity supports many frequency modes with frequencies, v_m, given by requiring standing waves within the cavity. Since the mode m_{th} mode obeys $m\lambda = 2nL$, where n is the refractive index experienced by the mode, then $v_m = \frac{mc}{2nL}$. The frequency difference between modes is $\triangle v = \frac{c}{2nL}$ [71].
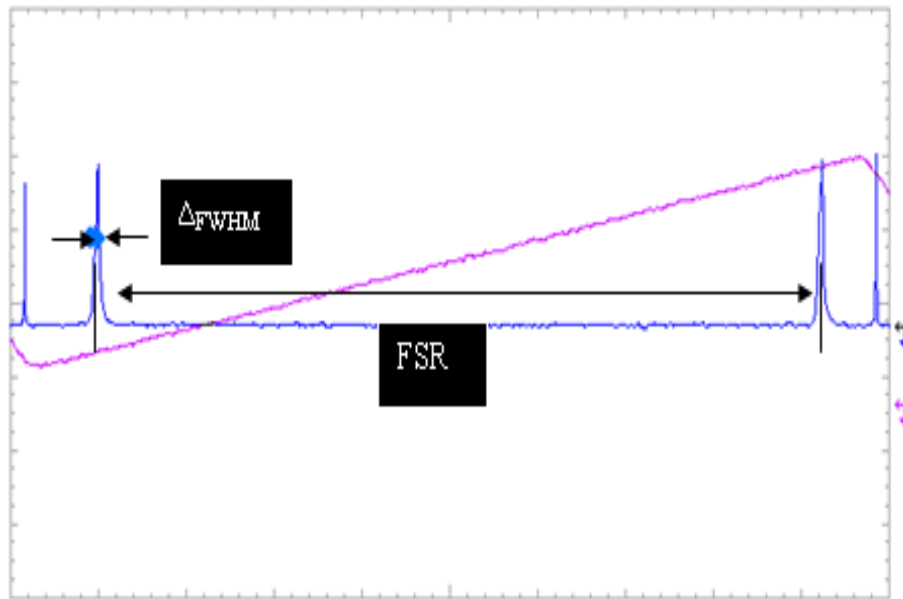
Figure 5.12: Output of Fabry Perot spectrometer showing single mode repeated at the FSR. The lower trace shows the change in length of the FP

The DFB-FL output was observed on a 1.5 GHz Agilent Infiniium Oscilloscope as depicted in Figure 5.12 which shows the recorded spectrum of the single mode laser. Two peaks can be seen from the oscilloscope trace. Since the distance between two similar peaks is known as the free spectral range (FSR), their difference in frequency can be measured precisely. The

119

free spectral range (FSR) of the Fabry Perot spectrometer (FPS) used was 300 MHz with finesse of 301 which is the highest resolution available in the lab.

From the experimental trace of Figure 5.12, the time scale corresponding to the FSR is $\triangle t = 8$ms and the FWHM width of the laser mode is $\triangle_{FWHM} = 46$ μs, giving the FWHM linewidth as:

$$\triangle v = \frac{FSR}{\triangle t} . \triangle_{FWHM} = 1.725 MHz \tag{5.2}$$

From the DFB-FL datasheet, the linewidth is less than 10 kHz. However the resolution, R of the FPS only allows a minimum of linewidth of 1MHz to be measured which is calculated through equation 5.3:

$$R = \frac{FSR}{Finesse} \tag{5.3}$$

5.5.4   Temperature Effect on Pump Laser

For the pump laser, the dependence on the operating current also includes temperature effects, since a larger operating current also heats up the laser. A thermistor is the temperature sensing element in the pump laser module. It provides excellent wavelength stability for the laser module, when the laser is held at constant temperature using the thermistor feedback. The thermistor resistance, R is inversely proportional to temperature, T, by equation (5.4) [90]:

$$T(°\mathcal{C}) = [\frac{3892}{ln(R(k\Omega)/2.142 * 10^{-5})}] - 273.15 \tag{5.4}$$

Temperature was increased gradually from 20 ° C to 30 ° C to see the effect of the temperature of the pump laser on the output wavelength of the DFB-FL. It was observed, as shown in Figure 5.13, that a small shift of $\sim$ 0.01nm in the lasing wavelength occurred,

$\sim 0.001 \text{nm}/°\text{C}$, which is tolerable for measurements on pressure broadened gas absorption lines where the line-width is $\sim 0.05 \text{nm}$.

However, the wavelength of the DFB-FL depends strongly on the DFB fibre's temperature and this will be discussed in detail later in this chapter.
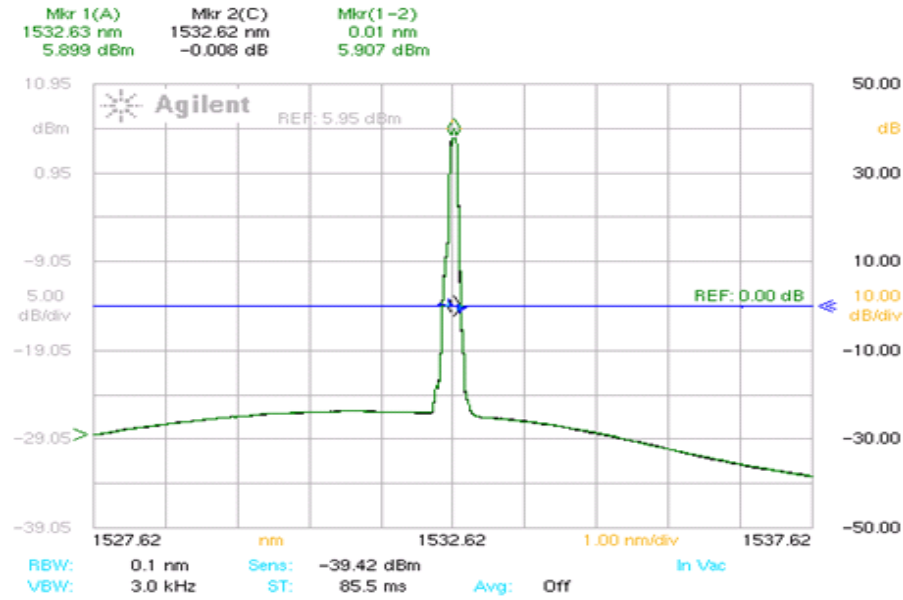
Figure 5.13: Effect of temperature on the operating wavelength of the DFB fibre laser

5.5.5 Dynamic Response

The set-up to measure the dynamic response of the DFB-FL system is shown in Figure 5.14. A square wave of frequency (0-100kHz) from a signal generator was used on P1 for pump modulation, with a positive dc offset to maintain the peak-to-peak value between 0 to 5 V at the input and P2 was set to 10mW to prevent saturation of the photoreceiver.

Figure 5.15 shows the time delay between the launch of the pump power (t_0) and start of laser spiking (t_b) using a 100 Hz square wave with amplitude of 500mVpp on the signal generator. It was observed that at the pump power of 6.04mW, the build-up time was 0.347ms.

121
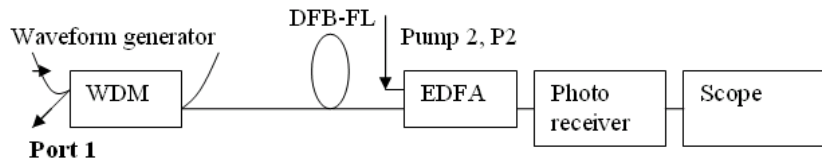
Figure 5.14: Transient Response Measurement Setup
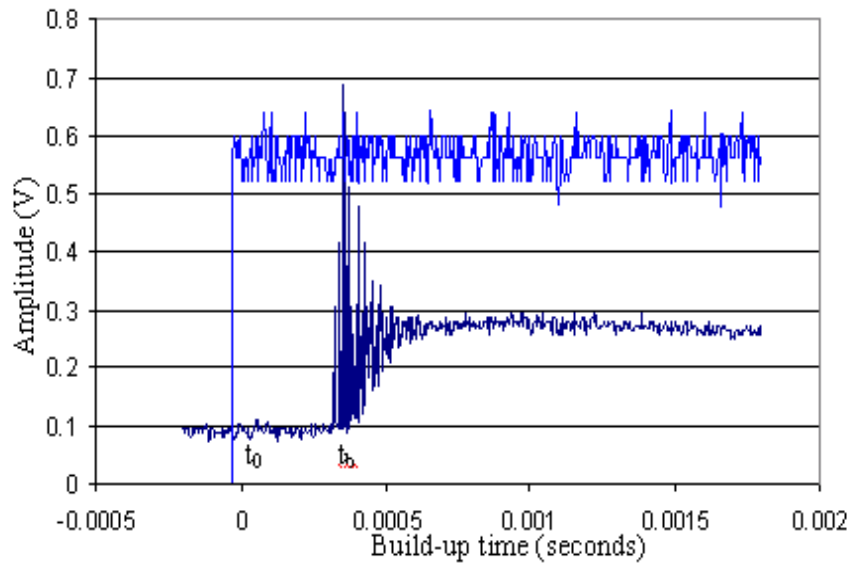
Figure 5.15: Time Delay between the launch of pump power (t_0) and start of laser spiking (t_b) with 100Hz, 500mVpp square wave (6.04mW for Pump 1 and 10mW for P2)
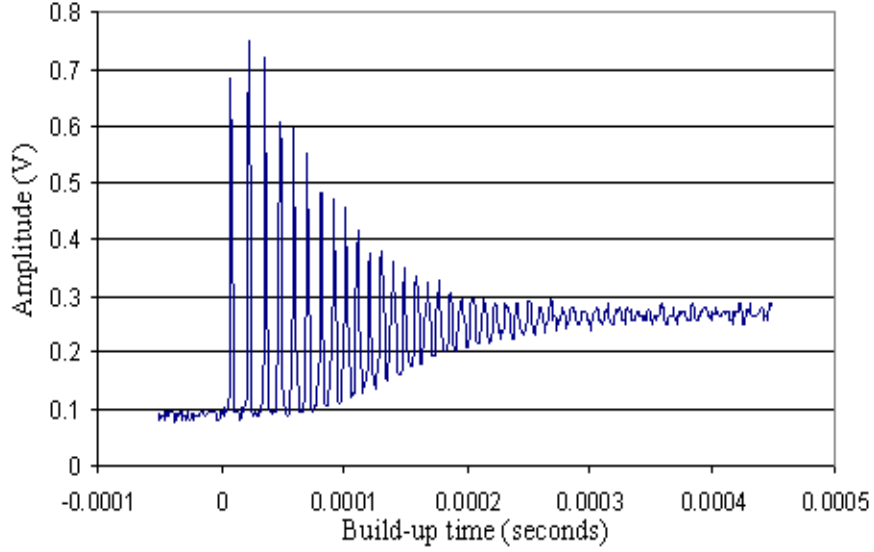
Figure 5.16: Relaxation oscillations of DFB-FL

After the build up time and before the steady state, the actual transient response can be observed by zooming-in on the time axis of the oscilloscope. The transient peaks follow a decaying oscillatory pattern before the output stabilised to its steady state, as shown in Figures 5.15 and 5.16.

As noted the experimental build-up time $(t_b - t_0)$ from Figure 5.15 is 0.347ms. Theoretically, the build-up time can be calculated from

$$t_b - t_0 = \tau_0 In(\frac{P_{in}}{P_{in} - P_{th}}) \tag{5.5}$$

where $P_{in}=$ P1 is 6.04mW, P_{th} is 2.22mW and τ_0 is 10ms to give a value of 4.2ms for the build-up time.

The value of the build-up time obtained from the experiment is very different from the theoretical value computed from equation 5.5. However equation 5.5 is based on the approximation of good pump power absorption. It is expected a large percentage of the input pump power is not fully absorbed due to the short length of DFB fibre (only $\sim$ 5cm).

123

From Figure 5.16, the relaxation oscillation frequency is ~175 kHz for P1 of 25mW. This is similar to the result obtained in the RIN section.

5.5.6   Pump Modulation

The characteristics of the DFB-FL system with pump modulation was investigated by applying a sinusoidal modulation to the pump current. As with the EDFL ring lasers, this allows the use of phase-sensitive detection (PSD) in order to increase the signal to noise ratio in measurements of attenuation or absorption lines.

Figure 5.17 displays the experimental setup with a Lock-in Amplifier (LIA) SR850 using a frequency reference from the waveform generator used to modulate the pump current.
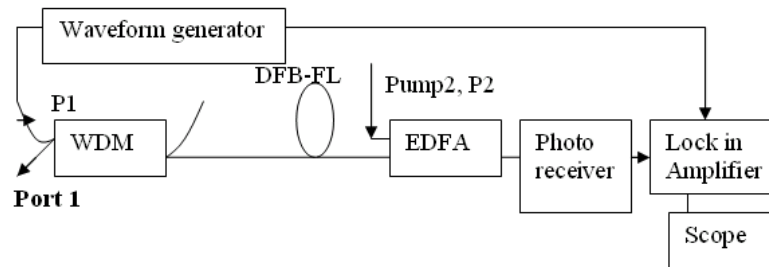
Figure 5.17: Pump modulation of the DFB-FL

A variable attenuator was connected into the system in order to measure the sensitivity to changes in loss. The effect of attenuation on the lock-in output can be seen in Figure 5.18 where 10kHz frequency was used for the measurement. As expected the LIA's output decreases when the attenuation was increased. The DC output of the lock-in could be increased by increasing the gain (P2) of the EDFA.
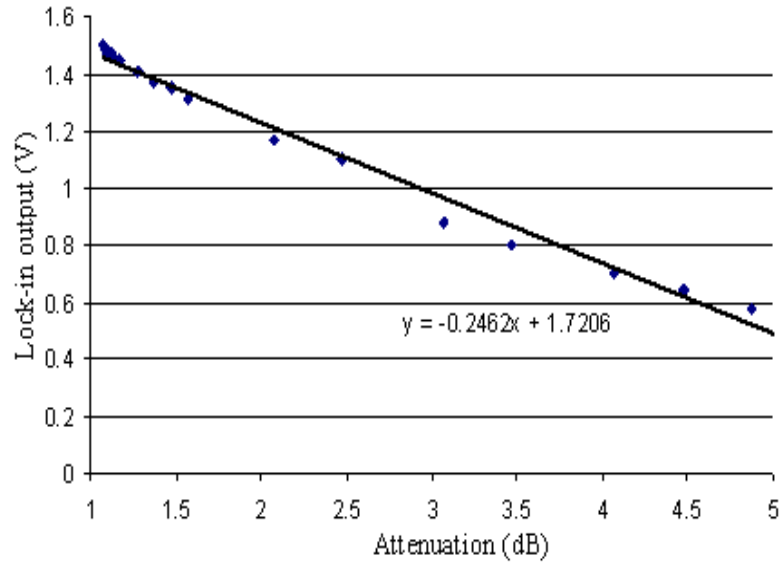
Figure 5.18: DC output of lock-in versus attenuation for P1 of 55.3mW and P2 of 10mW

5.5.7 Wavelength Tuning

One of the desired features for spectroscopy is the ability to scan across an absorption line i.e. wavelength tuning via mechanical stretching where the conventional method is to apply a strain along the grating using a PZT stretcher or by bending the grating. However, the spliced connection can easily be broken, especially when the grating is over stretched. Hence thermal tuning using a uniform temperature change along the grating was also investigated.

5.5.7.1 Wavelength Tuning with a PZT

The Bragg wavelength is determined by the well-known equation:

$$\lambda_B = 2n_{eff}\Lambda \qquad (5.6)$$

where Λ is the period of index modulation in the optical fibre and calculated for a given grating by:

125

$$\Lambda = L/n \tag{5.7}$$

where L is the total length of the grating and n is the number of sequential index changes in that length for a linearly indexed common Bragg reflector. If the length of the fibre is increased by mechanical stretching, the Bragg wavelength will then shift towards longer wavelengths (the change in the index of refraction of the fibre under strain has less effect than the length change).

When stretching a fibre, the Bragg wavelength will be changed according to:

$$\triangle\lambda_B = \lambda_B(1 - p_e)\varepsilon_z \tag{5.8}$$

The applied strain (ε_z) is found by:

$$\varepsilon_z = \triangle L/L \tag{5.9}$$

where $\triangle L$ is the change in length of the grating and L is the original length of the grating. The strain-optic constant (p_e) is usually about 0.22 for silica fibre material [91, 92] and this value is used in this study.

The experimental configuration used for wavelength tuning by stretching shown in Figure 5.19. The device consisted of one PZT and the DFB-FL. The fibre was glued on the two blocks at both sides of the PZT which consists of piezo-ceramic disks (0.2-1.0mm thick), separated by thin metallic electrodes with a PTFE insulated wires connected to the voltage supply.
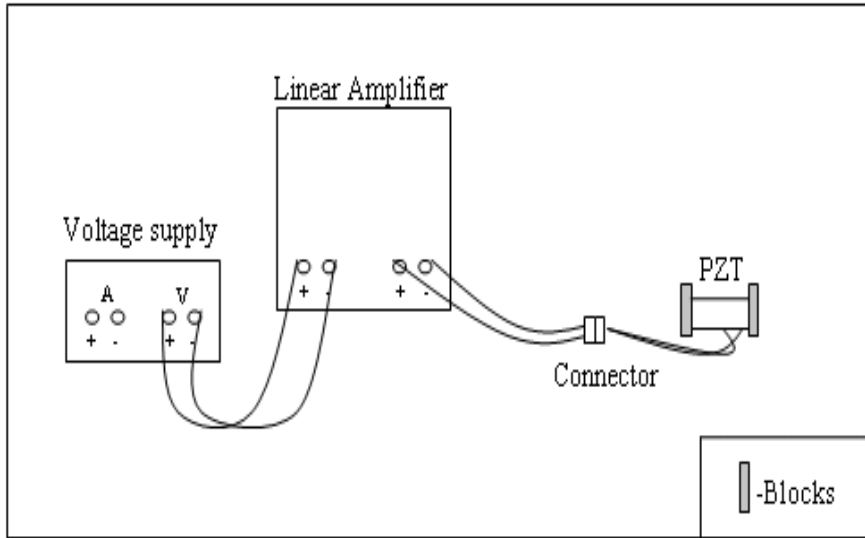
Figure 5.19: Setup for wavelength tuning with a PZT

When a DC voltage is applied to the PZT, the grating is pulled from each side of the PZT. As a result, the Bragg wavelength is shifted; this can be measured by the OSA with a resolution of 0.06nm. The maximum voltage that can be supplied with the voltage amplifier is ±200V [93].

In performing the mechanical stretching of the grating, one must take care not to exceed the deformation strain of the fibre. This value can be found in the datasheet provided by supplier. However, since the amount stretched is very small (nanometres), the displacement is estimated by using a ratio calculation based on the equation in [94] given below:

$$\triangle L = dU_n \tag{5.10}$$

where d is the deformation coefficient, U is the operating value and n is the number of discs.

The experimental relationship between the Bragg wavelength shift and the DC voltage is almost linear as depicted in Figure 5.20.
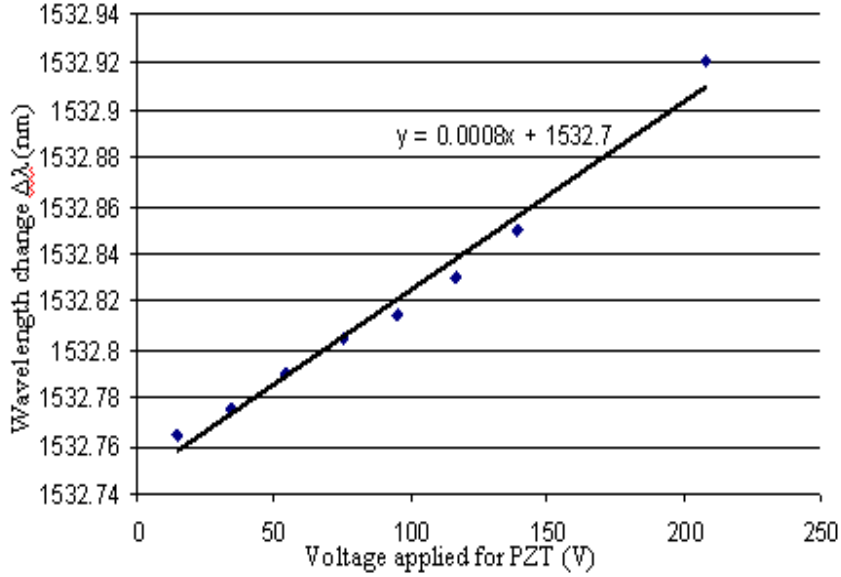
Figure 5.20: Wavelength change $\triangle\lambda$ as function of voltage applied to PZT

Observation showed a 0.155nm shift in the Bragg wavelength for the maximum voltage of 200V. giving an experimental tuning sensitivity of 0.0008nm/V. Wavelength shifts were very small at either end of the tuning range since the movement is very little. Based on the datasheet provided for the PZT, the maximum voltage is 1000V, and the maximum displacement is 60μm. Therefore an applied voltage of 208V gives $\triangle L$=0.01248mm and a strain of $\varepsilon_z = 0.2496 * 10^{-3}$ with a grating length of 50mm. From this result, $(1 - p_e) = 0.40$.

5.5.7.2 Thermal Tuning

Another effective method for wavelength tuning is to change the temperature of the grating. The lasing wavelength change resulting from a given temperature change is given by:

$$\triangle\lambda = \lambda * (\alpha + \xi)\triangle T \tag{5.11}$$

where α is the thermal expansion coefficient and ξ is the thermo optic coefficient. In this experimental, we assume α is $0.55 \times 10^{-6}/°C$ and ξ is $8 \times 10^{-6}/°C$ by referring to [77] for

128

the glass.

The setup for thermal testing of the DFB-FL is shown in Figure 5.21. A Fluke thermometer, a thermoelectric cooler (TEC) and a thermistor was used in the experiment. The DFB-FL was laid on the TEC and underneath was a metal base to act as a heat sink. Silicone heat sink compound (Servisrol) was put along the fibre to conduct the heat released by the TEC.
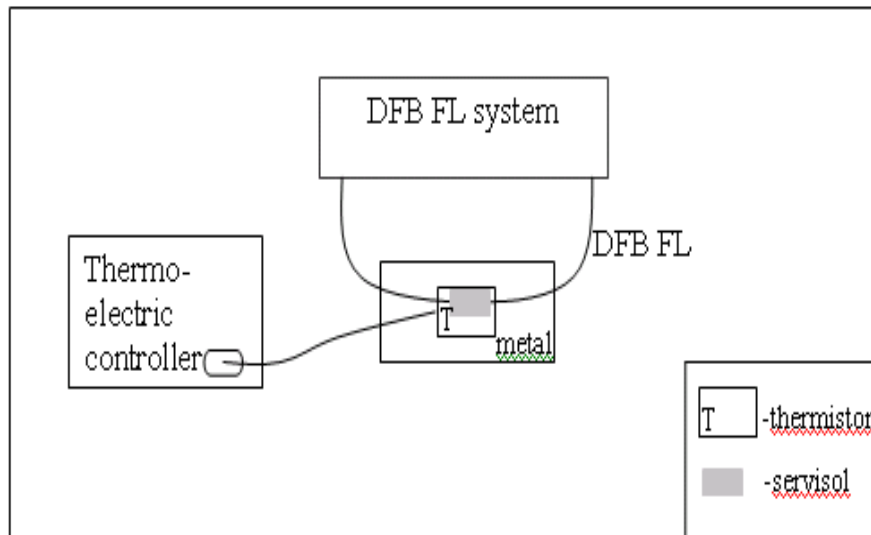
Figure 5.21: Setup for wavelength tuning with a TEC

A thermometer was used to measure the desired temperature of the TEC before the DFB-FL was laid on the TEC. The fibre was heated by the TEC yielding a shift in the Bragg wavelength when the temperature was changed.

Figure 5.22 illustrates the result of wavelength change with temperature showing that the tuning rate is relatively linear. A shift of 0.19nm in the Bragg wavelength was observed for an increase in temperature from 25 $^\circ$C to 40 $^\circ$C giving a tuning rate of ~0.01nm/ $^\circ$C .
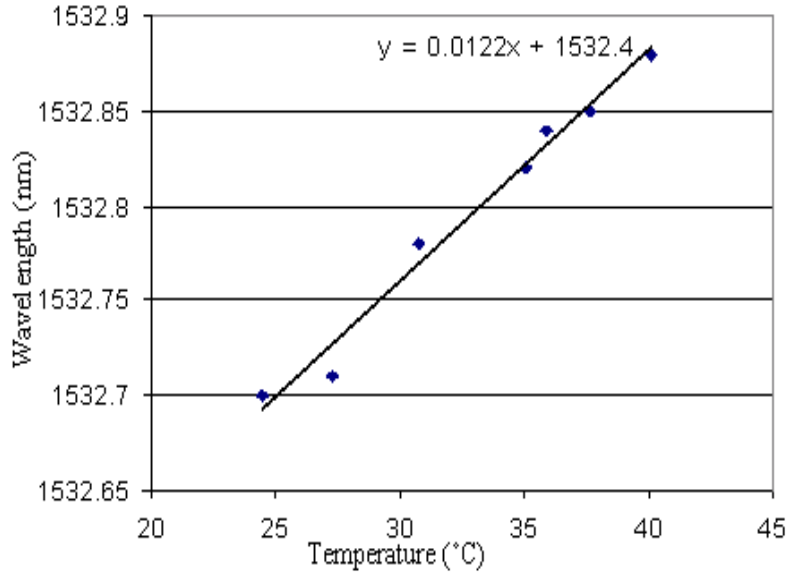
Figure 5.22: Laser wavelength versus temperature

Combining both equations for wavelength changes due to temperature and strain:

$$\triangle\lambda = \lambda_B * ((\alpha + \xi)\triangle T + (1 - p_e)\varepsilon_z \tag{5.12}$$

Values for standard silica fibre yield [91]:

$$\triangle\lambda = \lambda_B * (8.55 \times 10^{-6}\triangle T + 0.78\varepsilon_z) \tag{5.13}$$

Using the experimentally obtained thermal tuning rate in the equation above with λ_B =1532.4nm, $\Delta\lambda = 0.19$nm and $\triangle T$=15°C, gives $(\alpha + \xi) = 8.27 \times 10^{-6}$ which is nearly same as the quoted coefficient.

5.6 Tunable DFB Fibre Laser Spectroscopy

5.6.1 Experimental Arrangement

The proposed tunable DFB fibre laser system for spectroscopy is shown in Figure 5.23 below. It consists of the DFB-FL, an EDFA unit, AM nulling and output measurement devices. Double modulation was applied to the system, consisting of a ramp modulation applied at the controller of the TEC module and pump modulation to produce AM on the laser output. As shown, the system is divided into several sections to ease the conduct of the experiment.

For the first section, the wavelength of the DFB-FL was tuned by increasing the temperature of the TEC controller (TED200) to the desired gas absorption line. The objective of this experiment is to thermally scan over the width of an absorption line which needs about $\pm 10\,^{\circ}$C temperature. The thermoelectric cooler (TEC) module was laid underneath the DFB fibre laser and the controller was set to obtain minimum and maximum temperature values and a ramp signal applied from the signal generator with period of 2 seconds. A highly sensitive temperature measuring tool, namely PicoLog was used to get the reading.

The second section, namely, the erbium doped fibre amplifier (EDFA), was used to amplify the output from the DFB-FL as its output was low due to the short length of the DFB-fibre. A sinusoidal current modulation was applied to modulate the pump laser to produce intensity modulation of the laser output.

The third section was for background AM nulling and divided the light into two paths. The first path consists of standard fibre and an attenuator whereas the other path contains the micro-cell for gas detection. The first path serves as a reference arm and the attenuator was used to equalise the magnitude of the signals from the two paths in the absence of gas. The length of the AM nulling fibre depends on the modulation frequency according to:

$$L = \frac{1}{2}\frac{T}{a} \tag{5.14}$$

Or

$$\frac{nL}{c} = \frac{T}{2} \qquad (5.15)$$

where is the time it takes light in the fibre to travel 1 meter which is ~ 5 nanosecond. In the laboratory, it is difficult to get an exact value of fibre length, therefore the modulation frequency or period,T , is varied according to the value of the available fibre length.

The fourth section is the output part where the detected signal is fed to the LIA with the reference signal from the signal generator and the result observed on the oscilloscope.
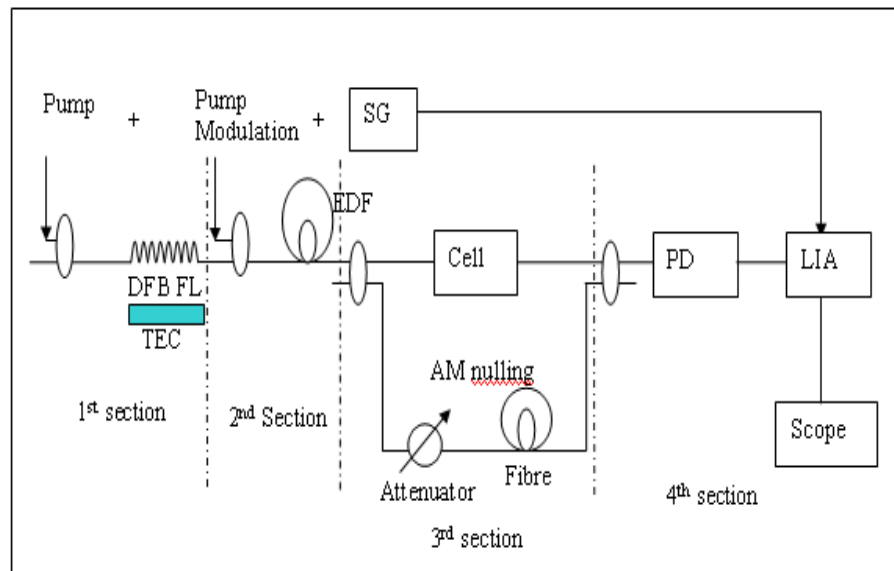
Figure 5.23: DFB-FL system setup

5.6.2 Test of the TEC Controller
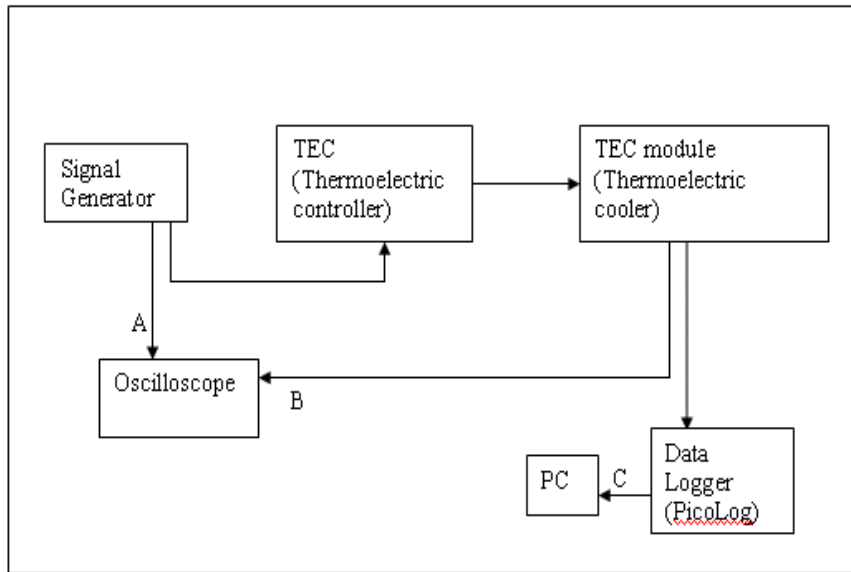
Figure 5.24: Setup for test of TEC controller

Figure 5.24 is the setup for testing the TEC controller performance. TED200 Thorlabs was used to control the temperature of TEC module and a oscilloscope data logger (Picolog) was used for the measurement.

A frequency of 500 mHz (period of two seconds) and a 1Vpp from a signal generator was applied to get an increment and decrement of 10 degree Celsius in temperature, however due to the limitation of the controller, the best response of the controller was for ~7 seconds per cycle as shown in the following figures. Figure 5.25 shows the results of snapshots of temperature variation for 2 second and 7 second periods, respectively. These were measured by using the more sensitive temperature tool namely PicoLog, as output signals were difficult to see on the oscilloscope. The amplitude of the temperature variation at the 2 second period is much less than that from the 7 second period of modulation and hence the 7 second period is better for producing a ramp signal of 10°C temperature change within it.
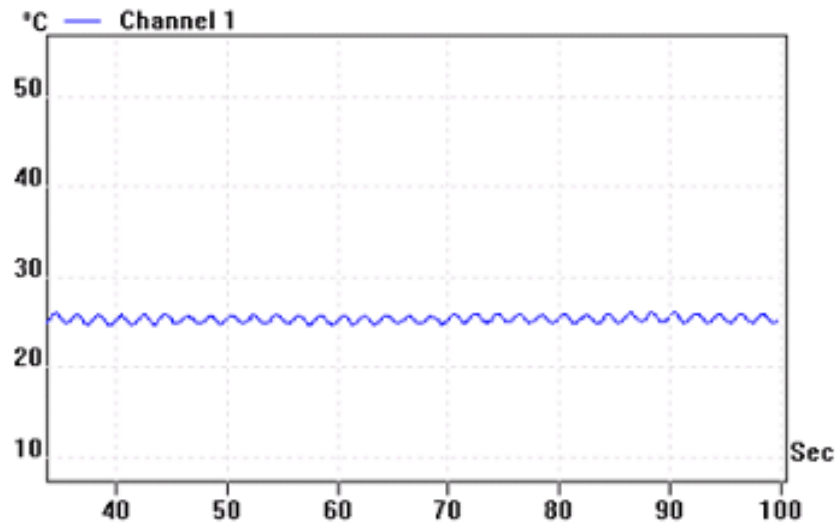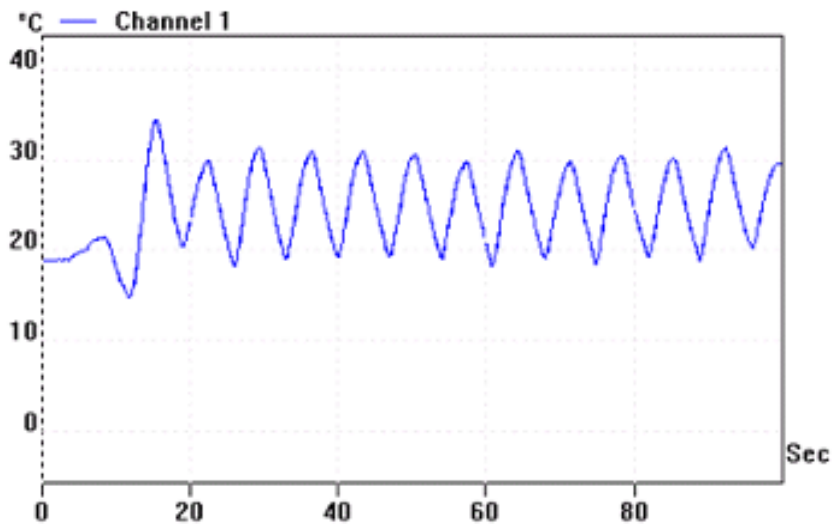
Figure 5.25: Temperature reading from PicoLog for (a) 2 sec and (b) 7 sec periods

An increment and decrement of 10°C within 2 seconds will only be possible (if at all) with a thermoelectric cooler which exploits the full power of the TED200, which means about 6V at 2A current. Furthermore the mounted thermal load has to be small. For the TED350, 5A was expected and would do the task though the device is very costly and this would increase the start up cost for the whole system. On the other hand, the signal generator cannot be

connected directly into the TEC module due to lots of noise from the signal generator since the TEC needs a smooth DC power supply and continuous voltage.

5.6.3 Test of Thermal Ramp Modulation on the DFB-FL for 1st Section

The experimental setup for thermal modulation of the DFB-FL with the TEC module is depicted in Figure 5.26. An OSA, oscilloscope and the PicoLog were used to measure the output signal. As shown in Figure 5.27, the TEC module functioned normally following the ramp signal pattern for t<150s, but then increased out of control. This may overcome by using a proper heat sink as only a piece of metal was used under the module.

Figure 5.26: Thermal ramp modulation in the 1st section layout

Figure 5.27: Temperature versus TEC operation time

5.6.4   Thermal Ramp Combined with Pump Modulation on the EDFA

A few Hertz frequency was applied to the TEC to scan the wavelength through an absorption line while simultaneous pump modulation was applied on the EDFA at a few kHz frequency. The wavelength shifted when heat was supplied to the TEC module as indicated in Figure 5.28 where (a) depicts the spectrum before heating and (b) after the TEC module was heated. However the optical spectrum analyser (OSA) has a resolution limit of 0.06nm and a hence a higher resolution is needed to the observe wavelength shift from the TEC modulation. Figure 5.29 shows the effect of the pump modulation on the spectrum observed on the OSA indicating the changing output power levels from the intensity modulation.

136
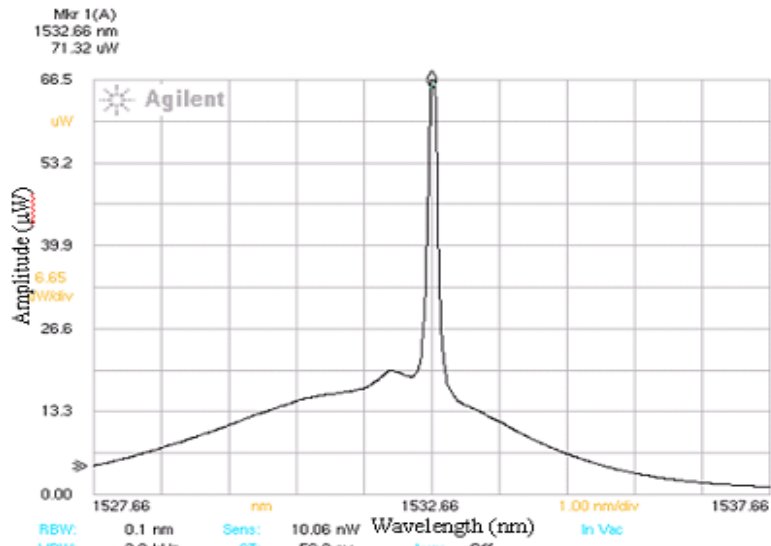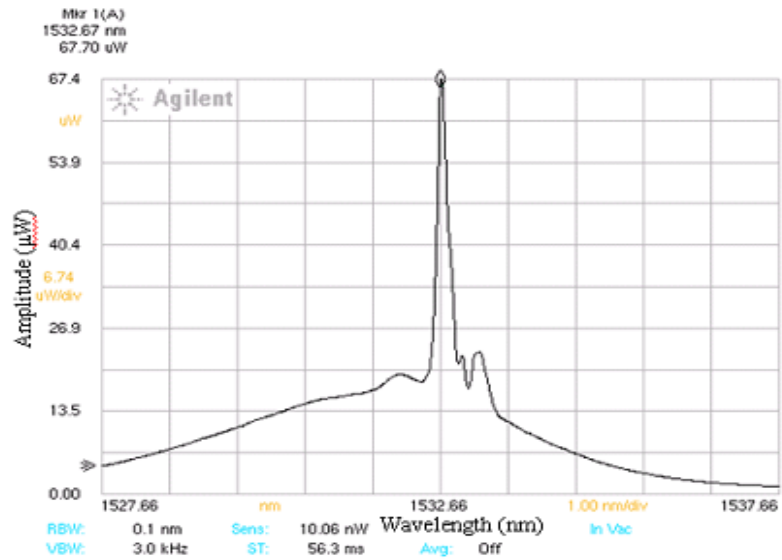
Figure 5.28: Initial DFB-FL wavelength (a) before and (b) after applying ramp modulation (thermal scanning) to the TEC module
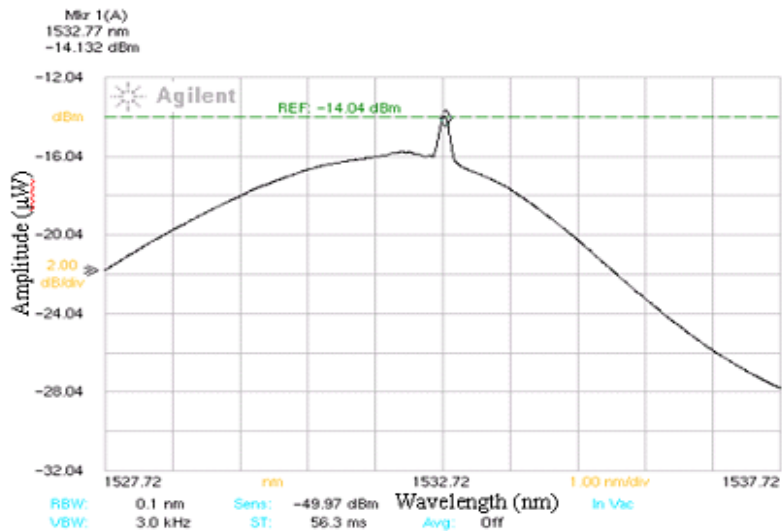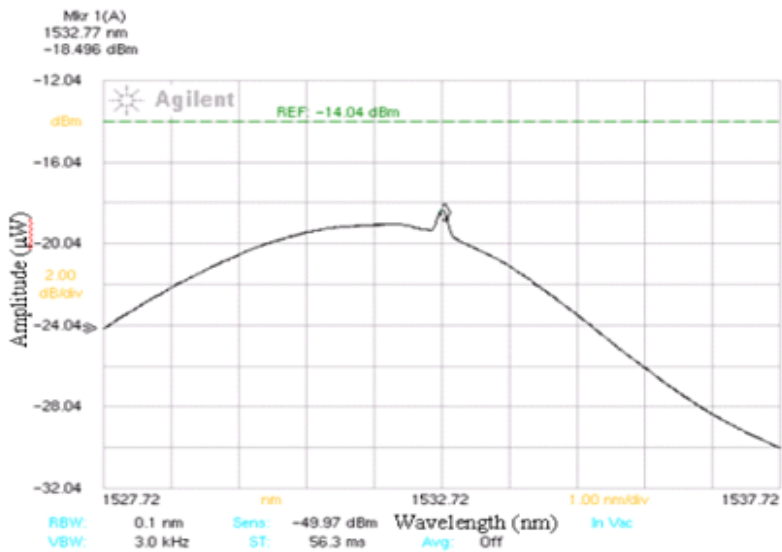
Figure 5.29: Changing in power level of spectrum with pump modulation

Due to the DFB fibre being broken in the middle of the experiment; it was not possible for the experiment to be continued. There were a number of improvements needed to be carried out even though the DFB-FL is feasible for spectroscopy applications. The technology of the DFB-FL is still in progress. From the results, the pump absorption was low and hence an amplifier is needed when conducting the experiments which poses an extra cost. Moreover

138

the DFB-FL itself is also expensive at this moment. This has resulted in a high cost in starting up the setup.

As for the tuning mechanism, it is preferable to use the PZT to stretch the fibre but there is a need to be extra careful in handling due to the fibre being very fragile and easily broken. Although heating is also one of the tuning method, the limitation of the controller and the slow thermal response means that the response was not fast enough to get the desired tuning rate hence making the overall process complex. Nevertheless, the work conducted here has provided a preliminary study for further development of the DFB-FL for gas spectroscopy.

5.7   Conclusion

This chapter gave a preliminary investigation into the use of the DFB-FL for trace gas detection. The DFB-FL system was constructed and experiments were conducted to characterize its performance. Results showed that the DFB-FL is a stable, single-mode laser which is alternative way of solving mode hopping problems that normally occur in long cavity fibre systems. It was observed that results such as lasing power, RIN and tuning wavelength for the DFB-FL matched well with the quoted values of coefficients and the associated theory.

After the characterization, further experiments were attempted by applying a double modulation to the system (thermal scan and laser intensity modulation) to test its viability for spectroscopy purposes. From the observations, operation of the tunable fibre laser system is feasible with double modulation; the pump laser current modulation produced intensity modulation of the output and the laser wavelength can be tuned by thermal means. However there are a number of drawbacks that need to be dealt with, such as the wavelength shift from the thermal scanning was very short and the duration of heating cannot be prolonged because of the limitation of the laser controller.

The other option is use of the PZT to stretch the laser wavelength to the desired absorption

wavelength, but the fragility of the fibre itself influenced its usefulness. The fibre laser was very fragile in stretching and extra care in handling is necessary since the DFB-FL is more expensive when compared to semiconductor lasers due to it being a newer technology and its relative lack of maturity.

Chapter 6

PHOTO-ACOUSTIC SPECTROSCOPY (PAS)

6.1 Introduction

The importance of monitoring more and more air pollutants continues to grow widely nowadays and this growth has ignited a desire to find and develop instruments that can provide rapid, real-time, accurate measurements of these various air pollutants. One class of instruments that can provide this is those based on the photoacoustic effect. The photoacoustic effect is based on the conversion of light energy into sound energy by a gas, liquid or solid. It was discovered around 1880 and was first reported by Alexander Graham Bell [38].

In this chapter, tuneable diode lasers in combination with photoacoustic spectroscopy (PAS) for high sensitivity gas detection is described. Preliminary measurements were made on the absorption lines of acetylene gas at 1531.59nm with the objective of becoming familiar with the working operation of diode lasers with PAS and WMS. For the initial work, detection of low concentrations of acetylene in a mixture of nitrogen gas was investigated from 1% (10000ppm) down to 0.5 ppm or 500ppb concentration of acetylene gas using a diode laser.

Several modulation formats were explored such as sinusoidal modulation, ramp modulation or direct detection and double modulation whereas wavelength scanning was done by using an arbitrary waveform which was automatically swept and manually tuned with a temperature controller.

After the preliminary study using the diode laser, a further investigation was carried out to study the potential of the erbium doped fibre laser (EDFL) systems with PAS using intensity modulation (IM) for gas spectroscopy. The setup of the EDFL is the same as in Chapter 3, the only difference is the structure of the gas cell which is a photo acoustic (PA) cell here. As mentioned in Chapter 3, the resulting output after processing through the lock-in amplifier (LIA) gives the gas absorbance which can be directly compared with the theoretical data. The result is very straightforward and has the advantage that PAS has an almost zero background when no gas is present in the cell. Thus, this system has higher sensitivity than the system using standard spectroscopy with the micro-optic gas cell.

6.2   Review of PAS

Photoacoustic spectroscopy (PAS) has become one of the most commonly used spectroscopy methods in gas sensing applications due to its high sensitivity, large dynamic detection range and good stability. The measured acoustic output results from the absorbed energy by gas molecules in the gas cell. Technical and historical reviews of this subject can be found in several sources [28, 95, 39].

The basic theory of the photoacoustic effect in gases using infrared radiation is straightforward. When a gas is irradiated with light of a frequency that corresponds to a resonant vibration frequency of the gas, some of the light will be absorbed. This will cause some of the molecules of the gas to be excited to a higher vibration energy state. These molecules will subsequently relax back to the initial vibration state through a combination of radiative

and non-radiative processes. For vibration excitation, the primary relaxation process is non-radiative vibration to translation energy transfer. This result is increased heat energy of the gas molecules and therefore a temperature and pressure increase in the gas. If the irradiating light is modulated, then the temperature and pressure will be as well. The modulated pressure will result in an acoustic wave, which can be detected with a sound measuring device, such as a microphone. The amplitude of the acoustic wave will depend upon such factors as the geometry of the gas cell, incident light intensity, absorbing gas concentration, absorption coefficient, and the background gas. For a non-resonant spherical gas cell under steady state conditions, the amplitude of the acoustic wave can be found from the following equation [96]:

$$P = K((C_p/C_v) - 1)I_o C(1/f) \tag{6.1}$$

In the above, P is the sound pressure, I_o is the incident light intensity, C is the absorbing gas concentration, f is the modulation frequency, C_p and C_v are heat capacities and K is a cell and gas dependent constant.

A crucial part of a PA gas detection setup is the cell in which the PA signal is generated and detected. The first "gas-microphone cells" that were reported [97] consisted of small cylindrical cavities with a transparent window. A microphone is used to convert the pressure wave into sound wave which is then converted to an electrical signal. R.E. Lindley et al. reported [98] the importance of the microphone's role in the gas cell, this is due to parameters such as the position of microphone and the manufacturing of the microphone in order to produce a good output signal. The microphone was connected to the cavity by a thin hole in one of the side walls of the cell. These PA sensors could be manufactured very easily; moreover, they were very cheap when miniature electret microphones were used.

Since the PA signal is inversely proportional to the cell volume and the modulation frequency, high PA signal levels can be obtained by taking a small cell volume (~ 10 cm^3) and low modulation frequencies (~ 100 Hz) [97].

As for the size of the gas cell, small gas-microphone cells; which are still the most suitable PA detectors for solid and liquid samples, are hardly used in gas phase photoacoustics anymore. The signal-to-noise ratio SNR of such a gas-microphone cell is usually quite small. Noise sources, for example, intrinsic noise of the microphone, amplifier noise, external acoustic noise show characteristic 1/f frequency dependence, and light absorbed in the windows and in the wall material generates a coherent background signal, which is practically impossible to separate from the PA signal generated by the gas absorption itself. Therefore, the SNR of a PA cell can be increased by applying higher modulation frequencies in the kHz region and acoustic amplification of the PA signals. Hence, the outstanding features of the PA cell, most importantly its small size, its simplicity, and robustness, can only be fully exploited when it is combined with a suitable laser source. Therefore, recent progress made in the development of diode lasers has had an increasing influence on the application of compact PA gas analyzers [97].

6.3   Principles of PAS with Tunable Diode Lasers

Principles of TDLS with PAS are similar to that discussed in Chapter 2 for operation of the spectroscopy. The transmitted intensity, I_{out}, at a specific optical frequency, v, associated with a rotation / vibration transition in a gas is given by Beer's law:

$$I_{out} = I_{in}e^{-\alpha(v)Cl} \tag{6.2}$$

where I_{in} is the incident intensity on the gas volume, $\alpha(v)$ is the absorption coefficient at frequency v, l is the length through which the beam and gas interact and C is the gas concentration expressed as $C = N/N_0$ (N_0 is the molecular density at STP and N is the actual molecular density of the target gas in units of No. of molecules per unit volume). The approximation shown is valid for small absorbance, A i.e. $\alpha(v)Cl \ll 1$.

In the case of high concentration or absorbance is larger than 1, the relative transmission, T is expressed as:

$$T = \frac{I_{out}}{I_{in}} = e^{-\alpha(v)Cl} = e^{-A} \tag{6.3}$$

The result measured in photoacoustic spectroscopy is the absorbed power by the gas, not the output optical power from the gas. Hence power absorbed by the absorption line for the case of lossless cell is:

$$P = I_{in} - I_{out} = I_{in}\alpha(v)Cl \tag{6.4}$$

For the gas absorption line, the absorption coefficient $\alpha(v)$ is described by:

$$\alpha(v) = \alpha_0 f(v) \tag{6.5}$$

where $f(v) = \left\{ \frac{1}{1 + \left(\frac{v - v_0}{\gamma}\right)^2} \right\}$ for a Lorentzian profile, v_0 and α_0 are the frequency and absorption coefficient at the line centre, respectively, and γ is the half-line width in units of cm^{-1}, α_0 is given by $\alpha_0 = \frac{N_0 S}{\pi \gamma}$, where S is the line strength of gas absorption line in units of $cm^2/(molecule\, cm)$. Therefore, the units of α_0 can be calculated as cm^{-1} based on previous description. The v_0 in equation 6.5 is the frequency at the absorption line centre. Figure 6.1 shows the absorption coefficient against frequency.

145
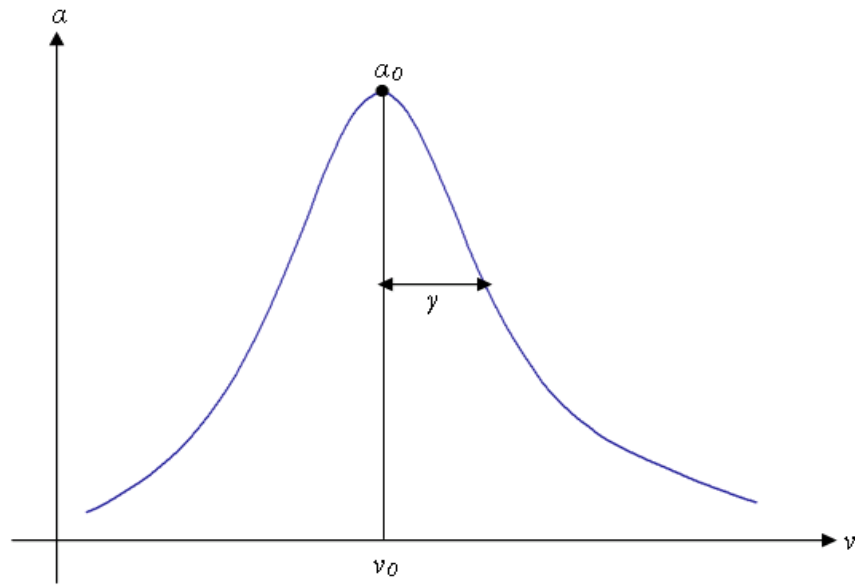
Figure 6.1: Absorption coefficient against frequency for a Lorentzian profile

In tuneable diode laser spectroscopy (TDLS) with wavelength modulation spectroscopy (WMS) the laser current is modulated by a ramp current and by a much higher frequency sine wave. The ramp slowly scans the centre frequency through the absorption line at typical rates of a few Hz to tens of Hz. The sinusoidal current modulation translates to a frequency modulation of amplitude, δv (deviation from the laser's centre frequency v_1), related to the amplitude of the current modulation through the tuning rate of the laser.

As well as frequency modulation and scan, the above current signals applied to the laser diode produce an increase in laser power as the ramp current level increases and sinusoidal modulation of the laser power. The amplitude, $\triangle I$, of the sinusoidal intensity modulation is determined by the slope of the laser power versus current characteristic, which changes slightly across the scan width.

Taking into account the above modulation effects on the intensity, the input intensity at a particular frequency,v_1 can be written as:

146

$$I_{in} = I(v_1) + \triangle I(v_1).cos(\omega t) \tag{6.6}$$

this with equation 6.4 gives the absorbed power as:

$$P = [I(v_1) + \triangle I(v_1).cos(\omega t)] . (\alpha(v_1)Cl) \tag{6.7}$$

where both the input intensity $I(v_1)$, and the intensity-modulation amplitude, $\triangle I$, depend on v_1 and w is the applied angular modulation frequency.

As mentioned earlier, the sinusoidal current modulation on the laser results in sinusoidal frequency modulation around v_1 given by:

$$v = v_1 + \delta v.cos(\omega t - \psi) = v_1 + \delta v.cos\theta \tag{6.8}$$

where ψ is the phase shift between the power and the frequency modulation and $\theta(t) = (\omega t - \psi)$ is defined. Substituting into equation 6.5 gives:

$$\alpha(v_1) = \alpha_0.f(\theta) \tag{6.9}$$

with $f(\theta) = \left\{ \frac{1}{1+(\triangle+mcos\theta)^2} \right\}$ for a Lorentzian profile, where $m = \delta v/\gamma$ is the modulation index and $\triangle = (v_1 - v_0)/\gamma$ is the deviation from the line centre.

The absorption coefficient, $\alpha(v_1)$ may be expanded as a Fourier Series in harmonics of the modulation frequency, ω. Since $f(-\theta) = f(\theta)$ for the Lorentzian, then $f(\theta)$ is an even function and the Fourier expansion is given by the following equation.

$$f(\theta) = \left\{ a_0 + \sum_{n=1}^{\infty} a_n cos(n\theta) \right\} = \left\{ a_0 + \sum_{n=1}^{\infty} a_n cos(n\omega t - n\psi) \right\} \tag{6.10}$$

where the Fourier coefficients are described as:

$$a_0 = \frac{1}{\pi} \int\limits_{0}^{\pi} f(\theta)d\theta = \frac{1}{\pi} \int\limits_{0}^{\pi} \frac{1}{\{1 + (\triangle + mcos\theta)^2} d\theta \tag{6.11}$$

$$a_n = \frac{2}{\pi} \int\limits_{0}^{\pi} f(\theta)cos(n\theta)d\theta = \frac{2}{\pi} \int\limits_{0}^{\pi} \frac{cos(n\theta)}{\{1 + (\triangle + mcos\theta)^2} d\theta \tag{6.12}$$

The maximum value for a_1 occurs [10] at $\triangle = \frac{\pm\{\sqrt{(3m^2+4)}-1\}}{\sqrt{3}}$ and for a_2 at $\triangle = 0$.

A lock-in amplifier is used to obtain the harmonic of the output signal which can be attained by substituting equations 6.9and 6.10 into equation 6.7 as follows:

$$P = A\{I(v_1) + \triangle(v_1)cos(\omega t)\} . \left[a_0 + \sum\limits_{n=1}^{\infty}a_n cos(n\omega t - n\psi)\right] \tag{6.13}$$

Expanding equation 6.13 gives:

$P = A.a_0(v_1).\{I(v_1) + \triangle(v_1)cos(\omega t)\}$for DC component

$P = A.a_1(v_1).\{I(v_1) + \triangle(v_1)cos(\omega t)\} .cos(\omega t - \psi)$ for first harmonic (1f)

$P = A.a_2(v_1).\{I(v_1) + \triangle(v_1)cos(\omega t)\} .cos(2\omega t - 2\psi)$ for second harmonic (2f)

$$\tag{6.14}$$

and so on.

The product term of the cosine can be written as follow:

$$cos(\omega t).cos(n\omega t - n\psi) = \frac{1}{2}\triangle I(v_1)\{cos\left[(n+1)\omega t - n\psi\right] + cos[(n-1)\omega t - n\psi]\} \tag{6.15}$$

The components of DC, first harmonic, second harmonic, etc., of absorbed power can be obtained from equation 6.14 and equation 6.15 as:

DC component:

148

$$P_{DC} = A[a_0(v_1).I(v_1) + \frac{1}{2}a_1(v_1).\triangle I(v_1).cos\psi] \tag{6.16}$$

1f component:

$$P_\omega = A\{a_0(v_1).\triangle I(v_1)cos(\omega t) + a_1(v_1).I(v_1)cos(\omega t - \psi) + \frac{1}{2}a_2(v_1).\triangle I(v_1)cos(\omega t - 2\psi) \tag{6.17}$$

Note that the first term arises from the effect of gas absorption on the AM, the second term is the signal arising from the FM (dependent on a_1 and at a phase of $-\psi$) while the third term (at phase -2ψ the AM on the second harmonic (using equation 6.15).

2f component:

$$P_{2\omega} = A\{\frac{1}{2}a_1(v_1).\triangle I(v_1)cos(2\omega t - \psi) + a_2(v_1).I(v_1)cos(2\omega t - 2\psi) + \frac{1}{2}a_3(v_1).\triangle I(v_1)cos(2\omega t - 3\psi)$$
$$\tag{6.18}$$

The first term (at phase $-\psi$ comes from the AM on the first harmonic, the second term is the second harmonic from the FM (dependent on a_2 and at a phase of -2ψ) while the third term (at phase -3ψ from the AM on the third harmonic. In case of low modulation frequencies, ψmay be small [10].

6.4 Experimental PAS system with Tunable Diode Lasers

The setup shown in Figure 6.2 depicts the experimental PAS system. The PA cell is placed in a grey nylon block to hold the cell which has a length of approximately 10cm and inside the block there is a white ceramic to absorb the light that has passed through the cell. A mixture of acetylene gas with 1% (10000ppm) concentration in nitrogen was used in the experiment.

A DFB diode laser (Anritsu AB5A232P1, Opto-Sci) emitting at 1531.59nm was selected for the acetylene gas detection. The diode laser wavelength was modulated by combining a drive current from a laser diode controller (LDC 202B, 200mA, Thorlabs) with a modulation signal from a function generator Agilent 33220A, 20MHz, LX1. A temperature controller (TED 200 Thorlabs) was used to vary the output centre wavelength of the laser. 10kΩ of load resistance was set on the signal generator to match the diode laser controller and a low frequency range of 1Hz-1kHz was used in the experiments. The diode laser is fibre-pigtailed which facilitates the construction of the system and the connection to an EDFA to boost the optical power launched into the PA cell. The output from the EDFA used here was in the 20-27dBm range which is equivalent to 500mW maximum output. This considerably improves the sensitivity, since the PA signal is directly proportional to the laser power. The output fibre from the EDFA is terminated by a GRIN lens which has low cost, low loss and low optical interference. As the light beam propagates along the PA cell, interaction of the light from the current-modulated laser and the gas molecules produces a sound wave which was detected by a microphone attached at the centre of the PA cell. The measured signal was amplified with a pre-amplifier, which used a battery as a power supply to reduce the mains pick up problem which occurred when using a mains current supply. Finally, the output signal was measured with an oscilloscope DS060034A Agilent Technologies, 300 MHz, 2GSa/s. Three modulation formats were investigated, namely, low frequency ramp signal only, large amplitude sinusoidal signal only, and combined ramp plus sinusoidal signal on the laser diode current.
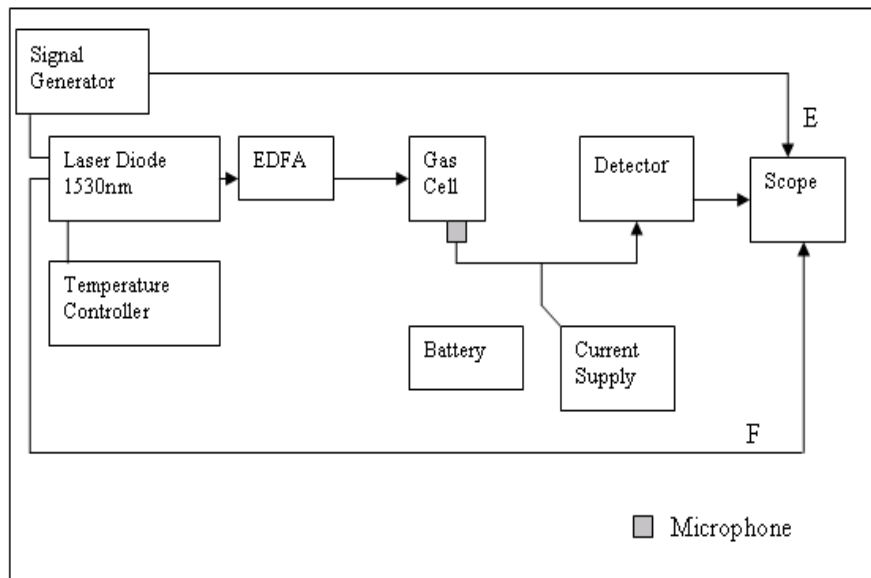
Figure 6.2: Experimental setup for PAS with a diode laser

6.4.1 Characteristics of Laser Diode

The characteristics of the laser diode (Anritsu 1530nm) was first studied before being employed in the system to determine its power output and wavelength.

6.4.1.1 Power Output versus Input Current
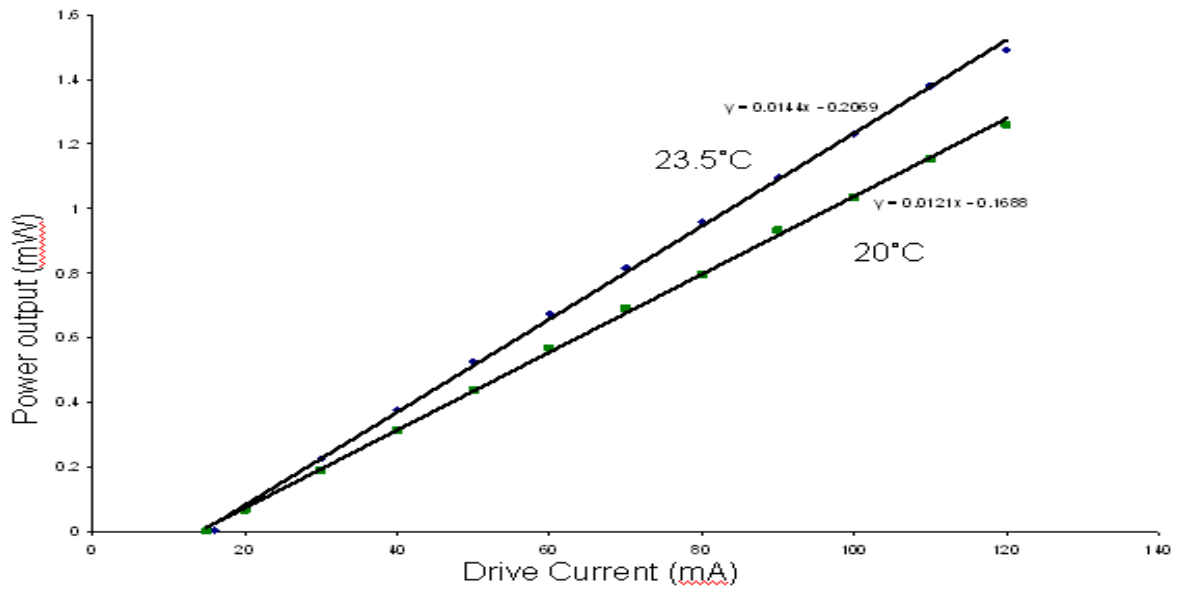
Figure 6.3: Power output of the 1530nm diode laser

Referring to the Figure 6.3, two different temperature measurements were taken to see the effect of temperature on the laser power. Power output of the laser diode increases linearly with the drive current applied, as expected, with threshold current around 15.96mA for both temperature settings.

6.4.1.2 Wavelength versus Input Current

When the input current of the laser diode is increased, the centre wavelength of the laser diode also increases and hence different settings of the input current gives a different wavelength as depicted in Figure 6.4. This was used to select the centre wavelength and tune to selected gas absorption lines.
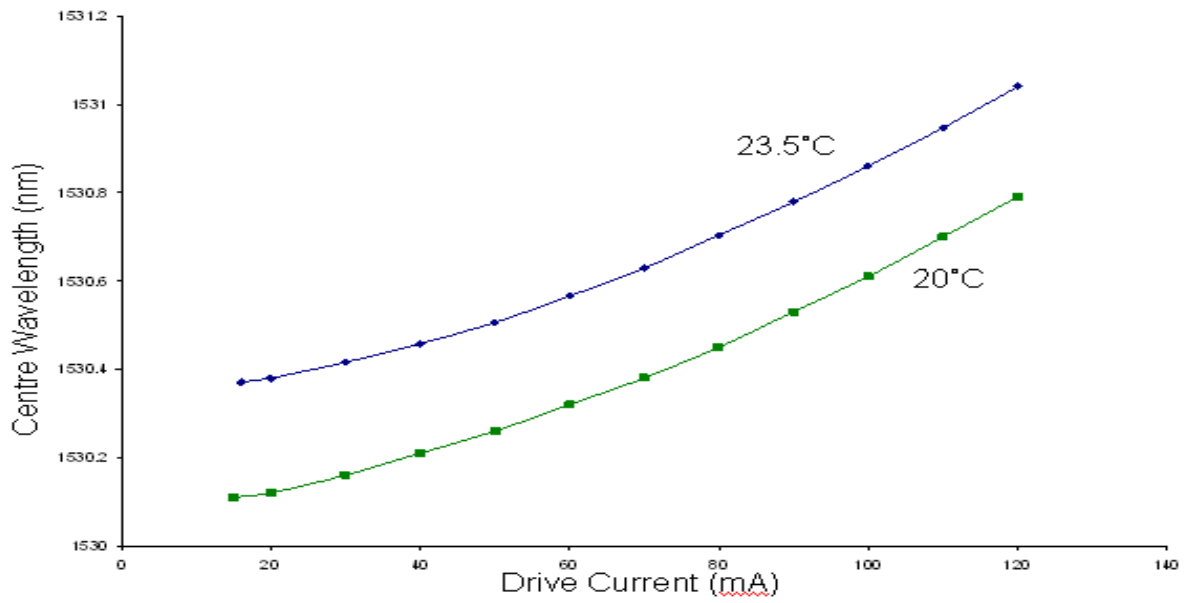
Figure 6.4: Diode laser wavelength versus input current

6.4.1.3 Wavelength versus Temperature

Figure 6.5 shows that the wavelength can also be shifted when the temperature is varied. Two different settings of drive current were applied during the experiment. About 1.32nm shift in the centre wavelength for both drive currents can be obtained for the range of temperature shown, and the tuning rate is $\sim$0.093nm/$^{\circ}$C.
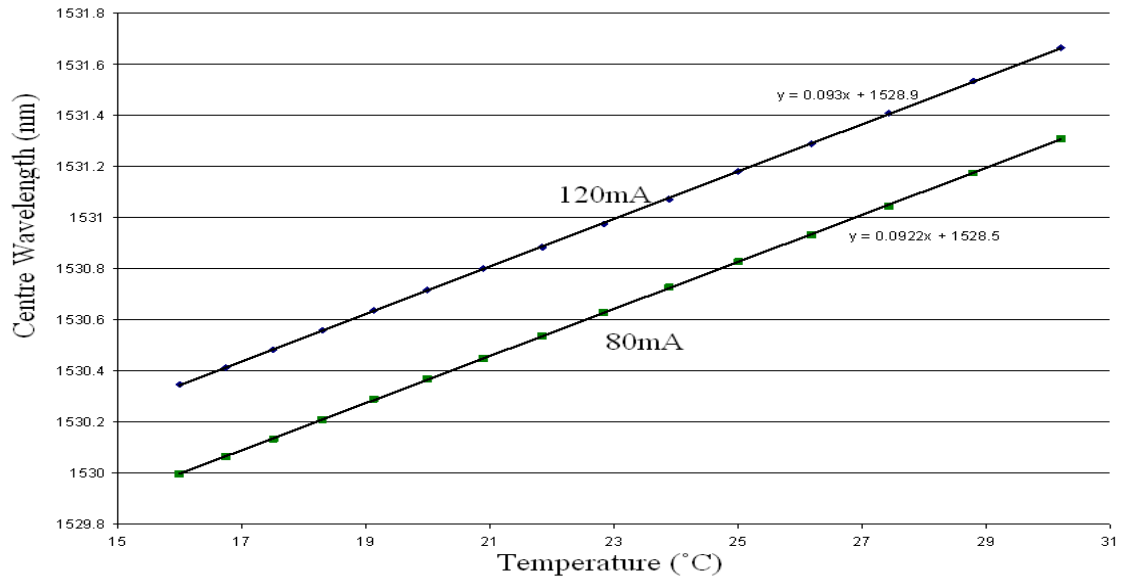
Figure 6.5: Laser wavelength tuned thermally by using a temperature controller

6.4.2 Ramp Signal only on Laser Diode Current (First Modulation Technique)

In order to repeatedly scan the laser frequency over the entire acetylene absorption line, a periodic ramp was applied to the injection current by the function generator connected to the modulation input at the rear panel of the current controller. The modulation frequency was set to 2.5Hz, with amplitude of Hilevel of function generator at 1.6V and Lolevel at 0V while the laser current was set to 80mA and temperature resistor setting was varied from 12kΩ to 14kΩ, with the EDFA in the range of 20-27dBm.

6.4.2.1 Dependence of PAS Signal on EDFA Pump Power

Figure 6.6 shows the output photoacoustic signal observed on the oscilloscope as the pump power of the EDFA amplifier was increased and the wavelength is scanned through the absorption line by the ramp signal. 27dBm output power from the EDFA gave approximately

154

a 2V amplitude signal.
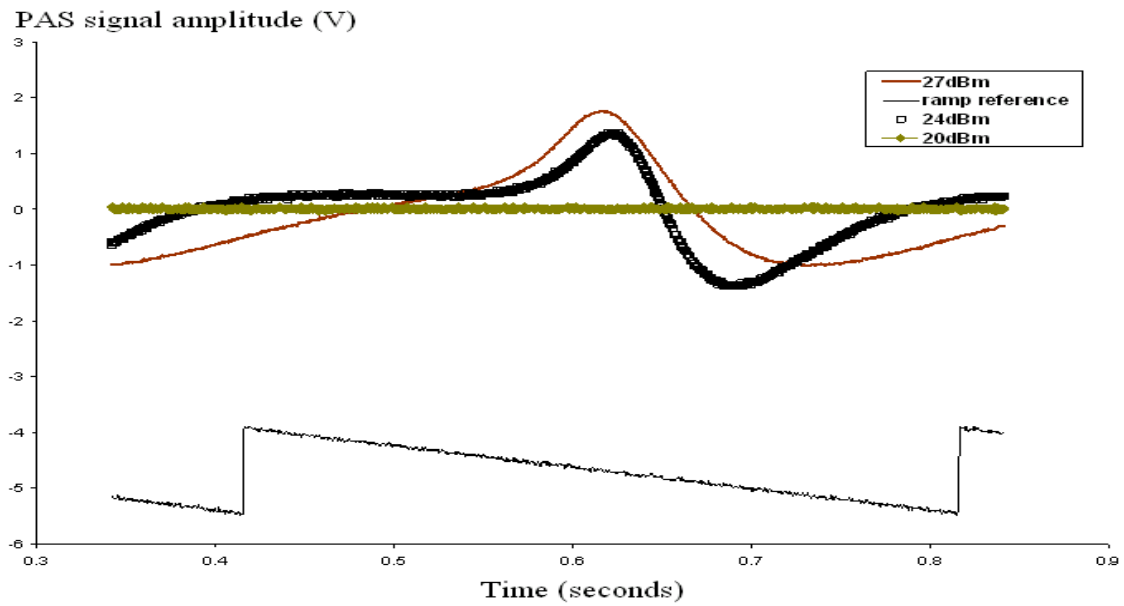
Figure 6.6: Effect of EDFA pump power on PAS signal

6.4.2.2 Effect of Ramp Frequency on PAS Signal
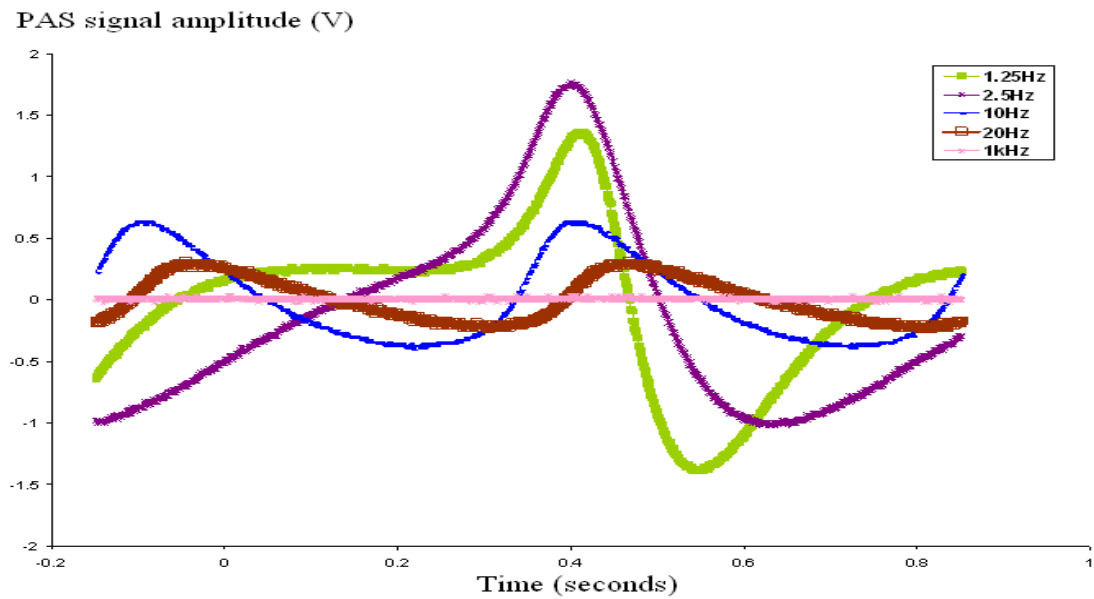
Figure 6.7: Effect of ramp frequency on PAS signal

155

Figure 6.7 displays the PAS signal for different ramp frequencies over the range of 1Hz to 1kHz. The optimum period of modulation was 500ms, equivalent to 2Hz frequency, which gave the highest peak value. When the period was shorter (higher frequencies), a lower peak voltage was obtained due to the energy absorption of gas molecule being less compared to long periods.

6.4.2.3 Wavelength Adjustment by Thermal Effect

The temperature was adjusted in order to shift the centre wavelength of the laser near the absorption line so that the ramp can be used to scan across the line.
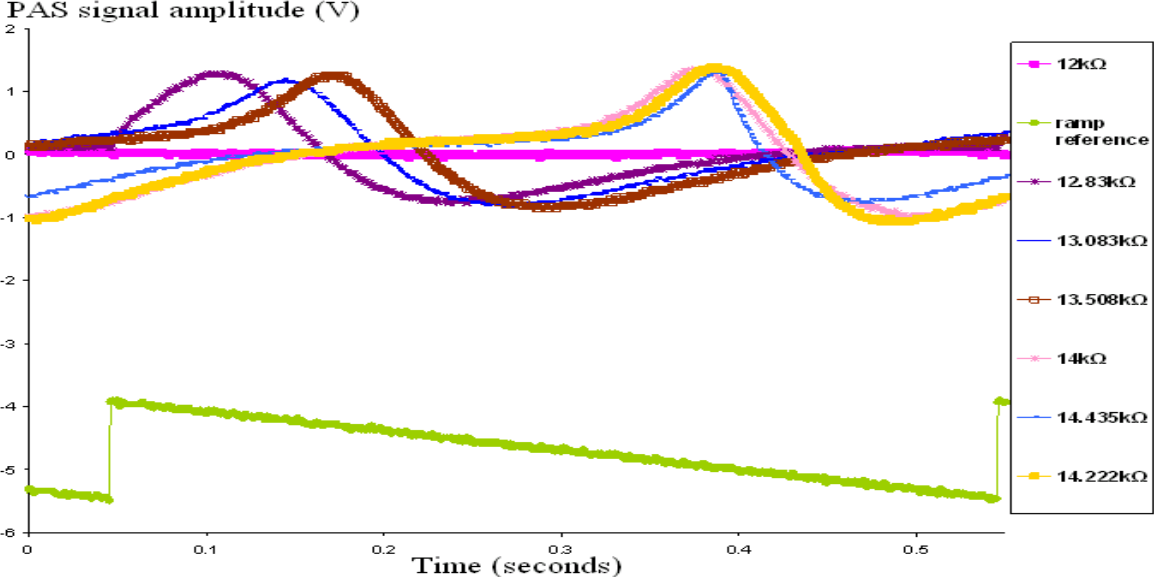
Figure 6.8: Shift of PAS signal in relation to ramp at different temperatures

Figure 6.8 shows the shift of the PAS signal in relation to the ramp as the thermal resistance was increased from 12 kkΩ to 14.646 kΩ (which is inversely equivalent to 20 ° C to 16.5 ° C). (Beyond this range of values, the waveform of the output signal will be clipped due to being at the end of the ramp tuning range. The range of thermal tuning was very short to see the actual effect of wavelength shifting; hence in general the OSA was used to see the

wavelength change against temperature).

6.4.3 Sinusoidal Modulation only (Second Modulation Technique)

For the second technique, a sinusoidal signal from the function generator, with amplitude of 450mV and 33Hz frequency was applied to the laser diode. The DC or bias current was set to 60mA and the temperature varied from 10kΩ to 13kΩ with the EDFA amplifier in the range of 20-27dBm.

6.4.3.1 Effect of Laser Diode DC current

The laser diode DC current was varied to see the effect on the waveform of the output signal. From the observation, the amplitude of the output signal was small at 40mA but increased when the current was set at 80mA as shown in Figure 6.9. The laser diode DC current shifts the wavelength of the laser and hence the position of the sinusoidal modulation in relation to the absorption line. In addition, the EDFA also influences the signal strength which is useful when dealing with low gas concentrations.
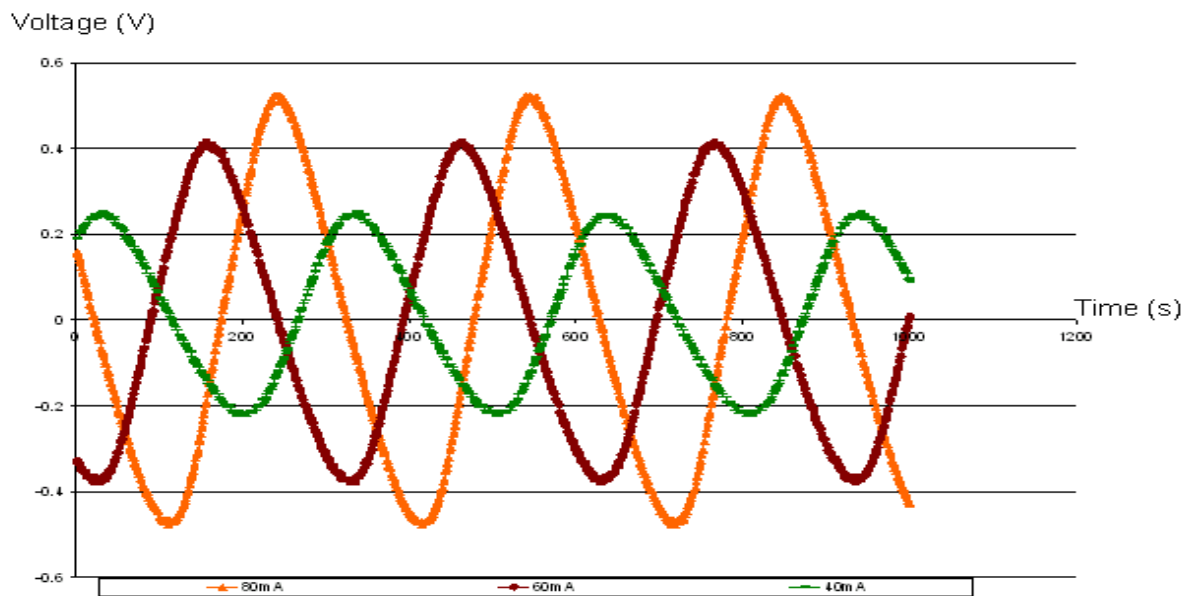
Figure 6.9: Effect of diode laser DC current on the output signal

6.4.3.2 Effect of Modulation Frequency on PAS Signal
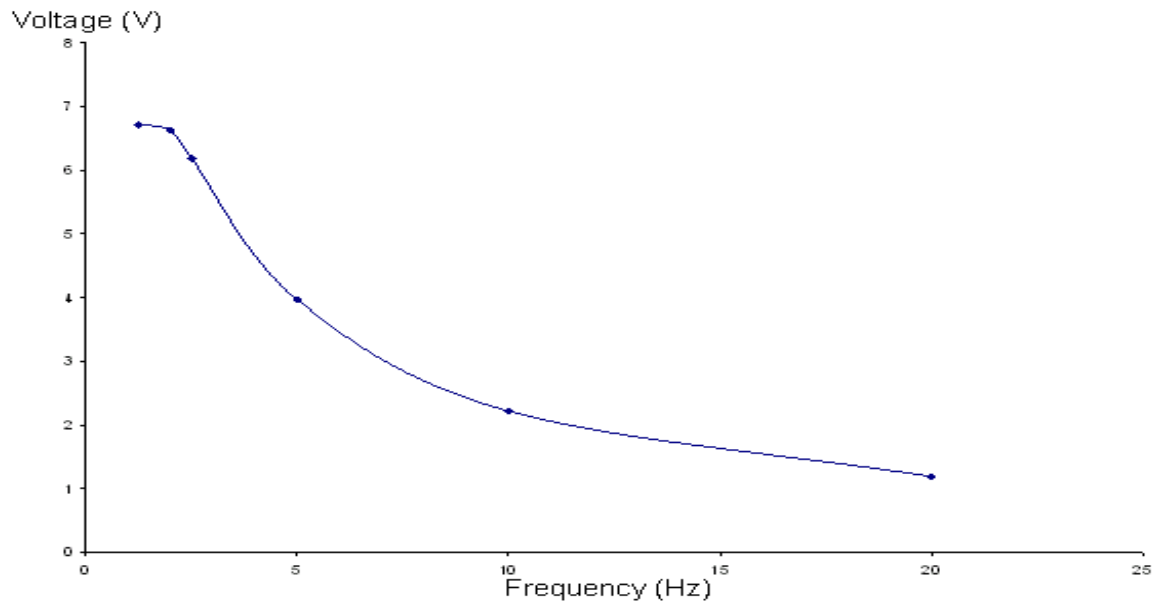
Figure 6.10: Variation of PAS signal with modulation frequency at laser DC current of 80mA, EDFA at 24dBm and temperature =12.801kΩ

Figure 6.10 shows the effect of the sinusoidal modulation frequency on the acoustic signal amplitude. The signal amplitude decreases as the modulation frequency is increased due to the decreased energy absorbed per cycle.

6.4.3.3 Wavelength Adjustment by Temperature

Figure 6.11 shows the effect of diode temperature changes, similar to the ramp modulation as discussed earlier. This is due to the shift in the centre wavelength of the laser diode which changes the harmonic content of the PAS signal according to the position on the absorption line as illustrated in Figure 6.12.
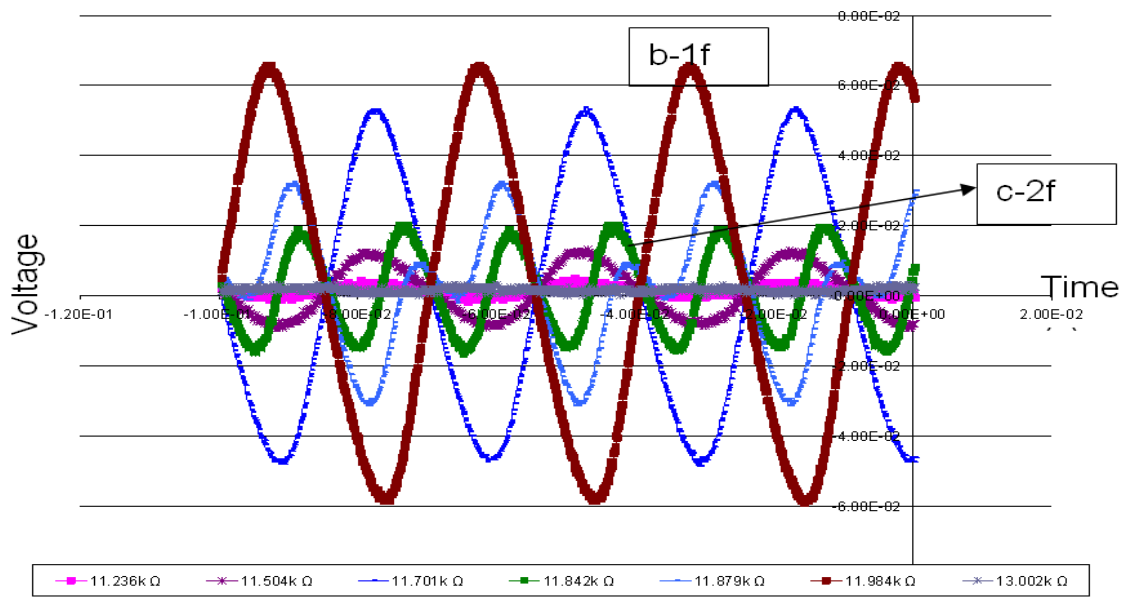
Figure 6.11: Effect of temperature on PAS signal
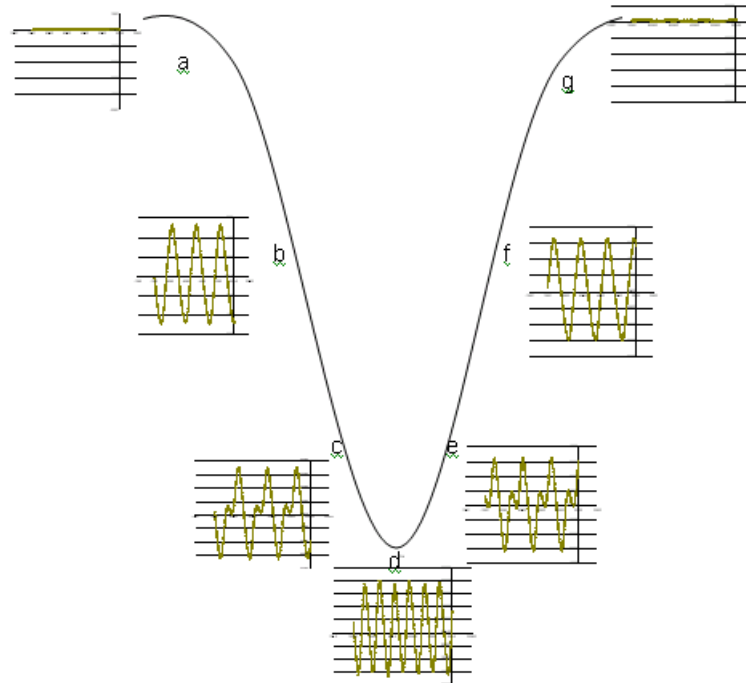
Figure 6.12: Output signal at different positions on absorption line

For Figure 6.12, the EDFA was set at 24dBm, the diode laser dc current was 60mA and

the frequency modulation at 33Hz. At the start of the sweep, before any absorption, there is zero intensity modulation induced by the FM, the temperature was at 10.995kΩ. Gradually the slope of the absorption profile increases negatively; thus the intensity modulation induced by the FM increases in magnitude but is 180° out of the phase relative to the FM induced signal on the right hand side of the gas absorption line. This is reflected in the negatively increasing 1st harmonic content. The gradient of the absorption line is at its maximum at point b (temperature at 11.705kΩ), giving rise to the maximum 1st harmonic. From this point the gradient decreases again to the absorption line centre where the 1st harmonic is zero. At this point the second harmonic is maximum and can be seen from the oscilloscope trace (temperature at 11.842kΩ). After the peak absorption point, the gradient of the absorption line increases positively to a maximum at f (temperature at 11.984kΩ). At the end of the scan the gradient of the absorption line and consequently the FM induced intensity modulation returns to zero. The 1st harmonic signal mapped out by the lock-in amplifier is presented in the following section.

6.4.3.4 Lock-in Amplifier (LIA) Experimental Results

From the experiment above, all harmonics can be seen by manually tuning the temperature resistance. To isolate the harmonics from the waveform and increase the signal to noise ratio, a lock-in amplifier (LIA) SR Stanford was employed. Meters on the front panel of the LIA showed the value of the X component and Y component for the selected harmonic. A sinusoidal waveform of 33Hz frequency was applied as the modulation signal with an amplitude of 450mV. The laser DC current was set to 60mA and temperature was varied from 10kΩ to 13kΩ with the EDFA in the range of 20-27dBm. The output of the laser diode controller was connected to the oscilloscope as a reference signal whereas the output from the detector was connected to the LIA and a BNC cable was used to connect the output of LIA either from channel X or channel Y to the oscilloscope as shown in Figure 6.13.

160
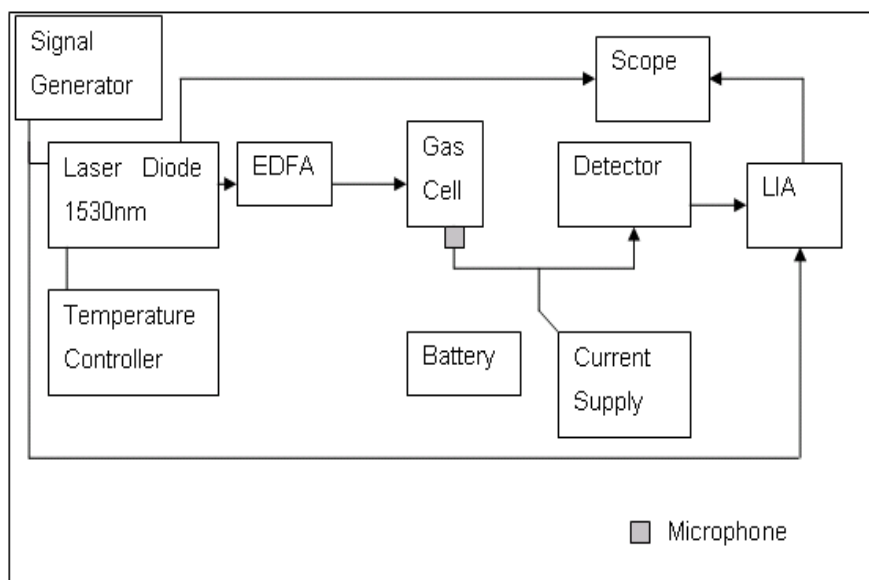
Figure 6.13: Experimental setup for lock-in detection of PAS signal

6.4.3.5 First and Second Harmonic Signals from LIA with Temperature Scan
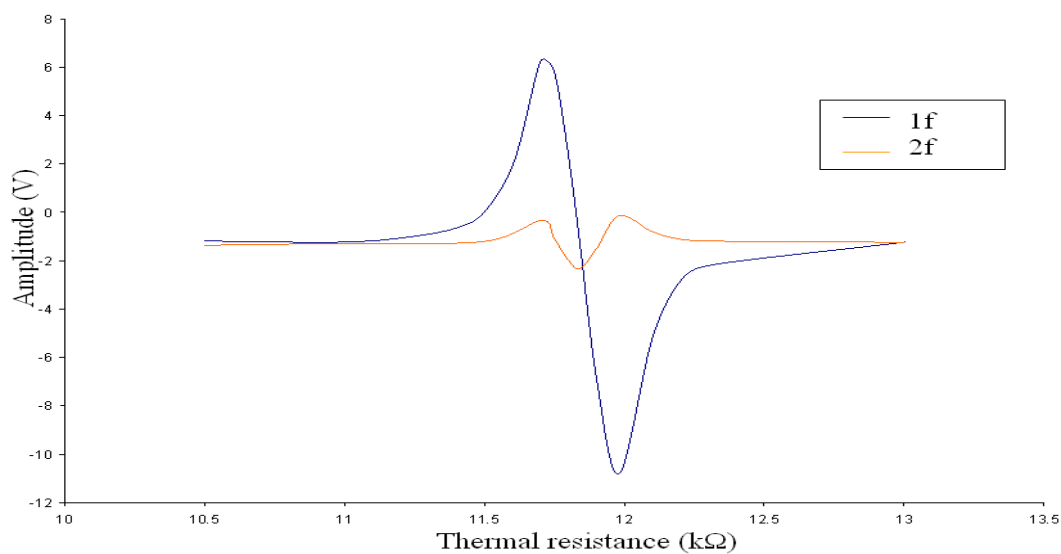
Figure 6.14: X-component for 1f and 2f from the LIA measurement at dc=60mA and EDFA=24dBm
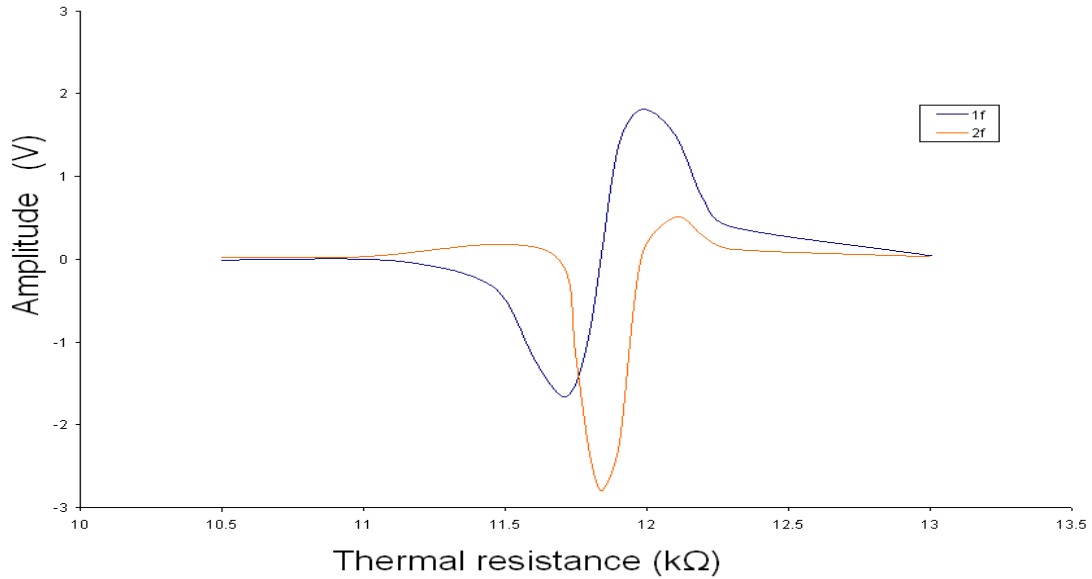
Figure 6.15: Y-component for 1f and 2f from the LIA measurement at dc=60mA and EDFA=24dBm

The laser was scanned around the absorption line of acetylene by adjusting the temperature resistance. Figure 6.14 and Figure 6.15 shows the X and Y components for 1f and 2f signals. The right peak is higher than the left peak due to the distorting effects arising from the simultaneous AM and FM which occurs when the diode laser current is modulated.

6.4.4 Application of Previous Techniques (Ramp or Sinusoidal Modulation) for Gas Detection

Both the techniques described in the previous sections were employed in this section and compared for measurement of low gas concentrations.

For the ramp modulation, with the intention of detecting a low concentration, a method of subtraction of the background signal and noise from the gas measurement was employed based on the off- and on-absorption line positions during scanning under the same operating conditions. The background signal and noise can be obtained when the laser is scanning

through the off-line position and was subtracted from the on-line signal. Two specific thermal resistances were determined for the on- and off-line wavelengths, namely, 13.9kΩ for on-line and 12kΩ for off-line. A 2Hz ramp signal of 1.6V amplitude was used for the experiment, which was the same as before. The power output of the laser diode was amplified by the EDFA at 27dBm due to the low gas concentrations used. Output of the detector was multiplied by 10 for clearer vision on the oscilliscope.

For the second method, sinusoidal modulation from a function generator was used to modulate the diode laser and, simultaneously, the wavelength was manually tuned across the absorption line by adjusting the thermal resistance of the temperature controller of the diode laser. A 33Hz frequency, 450mV amplitude signal was set on the function generator and the output of the laser was amplified by the EDFA at 27dBm. The acoustic signal detected by the microphone was amplified by a pre-amplifier (OptoSci, LNP 2A) and connected to the LIA.

6.4.4.1 Pure Nitrogen

Figure 6.16 presents the initial signals observed on the scope before the cell is filled with acetylene gas with the ramp modulation signal. This procedure is important to obtain a reference and background signal. A small difference for both the selected thermal resistances is observed although there was no acetylene gas in the cell. This was due to noise from the environment such as equipment, components and vibration.

(a) Ramp reference

(b) Signal at 12kΩ

(c) Signal at 13.9kΩ

(d) Difference between (b) and (c)
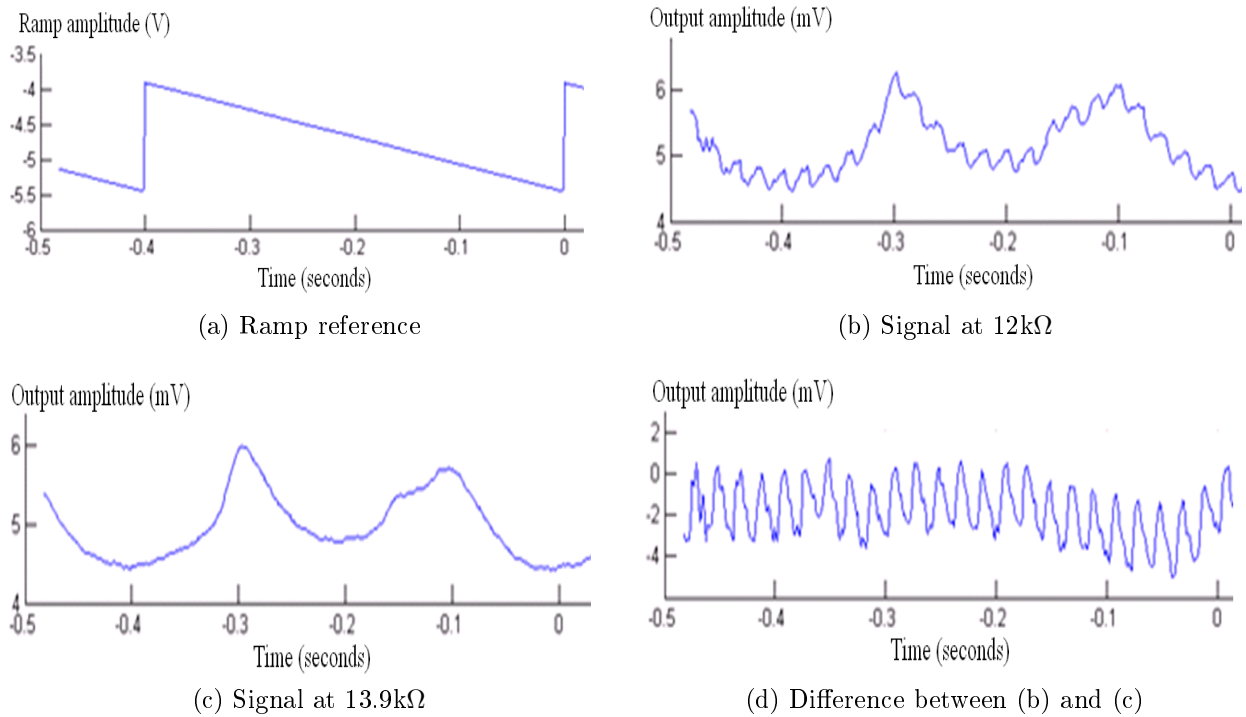
Figure 6.16: Signals observed on scope with ramp modulation for pure nitrogen at off- and on-acetylene line positions

Figure 6.17 shows the output from the LIA with a sinusoidal modulation signal, which was unstable and fluctuating during the measurement time.
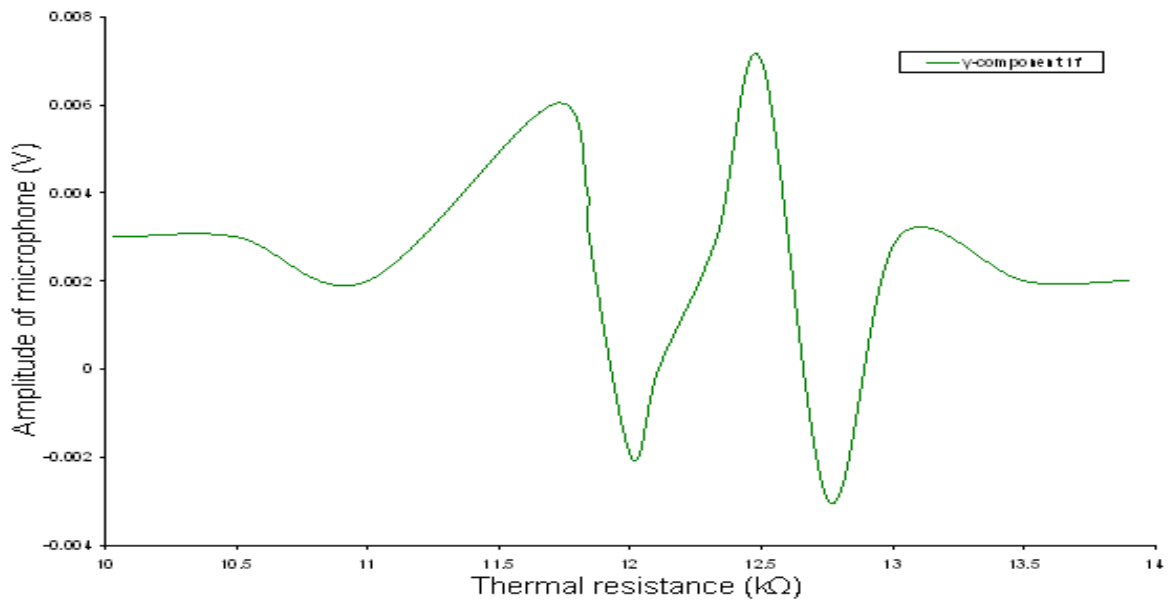
Figure 6.17: y-component of 1f for pure nitrogen in the gas cell with sinusoidal modulation

6.4.4.2   Signals for 10ppm of Acetylene Gas

10ppm of acetylene gas was now added to the cell and it was observed, for the ramp modulation, that there was significant difference in amplitude between the background signal and the combined signal as shown in the oscilloscope trace of Figure 6.18 where (a) is the combined signal and (b) is the gas signal after background subtraction. For the LIA measurement with sinusoidal modulation, even though the concentration is low, the first and the second harmonics can be clearly seen. From the magnitudes of the signals obtained, the system could be expected to detect <1ppm gas concentration.

(a) Signal at 13.9kΩ

(b) Difference
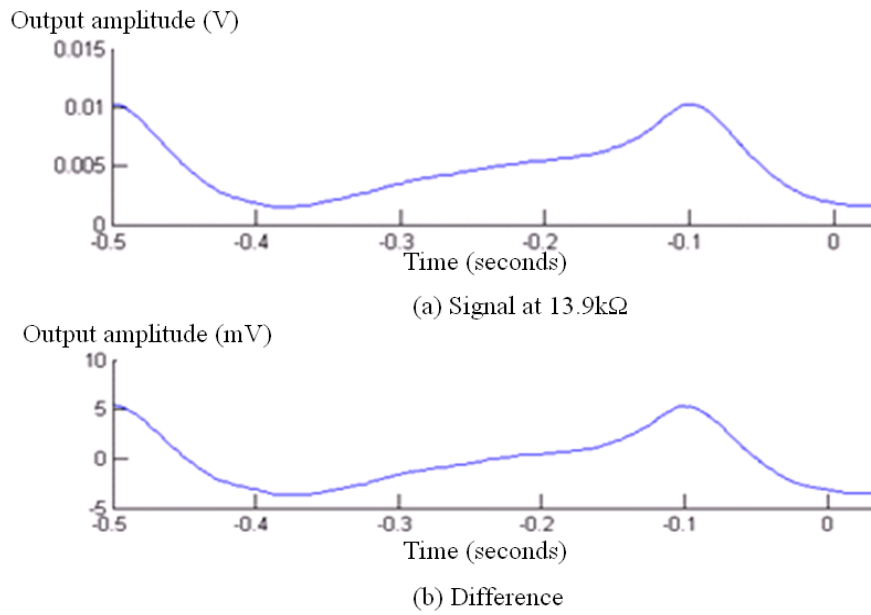
Figure 6.18: Oscilloscope trace for 10ppm of acetylene gas with ramp modulation
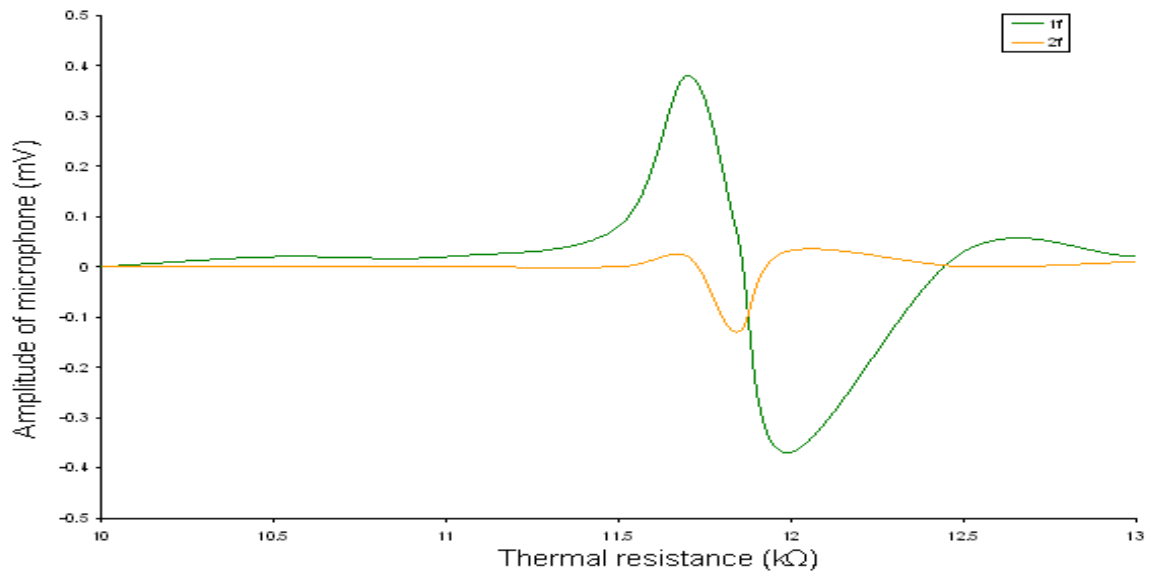
Figure 6.19: y-components of 1f and 2f for 10ppm acetylene gas and sinusoidal modulation

6.4.4.3 Signals for 1ppm and 0.5ppm of Acetylene Gas
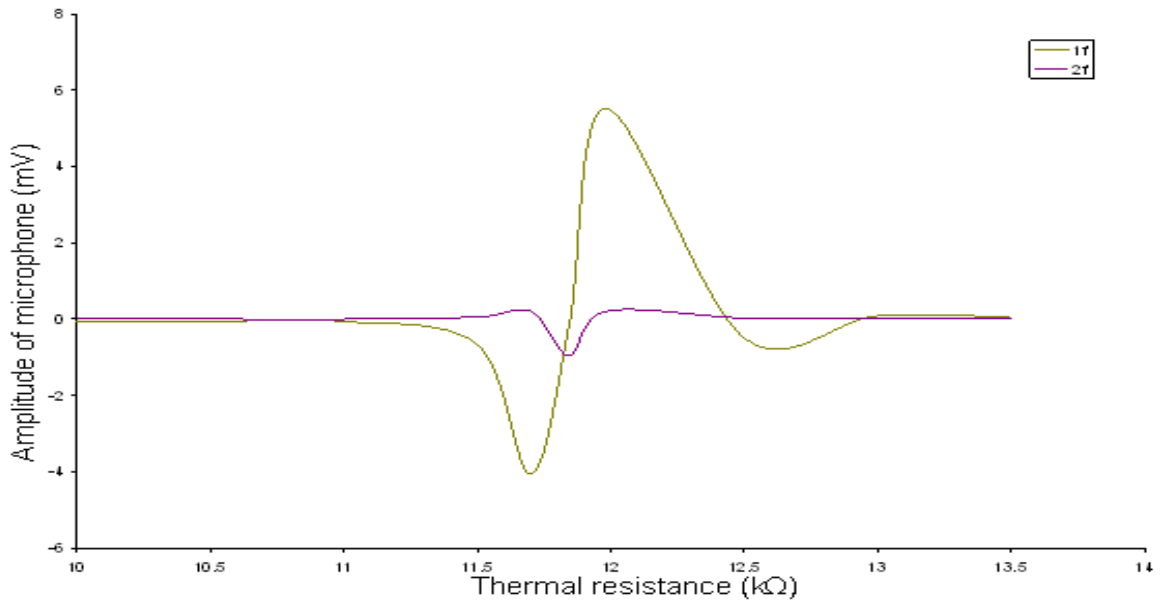
Figure 6.20: Harmonic signals for 1ppm acetylene using sinusoidal modulation
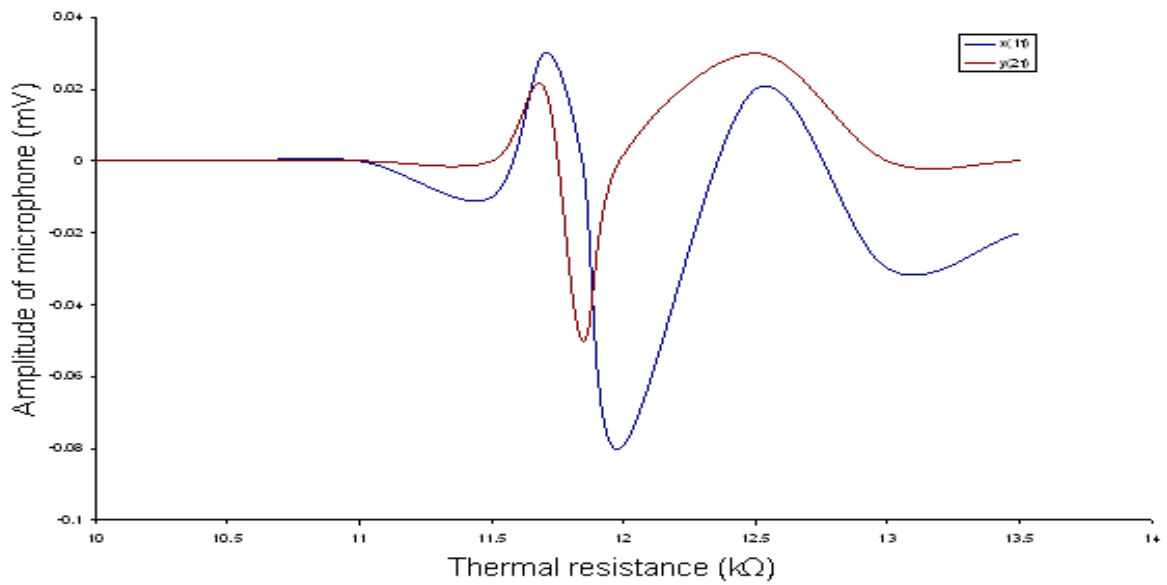
Figure 6.21: Harmonic signals for 0.5ppm acetylene using sinusoidal modulation

Referring to Figure 6.20, clear 1f and 2f signals were obtained with 1ppm of concentration. However signals fluctuated when lower concentrations such as 0.5ppm acetylene (as shown in Figure 6.21) were measured. It should be noted that water vapour and carbon dioxide are present in the atmosphere and likely in the cell during gas filling by a syringe. Also noise is more significant at lower concentration.

6.4.5 Combination of Ramp and Sinusoidal Modulation (Third Modulation Technique)

Instead of thermal scanning, combination of both the ramp and sinusoidal modulation of the diode laser current eases the process of scanning the centre wavelength automatically and fast. This can conveniently be done by creating an arbitrary waveform using software provided by Agilent, namely Waveform Editor which is available on the company's website. A frequency ratio of 1:33 was used for the combination signals, with 1Hz and 1.6Vp-p signal amplitude for the ramp signal and 33 Hz, 450mV amplitude for the sinusoidal signal. The waveform was sent to the function generator via a RS323 cable and output waveform is displayed in Figure 6.22
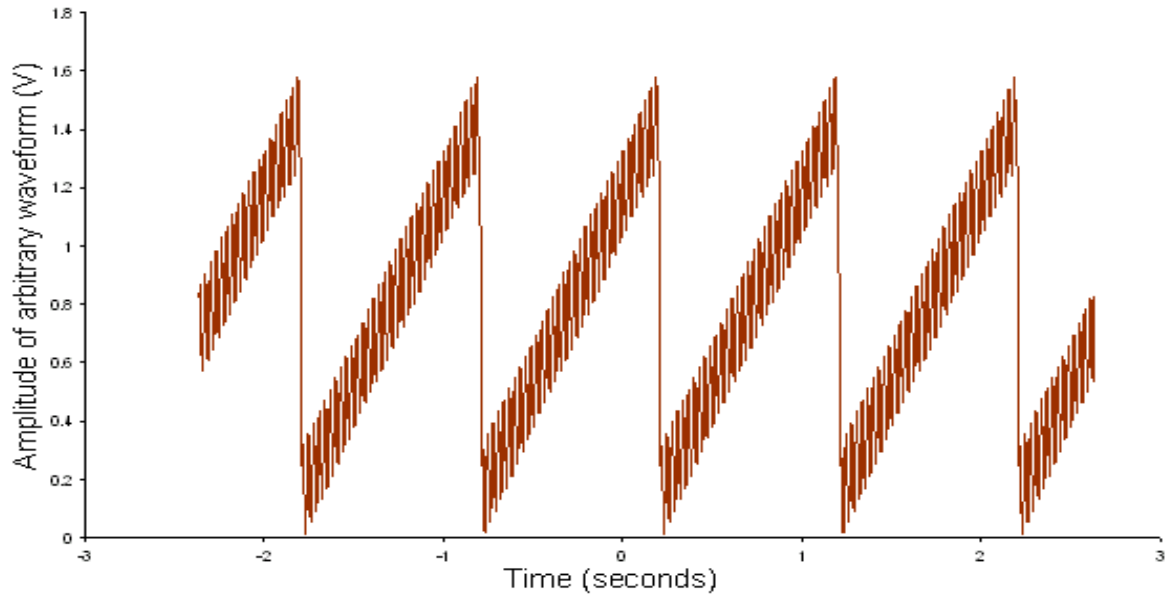
Figure 6.22: Combined sine and ramp waveforms from function generator with 1 Hz ramp and 33 Hz sinusoidal waveforms

For this investigation, the thermal resistance was set at 12.711 kΩ, DC laser current at 60mA and 27dBm of EDFA output power to test 1% of acetylene gas. 33Hz from internal source served as the reference signal at the LIA.

6.4.5.1 PAS Signals with 1% Acetylene Gas

Figure 6.23 shows the oscilloscope trace of the PAS signal (at thermal resistance of 12.117kΩ) around the middle of the absorption line as the wavelength is ramped across the absorption line by the combined modulation waveform. The variation of the first harmonic content and the appearance of the second harmonic around the line centre is clearly evident. Figures 6.24 and 6.25 show the results from the output of the LIA for first and second harmonics at the x channel. Time constant of 10ms and sensitivity of 200mV were set on the LIA.

169
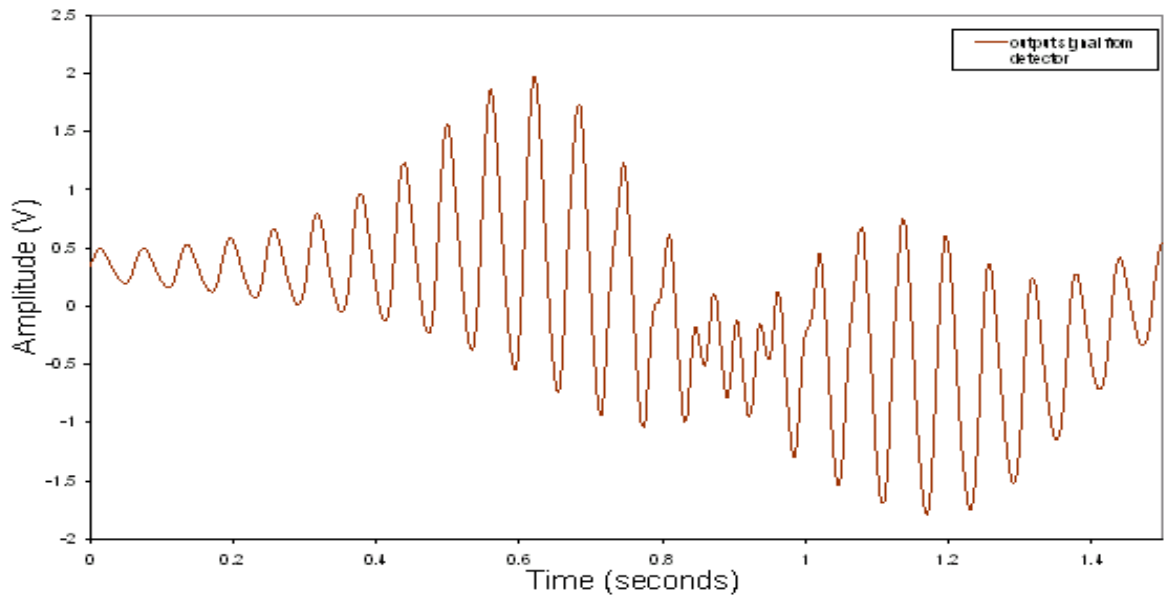
Figure 6.23: Output signal observed on oscilloscope for 1% acetylene at 12.117kΩ thermal resistance with laser bias current at 60mA
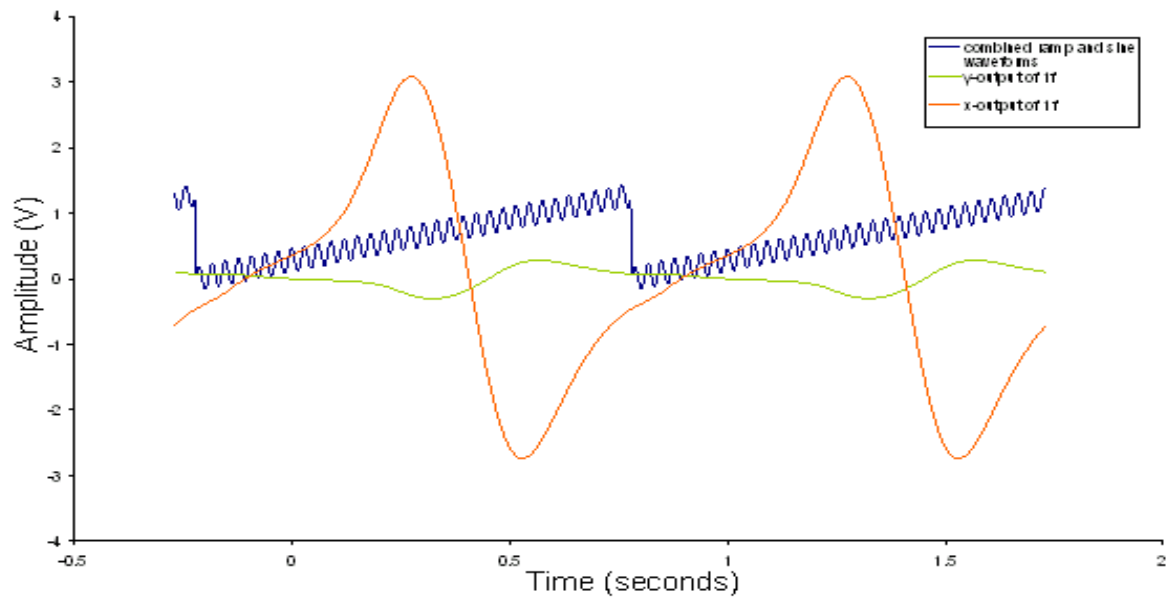
Figure 6.24: First harmonic from LIA for combined modulation waveform with ramp of 1Hz and sinusoidal modulation of 33Hz (1% acetylene)
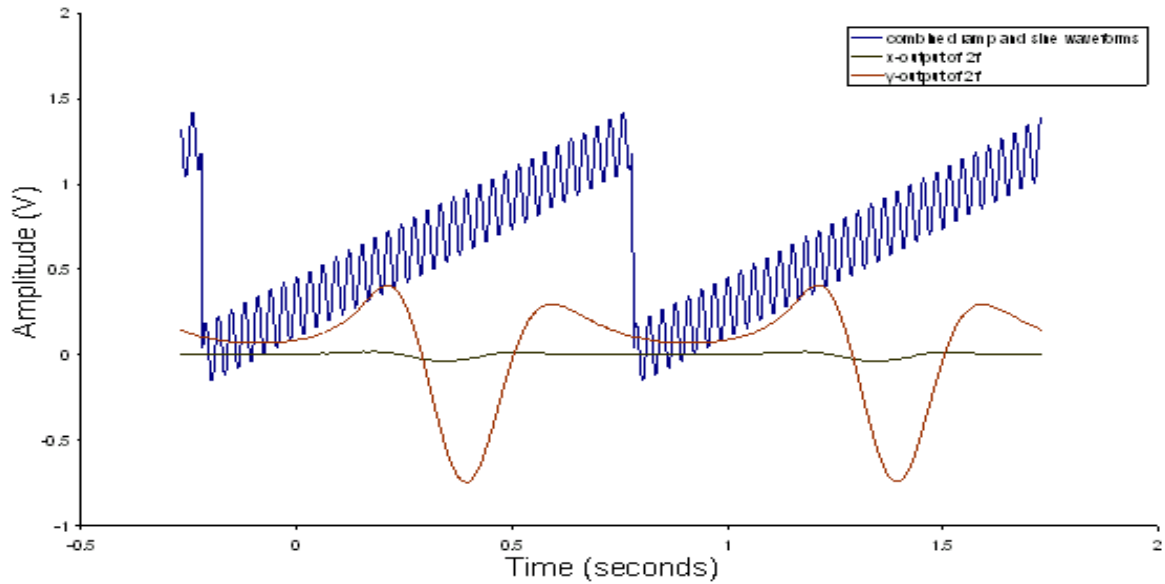
Figure 6.25: Second harmonic from LIA for combined modulation waveform with ramp of 1Hz and sinusoidal modulation of 33Hz (1% acetylene)

As shown by the above results, the combination of ramp and sine waveform has been successfully implemented, with only one function generator needed for the experiment. The results are very promising and reliable for gas detection especially with the use of the LIA.

The figures above show that the left peak is higher than right peak (reversed compared with Figures 6.14 and 6.15. As stated earlier, this distortion arises from the combined AM and FM when the laser diode current is modulated. The reason for the reversal is that the wavelength decreases with increased current which is the opposite characteristic with temperature tuning (in kΩ) as performed before. Therefore the harmonic signals for current tuning are reversed compared with temperature tuning and thermal resistance as shown below in Figure 6.26 and Figure 6.27.
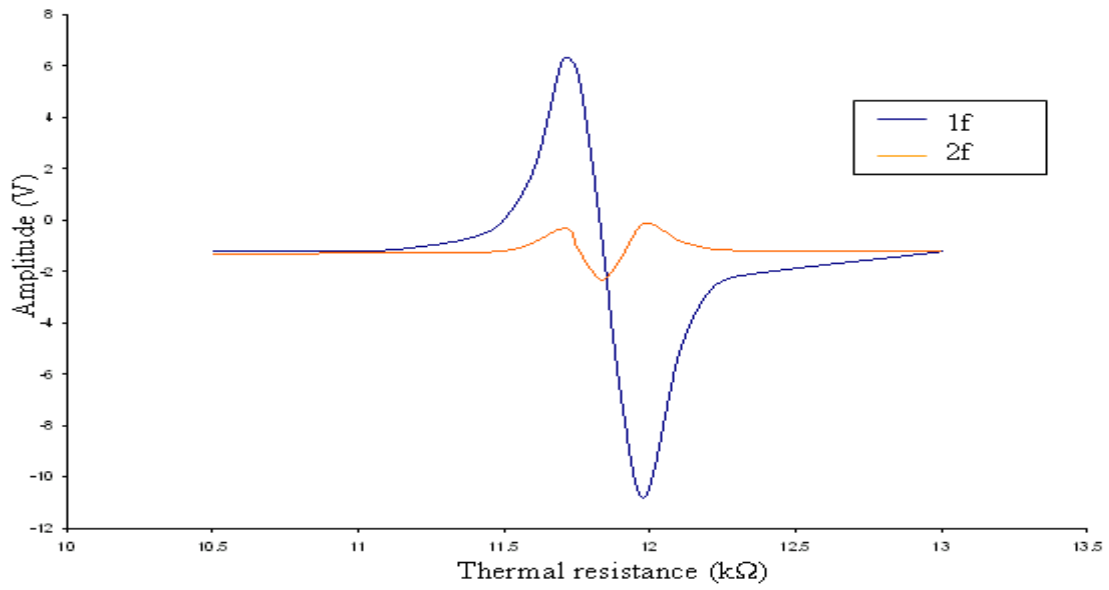
Figure 6.26: Temperature tuning in kΩ for X-component of 1f and 2f at dc=60mA and EDFA=24dBm
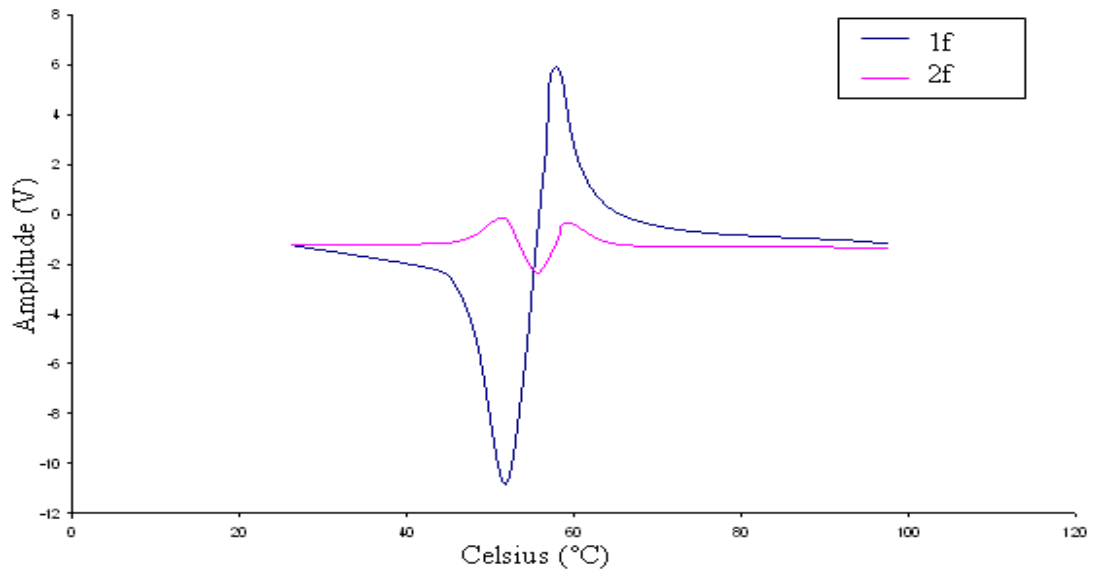
Figure 6.27: Temperature tuning in °C for X-component of 1f and 2f at dc=60mA and EDFA=24dBm

6.4.6 Combined Sinusoidal Modulation with Automatic Temperature Scan

Instead of using combined ramp and sinusoidal modulation signals applied to the laser diode current, there are some advantages in seeking to automatically temperature scan the wavelength if the response of the TEC is fast enough and can follow the ramp signal. This method is easier to implement since no programming is needed to create an arbitrary waveform as discussed above.

To investigate this, the PID of the TEC was adjusted to get a desired speed of temperature tuning in order to scan through the absorption line. It was difficult to get a fast response to follow the actual temperature setting due to the device limitations as most applications seek a stable temperature. A delay of about 200ms between input and output of the TEC was observed as depicted in Figure 6.28.
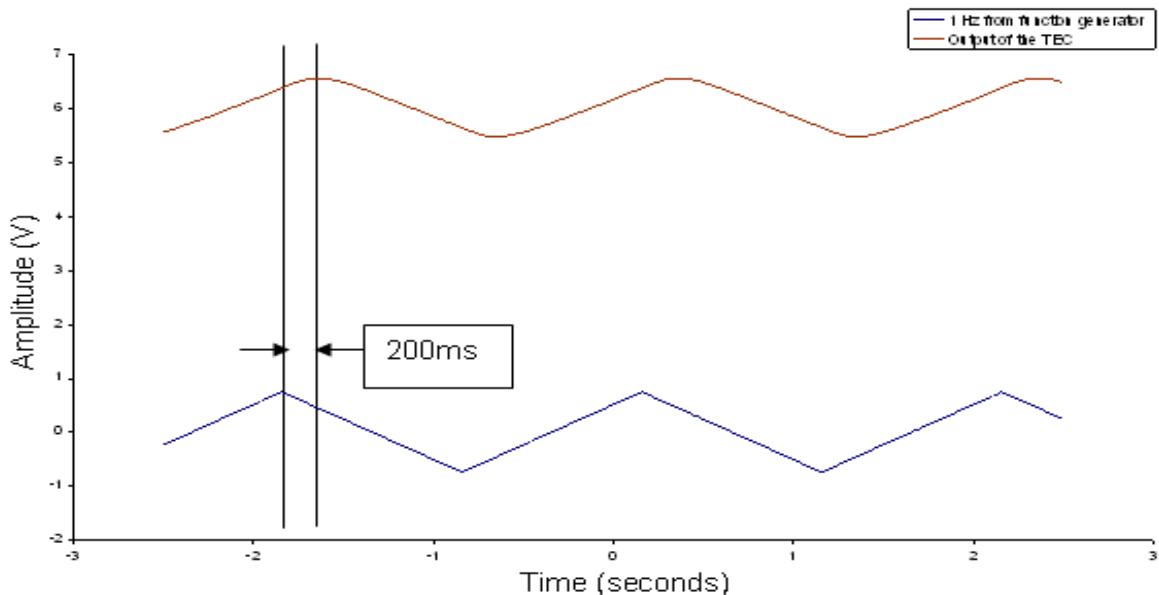
Figure 6.28: Delay between actual signal into the TEC and the output signal from the TEC

Figure 6.29 shows the amplitude of acoustic signal when the PID was adjusted. Results, displayed on the oscilloscope, were taken directly from the system with temperature scan

only. First and second peaks indicate increases and decreases of temperature automatically done by the TEC. However, the second peak of the backward scan was unstable due to the delay stated above.
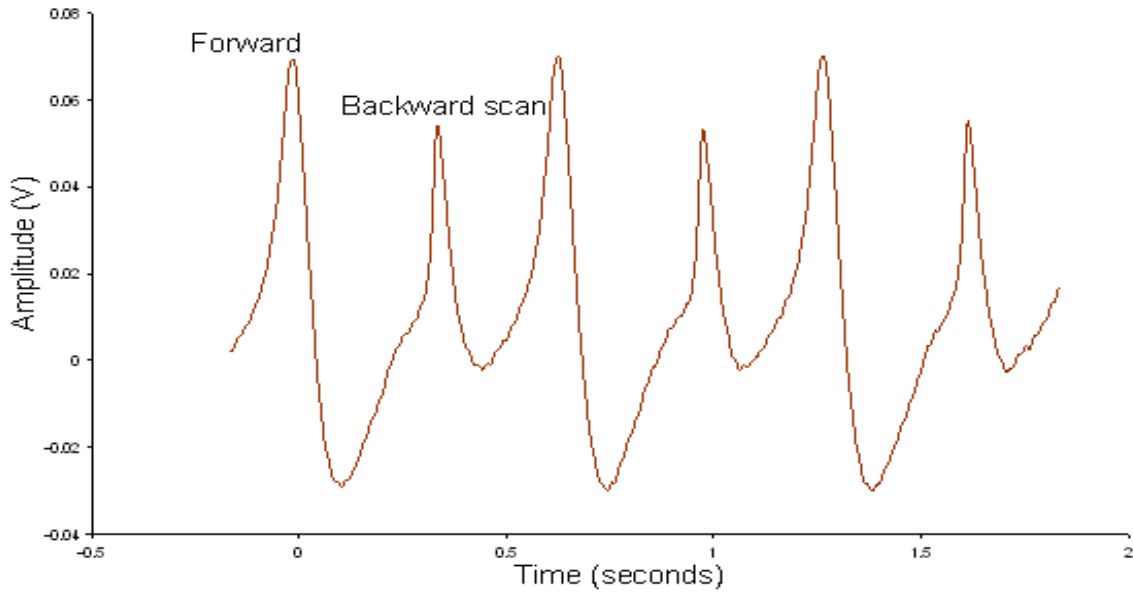
Figure 6.29: Output acoustic signal from automatic temperature scan by the TEC

Figure 6.30 shows the output observed on the oscilloscope and output from the LIA is shown in Figure 6.31 with combined sinusoidal modulation applied to the diode laser current and temperature scan.
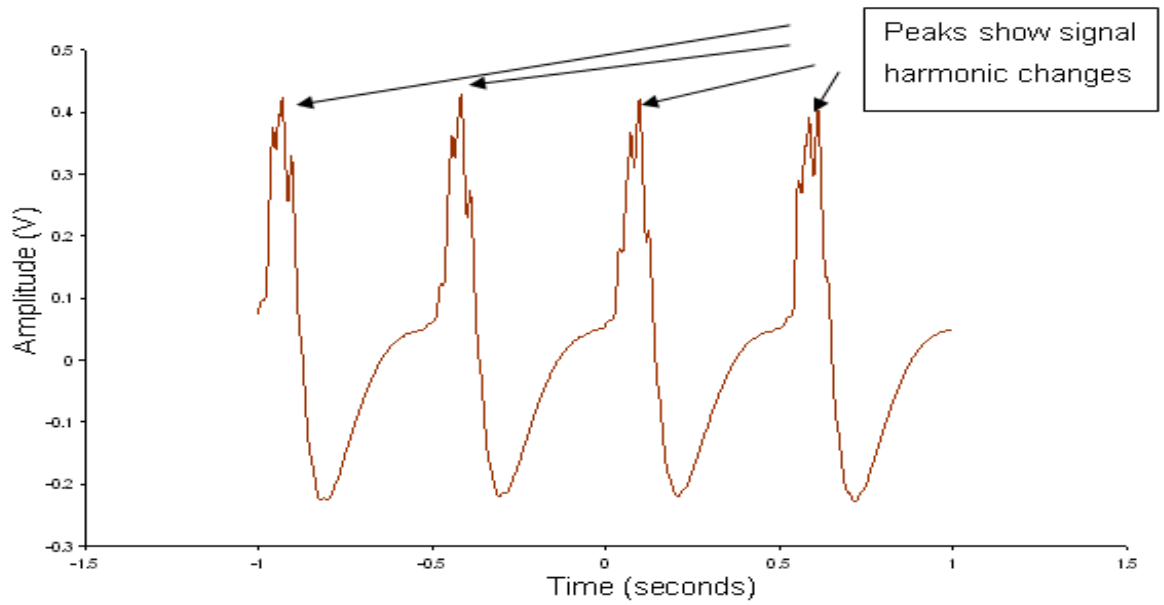
Figure 6.30: Output signal obtained from oscilloscope
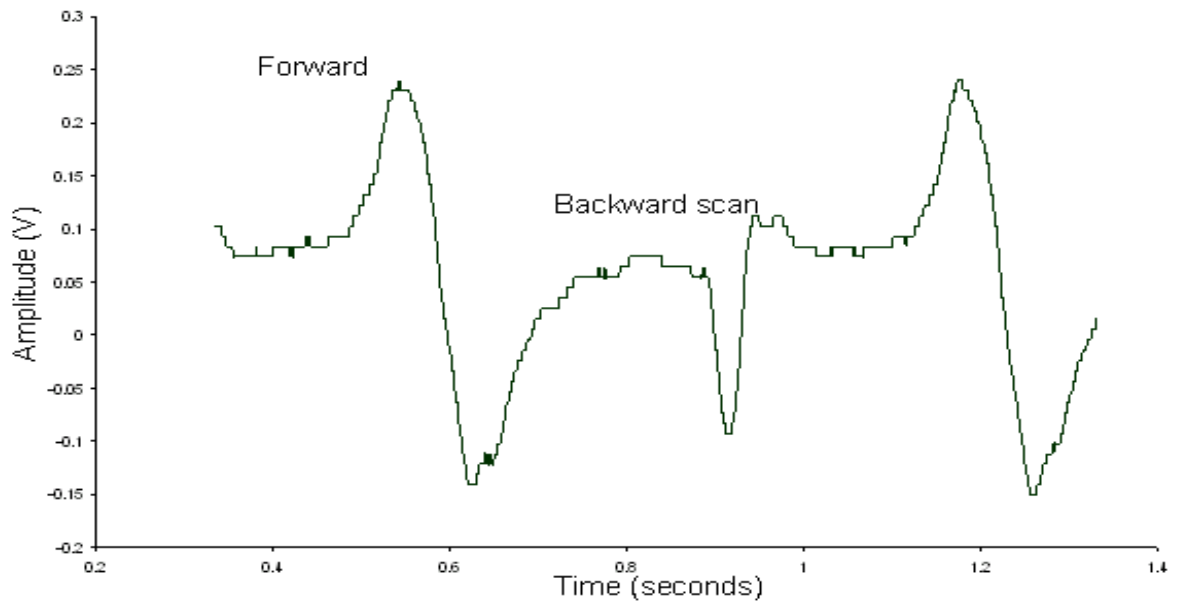
Figure 6.31: x- output of first harmonic for 1% of acetylene gas

The automatic temperature tuning is a potentially useful method if the response of the TEC can be adjusted faster and can follow the exact ramp signal without any delay.

6.5 Investigation of PAS with Erbium Doped Fibre Lasers System

From the previous section, the figures showed that different amplitudes of the right and the left peaks for the 1f and 2f harmonics were observed due to the simultaneous AM and FM which occurs when modulation is applied on the diode laser. The erbium doped fibre laser system with the PA cell was studied in this section in an effort to obtain undistorted signals and to explore the feasibility of EDFLs with PAS for trace gas sensing. Moreover the zero background of PAS is an important advantage for EDFL systems using simple intensity modulation. Figure 3.15 shows the schematic diagram of the experimental EDF ring laser with a saturable absorber (SA). A photoacoustic (PA) cell was utilised to differentiate this study with that previously reported in Chapter 3. As with the diode laser source, the acoustic signal produced from the microphone is amplified by a pre-amplifier before being connected to measurement equipment such as the oscilloscope and the LIA.

6.5.1 PAS using EDFL with Intensity Modulation for Spectroscopy

Operation of the EDFL source is similar to that reported in Chapter 3 where a micro-optic gas cell was used, but here a photoacoustic cell is used for PAS. For the EDFL source, instead of using wavelength modulation as was done with diode lasers in the previous section (resulting in both AM and FM), the EDFL pump current is modulated to obtain simple intensity modulation only, described by the following equation:

$$P = P_0 + \triangle P cos(\omega t) \tag{6.19}$$

where P is output of the laser in the frequency range of the gas absorption line, P_0 is the un-modulated laser power, ω is the angular frequency of the sinusoidal pump modulation

and $\triangle P$ is the intensity modulation amplitude.

6.5.2 Ramp Scanning and Direct Detection

A ramp of 5Hz frequency with 95% symmetry from a function generator was amplified by a voltage amplifier (OptoSci) to obtain enough voltage to stretch the PZT controlling the wavelength of the EDFL in order to scan over the acetylene absorption line at 1535.39nm. It was noted that 100V gave 0.1nm of wavelength shift. The experimental setup is depicted in Figure 6.32.
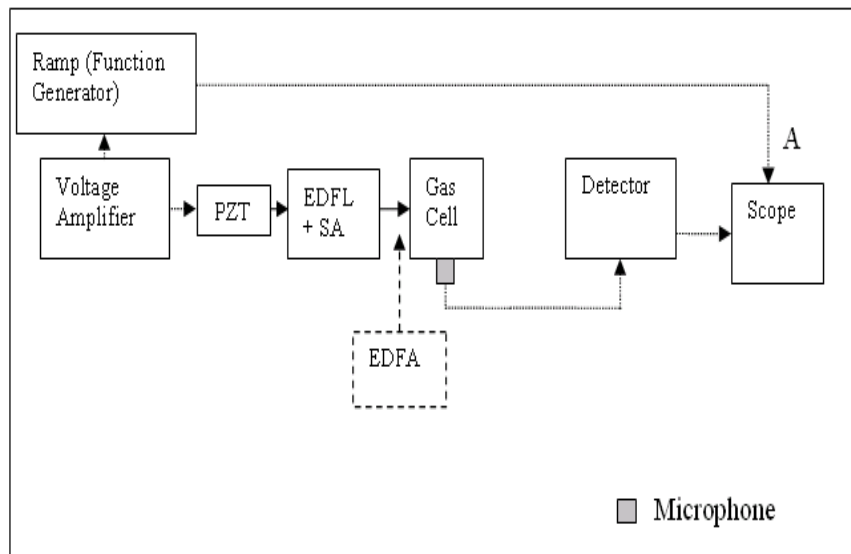
Figure 6.32: Experimental setup using an EDFL with a PA cell

6.5.2.1 Effects of the EDFA

An EDFA was employed at the output of the EDFL to amplify the laser output power to improve the signal to noise ratio as can be seen in Figure 6.33 which shows that the signal is noisy and unstable when operating without the EDFA. The improvement achieved is indicated in Figure 6.34 which shows that the output of the system is more stable and the amplitude is much greater with the EDFA. Note that Figure 6.34 shows the direct output

PA signal observed on the oscilloscope for 1% acetylene without modulation of the pump as the wavelength is scanned through the acetylene line.
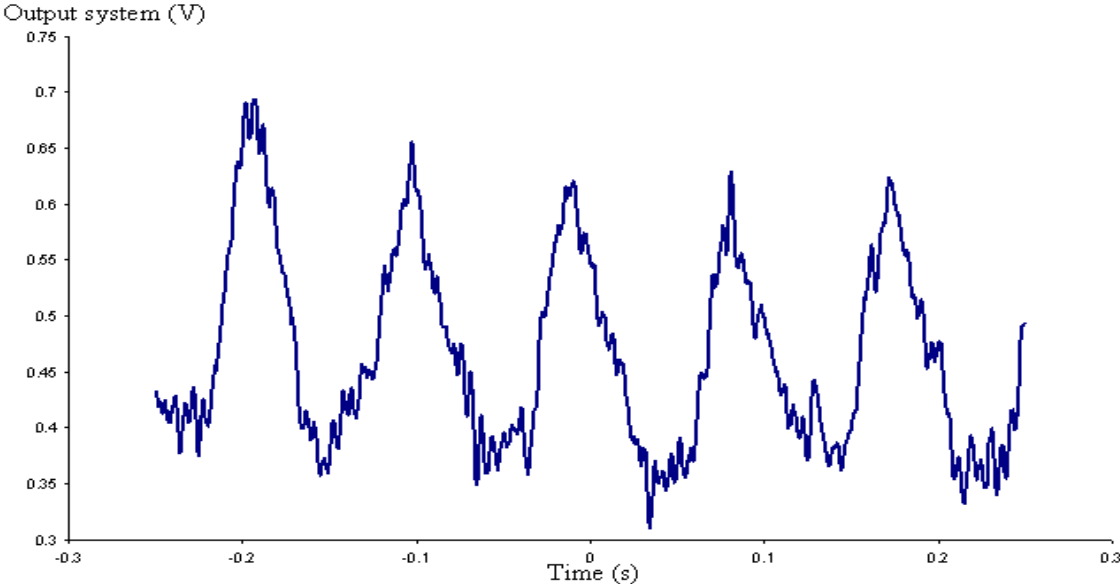
Figure 6.33: Output of the system without an EDFA
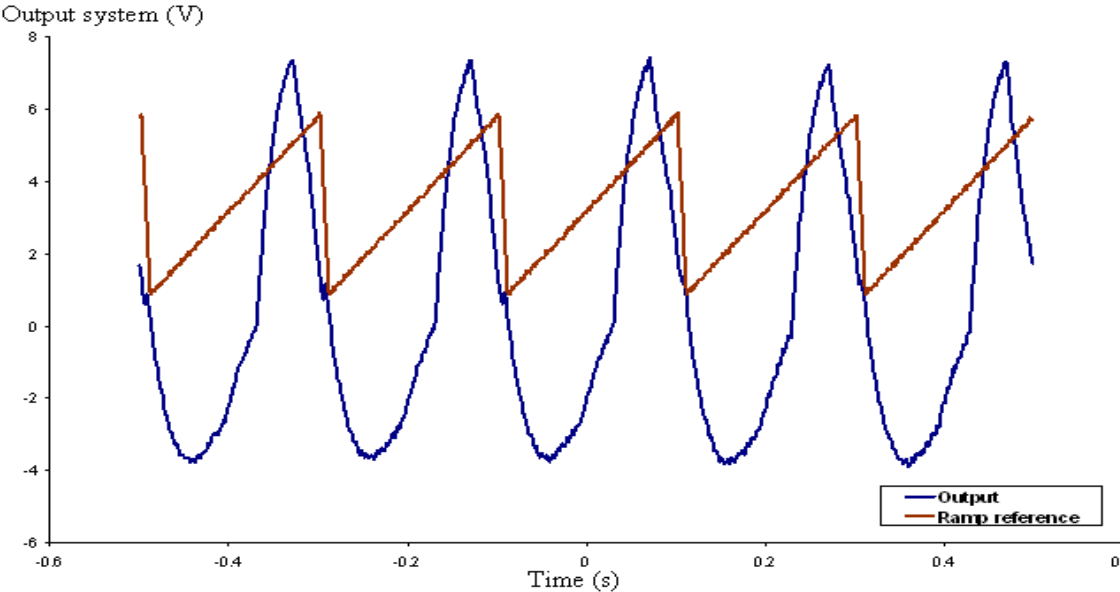
Figure 6.34: Output signal with 1% of acetylene gas (with EDFA at 80mW)

Only 150V was achieved with the available voltage amplifier and as mentioned earlier, the

tuning range of the PZT is 0.001nm/V. Thus the centre wavelength of the laser was situated at the edge of the ramp signal as indicated in Figure 6.34 since the scanning range is not fully across the absorption line.

6.5.2.2 No Gas (Nitrogen) Background Signal

Figure 6.35 shows that the output signal is almost zero when nitrogen gas is filled into the cell. The change is significant compared to Figure 6.34 where the peak output signal amplitude is 7.5V for 1% acetylene with a x60 multiplier setting of the pre-amplifier.
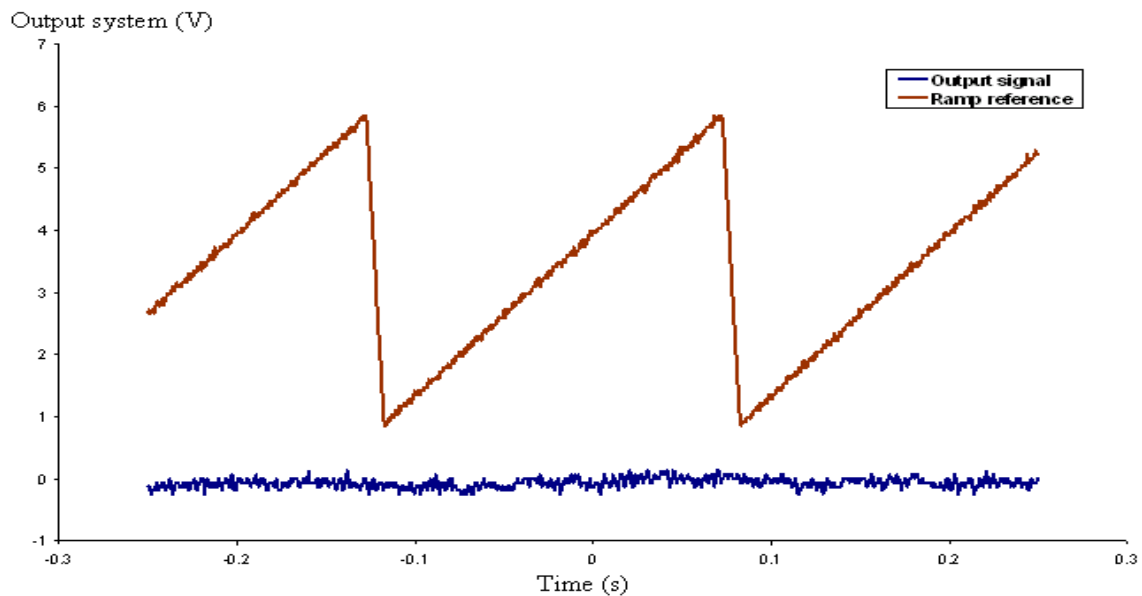
Figure 6.35: Output signal without gas in the cell

6.5.3 Sinusoidal Modulation

For pump modulation, a range of frequencies from 1 Hz to 3.5 kHz (with 800mVpp and 2.2V bias, based on earlier results) were applied to the EDFL pump in order to get the optimum frequency for maximum PA signal output. Results for the output PA signal are shown in Figure 6.36 which shows that the highest output is at 2.5 kHz which is the acoustic resonance frequency of the cell.
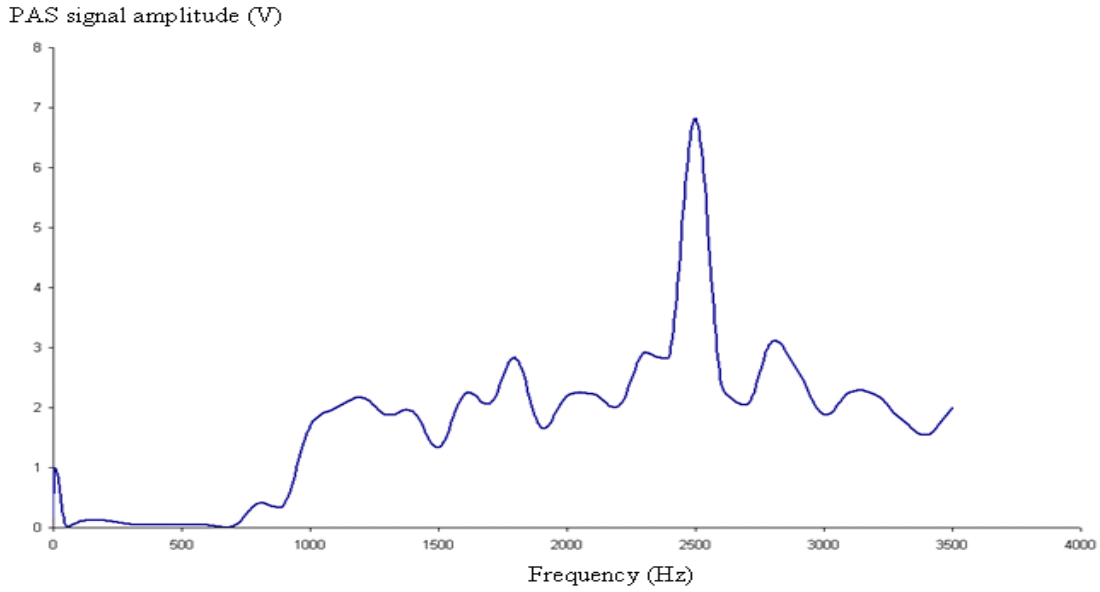
Figure 6.36: Variation of photoacoustic signal peak to peak amplitude with frequency of laser pump sinusoidal modulation

The resonance frequency of the first longitudinal resonance mode of the PA cell can be calculated by equation 6.20:

$$f = c/2L \tag{6.20}$$

where c is velocity of the acoustic wave which is 344 m/s at room temperature and atmospheric pressure, f is the first resonance frequency, and L is length of resonator. Substituting 2.5 kHz as the first resonance frequency into equation 6.20 the resonator length of the gas cell can be calculated as 7.0 cm which coincides approximately to the actual length of the cell. Full detail of the gas cell structure is presented in Figure 6.37.
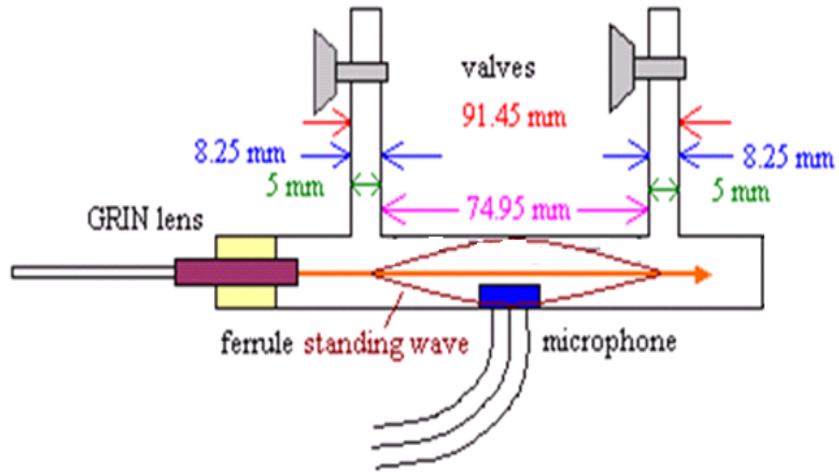
Figure 6.37: The PA cell structure

6.5.4 Gas Measurements Using the EDFL With Pump Modulation
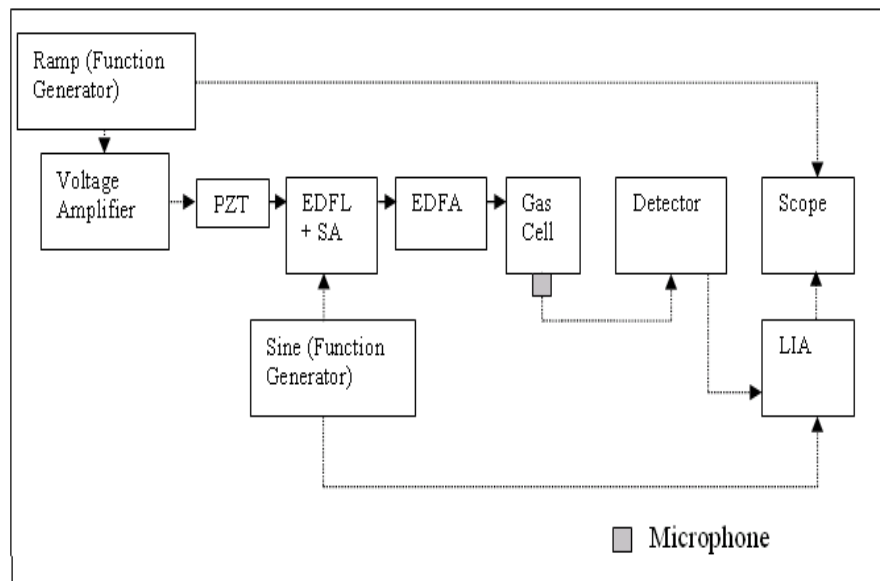
Figure 6.38: Setup of PAS experimental with pump modulation and wavelength scanning

The full experimental arrangement using the EDFL with pump modulation for gas measurements with PAS is shown in Figure 6.38.

The EDFL with SA is the same as that described in Chapter 3. A power of 70mW from the EDFA was set to avoid power overloading. A 20:80 single mode fibre coupler was used to tap off 20% of the output power to an optical spectrum analyzer (OSA: Agilent 86140B resolution of 0.06nm) for wavelength referencing and monitoring while the remaining 80% was launched into the PA cell. Output signals from the PA cell were measured by a lock-in amplifier and an oscilloscope for data collection.

6.5.4.1 Experimental Results on Gas Measurements

Figures 6.39 to 6.41 show the experimental results obtained for the Y component of first, second and third harmonic signals from the lock-in amplifier with 1% acetylene gas.
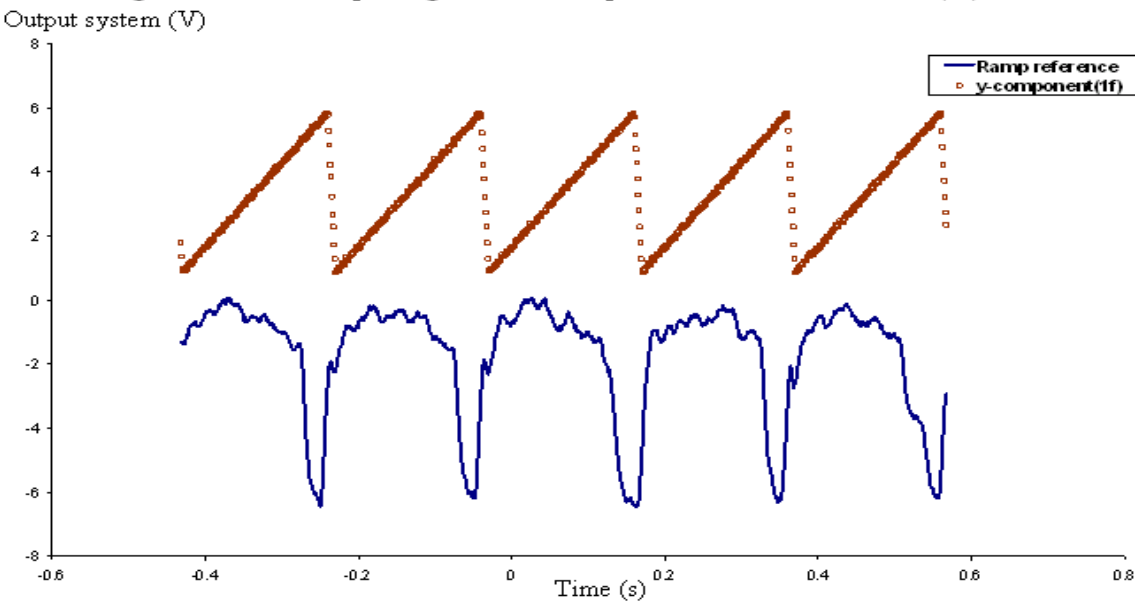
Figure 6.39: Output signal at y-component of first harmonic (1f)
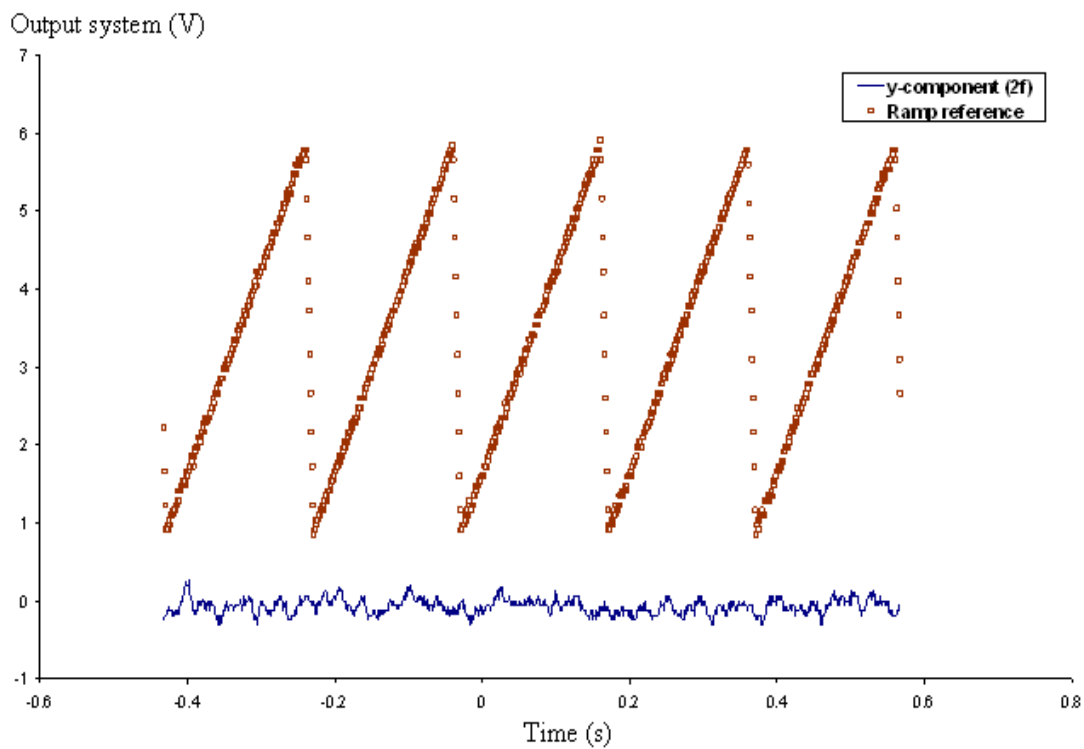
Figure 6.40: Output signal at y-component of second harmonic (2f)
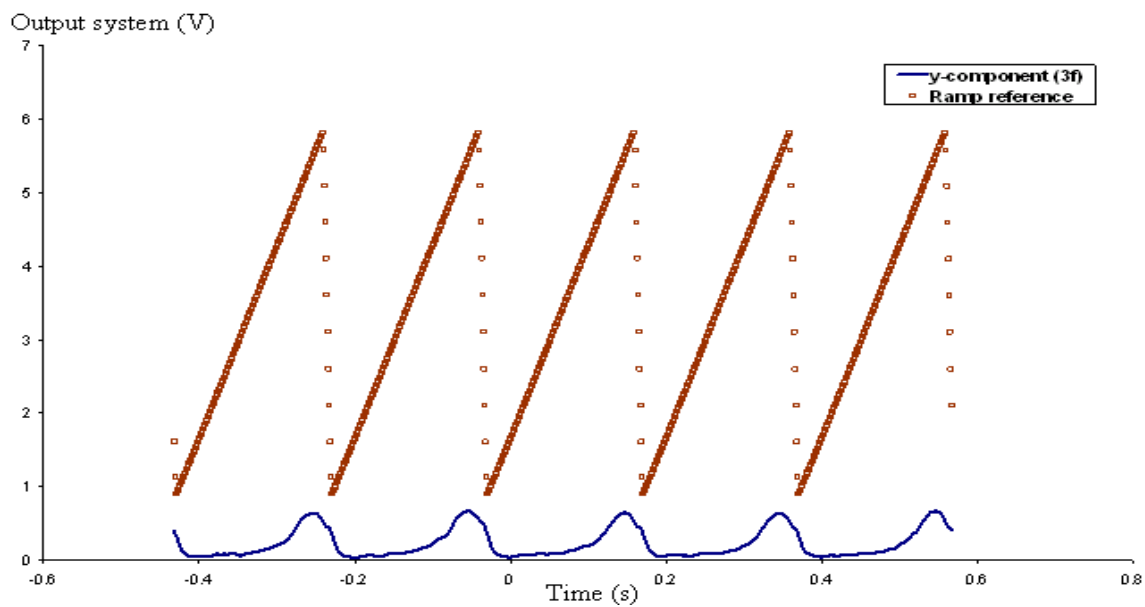
Figure 6.41: Output signal with 1% acetylene at y-component of third harmonic (3f) with amplitude of 0.67V

As shown in the figures above, large signals were obtained at the first harmonic, 6V for y-component in Figure 6.39. There was no signal at the second harmonic in Figure 6.40 as expected since there is only intensity modulation at 1f applied to the EDFL. The noise level was $\sim$ 80mV without gas and hence 1% was measured at a signal to noise ratio of $\sim$ 75. Hence a sensitivity of $\sim$ 100ppm is possible at a S/N $\sim$ 1. A signal was seen at the third harmonic in Figure 6.41 due to the coupling of acoustic resonance mode of cell to higher order acoustic resonance at 3f.

6.5.4.2 Wavelength Referencing and Comparison to Theoretical Profiles

The absorption profiles obtained (Figures 6.39 – 6.41 above) have a time x-axis corresponding to the ramp; therefore it is necessary to relate this axis to the corresponding change in the optical wavelength of the fibre laser in order to compare experimental observations with theoretical predictions in curve fitting. The wavelength range is shown in Figure 6.42, where the laser scans from 1535.248nm to 1535.428nm which is about 0.15nm with 300V output of the voltage amplifier.
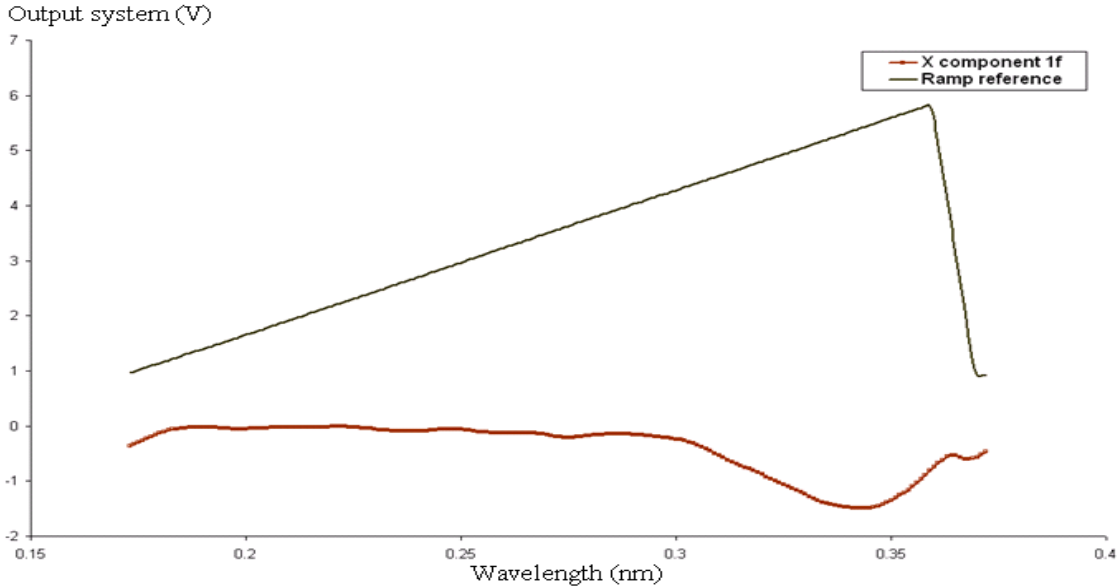
Figure 6.42: x- component of 1f from lock-in showing wavelength shift from ramp signal

184
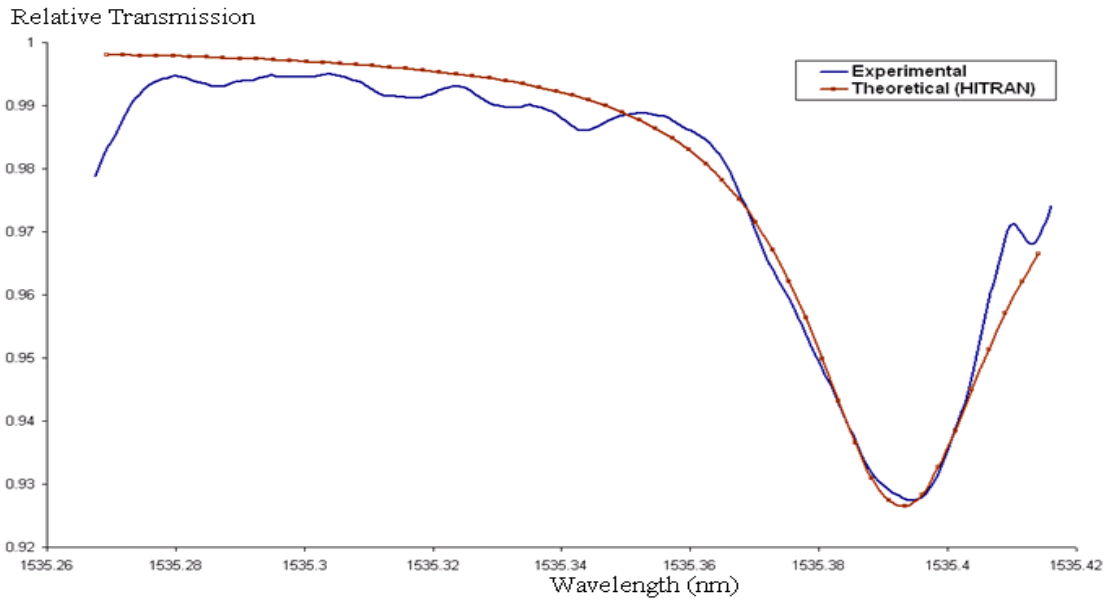
Figure 6.43: Relative transmission for 1% of acetylene at atmospheric pressure and room temperature

Figure 6.43 shows the experimentally measured absorption line compared with the theoretical line at 1535.395nm. As can be seen from Figures 6.42 and 6.43, the absorption line lies unfortunately at the edge of the ramp signal due to the limited stretch range of the PZT/grating. It was also observed that the grating was creeping due to the acrylate recoating material for the FBG (softer than a polyimide coating) and, as a result, the centre wavelength was progressively shifting backward to a shorter wavelength. In order to get the absorption at the centre of the ramp signal, a higher voltage is required to further stretch the grating but due to equipment limitations this was not possible. One solution was to peel off the coating and directly glue the core of the fibre to the PZT but this process needs careful handling to avoid breakage of the grating. The simplest way to solve the problem was to re-stretch the grating and re-glue to the PZT. Figure 6.44 is result obtained after re-stretching using the same limited voltage supply.
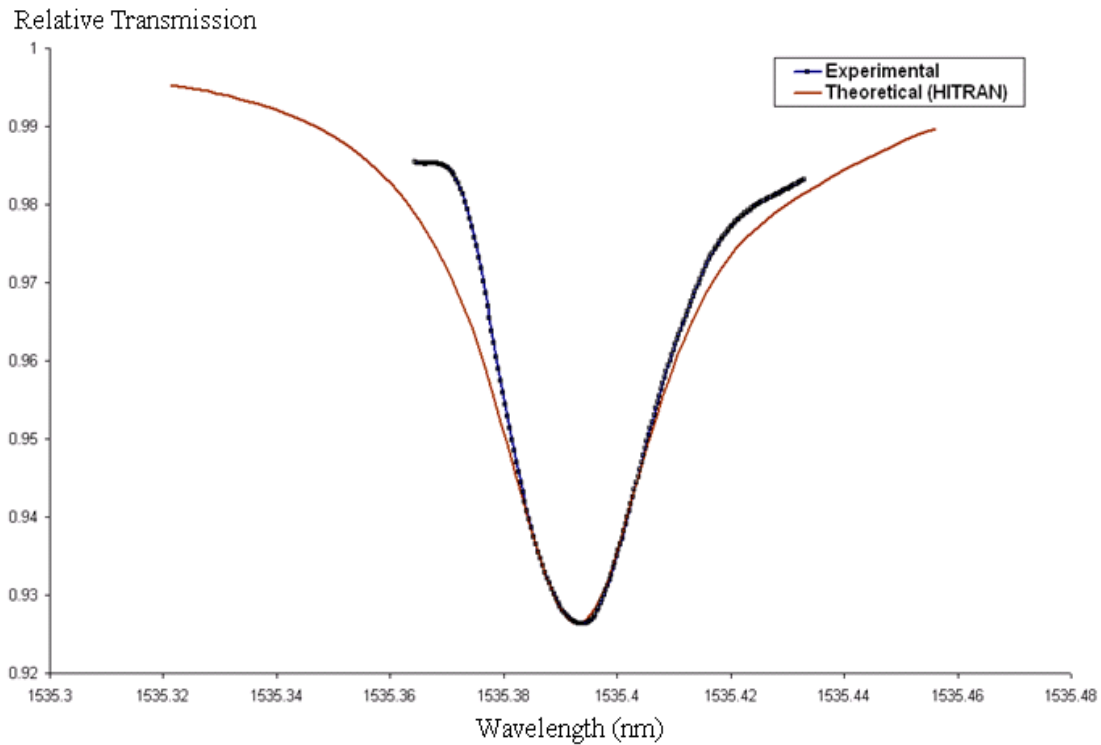
Figure 6.44: Absorption profile compared with theory after re-stretching of the grating

6.6   Conclusion

This chapter has reported an investigation into photo-acoustic spectroscopy, initially using diode lasers to become familiar with PAS and WMS techniques and then using the EDFL system for PAS. Several modulation formats were investigated in both cases.

Injection current modulation of diode lasers produces both wavelength and intensity modulation, with a phase shift dependent on the modulation frequency. This results in residual amplitude modulation on the output and in distortion of harmonic signals derived from the absorption line. Parameters such as the amplitude of the laser frequency dither, the relative phase of the laser frequency and intensity modulation, and the background RAM amplitude over the entire frequency sweep need to be accurately measured in order to successfully implement WMS with diode lasers if line-shape recovery is required. This results in increased

complexity of the system.

Hence the EDFL system was investigated where simple intensity modulation (without FM) can be obtained by pump modulation to directly obtain the absorption line profile. The performance of the EDFL system with PAS was much better and had a higher sensitivity compared to the spectroscopy system using the micro-optic gas cell described in Chapter 3. The output signal with the PA cell was more stable and has the very important advantage of having a zero or very low background 1st harmonic signal level at the output of the LIA. In contrast, the EDFL system of Chapter 3 has a high signal background level and the gas absorption produces only relatively small changes compared to background level, resulting in low sensitivity.

With further development , it is expected that the EDFL system with PAS can be improved and the system sensitivity enhanced. Currently, the PAS cell used in the system discards the output light. If a new cell is designed so that the output light is collected by a GRIN lens then the PAS cell could be placed within the EDFL cavity for combining ICLAS with PAS. Only a small amount of light needs to be tapped from the cavity (for optical monitoring purposes only) so that a high intra-cavity power could be realised, removing the need for an external EDFA.

Chapter 7

CONCLUSION AND FUTURE WORK

7.1 Summary of the thesis

The basic aim of the thesis was to investigate the compatibility of fibre laser systems with different spectroscopic techniques for the interrogation of the relatively weak overtone absorption lines of gases such as acetylene, carbon dioxide and methane.

Chapter 2 provided a review of spectroscopic techniques, including optical and acoustic detection, with a focus on gas spectroscopy. Use of different types of laser sources was reviewed along with the advantages of fibre lasers for gas spectroscopy. Since the performance of a gas sensing system using a particular technique depends on the components and devices involved in the setup, a summary of the required components was also included in this chapter. An explanation was provided on how experimental results may be compared with theoretical results by use of the HITRAN database.

Chapter 3 demonstrated the working operation of the erbium doped fibre laser system and optimisation was carried out in order to test its compatibility with gas spectroscopy requirements such as stable, narrow linewidth operation and wavelength tunability in order to scan through absorption lines. In contrast to current modulation with diode lasers which

produces both AM and FM modulation, the EDFL system employed simple intensity modulation (from modulation of the pump current) and scanning of the wavelength with a grating only. However, long cavity fibre lasers are normally associated with stability problems, such as frequent mode hopping, and this was suppressed by introducing a saturable absorber into the system. The saturable absorber was made of a length of unpumped erbium doped fibre with polarization maintaining components to improve the performance. Two different setup arrangements were investigated in the SA section, namely, a loop mirror as a reflector with a Sagnac loop filter, or a fibre Bragg grating with a PZT. The fiber Bragg grating was used to determine the lasing wavelength while the Sagnac loop filter or PZT provided a means for wavelength scanning. Preliminary results demonstrated that the system was feasible for detecting acetylene absorption lines (typically detecting $\sim$0.005dB of attenuation) but further work would be necessary to improve sensitivity and for accurate line shape recovery. The system was also rather complex.

A much simpler set-up was introduced in Chapter 4 by placing the micro-optic cell within the laser cavity and using the broad-band ASE already present within the cavity. The ASE provides a convenient broad-band source for the interrogation of several gases within the gain-bandwidth of the fibre laser and sensitivity enhancement was observed from the multiple circulations of the ASE light within the cavity near threshold conditions. Successful operation with several gases, such as 1% C_2H_2, 100% CO_2 and the very low strength lines of 10% CH_4, was demonstrated. For example, 16 absorption lines in the 1530nm region with a path length enhancement of $\sim$60 was observed for 1% acetylene gas, effectively transforming the 6cm micro-optic cell into a path length of $\sim$3.5m.

Chapter 5 reported a preliminary investigation into the use of the DFB-FL as alternative way of solving the mode hopping problems that afflict long cavity fibre lasers. The DFB-FL system was constructed and its performance was characterised. A thermal wavelength scan along with laser intensity modulation (by pump current modulation) was investigated

for spectroscopy purposes but a number of practical difficulties associated with the fragility of the DFB laser were encountered which prevented successful demonstration of a working system.

Chapter 6 introduced photo-acoustic spectroscopy and this was initially investigated with a diode laser (in order to become familiar with its principles and properties) and then with the EDFL system of Chapter 3. This system was much more stable and reliable compared to those of the previous chapters. In particular, the virtually zero background signal level with photo-acoustic spectroscopy means that the simple laser intensity modulation technique is very effective for sensitive gas concentration measurements (unlike the situation in Chapter 3 where the gas produces only a small change in a high background level). Additionally the problem of line-shape distortion from combined AM and FM modulation in diode lasers is avoided.

In summary the main contributions of the thesis have been:

1) Development of an EDFL system incorporating a saturable absorber for improved stability and use of intensity modulation (through pump modulation) combined with wavelength scanning for both standard and photo-acoustic spectroscopy. In particular, the system is viable in photo-acoustic spectroscopy where there is a zero background level with no gas present.

2) Demonstration of a simple method of ICLAS for sensitivity enhancement using the ASE present within the laser cavity. Approximately 2 orders of magnitude sensitivity enhancement has been conclusively demonstrated with the potential for multi-gas sensing.

7.2 Comparison of Systems Studied

Based on the previous chapters, a summary of the key results from the systems tested is tabulated in Table 7.1 as follows:

System	Estimated Sensitivity	Problems	Advantages
1. EDFL + SA	0.5% acetylene	High background signal with no-gas condition, thus only small changes could be detected when gas present. Only one absorption line can be detected due to specific wavelength of FBG used in system.	Pump modulation produces only intensity modulation of the laser output, with phase sensitive detection, hence easier line-shape recovery.
2. EDFL + SA with PAS	133ppm acetylene	Specific wavelength of FBG used in the system, thus only one absorption line can be detected.	Stable, zero-background, high sensitivity. Pump modulation produces only intensity modulation of the laser output, with phase sensitive detection, hence easier line-shape recovery.

System	Estimated Sensitivity	Problems	Advantages
3. Diode lasers with PAS	0.5ppm acetylene	Current modulation produces both amplitude and frequency modulation. Data processing is needed to recover actual line shapes and absorption strength of a gas line. Need a high power EDFA (250mW) for signal amplification.	Stable,high sensitivity and calibration-free line-shape recovery possible through special techniques such as residual amplitude modulation (RAM) and phasor decomposition (PD) approaches.
4. DFB FL	Not available	Specific wavelength, fragile device, expensive and lack of proper control in tuning.	Stable, single-mode, narrow-linewidth and mode-hop-free laser.
5. ASE with ICLAS	166ppm acetylene 100% carbon dioxide 10% methane	Careful calibration required to determine enhancement factor.	Simple set-up, using the broadband ASE already present within the cavity. Higher sensitivity and multi-gas lines can be detected.

Table 7.1: Summary of the characteristics of the different types of spectroscopy investigated

From the table above, the ICLAS would be the best and the most promising technique with erbium-doped fibre laser systems for further investigation in gas spectroscopy. If the calibration issues can be solved, this technique could provide a simple, sensitive and multi-gas sensor system.

7.3 Future Work

Future work relates to improving stability, dealing with calibration issues and extending the capabilities of the systems investigated in the thesis, bearing in mind that the basic reason for considering fibre lasers is to take advantage of properties such as their broad bandwidth and compatibility with fibre optic systems for remote, multi-point sensing.

The fibre laser systems constructed here were for test purposes and were mostly used in unshielded laboratory conditions with many fibre optic connectors for convenience in adding or removing components. Better stability would be expected if all the connections were spliced together to reduce loss and packaged in a proper casing or styrofoam case to lessen environmental perturbation and acoustic noise. For the DFB fibre laser, further investigation should be carried out to improve operation and to test its performance with gas in a cell to determine the sensitivity that can be achieved.

Calibration issues are important and a reference gas cell could be used to determine calibration factors. For the ICLAS system using ASE, it is necessary to calibrate the enhancement factor and one method under consideration is the use of the weak etalon fringes from a simple intra-cavity etalon formed by reflections from the ends of a $\sim$ 1cm length silica glass or quartz rod placed within the micro-optic cell. These fringes produce a defined intensity variation with wavelength across the ASE bandwidth and could possibly be used for calibrating the observed absorption lines.

Although PAS showed the most promising results compared with the other methods, there is still room for improvement in the gas cell design and system operation. Proper acoustic isolation from the outside world and the microphone configuration is critical to optimise the sensitivity. On-going developments in components and devices such as MEMS mirrors could be used for laser modulation in order to get better signal to noise ratios. Currently, the PAS cell discards the output light. If a new cell is designed so that the output light is collected by a GRIN lens then the PAS cell could be placed within the EDFL cavity for combining

ICLAS with PAS. Only a small amount of light needs to be tapped from the cavity (for optical monitoring purposes only) so that a high intra-cavity power could be realised, removing the need for an external EDFA.

Finally, all studies performed here have been at room temperature and atmospheric pressure. It would be useful for the system to be tested with various conditions of pressure and temperature to see its effectiveness in monitoring pressure or temperature variations as well as concentration. This would widen the scope of applications for fibre laser systems in the future.

.

Bibliography

[1] P. J. Lambert, A. G. Whitman, and O. F. Dyson, "Raman spectroscopy: The gateway into tomorrow's virology," *Virology*, vol. 3, no. 51, 2006.

[2] B. Culshaw, G. Stewart, F. Dong, C. Tandy, and D. Moodie, "Fibre optic techniques for remote spectroscopic methane detection- from concept to system realisation," *sensors and actuators*, vol. B 51, pp. 25–37, 1998.

[3] J. Marshall, G. Stewart, and G. Whitenett, "Design of a tunable l-band multi-wavelength laser system for application to gas spectroscopy," *Measurement Science Technology*, vol. 17, pp. 1023–1031, 2006.

[4] G. Whitenett, G. Stewart, K. Atherton, B. Culshaw, and W. Johnstone, "Optical fibre instrumentation for environmental monitoring applications," *Applied Optics*, vol. 5, no. 5, pp. S140–S145, 2003.

[5] G. Stewart, C. Tandy, D. Moodie, M. A. Morante, and F. Dong, "Design of a fibre optics multi-point sensor for gas detection," *sensor and actuator*, vol. B 51, pp. 227–232, 1998.

[6] G. Stewart, G. Whitenett, P. Shields, J. Marshall, and B. Culshaw, "Design of fibre laser and sensor system for gas spectroscopy in the near ir," *SPIE Photonics East 2003*, 2003.

[7] G. Stewart, B. Culshaw, W. Johnstone, G. Whitenett, K. Atherton, and A. Mclean, "Optical fibre sensors and networks for environmental monitoring," *Management of environmental quality*, vol. 14, no. 2, pp. 181–190, 2003.

[8] M. E. Webber, M. Pichael, and C. K. N. Patel, "Fibre-amplifier-enhanced photoacoustic spectroscopy with near-infrared tunable diode lasers," *Applied Optics*, vol. 42, pp. 2119–2126, 2003.

[9] R. T. Wainner, M. B. Frish, M. C. Laderer, M. G. Allen, and B. D. Green, "Tunable diode laser wavelength modulation spectroscopy (tdl-wms) using a fiber-amplified source," *Optical Society of America*, 2007.

[10] R. Arndt, "Analytical line shape for lorentian signal broadened by modulation," *J Applied Physics*, vol. 36, no. 8, pp. 2522–2524, 1965.

[11] D. T. Cassidy and J. Reid, "Atmospheric pressure monitoring of trace gases using tunable diode lasers analytical line shape for lorentzian signal broadened by modulation," *Applied Optics*, vol. 21, pp. 1185–1190, 1982.

[12] D. T. Cassidy and L. J. Bonnell, "Trace gas detection with short-external-cavity ingaasp diode laser transmitter modules operating at 1.58um," *Applied Optics*, vol. 27, pp. 2688–2693, 1988.

[13] K. Namjou, S. Cai, E. A. Whittaker, J. Faist, C. Gmachl, F. Capasso, D. L. Sivco, and A. Y. Cho, "Sensitive absorption spectroscopy with a room-temperature distributed-feedback quantum-cascade laser," *Optics Letters*, vol. 23, pp. 219–221, 1998.

[14] U. Gustafsson, G. Somesfalean, J. Alnis, and S. Svanberg, "Frequency-modulation spectroscopy with blue diode lasers," *Applied Optics*, vol. 39, pp. 3774–3780, 2000.

[15] S. Schilt and L. Thevenaz, "Wavelength modulation spectroscopy: combined frequency and intensity laser modulation," *Applied Optics*, vol. 42, pp. 6728–6738, 2003.

[16] S. K. Kim, G. Stewart, and B. Culshaw, "Mode-hop-free single-longitudinal-mode erbium-doped fiber laser frequency scanned with a fiber ring resonator," *Applied Optics*, vol. 38, no. 24, pp. 5154–5157, 1999.

[17] G. Whitenett, *The modelling and design of a fibre laser system with application to gas spectroscopy.* PhD thesis, University of Strathclyde, 2004.

[18] *Stanford Research Systems, 'Model SR850 DSP Lock-In Amplifier' revision 1.5(6/03).*

[19] A. M. Bullock, J. M. Barrington, C. M. Fitzgerald, B. Seavey, and A. N. Dharamsi, "Wavelength modulation of semiconductor lasers for absorption spectroscopy employing harmonic detection," in *Proc. SPIE 3945*, 2000.

[20] J. M. Supplee, E. A. Whittaker, and W. Lenth, "Theoretical description of frequency modulation and wavelength modulation spectroscopy," *APPLIED OPTICS*, vol. 33, no. 27, 1994.

[21] I. D. Lindsay, P. Gro, C. J. Lee, B. Adhimoolam, and K. J. Boller, "Mid-infrared wavelength and frequency modulation spectroscopy with a pump-modulated singly-resonant optical parametric oscillator," *Optics Express*, vol. 14, pp. 12341–12346, 2006.

[22] V. M. Baev, T. Latz, and P. E. Toschek, "Laser intra-cavity absorption spectroscopy," *Applied Physics*, vol. B69, pp. 171–202, 1999.

[23] M. Zhang, D. N. Wang, W. Jin, and Y. Liao, "Wavelength modulation techniques for intra-cavity absorption gas sensor," *IEEE Trans. on Inst. and Meas.*, vol. 53, pp. 136–139, 2004.

[24] Y. Zhang, M. Zhang, W. Jin, H. L. Ho, M. S. Demokan, B. Culshaw, and G. Stewart, "Investigation of erbium-doped fiber laser intra-cavity absorption sensor for gas detection," *Elsevier Optics Communication*, vol. 232, pp. 295–301, 2004.

[25] G. Stewart, P. Shields, and B. Culshaw, "Development of fibre laser systems for ring down and intra-cavity gas spectroscopy in the near ir," *Measurement Science Technology*, vol. 15, pp. 1621–1628, 2004.

[26] G. Stewart, G. Whitenett, K. Vijayraghavan, and S. Sridaran, "Investigation of the dynamic response of erbium fibre lasers with potential application for sensors," *Lightwave Technology*, vol. 25, no. 7, pp. 1786–1796, 2007.

[27] A. Stark, L. Correia, M. Teichmann, S. Salewski, C. Larsen, V. M. Baev, and P. E. T. P. E, "Intra-cavity absorption spectroscopy with thulium doped fibre laser," *Optics Communications*, vol. 215, pp. 113–123, 2003.

[28] S. Schilt, L. Thevenaz, M. Nikles, L. Emmenegger, and C. Huglin, "Ammonia monitoring at trace level using photoacoustic spectroscopy in industrial and environmental applications," *Elsevier Spectrochimica*, vol. 60, pp. 3259–3268, 2004.

[29] J. Li, X. Gao, L. Fang, W. Zhang, and H. Cha, "Resonant photoacoustic detection of trace gas with dfb diode laser," *Optics laser technology*, vol. 39, pp. 1144–1149, 2007.

[30] J. Li, X. Gao, W. Li, Z. Cao, L. Deng, W. Zhao, M. Huang, and W. Zhang, "Near-infrared diode laser wavelength modulation-based photoacoustic spectrometer," *Elsevier Spectrochimica*, vol. 64, pp. 338–342, 2006.

[31] J. P. Besson, S. Schilt, and L. Thevenaz, "Sub-ppb ammonia detection based on photoacoustic spectroscopy," *SPIE*, vol. 5855, pp. 415–418, 2005.

[32] B. A. Paldus, T. G. Spence, and R. N. Zare, "Photoacoustic spectroscopy using quantum-cascade lasers," *Optics Letters*, vol. 24, no. 3, pp. 178–180, 1999.

[33] A. Elia, P. M. Lugara, and C. Giancaspro, "Photoacoustic detection of nitric oxide by use of a quantum-cascade laser," *Optics Letters*, vol. 30, no. 9, pp. 988–990, 2005.

[34] L. B. Kreuzer, "Ultralow gas concentration infrared absoprtion spectroscopy," *J Applied Physics*, vol. 42, pp. 2934–2943, 1971.

[35] C. F. D. Jr, R. D. Kamm, and C. E. Hackett, "Acoustic amplifier for detection of atmospheric pollutants," *J Applied Physics*, vol. 23, no. 11, pp. 633–635, 1973.

[36] P. D. Goldan and K. Goto, "An acoustic resonant system for detection of low-level infrared absorption in atmospheric pollutants," *J Applied Physics*, vol. 45, no. 10, pp. 4350–4355, 1974.

[37] R. D. Kamm, "Detection of weakly absorbing gases using a resonant optoacoustic method," *J Applied Physics*, vol. 47, no. 8, pp. 3550–3558, 1976.

[38] A. Miklos, P. Hess, and Z. Bozoki, "Application of acoustic resonators in photoacoustic trace gas analysis and metrology," *Review of Scientific Instruments*, vol. 72, pp. 1937–1955, April 2001.

[39] J. P. Besson, S. Schilt, and L. Thevenaz, "Multi-gas sensing based on photoacoustic spectroscopy using tunable laser diodes," *Elsevier Spectrochimica*, vol. 60, pp. 3449–3456, Nov 2004.

[40] "Hitran database," 2004.

[41] L. S. Rothman, I. E. Gordon, A. Barbe, D. C. Benner, P. F. Bernath, M. Birk, and VBoudon, "The hitran 2008molecularspectroscopicdatabase," *Elsevier Quantitative Spectroscopy and RadiativeTransfer*, vol. 110, pp. 533–572, February 2009.

[42] G. S. Calculator, "www.spectralcalc.com."

[43] A. E. Siegman, *Lasers.* University Science Books, 1986.

[44] K. Walter, *Solid-state laser engineering*, vol. ISBN 3-540-60237-2. Springer, 1996.

[45] K. Duffin, A. J. McGettrick, W. Johnstone, G. Stewart, and D. G. Moodie, "Tunable diode laser spectroscopy with wavelength modulation: a calibration-free approach to the recovery of absolute gas absorption line shapes," *J Lightwave Technology*, vol. 25, no. 10, pp. 3114–3125, 2007.

[46] A. J. McGettrick, K. Duffin, W. Johnstone, G. Stewart, and D. G. Moodie, "Tunable diode laser spectroscopy with wavelength modulation: a phasor decomposition method for calibration-free measurements of gas concentration and pressure," *J Lightwave Technology*, vol. 26, no. 4, pp. 432–440, 2008.

[47] A. L. Chakraborty, K. R. W. Johnstone, M. Lengden, and K. Duffin, "Elimination of residual amplitude modulation in tunable diode laser wavelength modulation spectroscopy using an optical fibre delay line," *Optics Express*, vol. 17, no. 12, pp. 9602–9607, 2009.

[48] E. Snitzer, "Proposed fiber cavities for optical masers," *J Applied Physics*, vol. 32, no. 1, pp. 36–39, 1961.

[49] M. J. F. Digonnet, C. J. Gaeta, and H. J. Shaw, "1.064 and 1.32 pm nd:yag single crystal fibre lasers," *IEEE J Lightwave Technology*, vol. LT-4, no. 4, pp. 454–460, 1986.

[50] R. J. Mears, L. Reekie, S. B. Poole, and D. N. Payne, "Neodymium-doped silica single-mode fibre lasers," *Electronics Letters*, vol. 21, no. 17, pp. 738–740, 1985.

[51] H. Y. Ryu, W. K. Lee, H. S. Suh, and H. S. Moon, "Tunable erbium-doped fiber ring laser for applications of infrared absorption spectroscopy," *Elsevier Optics Communications*, 2007.

[52] Z. Meng, G. Stewart, and G. Whitenett, "Stable single-mode operation of a narrow-linewidth, linearly polarized, erbium-fiber ring laser using a saturable absorber," *J of Lightwave Technology*, vol. 24, no. 5, pp. 2179–2183, 2006.

[53] G. Stewart, W. Johnstone, N. Arsad, and K. Duffin, "Tunable diode and fibre laser spectroscopy in the near-ir for measurement of gas parameters," *SPIE Photonics Europe*, April 2008.

[54] I. J. Sola, J. C. Martin, and J. M. Alvarez, "980 and 1480 nm edf characterisation by ring tunable laser dynamic study," *Elsevier Optics Communications*, vol. 203, pp. 349–358, 2002.

[55] J. Cousin, P. Masselin, W. Chen, D. Boucher, S. Kassi, D. Romanini, and P. Szriftgiser, "Application of a continuous-wave tunable erbium-doped fiber laser to molecular spectroscopy in the near infrared," *Applied Physics Lasers and Optics*, vol. 83, pp. 261–266, 2006.

[56] G. A. Ball and W. H. Glenn, "Design of a single-mode linear-cavity erbium fiber laser utilizing bragg reflectors," *J of Lightwave Technology*, vol. 10, no. 10, pp. 1338–1343, 1992.

[57] D. J. Hill, B. Hodder, J. D. Freitas, S. D. Thomas, and L. Hickey, "Dfb fibre-laser sensor developments," *Proc. of SPIE*, vol. 5855, no. 17, pp. 904–907, 2005.

[58] M. Sejka, P. Varming, J. Hubner, and M. Kristensen, "Distributed feedback er3+-doped fibre laser," *Electronics Letters*, vol. 31, no. 17, pp. 1445–1446, 1995.

[59] J. T. Kringlebotn, J. L. Archambault, L. reekie, and D. N. Payne, "Er3+yb3+ codoped fiber distributed feedback lasers," *Optics Letters*, vol. 19, no. 24, pp. 2101–2103, 1994.

[60] K. Yelen, M. N. Zervas, and L. M. B. Hickey, "Fiber dfb laser with ultimate efficiency," *J. of Lightwave Tech.*, vol. 23, pp. 32–43, 2005.

[61] L. dong, W. H. Loh, J. E. Caplen, J. D. Minelly, K. Hsu, and L. Reekie, "Efficient single-frequency fiber lasers with novel photosensitive er/yb optical fibers," *Optics Letters*, vol. 22, no. 10, pp. 694–696, 1997.

[62] H. Kogelnik and C. V. Shank, "Coupled wave theory of distributed feedback lasers," *Applied Physics*, vol. 43, no. 5, pp. 2327–2335, 1972.

[63] L. B. Fu, M. Ibsen, P. W. Turner, D. J. Richardson, and D. N. Payne, "Single-polarization all-fiber dfb laser with keyed-axis output," *Optical Society of America*, vol. WJ5, 2002.

[64] H. H. Thanh, "Fabrication and characterization of tunable dfb fiber laser with the single wavelength and single polarization mode for optical communications," *International workshop on Photonics and application Vietnam*, 2004.

[65] P. Horak, N. Y. Voo, M. Ibsen, and W. H. Loh, "Pump-noise-induced linewidth contributions in distributed feedback fiber lasers," *IEEE Photonics Technology Letters*, vol. 18, no. 9, pp. 998–1000, 2006.

[66] J. F. Cliche, M. Allard, and M. tetu, "High power and ultranarrow dfb laser: the effect of linewidth reduction systems on coherence length and interferometer noise," *SPIE*, vol. 6216, 2006.

[67] V. C. Lauridsen, J. H. Povlsen, and P. Varming, "Design of dfb fibre lasers," *Electronics Letters*, vol. 34, no. 21, pp. 2028–2030, 1998.

[68] C. Yelleswarapu and A. Sharma, "A simple technique for indirect measurement of absorption line widths in voigt profile regime," *J. of Quantitave Spec. and Radiative Transfer*, vol. 72, no. 5, pp. 733–740, 2002.

[69] M. A. Mirza, *Design of a tunable multi-wavelength erbium doped fibre laser using periodic filtering and phase modulation.* PhD thesis, University of Strathclyde, Dept of Electronic and Electrical Engineering, November 2008.

[70] C. Svelto, E. Bava, S. Taccheo, and P. Laporta, "Pound-drever frequency-stabilised yber: glass laser against c2h2 molecules at 1.534097 um," *Electron. Lett*, vol. 34, no. 5, pp. 1004–1005, 1993.

[71] M. Bass and E. W. V. Stryland, *Fiber Optics Handbooks- Fiber, Devices and System for Optical Communications.* McGraw-Hill Telecom Engineering, 2002.

[72] R. J. Zhang, B. L. Yu, Z. Cao, S. Zhen, J. Zhu, and R. Liu, "Frequency modulated and polarization maintaining fibre laser with narrow linewidth," *Elsevier Optics Communication*, vol. 274, pp. 392–395, 2007.

[73] A. Mirza and G. Stewart, "Theory and design of a simple tuneable sagnac loop filter for multi-wavelength fibre lasers," *Applied Optics*, vol. 47, no. 29, pp. 5242–5252, 2008.

[74] G. Whitenett, G. Stewart, H. Yu, and B. Culshaw, "Investigation of a tunable mode-locked fibre laser for application to multi-point gas spectroscopy," *Lightwave Technology*, vol. 22, no. 3, pp. 813–819, 2004.

[75] K. Yelen, *Design method for ultimate efficiency in linear-cavity continuous-wave lasers using distributed-feedback.* PhD thesis, University of Southampton, June 2004.

[76] H. Kogelnik and C. V. Shank, "Stimulated emission in a periodic structure," *Applied Physics Letters*, vol. 12, no. 18, pp. 152–154, 1971.

[77] A. Othonos, "Fiber bragg gratings," *Review Science Instrument*, vol. 68, pp. 4309–4341, Dec 1997.

[78] K. O. Hill, Y. Fujii, D. C. Johnson, and B. S. Kawasaki, "Photosensitivity in optical fiber waveguides: Application to reflection filter fabrication," *Applied Physics Letters*, vol. 32, no. 20, pp. 647–649, 1978.

[79] G. Meltz, W. W. Morey, and W. H. Glenn, "Formation of bragg gratings in optical fibers by a transverse holographic method," *Optics Letters*, vol. 14, no. 15, pp. 823–825, 1989.

[80] D. Z. Anderson, V. Mizrahi, T. Erdogan, and A. E. White, "Production of in-fiber gratings using a diffractive optical-element," *Electronics Letters*, vol. 29, no. 6, pp. 566–568, 1993.

[81] K. O. Hill, B. Malo, F. Bilodeau, D. C. Johnson, and J. Albert, "Bragg gratings fabricated in monomode photosensitive optical fiber by uv exposure through a phase mask," *Applied Physics Letters*, vol. 62, no. 10, pp. 1035–1037, 1993.

[82] G. A. Ball and W. W. Morey, "Continuously tunable single-mode erbium fiber laser," *Optics Letters*, vol. 17, no. 6, pp. 420–422, 1992.

[83] M. J. Cole, H. Geiger, R. I. Laming, S. Y. Set, M. N. Zervas, W. H. Loh, and V. Gusmeroli, "Broadband dispersion-compensating chirped fibre bragg gratings in a 10gbit/s nrz 110km non-dispersion-shifted fibre link operating at 1.55um," *Electronics Letters*, vol. 33, no. 1, pp. 70–71, 1997.

[84] V. C. Lauridsen, J. H. Povlsen, and P. Varming, "Optimising erbium-doped dfb fibre laser length with respect to maximum output power," *Electronics Letters*, vol. 35, no. 4, pp. 300–302, 1999.

[85] M. J. Cole, W. H. Loh, R. I. Laming, M. N. Zervas, and S. Barcelos, "Moving fibre/phase mask-scanning beam technique for enhanced flexibility in producing fibre gratings with uniform phase mask," *Electronics Letters*, vol. 31, no. 17, pp. 1488–1490, 1995.

[86] G. Bonfrate, F. Vaninetti, and F. Negrisolo, "Single-frequency mopa er3+ dbr fiber laser for wdm digital telecommunication systems," *IEEE Photonics Technology Letters*, vol. 10, no. 8, pp. 1109–1111, 1998.

[87] M. Ibsen, A. Fu, H. Geiger, and R. I. Laming, "All-fibre 4 x 10 gbit/s wdm link with dfb fibre laser transmitters and single sinc-sampled fibre grating dispersion compensator," *Electronics Letters*, vol. 35, no. 12, pp. 982–983, 1999.

[88] M. Ibsen, S. U. Alam, M. N. Zervas, A. B. Grudinin, and D. N. Payne, "8-16 channel all-fiber dfb laser wdm transmitters with integrated pump redundancy," *IEEE Photonics Technology Letters*, vol. 11, no. 9, pp. 1114–1116, 1999.

[89] H. Simonsen, J. Henningsen, and S. Sogaard, "Dfb fibre lasers as optical wavelength standards in the 1.5um region," *IEEE Transactions on Instrumentation and Measurement*, vol. 50, no. 2, pp. 482–485, 2001.

[90] J. Uniphase, *Butterfly Laser Modules-DC Operating Instructions*, August 2000.

[91] C. D. Butter and G. B. Hocker, "Fibre optic strain gauge," *Applied Optics*, vol. 17, no. 18, pp. 2867–2869, 1978.

[92] N. F. Borrelli and R. A. Miller, "Determination of the individual strain-optic coefficients of glass by an ultrasonic technique," *Applied Optics*, vol. 7, pp. 745–750, May 1968.

[93] F. E. AB, *General purpose analogue amplifier-Model A400*.

[94] P. P. Actuator, *Product description and operating notes*, 1.0.0 ed., Feb 2004.

[95] M. Wolf and H. Harde, "Photoacoustic spectrometer based on a dfb-diode laser," *Elsevier Infrared Physics and Technology*, vol. 41, pp. 283–286, 2000.

[96] C. Haisch and R. Niessner, "Light and sound - photoacoustic spectroscopy," *Spectroscopu Europe*, pp. 10–15, 2002.

[97] A. Schmohl, A. Miklos, and P. Hess, "Detection of ammonia by photoacoustic spectroscopy with semiconductor lasers," *Optical Society of America*, vol. 41, pp. 1815–1823, March 2002.

[98] R. E. Lindley, A. M. Parkes, K. A. Keen, E. D. Mcnaghten, and A. J. Orr-ewing, "A sensitivity comparison of three photoacoustic cells containing a single microphone, a differential dual microphone or a cantilever pressure sensor," *Applied Physics*, vol. B86, pp. 707–713, 2007.